ALMA MATER STUDIORUM - UNIVERSITÀ DI BOLOGNA

DOTTORATO DI RICERCA IN

CHIMICA

Ciclo XXVIII

Settore concorsuale di afferenza: 03/C2
Settore scientifico disciplinare: CHIM/04

New insights on the mechanism of interaction between light (bio) alcohols and metallic mixed oxides catalysts

Presentata da: Juliana Velasquez Ochoa

Coordinatore Dottorato — Prof. Aldo Roda

Relatore — Prof. Fabrizio Cavani

Esame finale anno 2016

SUMMARY

1 INTRODUCTION

The use of ethanol and other bio-alcohols as building blocks for the chemical industry continues to be one of the pillars of the growing concept of *biorefineries*. One reason is that alcohols such as ethanol and butanol obtained directly from biomass are already available at a reasonable price and this makes them attractive as platforms to try to transform them in higher added value compounds. Among the different molecules that can be produced from ethanol (or butanol), the 1,3-butadiene represents one of the most valuable derivatives due to its high demand. In fact, the production of this monomer is driven by its importance for the synthesis of polymers such as styrene-butadiene rubber (SBR) used in the manufacture of tires, a market that is constantly growing, especially in developing countries. The direct production of butadiene from ethanol is a complex process known as "Lebedev" reaction (in honor of his first inventor). So far, the conclusion is that the on-purpose production of butadiene from alternative renewable sources is an interesting approach for obtaining this added value product that nowadays is mainly formed as a by-product of the steam cracking of naphtha or natural gas.

As regards the catalyst for the Lebedev process, the composition is based on the basic/acid pair Mg-Si in mixed oxides. Modifications of the Mg/Si/O catalyst by addition of metals such as Zn, Ag, Cu, Ni and so on, have been also investigated in the literature and they improved the yield of the desired product. However, until now there is no clear explanation on why catalysts with a similar composition differ so much in terms of activity. Moreover, the mechanism of this reaction is supposed to share the same intermediates than those that produce *n*-butanol from ethanol; this reaction of higher alcohols formation (known as Guerbet reaction) is indeed usually carried out with similar catalysts than those for the Lebedev process. However, recently it has been stated that they might proceed by different mechanisms [1], [2].

This research intends to explore the mechanism behind the transformation of ethanol over basic and acid/base catalysts. The approach used was first to explore in depth the role of the MgO which is a common component of both reactions (Lebedev and Guerbet) and then to study the incorporation of Si ion and the effect on the acid/base properties of the resulting materials. Moreover, the addition of a dopant with acid/dehydrogenating

properties was also explored. Further on, several catalysts were tested under the usual conditions for this reaction and characterization was made in order to understand their particular behavior. An important tool in this research was the in-situ infrared diffuse reflectance spectroscopy (DRIFTS) coupled with mass spectrometry (MS) due to the possibility that it offers to study what occurs on the catalysts surface under real working conditions. This study allowed to gain new insights on the mechanism behind the catalytic upgrading of ethanol on basic and acid/base mixed oxides, giving an alternative view of the mechanism for the Lebedev and Guerbet reactions that permitted us to discard the key role of the generally accepted intermediates and helped to explain several experimental findings not clear before.

1.1. Ethanol

Nowadays, the increasing concerns about climate change and energy security have motivated the search for alternatives to petroleum to produce fuels and chemicals. Even if ethanol may be a simple molecule, it has the potential to be a building block for a significant number of compounds usually obtained from fossil fuels [3]. This seems to be a huge opportunity for the ethanol industry, but there are still some challenges to overcome.

In general, the utilization of biomass as a raw material to produce ethanol and other commodities has attracted great interest [4]; in fact nowadays biomass is seen as the only renewable source of organic carbon currently able to replace petroleum in the production of fuels and chemicals. However, it requires new approaches in terms of processing since from the chemical standpoint biomass and fossil oil are diametrically opposed. Indeed, petroleum is composed of a mixture of hydrocarbons (e.g., linear, cyclic, aromatics, etc.) whereas biomass feedstock typically comprises highly-oxygenated compounds embedded in some cases in a complex polymeric matrix. Consequently, the highly-optimised catalytic processes that have been developed over the past years in the petrochemical industry cannot be directly extrapolated for their use with biomass, and this includes as well the catalysts design.

Typical petroleum catalysts are designed to resist high temperatures and hydrophobic environments but this might not be effective in the conditions required to process

biomass. Thus, to be successful, efficient processes for converting biomass to ethanol and then the alcohol into chemicals have yet to be developed. Moreover, the markets have to be settled for these ethanol-based chemicals. Nevertheless, in the last decade the production of ethanol has been growing and it reached values of more than 20 billion of gallons per year (See Figure 1); and also every day there are advances in the technology to obtain it from different sources making it a very attractive molecule for its transformation into added value products.

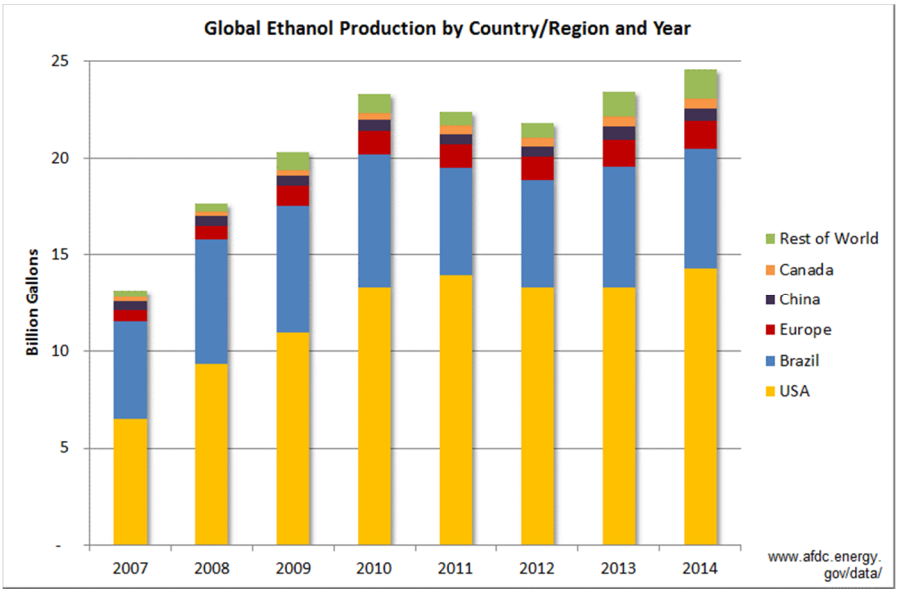

Figure 1. Global Ethanol production by country/region and year. Source: F.O. Licht, cited in Renewable Fuels Association, Ethanol Industry Outlook 2008-2014 reports.[1]

1.1.1. Ethanol production

Ethanol can be produced in two ways. The first is the route starting from petrochemical feedstock. This accounts for an annual world production of 850000 tonnes (470000 tonnes for Europe in 2013 not including alcohol produced biosynthetically).[2] In this method, ethanol is obtained by the direct catalytic hydration of ethylene in presence of steam, using phosphoric acid adsorbed on the surface of a solid silica as a catalyst, the whole in a fixed bed reactor. The reaction is reversible and exothermic:

[1] www.ethanolrfa.org/pages/annual-industry-outlook
[2] http://www.essentialchemicalindustry.org/chemicals/ethanol.html

$$C_2H_4(g) + H_2O(g) \overset{\text{catalyst}}{\rightleftharpoons} C_2H_5OH(g)$$

In this case, the production of ethanol is favored by low temperature, high pressure and high steam concentration. To achieve acceptable reaction rates, a temperature of ca 250 °C is used in the presence of the catalyst. An increase in the pressure pushes the reaction to the product side but also causes polymerization of ethylene. Besides, higher pressures mean increased capital and operating costs as well. In practice, the process is generally operated at about 60-70 atm. This reaction has a theoretical atom economy of 100%, but some side reactions occur producing by-products such as methanol, acetaldehyde and ethoxyethane. The ethanol obtained by this method is usually purified by fractional distillation which always results in a mixture of 96% ethanol and 4% water (azeotropic or constant boiling mixture). Conventionally, this last 4% water is removed from the mixture either by refluxing with calcium oxide, a dehydrating agent, or by mixing with benzene, which breaks up the azeotrope and produces pure ethanol when further distilled. However, these processes increase the energy costs of production, and benzene is also highly toxic and carcinogenic. Some new purification techniques that avoid the use of benzene involve the use of zeolites, which are a sort of molecular sieves that can retain and hence remove water from the final mixture. Some of these compounds (for instance the Zeolite 3A) have a particularly strong attraction, and they act as dehydrating agents at normal temperatures and pressures and can then be dried by heating and re-used. This produces considerable savings in energy.

The other way to produce ethanol is by fermentation of plant sugars; the alcohol obtained in this way is usually called bio-ethanol[3]. The most commonly used plants to produce ethanol are sugar cane and sugar beet since the saccharose contained in them is easily accessible for the fermentation organisms. Other plants used for fermentation are the corn, wheat potatoes or barley. The ethanol produced from these crops is known as *first generation* ethanol and it is nowadays the main route to bioethanol. However, there are two big concerns about it. The first one is ethical: the production of ethanol competes with the use of those crops as food, and the second one is practical: it excludes the use of most of the herbaceous biomass since the sugars in it are in the form of cellulose and hemicellulose which are more robust sugar polymers and thus less easily accessible. In fact, the main challenge to produce this so-called *second generation* bioethanol is the

[3] http://www.ethanolrfa.org/how-ethanol-is-made/

efficient breakdown of cellulose to the fermentable sugar monomers. Nevertheless, the efforts in this area have made available the technology to obtain ethanol from several lignocellulosic sources such as straw, nut shells, bagasse and so on. (Figure 2)

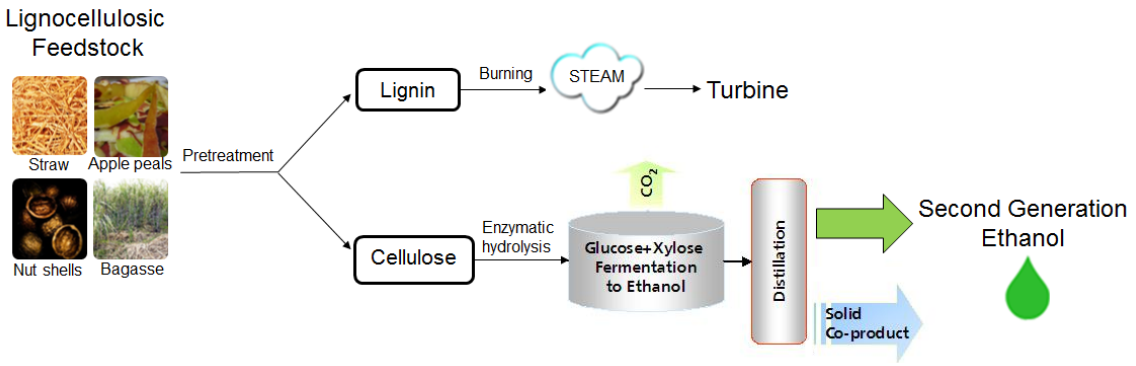

Figure 2. Production of second generation ethanol

In conclusion, with the advance of the technology to obtain it from a wider feedstock, together with the traditional sources, it can be stated that ethanol is already available in high quantity (and at a reasonable price) which makes it attractive to try to convert it into added value products.

1.1.2. Ethanol as a building block

Once the ethanol is obtained, there are numerous possibilities for its usage. For energy applications it can either be used directly as a fuel or transformed into hydrogen (mainly for energy production in fuel cells). On the other hand, it can be converted into several different chemical commodities (Figure 3). In general, chemical production from ethanol becomes attractive when there is an abundant ethanol supply and petroleum prices are high. Preliminary assessments of the sustainability of production of different chemicals from ethanol have been made and until now the conclusion is that 1,3-Butadiene and diethyl ether are the most promising derivatives followed by ethylene, propylene, acetaldehyde, ethylene oxide and ethyl acetate. On the other hand, iso-butylene, hydrogen, *n*-butanol, acetic acid and especially acetone did not seem to represent attractive options for bioethanol conversion.[5] Nevertheless, it is important to notice that purely industrial and economic factors, which are the usually considered aspects in those kind of studies, leave out of vision other elements which encourage the development of

this kind of chemistry from renewables that are more social and political in nature. For instance: (i) The Kyoto and related politics to reduce carbon footprint, (ii) security of supply, (iii) agricultural policies, (iv) sustainability and (v) support and growth of the local economics.[6]

This section gives a summary of the main aspect in the production of some of the chemical derivatives that could be obtained from ethanol and which are of interest for the present research, whereas the next section is dedicated to Butadiene as it was the main product intended to obtain in this particular study.

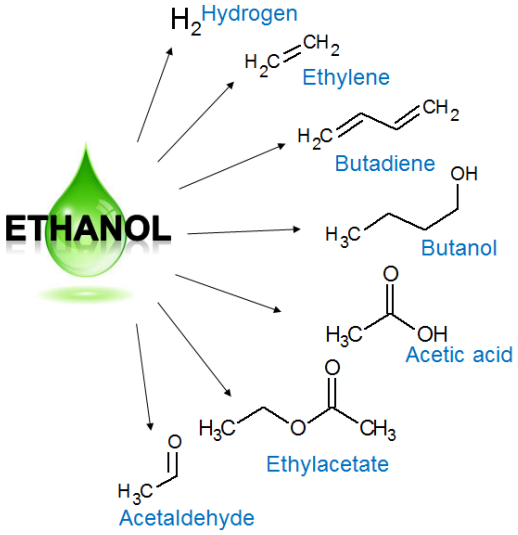

Figure 3. Bulk chemicals obtained from ethanol

Ethylene

Production of ethylene is of great importance; it is in fact the organic chemical of major production on the chemical industry in general. The market of this olefin is continuously growing (4.5% per year during 2009-2014, while capacity increased at a slower rate of about 3.5%.)[4] as well as the demand for renewable polyethylene. However, the possibility of synthesizing ethylene from steam cracking (or oxidehydrogenation -ODH-) of ethane (available at cheap prices from natural or shale gas), might represent an economic obstacle for further developments of the production of ethylene from bioethanol. Indeed, due to economic reasons, until now this process has been implemented only in regions were the cost of sugars (and thus bioethanol) is very low, such as in Brazil and India.[7], [8]. In spite of these economic drawbacks, this reaction has been the subject of a vast

[4] https://www.ihs.com/products/ethylene-chemical-economics-handbook.html

scientific production [9] and patents from companies such as as BP, Total Petrochemicals and Solvay.[10]–[12] A niche production of bio-ethylene might however be possible in those markets looking for smaller-scale volumes where full-scale crackers (using either naphtha or natural gas) would not be commercially viable.

From the catalytic point of view, several materials (mainly of acidic character) have been tested in order to decrease the temperatures usually required for this endothermic dehydration reaction (>500°C) which are, in part, the cause of the high cost of the process. Many of the catalysts tested are able to dehydrate ethanol with selectivity and conversion higher than 95%, but only few of them resist coke deactivation for long periods of time, making compulsory the periodic regeneration of the catalyst [8], [9]. The problem might be solved utilizing fluidized bed reactors that present a more uniform temperature profile and which allow the regeneration of the spent catalyst under continuous conditions. Nevertheless, friction and collision problems between catalyst particles remain general issues of this kind of reactors and favour the more conventional fixed-bed approach. The first catalysts used industrially for this process were based on immobilized phosphoric acid at 500°C; however, the severe coke formation and the high temperatures required, encouraged the development of more efficient systems. The following table (Table 1) summarizes some of the more active catalysts working at Temperatures < 300°C (adapted from[8]).

Table 1. Promising catalytic systems for dehydration o ethanol to ethylene

Catalyst	*Ethanol Conversion*	*Max. Ethylene Selectivity*	*Reaction Temperature*	*Life Span, Stability*
0.5%La-2% PHZSM-5	100%	99,9%	240-280°C	Very Stable
Nano-CAT	100%	99,7%	240°C	630h, Very Stable
$Ag_3PW_{12}O_{40}$	100%	99,2%	220°C	Stable in 9% humidity
STA-MCM-41	99,0%	99,9%	250°C	Stable
TRC-92	70,0%	99,0%	280°C	Very Stable

As regards the reaction mechanism, it is generally accepted that with acid/base catalysis formation of an intermediate ethoxy- and hydroxy-species on the catalyst surface occurs, with the consecutive water desorption as the rate-determining step (Figure 4) [6], [8].

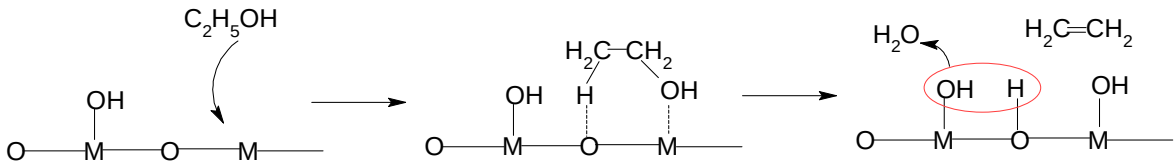

Figure 4. *Dehydration of ethanol to give ethylene*

However, as highlighted by the number of papers recently published on this topic [13]–[18], the reaction mechanism might be more complicated than expected; in particular, because reaction temperature, nature of the acid-base sites and ethanol partial pressure are fundamental variables that govern the phenomenon at the molecular level and need to be carefully tuned, especially to avoid consecutive reaction of ethylene with surface acid sites (which might generate coke) and redox reaction leading to dehydrogenation rather than dehydration.

New insights obtained on the reaction mechanism for ethanol transformation into 1-butanol (Guerbet reaction) and 1,3-Butadiene (Lebedev reaction) on oxide catalysts with basic features [1] showed that a C_2-carbanion could represent the real transient species that could explain the formation of ethylene on basic oxides. Indeed, oxides such as MgO or CaO form ethylene and other by-products (e.g. acetaldehyde, hydrocarbons, methane, COx, H_2 etc.) that are also observed on acid systems [9]. Nevertheless, the final product distribution is clearly a function of acid-base properties of the catalyst surface, which favour or hamper the different parallel and consecutive pathways thermodynamically possible.

Butanol

Higher alcohols, such as butanol, have fuel properties that resemble those of gasoline: this compound is essentially noncorrosive and immiscible with water and the energy density of butanol is close to that of gasoline (90%). This characteristics make butanol very attractive as an “advanced biofuel” and the commercial availability of this material as a

green “drop-in” chemical is gathering pace. Butanol has also been considered for the production of more valuable chemicals such as butenes, butadiene and maleic anhydride [19], [20].

The production of butanol from biosustainable feedstocks usually comes from the so-called ABE fermentation which uses wild and genetically modified strains (from the Clostridium family) in an anaerobic fermentation process that produces solvents in a ratio of 3 parts Acetone, 6 parts Butanol and 1 part Ethanol. Even when this process has been known for a long time, there are still many aspects to improve in order to produce n-butanol at commercially attractive prices, such as (i) increase the yields of bio-alcohol, (ii) expanding substrate utilization and (iii) minimizing energy consumption during separation and purification [21]. The cost of producing butanol by this method is then still high. It is necessary to develop micro-organisms able to give the selective fermentation to *n*-butanol to make competitive this type of synthesis. Another option is to obtain butanol from bio-ethanol. The process of increasing the carbon chain to produce higher alcohols is usually known as Guerbet reaction, named after the French scientist Marcel Guerbet (1861–1938) who first described the conversion of n-butanol to 2-ethyl-1-hexanol.

In the open literature, only a few reports describe the direct conversion of ethanol to 1-butanol and other alcohols in gas phase. The described technologies suggest a process where ethanol vapor is passed through a solid catalyst packed in a fixed bed. The reaction temperatures vary from 200 °C up to 450 °C, with a relatively low conversion (10–20%) and selectivity approaching 70%. In the recent literature, a novel catalytic process utilizing a non-stoichiometric hydroxyapatite was found to be very promising.[22] In addition, solid bases, some zeolites, and supported metals have been reported to convert ethanol to 1-butanol [23], [24].

As regards the mechanism of reaction, the generally accepted one states that an alcohol is dehydrogenated to form an aldehyde, which then undergoes aldol coupling and rehydrogenation of the product to give a longer-chain alcohol. This mechanism happens to be as well the accepted mechanism for butadiene production except for the final step (Figure 5) [25]. However, recently the aldolic condensation route has been questioned especially for the catalytic upgrading using materials of basic character [1], [2].

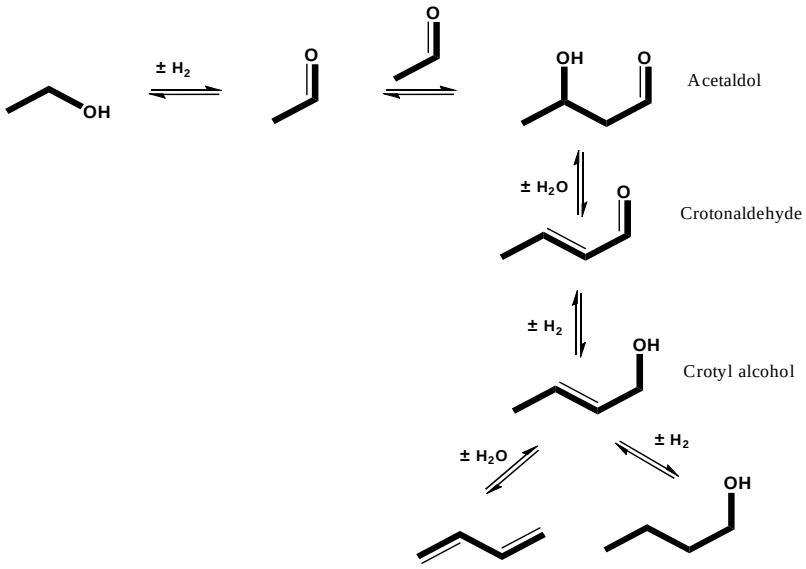

Figure 5. *Production of butanol (and butadiene) from ethanol*

Acetaldehyde

Acetaldehyde is another valuable molecule that can be obtained from ethanol. It is a low-boiling, highly flammable liquid with a pungent odor. Due to its high chemical reactivity, acetaldehyde is an important intermediate in the production of acetic anhydride, peracetic acid, butanol, 2-ethylhexanol, chlorinated acetaldehydes (chloral), glyoxal, alkyl amines, pyridines, and many other chemicals [26]. Commercial production processes to obtain acetaldehyde include hydration of acetylene, partial oxidation of hydrocarbons, direct oxidation of ethylene and the gas-phase oxidation of ethanol.

This last reaction belongs to the class of oxidative dehydrogenations and is one of the oldest routes for the preparation of acetaldehyde which may be the preferable choice when small capacities are needed. This process is exothermal (ΔH° -43 kcal/mol), and sometimes is also referred to as autothermal dehydrogenation. The nature of the mechanism is a function of the catalyst type and reaction conditions used; for instance, when a silver (Ag) catalyst is used (as in the case of the Veba-Chemie process) the mechanism is a dehydrogenation combined with hydrogen combustion. The conversion per pass usually varies between 30 and 70%, with a selectivity between 90 and 99%, depending of course on the reaction temperature (which can range from 500 to 650°C), on the alcohol/air inlet ratio used, and of the type of oxidant reactant (either air or oxygen). Main by-product for this reaction is acetic acid, but also minor amounts of formic acid, ethylacetate, CO and CO_2 may form [27].

The catalysts for this reaction might be either metallic or mixed oxides. In the first category, noble metals and especially gold-based catalysts have attracted the attention of researchers as catalysts for both liquid-phase and gas-phase oxidations [28]–[37]. These catalysts show peculiar reactivity properties because in general, they show high selectivity to acetaldehyde with very low selectivity to CO_2, which is unexpected because of the generation of highly electrophilic O species on the Au surface when nanoparticles (NPs) are supported over materials such as silica or titania. Nevertheless, in function of reaction conditions and catalyst type, the main product can be either acetic acid or ethylacetate (formed by consecutive dimerization of acetaldehyde). The behaviour is different from what is shown in liquid phase oxidation with Au-based catalysts, where quite high selectivity to acetic acid and ethylacetate (by esterification of acetic acid with ethanol) under moderate temperature and pressure is obtained [38], [39]. Recently, an outstanding performance of 95% yield of acetaldehyde at total ethanol conversion was achieved using Au nanoparticles supported over $MgCuCr_2O_4$-spinel. Moreover, the catalyst showed a stable performance over 500 h. This particular behaviour was attributed to the synergy between metallic Au NPs and the surface Cu^+ species, which act as sites for oxygen activation [40].

The second family of catalyst, i.e mixed oxides, include several compounds among which some recently published are V_2O_5/TiO_2, Mo/V/Nb/Te/O, P/Mo/V/O polyoxometalate, $CeOx/TiO_2$, CuO/Fe_2O_3, and $Co_3O_4/\gamma Al_2O_3$/cordierite [41]–[46]. An unconventional oxidic catalyst based on graphite nanofibers, has been also claimed to work for this reaction. In this case the oxygen groups terminating the prismatic edge sites of graphene planes were supposed to be responsible for the catalytic activity in oxidative dehydrogenation [47]. The results for this type of materials highlight that catalysts based either on Molybdenum or Vanadium oxide show the greatest selectivity to acetaldehyde, in the presence of co-fed steam, especially at temperatures lower than 200-250°C. Conversely, higher temperatures lead to the preferential formation of acetic acid.

Acetonitrile

Acetonitrile is a compound whose chemical properties (such as polarity, miscibility with water, low boiling point, low acidity, and low UV cut-off) make it a good solvent for the synthesis of oligonucleotides and peptides, as well as a reactant in chemical syntheses of malononitrile, pesticides or pharmaceuticals. Despite its wide spread usage, commercial acetonitrile is not obtained by a direct synthesis method but as a by-product of the

industrial-scale production of acrylonitrile. Acrylonitrile is the primary product of propylene ammoxidation, and from there, only 2-4% acetonitrile is formed and recovered by distillation; depending on the waste stream and the distillation capability, different acetonitrile qualities are obtained [48].

A dedicated process for the production of acetonitrile might be interesting since for example in the late in 2008 there was a severe acetonitrile shortage in the chemical industry, because several acrylonitrile production plants were temporarily shut down. An acetonitrile process based on a renewable source could include the use of ethanol as the reactant. In general, the ammoxidation of alcohols has been much less discussed in the literature than other substrates, with the very few examples limited to the liquid-phase ammoxidation of benzyl alcohol [49]–[53], glycerol and ethanol, and to the gas-phase ammoxidation of glycerol [54] and ethanol [55]–[58]. Indeed, ethanol ammoxidation can be carried out in the same reactor and process where propylene is ammoxidized into acrylonitrile. The conditions for the ammoxidation of ethanol are claimed to be not very different from those necessary for conducting propylene ammoxidation, while the co-feeding of ethanol and propylene has been proposed as a tool to increase the acetonitrile/acrylonitrile selectivity ratio [59].

As regards the mechanism, in some cases, they propose the formation of carboxylic acid, then amide, which, in turn, is dehydrated to nitrile.[57] In other cases the mechanism proposed is either via an exchange between water and ammonia with the formation of an amine and subsequent oxidehydrogenation to nitrile [55] or via aldehyde formation, then imine and final oxidehydrogenation to nitrile [51]–[53], [55], [56]. In this last case, it is claimed that the presence of an acid functionality in the catalyst may be essential to accelerate the dehydration of 1-aminoethanol during the non-reductive amination of ethanol. The catalysts described for this reaction are based $Ru(OH)_3$-alumina as well as manganese oxide-based molecular sieves (KMn_8O_{16}: OMS-2).[60] Manganese oxide is also a catalyst for the oxidative desulphurization of primary thioamides into the corresponding nitriles [61], while Ru hydroxide is a catalyst for the oxidative transformation of primary azides into nitriles [62]. In general, in the aerobic ammoxidation of alcohols into nitriles, the activation of the strong N-H bond in ammonia (107 kcal/mole) may require hard reaction conditions.

1.2. Butadiene

Butadiene (that usually refers to the most stable 1,3 isomer) is a chemical commodity with a very high demand. It finds application in the production of Styrene Butadiene Rubber (SBR), Styrene Butadiene Latex, Acrylonitrile Butadiene Styrene (ABS), Adiponitrile and so on (Table 2). The constantly growing automobile industry has pushed the global butadiene market in the last few years. In fact, recent studies point out that the flourishing automotive market in countries like China, India, Brasil and Rusia will increase the volume of tires to be manufactured during the period 2014-2023 and estimates the demand for butadiene to grow accordingly [63].

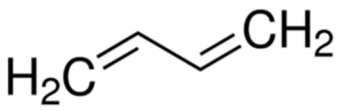

Figure 6. 1,3-Butadiene molecule

Table 2. End uses of Butadiene

End use of butadiene	*PERCENTAGE*
SYNTHETIC ELASTOMERS	***63,3***
Styrene-butadiene rubber (SBR)	32,0
Polybutadiene (BR)	23,0
Polychloroprene (neoprene)	5,6
Nitrile Butadiene rubber (NBR)	2,7
POLYMERS AND RESINS	***15,7***
Acrylonitrile-butadiene-styrene (ABS)	4,7
Styrene-butadiene copolymer (latex)	11,0
CHEMICALS AND OTHER USES	***21,0***
Adiponitrile	13,0
Others	8,0
TOTAL	100

1.2.1. Butadiene Production

Historically butadiene was industrially produced from acetylene by two processes called the Aldol process and the Reppe process, both of them using acetylene as reagent (Figure 7). These methods are no longer used as the production of acetylene requires much energy and becomes expensive. Only the first steps of the Reppe process leading to 1,4-butanediol and tetrahydrofuran are commercially employed nowadays.

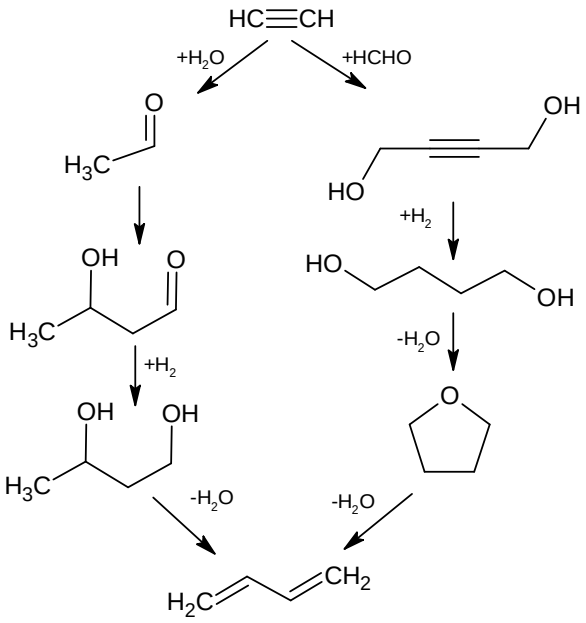

Figure 7*.Production of butadiene from acetylene by the Aldol process (Left) and Reppe process (Right).*

Another way to obtain Butadiene is by catalytic dehydrogenation of butane or butenes. The dehydrogenation reactions are highly endothemic:

Butane $\rightarrow$1-Butene $+H_2$ $\Delta H = 131 kJ/mol$

Butane $\rightarrow$cis-2-Butene$+H_2$ $\Delta H = 118 kJ/mol$

cis-2-Butene$\rightarrow$Butadiene$+H_2$ $\Delta H = 126 kJ/mol$

Nevertheless, the yield can be increased by lowering the partial pressure of the reaction products or by addition of steam. An example of one-step dehydrogenation reaction is the Houdry Catadiene process from ABB Lummus (Figure 8). In this adiabatic process, several packed bed reactors, arranged parallel to each other, are operated alternatingly. The catalyst is aluminum oxide mixed with approximately 20 % chromium oxide. *n*-

Butane is subjected to dehydrogenation as such or in a mixture with *n*-butenes at 600–700◦C and 10–25 kPa and it reaches conversion of 30-40% and butadiene yields up to 63%. However, the use of high temperatures results in by-products like C1 –C3 hydrocarbons and carbon deposition on the catalyst. After only 5–15 min of running time, the reactor has to switch to regeneration [64].

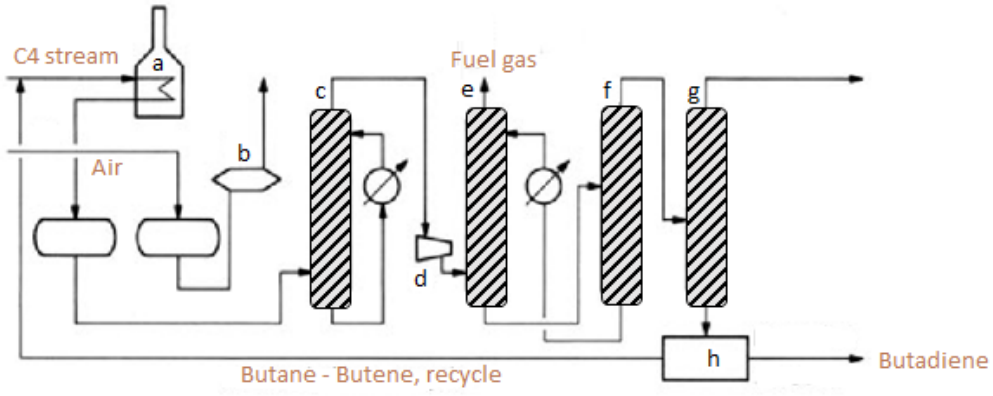

Figure 8. Houdry - Catadiene process. a) Reactor; b)Waste-heat boiler; c) Quench column; d) Compressor; e) Absorber; f) Stripper; g) C3 Column; h) C4 Separation (adapted from [64]*)*

In the case of butenes, the conversion and the selectivity of the dehydrogenation can be significantly improved by removing the hydrogen from the equilibrium and this can be achieved by addition of oxygen to promote the oxidation of hydrogen to water): $2C_4H_8 + O_2 \rightarrow 2C_4H_6 + 2H_2O$. The addition of oxygen to the dehydrogenation of butane is not meaningful because at the high temperatures required, oxygen reacts with the reaction products to give undesired by-products. The exothermic oxidation of hydrogen partially covers the heat requirements of the endothermic dehydrogenation reaction and, additionally, the oxygen together with the steam added during the reaction, decrease catalyst coking [65]. A commercial application of this approach is the so-called Oxo-D process of Petro-Tex (now TPC group) and the O-X-D process of Phillips. Petro-Tex process reaches a 65% conversion and a butadiene selectivity of 93 % by using a molar steam/butene ratio of 12/1 and a catalyst that is probably a ferrite with Zn, Mg or Mn. Phillips, on the other hand, obtains high conversion as well (75-80%) and a 88–92% selectivity to butadiene. The company Shell, alternatively, developed a one-step dehydrogenation of butane to butadiene with iodine as the hydrogen acceptor. The addition of iodine enables a high conversion and yield of butadiene but causes serious corrosion problems in the plant [66].

Today, butadiene is obtained mainly as a by-product of the steam cracking of ethane, naphtha, gas oil, and other higher boiling hydrocarbon fractions used to obtain ethylene and homologous compounds (Figure 9). Gas crackers that process ethane-rich gas, produce less C4 fraction than those based on heavier feedstock, and since most of the new crackers that started up since 2003 are based on ethane, there is a reduction in butadiene production by this conventional method. This aspect has driven the interest for the on-purpose production of butadiene, together with the possibility to obtain it in a more sustainable way.

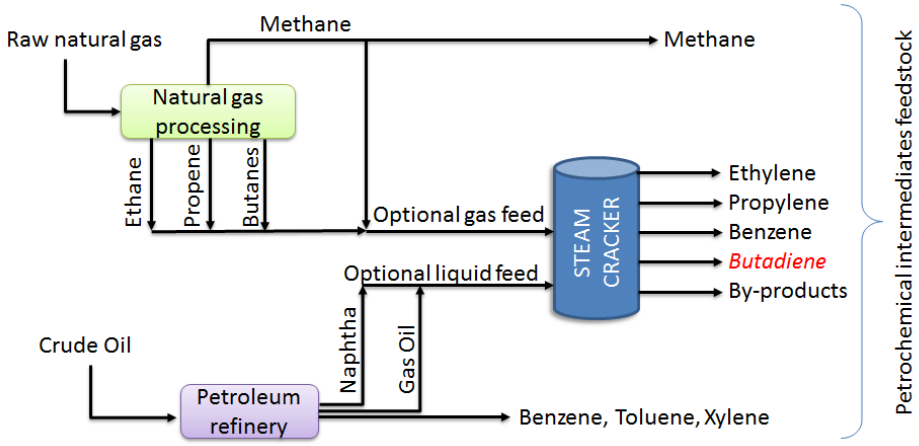

Figure 9. Production of Butadiene by steam cracking. Amount of butadiene without naphtha or gas oil is very low

1.2.2. Butadiene from ethanol

The production of butadiene from renewable resources has found support in the forecasted decrease of butadiene production by means of the conventional routes. Currently several alternatives are being considered for the synthesis of the so-called bio-butadiene (or green butadiene). Figure 10 shows different routes that are currently under investigation by different companies [67]. Nevertheless, the pathway from ethanol to bio-butadiene continues to be of great interest because ethanol is already available in high amounts and reasonable price, it is as well one of the more direct routes and it was already practiced at an industrial level during the period 1930-1970 (before being abandoned when the naphtha cracking made all the synthetic routes economically less convenient).

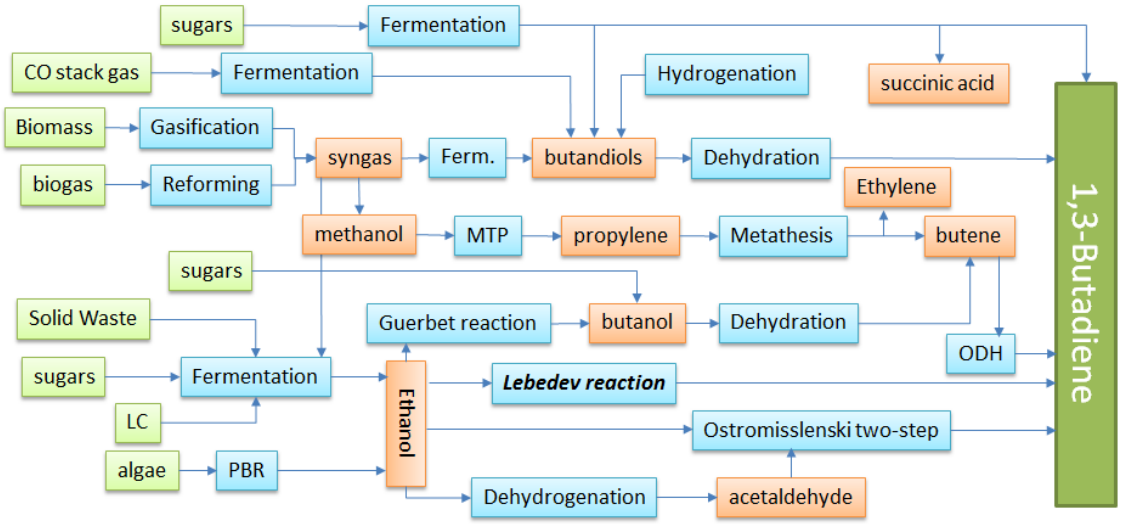

Figure 10. Different alternatives to obtain bio-butadiene

In fact, ethanol conversion into butadiene is a reaction with a very long history in the chemical industry but it has found renewed interest nowadays within the bio-refinery context. This process was first developed in Russia at the beginning of the XX century and it continued to develop until the industrial scale during the 1920-30 decade [68]. With the beginning of the World War II, many of the belligerent nations realized that they could be cut off from rubber plantations controlled by the British Empire, and sought to remove their dependence on natural rubber. In fact, three months after the attack on Pearl Harbor, Japan invaded Malaysia and the Dutch East Indies, desperate to take over natural rubber production from the allies. This gave the Axis control over 95% of world rubber supplies, and pushed the allies to develop the synthetic rubber industry. Fortunately, in 1929 it was discovered that a copolymer of styrene and butadiene could be used for automobile tires with improved mechanical properties. From that point until the end of the war, the butadiene production from ethanol represented the main route for the manufacture of synthetic rubber.

To carry out the transformation of ethanol into butadiene there were mainly two methods, a single-step approach where ethanol was directly made react on a multifunctional catalyst, and a two-step synthesis, where the dehydrogenation step of ethanol to acetaldehyde was separated from the condensation and dehydration ones. The two processes are known as the Lebedev (one-step) and the Ostromislensky (two-step) reactions, taking their name after their first inventors [68].

Details on the kind of technology used at an industrial level can be found in the patent literature for the two-step approach, which was the one adopted in U.S.A and it was operated by the Carbide and Carbon Chemicals Corporation [69]. A simplified flow sheet of the chemical plant is reported in Figure 11. Ethanol is first dehydrogenated to acetaldehyde in a reactor of the shell-and-tube type (R1 in Figure 11); the catalyst used in the this step contained copper and the reaction was conducted at 280°C with 10% water vapor in the inlet feed. In the second reactor (R2) the ethanol was made react with acetaldehyde in a molar ratio of about 3 to 1 and operating between 300-350°C. The catalyst used in this second step was composed by Ta_2O_5 on doped silica gel, even if other kind of silica-doped catalysts could have been applied [70], [71].

Unconverted ethanol and reaction products such as hydrogen and acetaldehyde were sent to a preliminary separation zone (Separation zone 1) along with some products (acetaldehyde, butadiene, diethyl ether, ethanol, mono-olefins, hydrogen and saturated hydrocarbon gases) coming from the second reactor (R2). In the Separation zone 1, a series of scrubbing towers were used to separate pure hydrogen from all the other molecules. In the same zone of the chemical plant a stream of light gases was vented ("gases" in Figure 11) and it was composed of a mixture of ethylene, propylene, saturated hydrocarbons, carbon dioxide and carbon monoxide; no butadiene should be present in this stream, since it was most likely all absorbed in the first scrubber and sent to separation zone 2. The outlet-stream from R2 was sent to the separation zone 2 together with the butadiene-rich flow derived from the first scrubbing tower of the zone 1. The separation zone 2 was composed of a distillation column and a scrubbing tower, both necessary to obtain a pure stream of butadiene. The bottom fractions from both rectification columns, containing water, acetaldehyde, diethyl ether, ethanol and by-products, were collected and mixed with the bottoms fractions coming from zone 1. The inlet feed of separation zone 3 was thus composed of a mixture containing approximately 15% acetaldehyde, 5% diethyl ether, 40% ethanol, 35% water and 5% by-products. Distillation columns in zone 3 had to separate both water and by-products from acetaldehyde and ethanol, which were recycled to both R1 and R2. The by-products withdrawn from zone 3 were composed of acetaldehyde, diethyl ether, ethyl acetate, butyraldehyde, methyl ethyl ketone and other minor impurities. It is important to note that both out-streams leaving zone 3 were not pure streams of ethanol and acetaldehyde respectively: the acetaldehyde-rich stream was actually composed of 75% acetaldehyde,

20% diethylether and 5% by-products, whereas the ethanol-rich stream was a mixture of 85% ethanol, 10% water and 5% by-products.

During the same decade Carbide and Carbon Chemicals Corporation submitted other patents discussing alternative plant configurations with the aim of improving the overall process economy [69], [72]; hence, compared to the reaction scheme just discussed, some differences might have been used in the actual industrial plant. Nonetheless, these alternative configurations are only minor variations concerning the separation zones and the technology used for products recovery, which, in the end, do not alter significantly the general plant configuration as reported in Figure 11.

The Lebedev (one-step) process was used mainly in Russia were it was first developed. However, the details on the chemical plant configuration used are much more difficult to find. Even if the general approach should be similar to the American technology, the lower butadiene purity known to be obtained with the one-step approach, suggests a more complex separation procedure so as to finally gain the high-purity butadiene required for an efficient polymerization of the olefin.

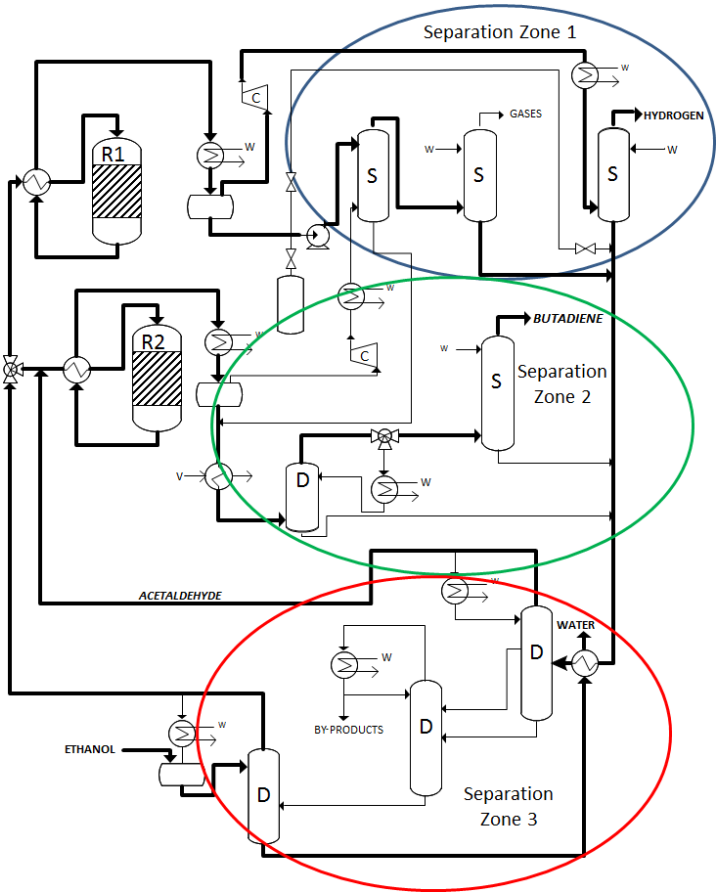

Figure 11. Scheme of the Two steps production of butadiene

Catalysts

Nowadays, the optimal catalyst composition for the Lebedev reaction is still subject of debate, whether talking about the one- or the two-step approach. In the last years, an increasing number of papers and reviews have been published on this topic, especially as regards the Lebedev approach, due to the less-demanding economic and engineering requirements theoretically needed by a one-pot synthesis. A comprehensive review was published in 2014 by Sels and co-workers [73]. According to these authors, the catalysts for the Lebedev one-step process can be divided into three main families: (i) doped alumina catalysts, (ii) magnesia–silica catalysts and (iii) other catalysts. Some of the most interesting results obtained for catalysts belonging to each category are reported in Figure 12 and the associated Table 3 (adapted from [67]). From there it is possible to see that most of them are in the 20 to 40% yield range and only few of them overcome the 60% including the ones reported by Ohnishi et. Al, whose values however, were taken during the first 10 minutes of reaction and thus are not representative of the steady state of the reaction.

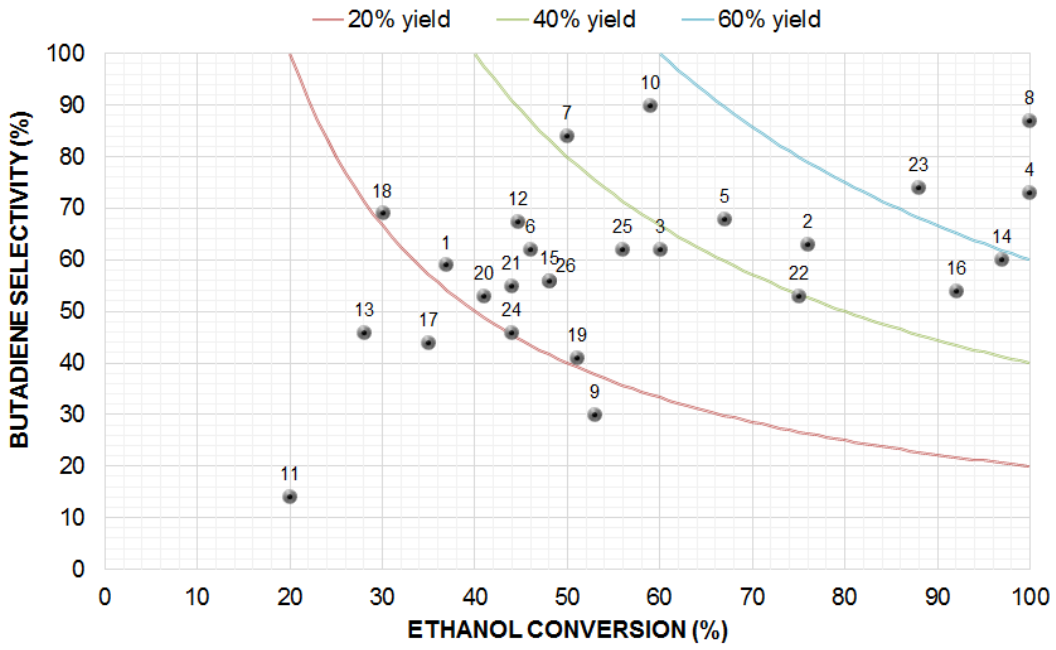

Figure 12.Butadiene selectivity vs. ethanol conversion for representative catalysts.

Table 3. Active systems in the transformation of Ethanol to 1,3-Butadiene

Number	*Catalyst*	*T [°C]*	*Ethanol conv. [%]*	*1,3-BDE Select. [%]*	*1,3-BDE Yield [%]*	*Reference (year)*
1	Mg/Si (2/3) wet kneading with acetic acid	380	36,9	59,0	21,8	[74] (1947)
2	2%Cr_2O_3–76%MgO–11%SiO_2–11% kaolin	435	76,0	63,0	47,9	[75] (1954)
3	2%Cr_2O_3–79%MgO–19%SiO_2	400	60,0	62,0	37,2	[76] (1960)
4	Al/Zn 6/4 (fluidized bed)	425	100,0	73,0	73,0	[77] (1963)
5	ZnO-MgO-SiO_2-kaolin	410	67,0	68,0	45,6	[78] (1966)
6	$Mg(OH)_2$ + colloidal SiO_2	380	46,0	62,0	28,5	[79] (1972)
7	Mg/Si wet kneading 1/1	350	50,0	84,0	42,0	[80] (1985)
8	Mg/Si wet kneading 1/1 + 0,1% Na	350	100,0	87,0	87,0	[80] (1985)
9	MgO/SiO_2 (0,83:1)	350	53,0	30,0	15,9	[81] (1988)
10	10%NiO–28%MgO–62%SiO2	280	59,0	90,0	53,1	[82] (1996)
11	(Ca/P = 1,62) hydroxyapatite	350	20,0	14,0	2,8	[83] (2008)
12	Cu(1%)Zr(1%)Zn(1%)/SiO_2	375	44,6	67,4	30,1	[84] (2011)
13	Mg/Si 2/1 Mechanical mixing (with $Mg(OH)_2$)	350	28,0	46,0	12,9	[85] (2012)
14	Mg/Si 2/1 wet kneading + Cu 5%	350	97,0	60,0	58,2	[85] (2012)
15	Mg/Si 2/1 wet kneading + Cu 5%	350	46,6	56,0	26,1	[85] (2012)
16	4%Ag-55%MgO-41%SiO_2	400	92,0	54,0	49,7	[85] (2012)
17	Mg/Si 3/1	325	35,0	44,0	15,4	[86] (2014)
18	Mg/Si 95/5 + Zr 1,5% + Zn 0,5%	325	30,0	69,0	20,7	[86] (2014)
19	Mg/Si 1/1 + Zr 1,5% + Zn 0,5%	325	51,0	41,0	20,9	[86] (2014)

Number	*Catalyst*	*T [°C]*	*Ethanol conv. [%]*	*1,3-BDE Select. [%]*	*1,3-BDE Yield [%]*	*Reference (year)*
20	Al and Zn nitrate impr. in γ-Al_2O_3	400	41,0	53,0	21,7	[87] (2014)
21	Al and Zn nitrate impr. in γ-Al_2O_3 + H_2O_2 in the feed	395	44,0	55,0	24,2	[87] (2014)
22	CuO/SiO_2–MgO	425	75,0	53,0	39,8	[88] (2014)
23	$Ag/ZrO_2/SiO_2$	314	88,0	74,0	65,1	[89] (2014)
24	1.0Ag/MgO-SiO_2	400	44,0	46,0	20,2	[90] (2015)
25	4 %ZnO/MgO–SiO_2(1:1)	375	56,0	62,0	34,7	[91] (2015)
26	Ag/ZrBEA	327	48,0	56,0	26,9	[92] (2015)

In the case of the Ostromislensky or two-step approach, the main difference with the Lebedev one is obviously the separation of the rate-determining dehydrogenation step (i.e. ethanol dehydrogenation into acetaldehyde) to a dedicated unit. Apart from this, the remaining catalysts' features for both approaches remain the same. Acetaldehyde can be produced from ethanol with or without oxygen in the feed [68], leading to water or hydrogen as a co-product, respectively. Some of the most efficient catalysts are summarized in Table 4.

Table 4. Catalysts for the conversion of ethanol into acetaldehyde.

Catalyst	*T [°C]*	*EtOH conv. [%]*	*C_2H_4O Sel. [%]*	*Ref.*
0.2%Au-0.2%Cu/SiO_2	250	100	100	[93]
5% WO_3 – 95% V_2O_5	280	48	98	[94]
5.75 wt%Cu supported on rice husk ash [a]	275	80	100	[95]
Au(4.9)/SBA-15 and Au(5.8)/SBA-16 [a]	350	95	90-100	[96]

[a] without oxygen in the feed

Mechanism of reaction

Another important aspect in the debate of the conversion of ethanol into butadiene is undoubtedly the reaction mechanism. Until now, several routes have been proposed; some of them are illustrated in Figure 13. [73]

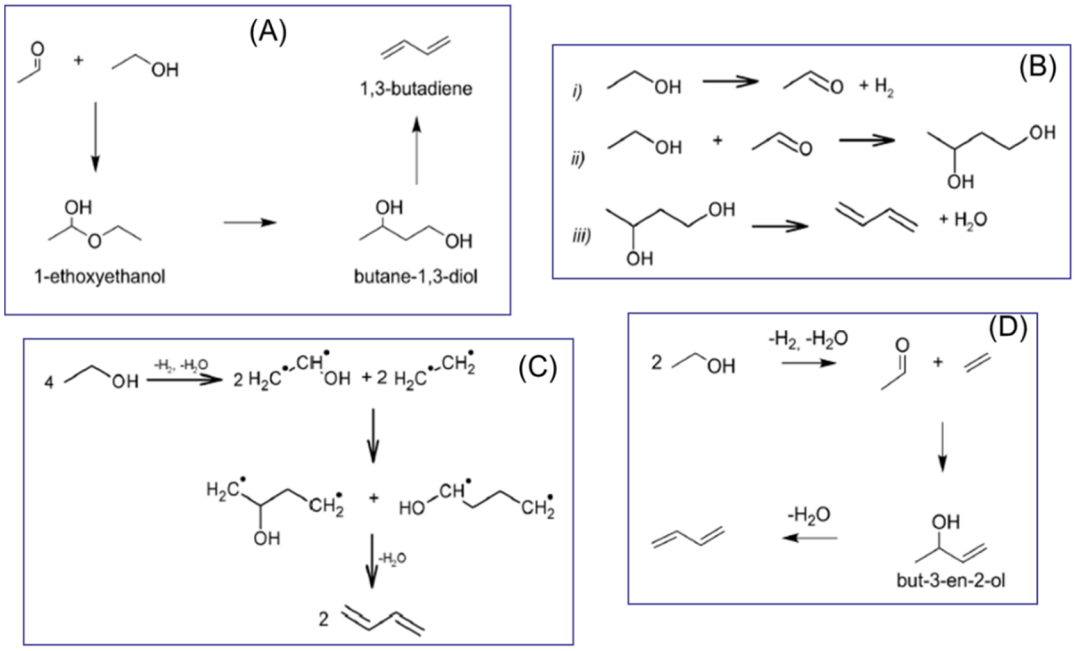

Figure 13. Alternative mechanisms proposed for butadiene production from ethanol

The first mechanism (A in Figure 13) was proposed by Ostromislensky for the two-step process, but it was said to apply as well for the one step approach [97]. The formation of the hemiacetal and its rearrangement were considered unlikely later on but the formation of 1,3-Butanediol was supported later by Balandin who proposed the mechanism shown in Figure 13 B [98]. On the other hand, the radicalic mechanism was the one originally proposed by Lebedev where the species (*CH_2CH_2* and *CH_2CHOH*) after a complex sequence of reactions would yield butadiene and other by-products. Lebedev also tested the addition of up to 20% ethylene to the feed, without observing any increase in the yield of butadiene [99]. He explained this behaviour by assuming that ethylene could only take part in the reaction when it was in a so-called activated form (i.e., just formed from ethanol and, therefore, still in its radical form). The proposal by Lebedev involving radical species is now considered unlikely and can probably be discarded. The mechanism in Figure 13D was proposed by Gruver et al. based on their studies with aluminated sepiolite catalysts [100]. They confirmed the importance of acetaldehyde as a precursor for butadiene formation, but they also proposed that ethylene was involved as

an intermediate (since both butadiene and ethylene selectivity increased as the total conversion increased). This mechanism that resembles a Prins-like reaction is considered now unlikely due to the need of protonation of ethylene that would create a very unstable primary carbocation.

Nonetheless, the most generally accepted mechanism for the production of butadiene from ethanol is the one depicted in Figure 14. In this mechanism, the key-step is believed to be the aldol condensation of acetaldehyde. Remarkably, this is also supposed to be the key-step for the synthesis of 1-butanol from ethanol, i.e. the gas-phase Guerbet synthesis. Nonetheless, since the beginning, the aldol route has often been criticized [69].

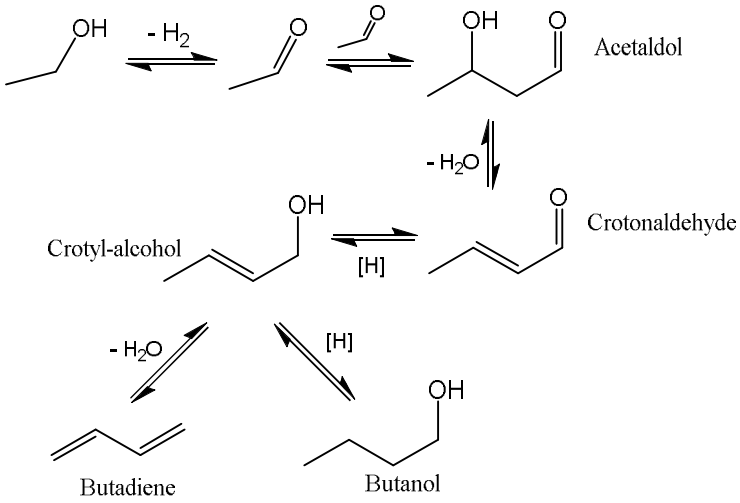

Figure 14.Generally accepted mechanism for Guerbet and Lebedev reaction

First of all, the aldol condensation is thermodynamically unfavored and also the intermediate acetaldol has never been detected among reaction products (however this could be due to its fast conversion, thus being a non-sufficient detail to exclude this route). Moreover, already in the 1949, the engineers working for the Carbide and Carbon Chemicals Corporation claimed that if the acetaldol was fed on the industrial catalyst to make butadiene, it was reversed to acetaldehyde and not dehydrated to crotonaldehyde, thus making clear that the acetaldol cannot be the key intermediate for the production of butadiene from ethanol [101]. More recently, Meunier and co-workers [2] also ruled-out the acetaldehyde self-aldolization as a main reaction pathway for the gas-phase transformation of ethanol into 1-butanol over hydroxyapatite, i.e. the best catalysts so far reported in literature for this reaction. In conclusion, there is a need to clarify this subject in order to make a real advance towards the commercial implementation of this kind of process.

2 METHODOLOGY

2.1 Reagents

The following table indicates the reagents used for the synthesis of the materials.

Table 5. Reagents used in the synthesis

Compound	*Formula*	*Purity*	*CAS*	*Brand*
Magnesium nitrate	$Mg(NO_3)_2 \cdot 6H_2O$	99%	13446-18-9	Sigma-Aldrich
Tetraethyl-orthosilicate (TEOS)	$SiC_8H_{20}O_4$	98%	78-10-4	Sigma-Aldrich
Nitric acid	HNO_3	68%	7697-37-2	VWR chemicals
Ammonium hydroxide solution	$NH_4(OH)$	28-30% NH_3 basis	1336-21-6	Sigma-Aldrich
Gallium nitrate	$Ga(NO_3)_3 \cdot XH_2O$	99.9%	69365-72-6	Alfa Aesar
Aluminium nitrate	$Al(NO_3)_3 \cdot 9H_2O$	98%	7784-27-2	Vetec (Sigma-Aldrich Brazil)
Zinc nitrate	$Zn(NO_3)_2 \cdot 6H_2O$	98%	10196-18-6	Vetec (Sigma-Aldrich Brazil)
Sodium carbonate	Na_2CO_3	≥99.5%	497-19-8	Sigma-Aldrich
Sodium hydroxide	NaOH	>98%	1310-73-2	Sigma-Aldrich

2.2 Synthesis

2.2.1 MgO

Several catalysts were prepared in the different stages of the research project. The first material studied was the MgO as a purely basic model material. The synthesis of this sample was made by precipitation from an aqueous solution containing $Mg(NO_3)_2 \cdot 6H_2O$. This solution was added dropwise to another one containing Na_2CO_3 dissolved in distilled water; the pH was continuously adjusted in order to keep it close to 10. The obtained slurry was left under stirring for 40 min; then the precipitate was filtered and washed with distilled water at 40°C. Finally, it was dried at 110°C overnight and calcined at 450°C for 8 h in air.

2.2.2 MgO-SiO_2 oxides

-*Varying the Mg to Si ratio:* A series of materials having Mg to Si ratio from 1 to 30 were prepared by the sol-gel method dissolving appropriate amounts of $Mg(NO_3)_2 \cdot 6H_2O$ and Tetraethyl orthosilicate (TEOS) in a solution of ethanol + distilled water maintained at 50°C using a water bath. The pH was hold below 2 by adding HNO_3. When the gel started to form, the stirring was stopped and the remaining liquid was left to evaporate in the oven at 65°C. The gel obtained was dried at 120°C overnight and calcined at 600°C for 5h in static air.

- *Varying the Preparation Method: The methods compared include, i) Sol-gel (as in the Mg/Si variation section). ii) The "Ohnishi-like" method:* In this case the Mg source was $Mg(OH)_2$ prepared by precipitation of $Mg(NO_3)_2 \cdot 6H_2O$ with NH_3. The Si source was obtained by precipitation of TEOS with NH_3. Afterwards, the Mg and Si sources were mixed with water for 4h and then dried at 120°C during the night to be finally calcined at 500°C for 3h in static air. iii) The *Lewandowsky-like* method: The Mg source was MgO prepared by precipitation of $Mg(NO_3)_2 \cdot 6H_2O$ with $Na_2CO_3 * 10H_2O$ at pH 10. The SiO_2 "Grace" of $320 m^2.g^{-1}$ was used in this case.

-*Modified Mg-Si oxides:* Some of the previous catalysts were modified by adding Gallium, the adding of the Ga was made in three forms. i) Simple impregnation: Dissolution of the dried $Ga(NO_3)_3$ in water and addition of the catalyst powder. ii) Incipient wetness impregnation: Dissolving the Ga source in the minimum amount of water needed to wet the catalyst, then drop this solution to the catalyst with a Pasteur pipette and mixing afterwards with a spatula. iii) In situ: the Ga source was added directly during the synthesis of the Mg-Si catalyst.

2.2.3 Alternative systems

The materials synthesized for chapter 3.5 (hydrotalcites) were prepared as follows: For the ZnMgAl-CO_3, a solution of NaOH 3.6M and Na_2CO_3 1.3M was added dropwise to another solution, previously heated to 60°C in an oil bath, containing the metallic salts (Aluminium, Magnesium and Zinc nitrates) in a proportion of Zn+Mg/Al = 3. The addition time was ca 1h and the final pH reached was 10. Then, the slurry obtained was left under stirring for 14h and later on it was filtered, washed with 2L of hot destilled/deionized water and dried at 110°C for 5h. In the case of the Si- containing samples the procedure is similar but it is made without carbonate in the first solution and the whole synthesis is done under N_2 atmosphere in order to avoid the uptake of CO_2

from the atmosphere. The Si source was added either as an excess of TEOS dissolved with the nitrates, ZnMgAl-SiO_4-TEOS, or adding SiO_2 to the sodium hydroxide solution, ZnMgAl-SiO_4-Silica.

2.3 Lab-scale catalytic tests

Reactivity experiments were carried out using a continuous flow reactor, operating under atmospheric pressure. For most of the experiments the Ethanol percent was fixed to a 2% in N_2. The catalyst amount and flux of the carrier were varied in order to achieve the desired residence time. Downstream products were continuously monitored by online gas chromatography (GC) using an Agilent-6890 instrument equipped with two columns (HP-5 50 m, 0.20 mm and HP-plot Al_2O_3-KCl 30 m, 0.50 mm) and two detectors (FID and TCD). Compounds were identified by means of GC-MS and then quantified by external standard calibration curve

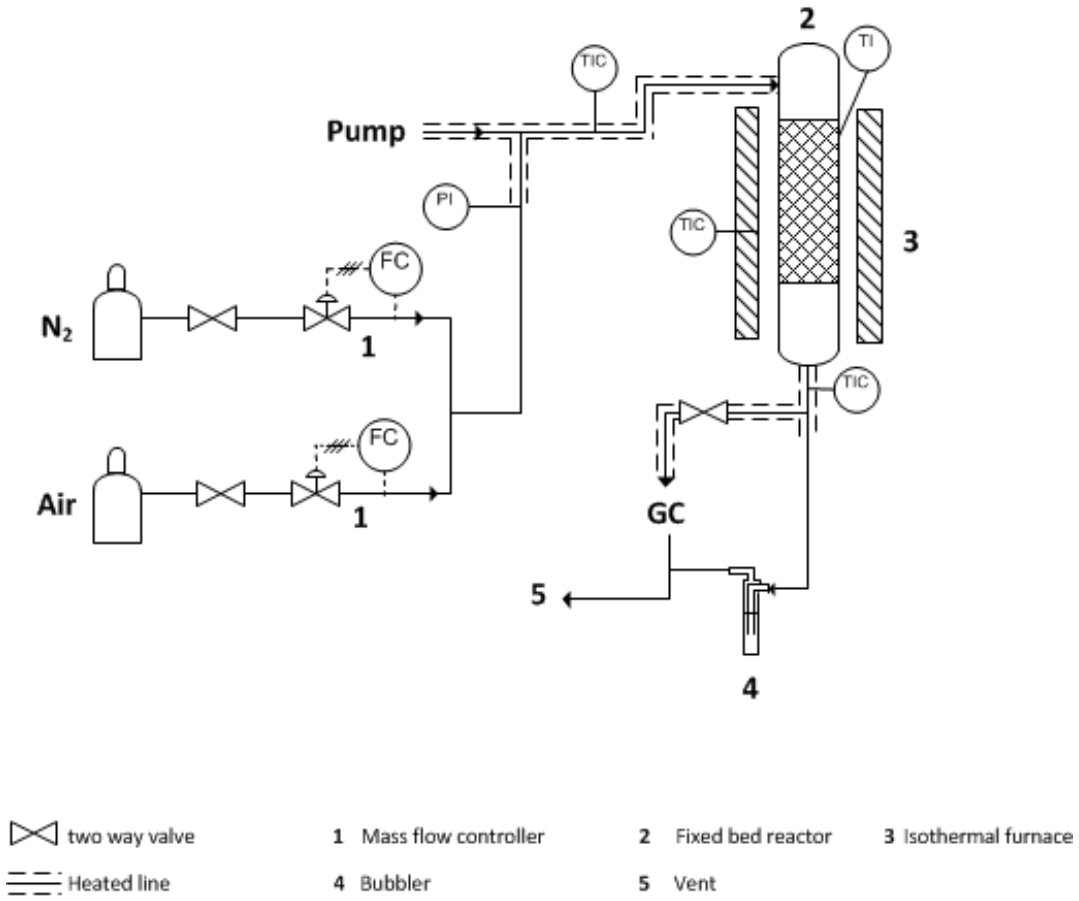

Figure 15. Lab-scale reactor scheme

2.4 Data elaboration: conversion, yield and selectivity

By means of gas chromatograph analyses the percentage values of conversion, yield and selectivity were determined, using the following equations:

$$Conversion = \frac{n° \, mols \, of \, converted \, reactant}{n° mols \, of \, fed \, reactant} \times 100$$

$$Yield = \frac{n° \, mols \, of \, product/stoichiometric \, coeff.}{n° \, mols \, of \, fed \, reactant/stoichiometric \, coeff.} \times 100$$

$$Selectivity = \frac{Yield}{Conversion} \times 100$$

2.5 Characterization techniques

X-ray diffraction (XRD)

The XRD measurements were carried out using a Philips PW 1710 apparatus, with Cu Kα (λ = 1.5406 Å) as radiation source in the range of 5°<2θ<80°, with steps of 0.1 grade and acquiring the signal for 2 seconds for each step. Reflects attribution is done by the Bragg law, using the d value: 2d senθ = nλ.

Nitrogen physysorption (BET)

The specific surface area was measured applying the single point BET method. The instrument used for this analysis was a Carlo Erba Sorpty 1700. The BET method (Brunauer Emmet Teller) calculates the surface area of the sample from the volume of the gas corresponding to the monolayer adsorption. The single-point approximation consists in the measurement of the pressure of adsorption and the corresponding gas volume adsorbed. The equation correlating this with the monolayer gas volume is:

$$\frac{P}{V(P_s - P)} = \frac{1}{V_m} \cdot \frac{P}{P_s}$$

Where P is the pressure, P_s is the surface tension of the adsorbed gas (nitrogen in this case), V is the adsorbed gas volume and Vm is the monolayer gas volume. The percent error that derives from these approximations is about 5% on values over 3 m^2; below this limit, the surface area calculated cannot be considered reliable.

In the analysis around 0.5g of the sample was placed inside the sample holder and then heated at 150°C under vacuum (4 Pa) in order for it release the water, air or other molecules adsorbed. Afterwards the sample was put in liquid nitrogen and the adsorption of the gaseous N_2 was carried out.

Attenuated total reflection (ATR)

Attenuated total reflectance spectra of the materials were recorded at room temperature with an ALPHA-FTIR instrument at a resolution of 2 cm^{-1}. First a background was taken to eliminate the contribution of atmospheric water and carbon dioxide. Later on, the powder was put in intimate contact with the crystal to perform the measurement. Figure 16 illustrates the principle of this technique also known as Multiple Internal Reflection Spectroscopy (MIR). Here the IR beam is passed through a thin, IR transmitting crystal in a manner such that it alternately undergoes total internal reflection from the interface with the sample. At each reflection, some of the IR radiation may be absorbed by species adsorbed on the solid surface. After one or several internal reflections, the IR beam exits the ATR crystal and is directed to the IR-detector.

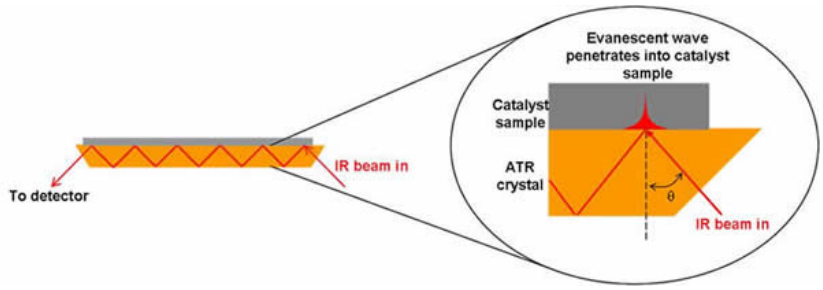

Figure 16. ATR principle.[5]

[5] http://www.qub.ac.uk/centacat/castech/httpwww.qub.ac.ukcentacatcastechsubtopic_1.3.htm

Scanning Electron Microscopy (SEM)

This technique allows the observation of high resolution images of the surface topography, with excellent depth of field. The images are produced using a highly-focused, scanning (primary) electron beam. The primary electrons enter a surface with an energy of 0.5 – 30 kV and generate many low energy secondary electrons. The intensity of these secondary electrons is largely governed by the surface topography of the sample. An image of the sample surface can thus be constructed by measuring secondary electron intensity as a function of the position of the scanning primary electron beam. High spatial resolution is possible because the primary electron beam can be focused to a very small spot (<10 nm). High sensitivity to topographic features on the outermost surface (< 5 nm) is achieved when using a primary electron beam with an energy of < 1 kV. In addition to low energy secondary electrons, backscattered electrons and X-rays are generated by primary electron bombardment. The intensity of backscattered electrons can be correlated to the atomic number of the element within the sampling volume. Hence, some qualitative elemental information can be obtained. The analysis of characteristic X-rays (EDX or EDS analysis) emitted from the sample gives more quantitative elemental information. Such X-ray analysis can be confined to analytical volumes as small as 1 cubic micron. SEM, accompanied by X-ray analysis, is considered a relatively rapid, inexpensive, and basically non-destructive approach to surface analysis. It is often used to survey surface analytical problems before proceeding to techniques that are more surface-sensitive and specialized.

The apparatus used in this research is a Zeiss EP EVO 50 operated at 20KeV, 10^{-6} Pa and variable pressure (90 or 100 Pa). The EDS attachment is an Oxford Instruments INCA ENERGY 350 [z>4 (Be), resolution 133eV (MnKa @ 2500cps)] with an automatic software for peaks recognition with respect to an internal standard.

Temperature programmed desorption (TPD)

NH_3-temperature-programmed desorption (TPD) measurements were obtained with a TPD/TPR/TPO Micromeritics instrument. 50–100 mg of catalysts were pre-treated at the calcination temperature for 1 h under a He flow. After cooling down to 80 °C, NH_3 was adsorbed by flowing of a 10% NH_3 in He gas mixture for 30 min (30 mL min^{-1}, NTP),

with subsequent He treatment at 80 °C for 15 min to remove physisorbed molecules. Catalysts were then heated under He flow (50 mL min^{-1}, NTP) at a heating rate of 10 °C min^{-1} up to the calcination temperature.

In-situ Diffuse Reflection Infrared Spectroscopy - Mass Spectrometry (DRIFT-MS)

DRIFTS is an important spectroscopic technique for investigating species adsorbed on a catalyst surface under dynamic reaction conditions. In this technique, the diffusely scattered IR radiation from a sample is collected, refocused and analyzed. This modification of the IR traditional set-up can be employed with samples that are not sufficiently transparent to be studied in transmission.[102] This session is dedicated to this particular experimental setup since it was one of the main techniques employed during the present work.

When an infrared beam reaches a sample, the incoming light can be reflected, scattered or transmitted. Only the part of the beam that is scattered within a sample and returned to the surface is considered to be diffuse reflection. As the light that leaves the surface has passed through a thin layer of the material, the intensity of the incident wavelength will be modified and this will give the structural information about the substrate. The principle of this technique is illustrated in Figure 17.

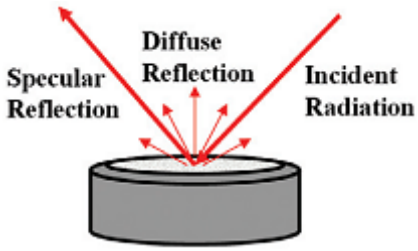

Figure 17. Infrared diffuse reflectance optical path.[6]

In DRIFTS the light intensity scattered at a given wavelength from an “infinitely thick” closely packed catalyst layer is compared with that scattered of a non-absorbing (white) reference. The light scattered is then collected in an integration sphere and detected.

[6] http://www.piketech.com/files/pdfs/DiffuseAN611.pdf

Regarding the intensity of the scattered light collected, generally the Kubelka-Munk theory is accepted. It provides a correlation between reflectance and concentration expressed with the Kubelka-Munk formula:

$$F(R) = (1-R)^2/2R = k/s = Ac/s$$

Where,

R = reflectance
k = absorption coefficient
s = scattering coefficient
c = concentration of the absorbing species
A = absorbance

The original theory has some limitations since it assumes infinite sample dilution in a non-absorbing matrix, a constant scattering coefficient and an "infinitely thick" sample layer.[102] However, with proper sample preparation diffuse reflectance spectroscopy can provide ppm sensitivity and high quality results. It is also stated by G. Busca in his review about infrared of organic molecules adsorbed on metal oxides [103] that the performances obtained using the transmission/absorption technique and those with the diffuse reflectance technique are today quite comparable.

Among the different experimental setups for infrared spectroscopy, diffuse reflectance is maybe the one giving the easiest access to the study of the surface of materials. One of the great advantages of this technique is that it does not require a complicated sample preparation, the catalyst powder is directly put in the sample holder and diluted with KBr if needed, and this avoids the mass transport limitations that are usually a drawback when using pressed discs (as in transmission) for kinetic studies for example.

Another characteristic that makes this technique attractive is the possibility to perform *in-situ* and even *operando* studies of reactions. The former term refers to the study of the catalyst under controlled atmosphere including the actual reaction mixture. Operando definition requires the simultaneous measure of the conversion or a reaction rate alongside the spectroscopic data on the same cell and catalyst bed [104]. However, this last aspect is still under development since the determination of an intrinsic reaction rate would require the careful consideration of the chemical engineering aspects of the reactors when designing the spectroscopic cells since normally they are not ideal reactors.

In a typical experiment, the samples were pre-treated at 450°C in a He flow (10 mL min^{-1}) for 45 min, in order to remove any molecules adsorbed on the material. Then the sample was cooled down to room temperature and ethanol was fed at 0.6 mL min^{-1} and vaporized. Subsequently, He was left to flow until weakly adsorbed ethanol was evacuated. The temperature was raised to 400°C at 10°C min^{-1} while registering the spectra (DRIFT an on-line MS). The following selected mass spectroscopy signals (m/z) were monitored continuously with time (and temperature): 2, 16, 25, 28, 29, 30, 31, 40, 41, 43, 44, 45, 56, 58, 59, 60, and 61. By combining the information obtained from several different m/z signals, it was possible to obtain unambiguous information on the various products formed. The IR apparatus used was a Bruker Vertex 70 with a Pike DiffusIR cell attachment. Spectra were recorded using a MCT detector after 128 scans and 2 cm^{-1} resolution. The mass spectrometer was an EcoSys-P from European Spectrometry Systems.

2.6 Theoretical modelling

The modelling of the processes involved in the reactivity of ethanol on MgO was carried out employing gas phase electronic structure calculations by means of the Gaussian09, [105] suites of codes at the Density Functional Theory (DFT) level. Specifically, we used the B3LYP DFT functional [106] together with the 6-31++G(d,p) basis set, a level of theory commonly employed for similar tasks [107], [108].

As previously done,[109] MgO nano-crystals were modelled using a cluster approach mainly with $Mg_{10}O_{10}$ as the model of the crystal corners (Mg3C and O3C sites, e.g. see Fig. 9). Whenever edge-proximity effects may have introduced a bias in the energetic profile being studied, the largest $Mg_{16}O_{16}$ cluster (e.g. see Fig. 11) was used to limit polarization-induced artefacts. The geometrical parameters of the clusters (right angles and d_{MgO}= 2.1084 Å) were kept frozen [107] while the degrees of freedom of the adsorbed species were optimized. In many cases, putative TS structures were generated by means of relaxed scans along chosen reaction coordinates (e.g. atom-atom distances), and subsequently fully optimized by using analytical second derivatives of the energy surface. All stationary points were characterized using frequency calculations. As these interesting processes involve heavy atoms or groups, no correction for zero point effects was introduced.

3 RESULTS AND DISCUSSION

3.1 MgO

Part of this chapter was included in the publication "On the Chemistry of Ethanol on Basic Oxides: Revising Mechanisms and Intermediates in the Lebedev and Guerbet reactions" A. Chieregato, J. Velasquez Ochoa, C. Bandinelli, G. Fornasari, F. Cavani, and M. Mella, *ChemSusChem*, vol. 8, pp. 377–388, 2015.[1]

3.1.1 Synthesis

The MgO catalysts used in this study was prepared by precipitation from an aqueous solution containing $Mg(NO_3)_2 \cdot 6H_2O$. This solution was added dropwise to another one containing Na_2CO_3 dissolved in distilled water; the pH was continuously adjusted in order to keep it close to 10.0. The obtained slurry was left under stirring for 40 min; then the precipitate was filtered and washed with distilled water at 40°C. Finally, it was dried at 110°C overnight and calcined at 450°C for 8 h in air. MgO was used as a model catalyst with pure basic features to explore ethanol conversion from its very early stages. In this point the idea was to understand the role played by the basic properties of the material and to see if there was an interconnection between the Lebedev and Guerbet reactions.

3.1.2 Catalytic tests

Ethanol reactivity

MgO performance on ethanol transformation was tested at 250°C and 400°C which were found to be the most representative temperatures (T) to evaluate the reaction pathways. In fact, 250°C was the minimum temperature to obtain detectable conversion of ethanol in the reaction conditions used, whereas 400°C was the temperature at which MgO showed

a good activity and a relatively limited yield to heavy products. Very low contact times were used in these tests compared to those normally applied to maximize the yield of C_4 compounds because in this stage the idea was to investigate the very early stages of the reaction. In this situation, however, poor carbon balance may be registered during the initial period of reactivity because of severe heavy compound deposition on the catalyst surface [70], [110].

Results for ethanol reaction over MgO at 250°C and different contact times are presented in Figure 18. It is observed that at low contact (< 0.4 s) the main product obtained is acetaldehyde, with traces of 1-butanol. At higher contact time, 1-butanol, 2-buten-1-ol (crotyl alcohol) and 3-buten-1-ol are detected as well; together with some trace compounds. In this experiment, neither C_4 aldehydes (3-hydroxybutanal, crotonaldehyde and butyraldehyde) nor C_4 olefins (butenes and butadiene) were detected.

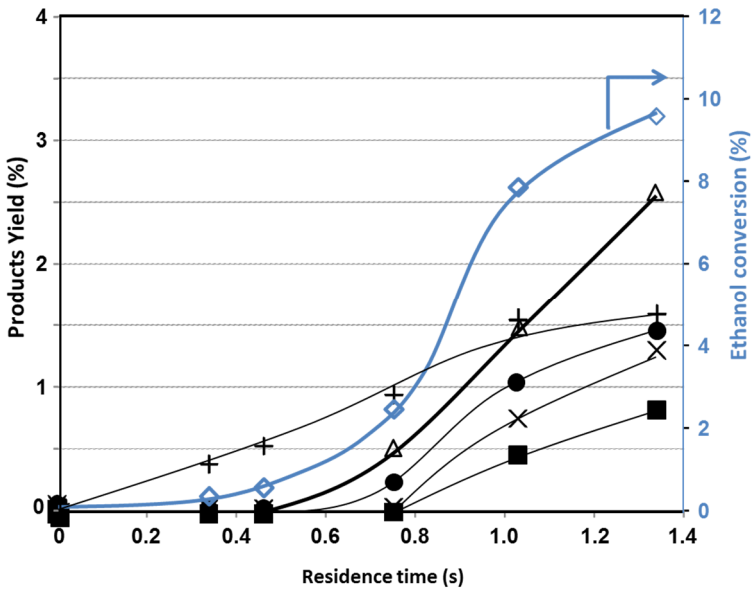

Figure 18. Ethanol conversion at 250°C on MgO. Symbols: ethanol conversion (◊); yields: acetaldehyde (+), 1-butanol (Δ), crotyl alcohol (●), 3-buten-1-ol (x), others (■). Others: 2-pentanol, 2-butanol and 3-buten-2-ol.

Additionally, reactivity experiments were carried out at 250°C and 0.6 s residence time for 24 hours in order to confirm the absence of C_4-aldehydes; the products collected during this run were analyzed by GC-MS and ESI-MS and revealed no trace of these compounds. The fact that neither 3-hydroxybutanal nor crotonaldehyde were detected opens important questions on the reaction mechanism, since these are the generally accepted intermediates for C_4-compound formation from ethanol. However, these tests are not conclusive because the lack of C_4 aldehydes might be also attributed to a fast

conversion to crotyl alcohol (via MPV reduction) and then 1-butanol. Nevertheless, it is important to highlight the direct formation of 1-butanol as a kinetically primary product, which clearly goes against the widely accepted mechanism postulating the formation of butanol after the in-situ reduction of crotonaldehyde. This unexpected feature was recently pointed out as well by other authors [2], [68].

The results for ethanol transformation over MgO at 400°C are presented in Figure 19. In this case ethylene was detected in large amounts, followed by acetaldehyde and 1-butanol, and finally butadiene was also detected as a consecutive product. Ethylene formation was not expected to be important on a pure basic oxide and its presence was discarded to be due to gas phase homogeneous reaction. In this case as well, acetaldehyde and 1-butanol appear to be kinetically primary products, even though selectivity extrapolation towards zero contact time may be non-unambiguous at such a high temperature.

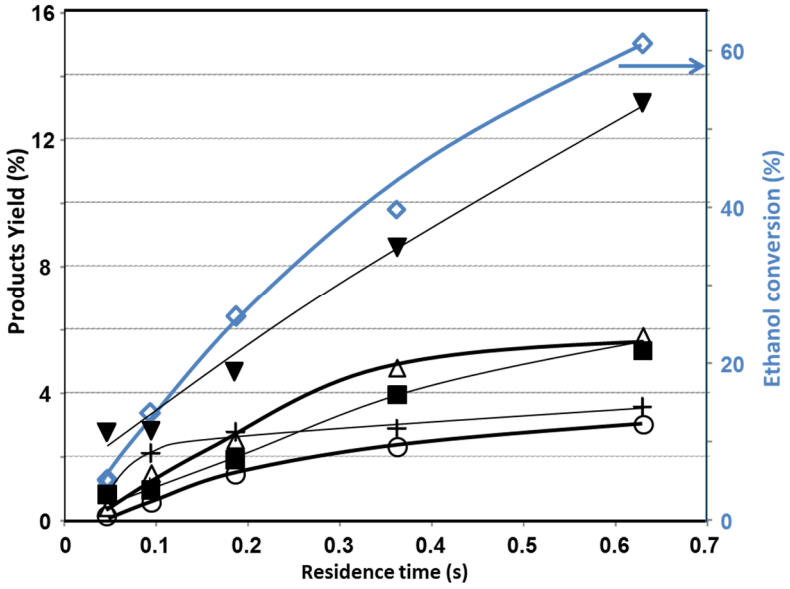

Figure 19. Ethanol conversion at 400°C on MgO. Symbols: ethanol conversion (◊); yields: ethylene (▼), acetaldehyde (+), 1-butanol (Δ), 1,3-butadiene (○), others (■).

Reactivity of proposed intermediates

Aiming a better understanding of the reaction, several tests were performed by feeding some of the molecules proposed in the literature as possible intermediates during the formation of C_4-compounds from ethanol.

One of the compounds fed was 1,3-Butanediol (1,3-BDO). This molecule has been suggested to form from either acetaldol MPV reduction or the reaction of ethanol with acetaldehyde.[111] The reaction products obtained at 400°C by feeding 1,3-BDO are shown in Figure 20.

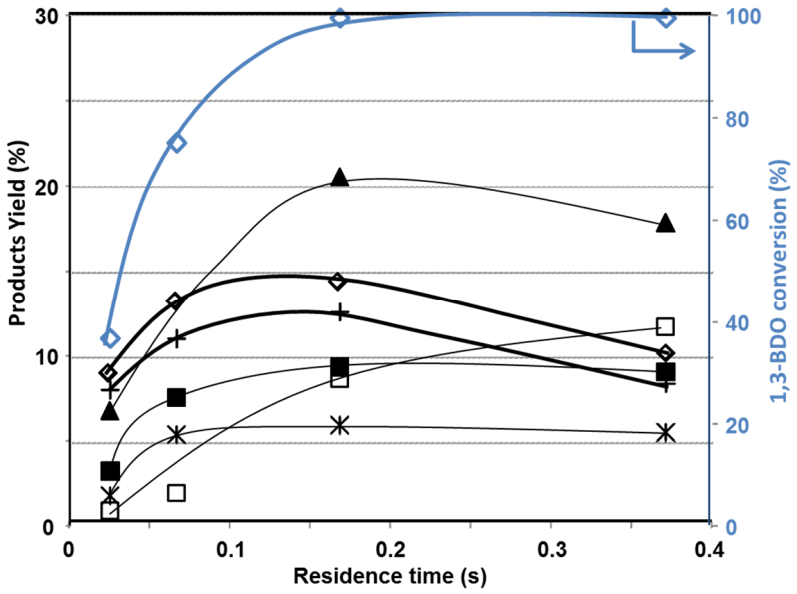

Figure 20. 1,3-Butanediol conversion at 400°C over MgO. Symbols: 1,3-butanediol conversion (◊); yields: methylvinylketone (▲), ethanol (◊), acetaldehyde (+), aromatic compounds (□), methylethylketone (x), others (■).

Because of the higher reactivity of the 1,3-BDO with respect to ethanol, the residence time for this experiment was kept lower. The two main products were ethanol and acetaldehyde; other products form were methylvinylketone (MVK) and methylethylketone (MEK), as well as minor amounts of other compounds, including aromatics. This results indicate that 1,3-BDO undergoes a reverse addition. Moreover, the catalytic behaviour was also studied at 250°C for this compound (Figure 21) and similar results were obtained.

Only minor changes were observed in the product distribution even when co-feeding ethanol and 1,3-BDO in an equimolar amount; specifically, a slight increase in MVK, 2-butanone, and aromatic compounds yield was noticed. These evidences and the fact that formation of 1,3-BDO was never detected during ethanol transformation, suggest that this compound does not form under our reaction conditions. In fact, any adsorbed intermediate compound desorbing into the gas-phase as 1,3-BDO would mainly decompose into ethanol and acetaldehyde.

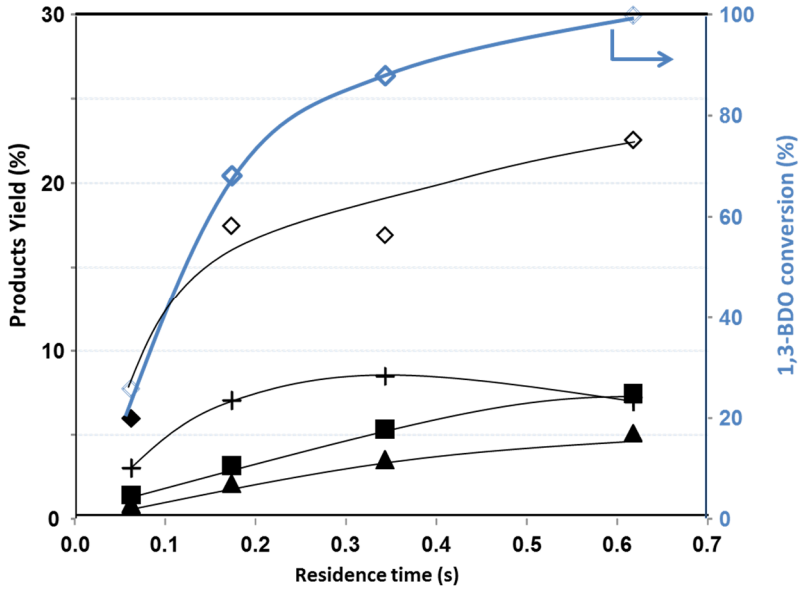

Figure 21. 1,3-Butanediol conversion at 250°C on MgO. Symbols: 1,3-butandiol conversion (◊); yields: methylvinylketone (▲), ethanol (◊), acetaldehyde (+), others (■).

Another compound studied was the Crotyl-alcohol (2-buten-1-ol) which was also suggested as a possible intermediate before [112], [113]. It was tested on the reaction at both 250°C and 400°C, results are presented in Figure 22 and Figure 23. The major product obtained was 1-Butanol; this could be obtained via MPV reduction of the carbonyl group in butanal, the latter being formed in a relatively large amount[23], [114], [115] by tautomery of the alkenol obtained via isomerization of the double bond in crotyl alcohol. The MPV-reduction can occur through the reaction with crotyl alcohol itself (which is dehydrogenated to crotonaldehyde), a hypothesis confirmed by a catalytic test carried out by co-feeding crotyl alcohol and ethanol (molar ratio 1:1) (Table 1). This did not show any significant difference from the test carried out by feeding crotyl alcohol alone. Overall, the distribution of the products obtained by reacting crotyl alcohol on MgO was very similar to the distribution shown from ethanol.

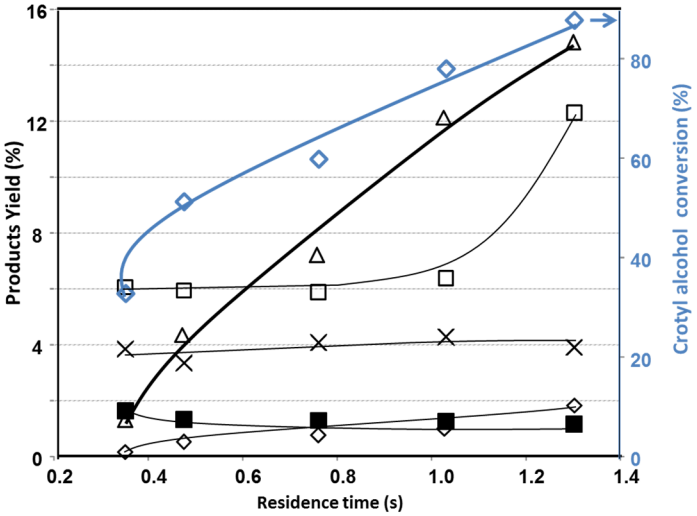

Figure 22.Crotyl alcohol conversion at 250°C on MgO. Symbols: crotyl alcohol conversion (◊); yields: 1-butanol (Δ), aromatic compounds (□), 3-buten-1-ol (X), ethanol (◊), others (■).

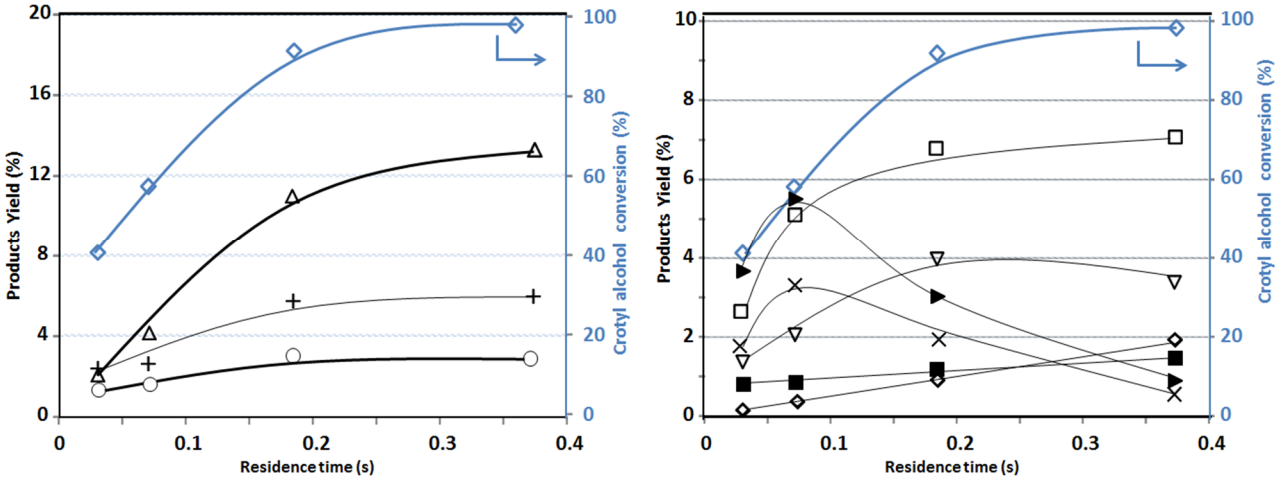

Figure 23. Crotyl alcohol conversion at 400°C on MgO. Main products (LEFT) and minor products (RIGHT) symbols: crotyl alcohol conversion (◊); yields: 1-butanol (Δ), acetaldehyde (+),1,3-butadiene (○),aromatic compounds (□), 2-butenal (crotonaldehyde) (▶), butanal (▽), ethanol (◊), 3-buten-1-ol (X), others (■).

Finally, catalytic tests were performed with acetaldol (3-hydroxybutanal) to elucidate additional key points in the mechanism since this molecule has been accepted for decades to be the key intermediate towards C4-compounds from ethanol. But it was never detected in our experiments (and also has not been reported in literature). First, we examined the conversion of this molecule in different conditions. From the results obtained at both 250°C and 400°C (Table 6), it is possible to see that the dehydration of the aldol to crotonaldehyde was only a minor reaction. Indeed, the main reaction observed was the reverse aldolization to acetaldehyde, clearly indicating that the aldol condensation is thermodynamically unfavourable at these temperatures. As no significant changes in

the product distribution appeared even when co-feeding ethanol and the aldol, any option presenting acetaldol as key intermediate in C_4-compound formation could either be ruled out or its role limited only to a minor one. This idea has gained theoretical support in the recent literature [2].

Table 6. Main catalytic results for proposed intermediates in ethanol conversion on MgO (in gas-phase).

				Yield (%)[a]							
Feed	T (°C)	τ (s)	Conv.(%)[a]	C_2H_4O[b]	C_4H_6O	C_4H_9OH	C_4H_6	C_2H_4	MVK	C_4H_8O	$C_4H_{10}O$
Acetalaldol	250	0.5	100	32 (+7)	9	tr	-	-	tr	tr	-
Acetaldol / ethanol	250	0.5	100	36 (+7)	8	tr	-	-	tr	tr	-
Acetaldol	400	0.2	100	11	2	-	tr	-	tr	tr	-
3-Buten-2-ol	250	0.0	14	-	-	-	tr	-	tr	tr	1
3-Buten2-ol	400	0.3	58	-	-	-	1	tr	5	10	9
Crotyl alcohol / ethanol	400	0.4	97	8	1	18	1	2	-	tr	-

[a] When two different products are co-fed, conversion and yield refers only to the C_4 compounds. **[b]** In parenthesis the yield obtained as paraldehyde is shown. **Explanation**: C_2H_4O, acetaldehyde; C_4H_6O: crotonaldehyde; C_4H_9OH: 1-butanol; C_4H_6: 1,3-butadiene; C_2H_4: ethylene; MVK: methyl vinyl ketone; C_4H_8O: 2-butanone; $C_4H_{10}O$: 2-butanol. "tr": trace amount (yield <1%)

In conclusion, the main results obtained with reactivity experiments may be summarized as follows:

(a) The main primary product of ethanol transformation was acetaldehyde; immediately after this, the main products obtained were 1-butanol and crotyl alcohol. Conversely, butanal, crotonaldehyde and butadiene were all kinetically consecutive compounds (compared to acetaldehyde).

(b) 3-hydroxybutanal (acetaldol), crotonaldehyde, or gas-phase 1,3-BDO are not key intermediates during ethanol transformation to C_4 compounds over MgO;

(c) The intermediate compound showing a product distribution closest to that shown from ethanol was crotyl alcohol.

3.1.3 In-situ DRIFTS-MS

In-situ DRIFTS experiments were performed to understand the way ethanol adsorbs on the surface of MgO and its further transformation with temperature. At room temperature (Figure 24), the observed bands correspond to undissociated H-bonded and O-bonded ethanol (broad band between 3500-3000 cm^{-1} for the OH_v stretching and small bands at 1377 and 1270 cm^{-1} for the OH_δ and $CH_{3\delta}$), and surface ethoxide (i.e. the product of ethanol dissociative adsorption), whose bands at 1062 and 1103 cm^{-1} can be assigned to coupled C-C and C-O stretching modes. Bands at 2972, 2928, and 2876 cm^{-1} are due to $CH_{3v(a)}$, $CH_{2v(a)}$ and $CH_{3v(s)}$ stretching modes. [116]

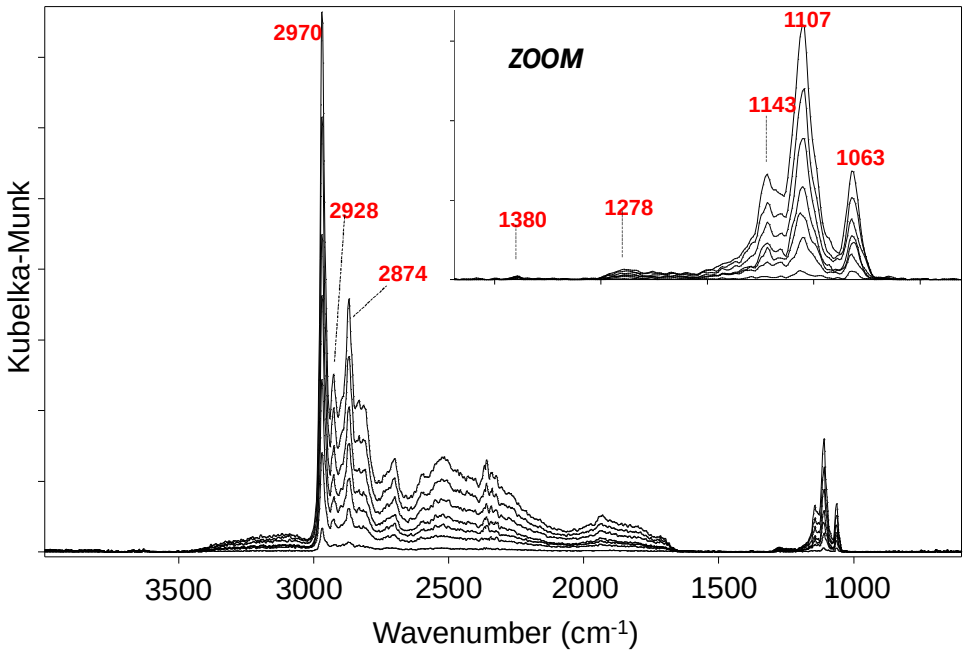

Figure 24. Adsorption of ethanol over MgO catalyst at 30°C

After adsorption at 30°C, ethanol feeding was stopped and the physically adsorbed ethanol was flushed with He. Then, a temperature program was followed from room temperature until 400°C at 10 °C min^{-1} while recording simultaneously DRIFTS and mass spectra at the different temperatures (Figure 25 and Figure 26 respectively). During the temperature program, the ethanol desorption is verified by the disappearance of the band at c.a 3200. As regards the ethoxy species (band at 1066 cm^{-1} for instance) it increase until 200°C and afterwards it seems to diminish. Similarly, in a recent paper, Davis et al [117] assigned the bands at 1119-1132 cm^{-1} as due to ethoxy species disappearing upon increasing T from 200 to 440°C. However, in our case a wider spectral range was covered and this allowed us to detect other species; for instance, there were bands appearing in the spectra at 1718 cm^{-1} and 1143 cm^{-1} as the temperature was increased to 150°C. While the first of the two bands can be attributed to the C=O stretching of acetaldehyde,[118] the second one corresponds to a species with a particular C-O stretching that is neither characteristic of the ethoxy nor of molecular ethanol. This band was tentatively attributed to the C-O stretching of a stabilized carbanion species formed by the abstraction of one H^+ from the methyl group in ethanol (this hypothesis is developed in the following Sections). This band seems to reach a maximum intensity and then it shifts towards lower wavenumbers in the same way some of the C-H vibration bands do.

The DRIFTS spectra were deconvoluted and the bands for each species were assigned, and its intensity was plotted against temperature to have a clearer view of bands behaviour and highlight correlations amongst them. This was performed using the built-in OPUS software fitting function. This command allows calculating single peak positions, widths and intensities in a system of overlapping peaks. Before starting the fitting calculation a model consisting of an estimated number of peaks and a baseline has to be set up. Of course the result of this calculation highly depends on the model selected, and it should be reasonable from the chemical point of view. This is performed by initially choosing the range of frequencies to be fitted and adding the obvious present peaks and then a few more for the doubtful ones. The model is then optimized during calculation. Peak shape, iteration time, optimization algorithm and so on, are also parameters that can be modified. In our case the peak shape used was Lorentzian and *Levenberg-Marquardt* optimization algorithm. Each spectrum at each temperature was divided in three frequency ranges to fit them separately, so at the end 24 fitting procedures were performed and the criteria to accept them was a residual root-mean-square (RMS) error

lower than 0.0009. An example of the fitting performed for the spectrum at 350°C is presented in Figure 27.

Afterwards results were put together in a table of Intensity vs temperature (Table 7) for each band found in that range of frequency, and plotted as in Figure 28. However, for sake of clarity Figure 28 presents only the bands that were evidently correlated (even visually) and that were representatives of a certain vibration. We further modified the figure by adding the intensity of the bands at 1124 and 1143 since they were attributed to the carbanion at low and high temperature. This analysis shows the evolution of the species as follows: First bands observed correspond to ethanol (bands at 2972 and 1270 cm^{-1}, with the maximum intensity at room temperature) and ethoxy (band at 1105 and 2925 cm^{-1} with maximum intensity at 100°C). Thereafter, acetaldehyde appeared at 100°C (bands at 1718 and 2813 cm^{-1}, also typical for aldehydes). In the middle range of temperatures (100-200°C), bands at 2957 and 1653 cm^{-1} seem to increase; the latter was reported to be the characteristic C=O stretching of acyl or acetyl species.[119] Upon increasing the temperature beyond 200°C, the acetyl band intensity decreased and the band tentatively attributed to a carbanion species began to shift towards lower wavenumbers (until 1124 cm^{-1} at T > 300°C). The intensity of ethoxy bands decreased, with no shift of the corresponding wavenumbers. The band at ca 1620 was assigned to crotyl alcohol; it is formed after reaction of the previous species and just before the formation of the final products making it a key reaction intermediate.

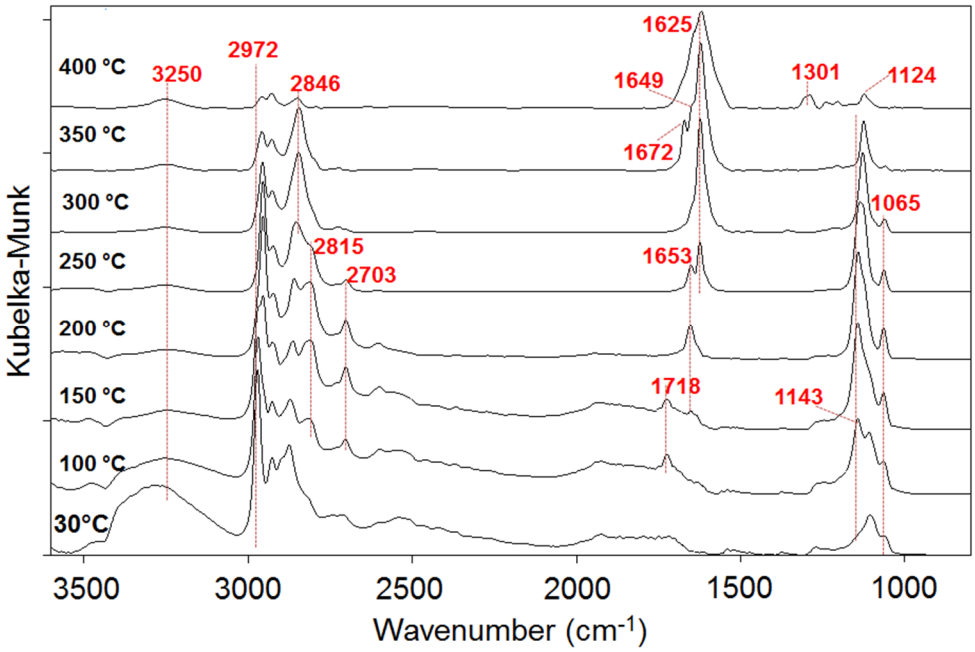

Figure 25. DRIFT spectra of ethanol adsorption on MgO and desorption / transformation with increasing temperature.

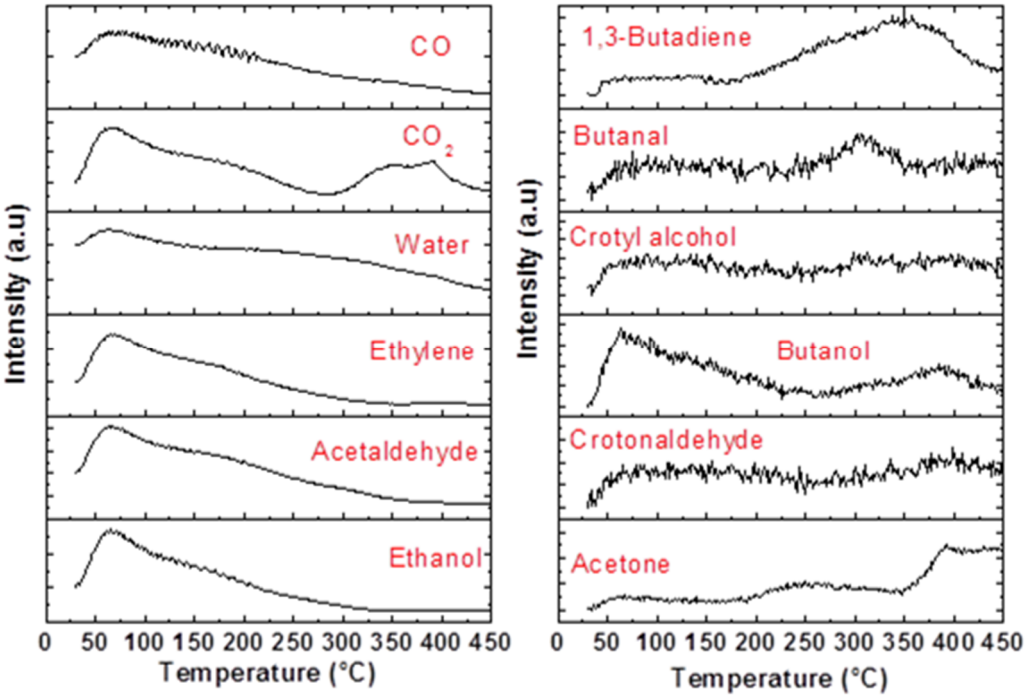

Figure 26. Ethanol Temperature Programmed Desorption on MgO.

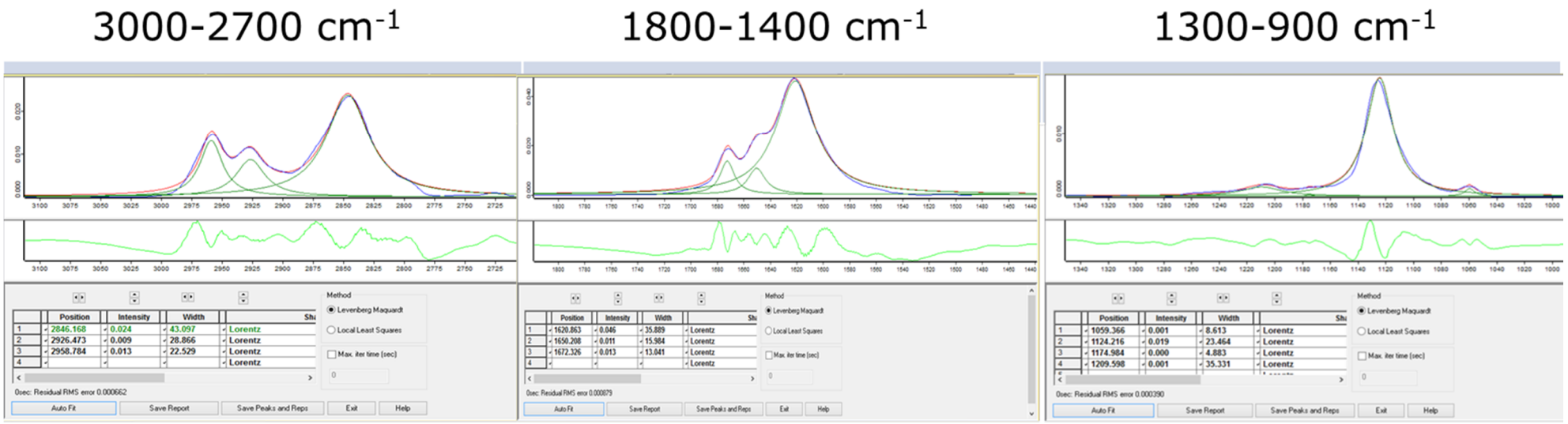

Figure 27. Example of the fitting procedure of Ethanol adsorption at 350°C on MgO

Table 7. Intensity of the detected bands during Ethanol adsorption over MgO at different temperature

Temp °C	*1058 cm^{-1}*	*1105 cm^{-1}*	*1124 cm^{-1}*	*1143-1124 cm^{-1}*	*1270 cm^{-1}*	*1380 cm^{-1}*	*1616 cm^{-1}*	*1625 cm^{-1}*	*1649 cm^{-1}*	*1653 cm^{-1}*	*1672 cm^{-1}*	*1718 cm^{-1}*	*2703 cm^{-1}*	*2813 cm^{-1}*	*2850 cm^{-1}*	*2870 cm^{-1}*	*2882 cm^{-1}*	*2920 cm^{-1}*	*2957 cm^{-1}*	*2925 cm^{-1}*	*2972 cm^{-1}*
30	2	11			7	5											40			16	66
100	8	18		23	2	7						9	9	19		20				22	47
150	10	15		35						5		8	18	26		22		16	46	16	
200	11		20	55						13			12	25		21		14	50	14	
250	8		24	50				18		8			4	12	23	23		11	40	11	
300	4		31	31				40	3	3					30	30		10	24	10	
350	1		19	19				43	11		13				24	24			13	9	
400			5	5			33		12						4				3	5	

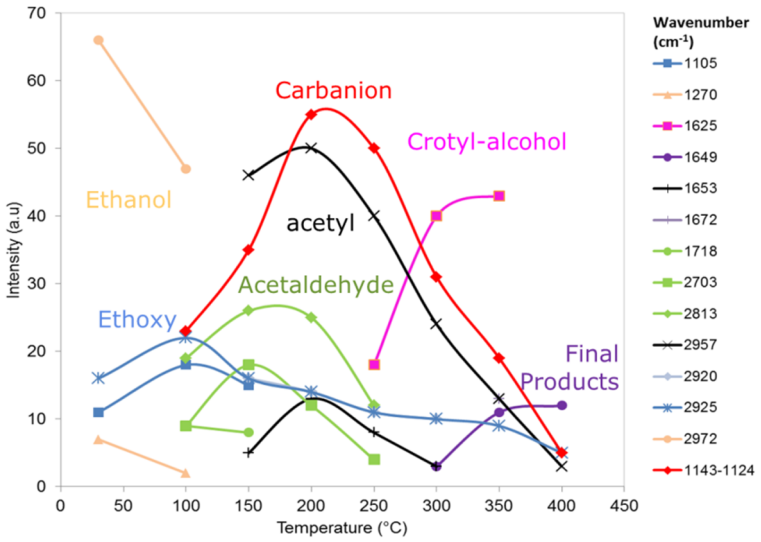

Figure 28. Ethanol on MgO: Infrared band intensity as a function of temperature.

On the other hand, additional clues emerged from the TPD experiments as the fact that 1-butanol is a primary product (especially at low temperature), that butadiene formation starts only when T is higher than 250°C, and that crotonaldehyde is observed only in traces at high temperatures. Acetyl species may also decompose into CO and methyl, which may end up forming acetone (band at around 1649 cm^{-1}, T > 350°C)[120] according to the following reactions:

$CH_3CHO \rightarrow CH_3CO_{ads} + H_{ads}$

$CH_3CO_{ads} \rightarrow CH_{3\,ads} + CO_{ads}$

$CH_3CO_{ads} + CH_{3\,ads} \rightarrow CH_3COCH_3$

With respect to lighter species, a partial adsorption of carbonates in the range of temperatures considered is evidenced by both the broadening of the band around 1600 cm^{-1} and the CO_2 detected in the TPD. In the case of ethanol observed at T < 250°C it may be related to both desorption of the molecularly adsorbed ethanol and recombination of the ethoxy species with protons. Other products observed were ethylene (only at low temperature, when ethanol was also present), hydrogen, methane, and carbon dioxide. The latter may be formed both by the decomposition of surface carbonates, and by the "reforming" of ethanol or other products due to the water generated in the reaction medium (e.g. via ethanol dehydration).

Further experiments were performed by adsorption of the potential intermediates directly on MgO under similar conditions in order to observe the way they adsorb. Results are presented in Figure 29 and it is clear that the adsorbed intermediate resembles crotyl-alcohol. Instead it seems that no traces of acetaldol or crotonaldehyde are found as

adsorbed intermediates (at low temperature) or desorbed to the gas phase, thus it seems again that the aldol condensation should not be the key reaction leading to the formation of C_4 compounds from ethanol on basic oxide materials.

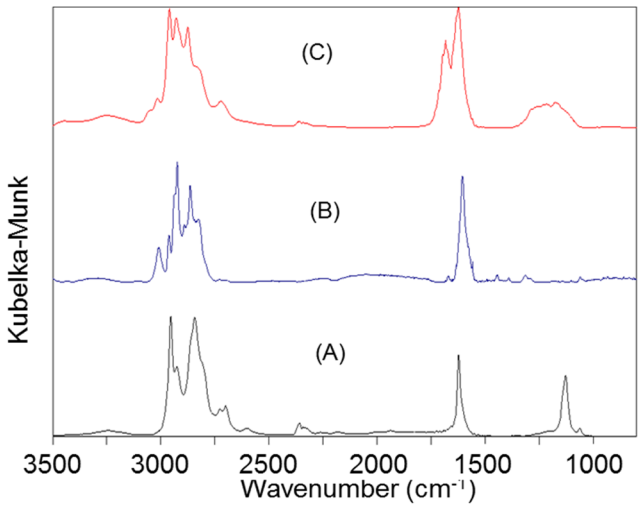

Figure 29. DRIFT spectra recorded after adsorption of crotonaldehyde (top), crotyl alcohol (middle) on MgO, at the temperature of 100°C, compared with the spectrum recorded during ethanol desorption at 300°C (bottom).

Experiments in continuous feeding at 400°C ("Operando mode")

To conclude this part, a set of experiments were performed by continuously feeding ethanol on MgO at 400°C, while the mass signals of desorbed products were also being monitored (so-called "operando mode"). These tests differed from those involving low temperature adsorption because the effective contact time of reactants is much shorter. In this respect, in the continuous feeding mode reaction conditions were certainly closer to those achieved in the flow reactor. However, they may make the identification of reaction intermediates more difficult due to their high concentration and fast transformation. Nevertheless, experiments at 400°C generated spectra that are similar to those recorded using the TPD approach at lower temperature, and thus support the hypothesis that intermediates observed during experiments in such conditions are likely precursors for the formation of the final products.

Figure 30 shows the spectrum recorded during an experiment carried out by directly feeding ethanol on MgO at 400°C; the mass signal (MS) of desorbed products was also registered (Figure 30). During the continuous feeding of ethanol, which lasted roughly 30 min, the spectra showed an increase of bands at 1672, 1647, and 1125 cm^{-1} with time. Such bands were also observed in the corresponding TPD experiments. Besides in the

bottom part (a zoom) the figure shows how the band at 1620 disappears to give place to those at 1672, 1647, and 1543 cm^{-1} typical of the formation of crotonaldehyde and probably butadiene (the former two) and acetates and carbonates (the last band). Therefore, it can be suggested that the acetaldehyde/acetyl and the carbanion may react together forming adsorbed crotyl alcohol, since the band at about 1620 cm^{-1} (appearing after 250°C) was also observed when crotyl alcohol was fed over MgO (Figure 25).

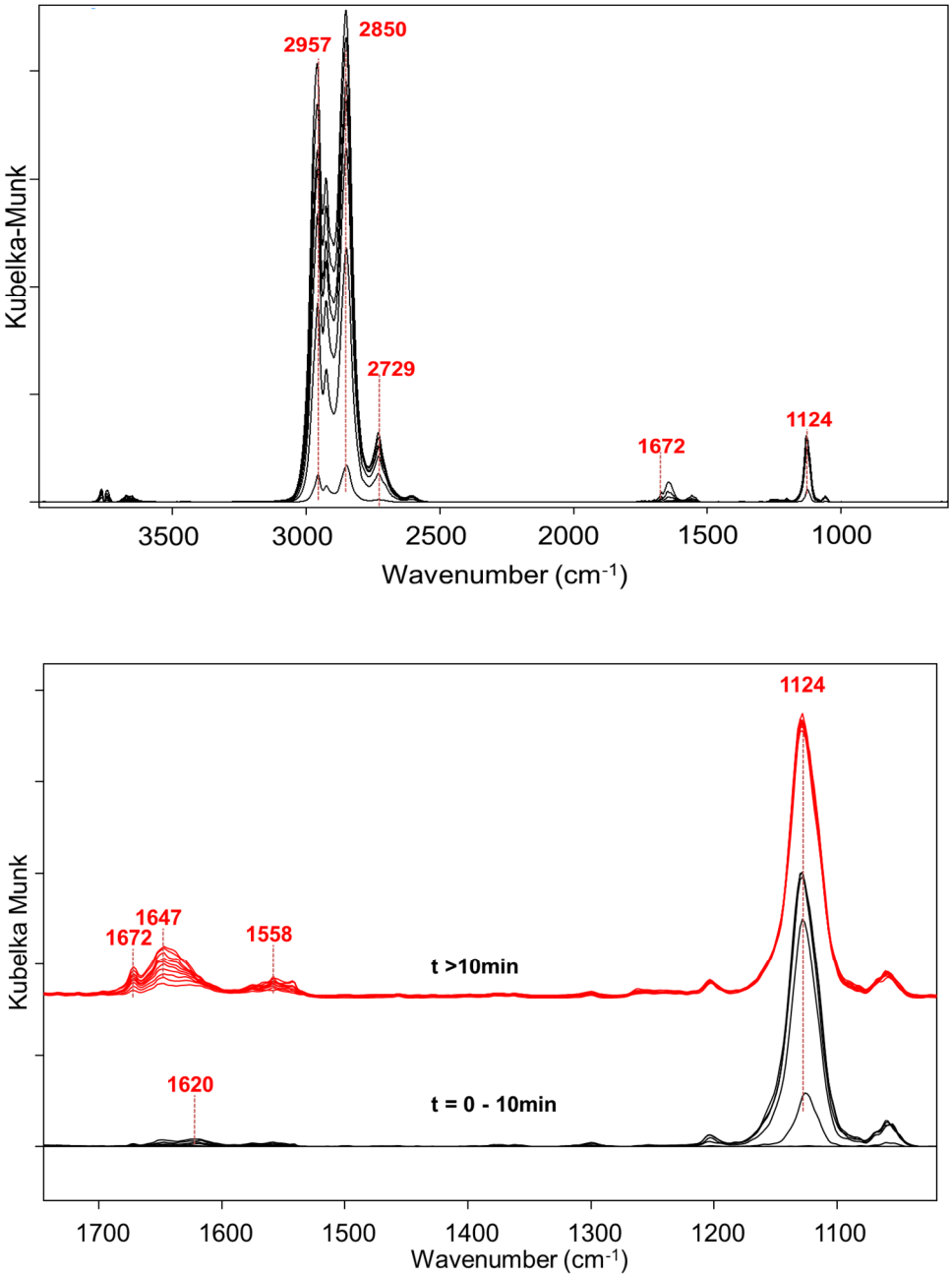

Figure 30. Spectra recorded during the continuous feeding of ethanol, at 400°C (UP) and detail for the first minutes in the low frequency region (BOTTOM).

Indeed, both similarities and differences were observed between these experiments and those carried out with the adsorption-TPD mode (See comparison in Figure 32): when constantly feeding ethanol at 400°C, there was prevalence of the C-H stretching bands of adsorbed molecular ethanol, which is expected due to the continuous supply of the alcohol. Another difference was that the broadening of the band of carbonates observed in the TPD appeared not to be predominant here, due also to the fact that the intermediates rapidly desorb and are not as promptly oxidized as in the former case. Nevertheless, it is interesting to note that the spectrum recorded was very similar to that one shown at 300-400 °C with the TPD mode (see Figure 32). This supports the hypothesis that the intermediates observed during the TPD experiments are those responsible for the formation of the final products in the actual reaction conditions. Moreover, the product distribution registered in these experiments at 400°C (by mass spectrometry) was similar to that obtained in the reactivity tests, as shown in Figure 31.

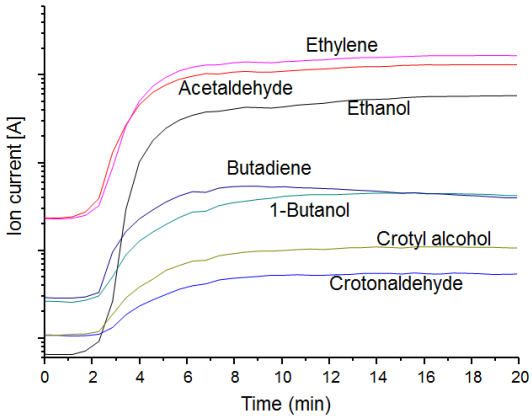

Figure 31. Products observed during the Ethanol continuous feeding on MgO at 400°C.

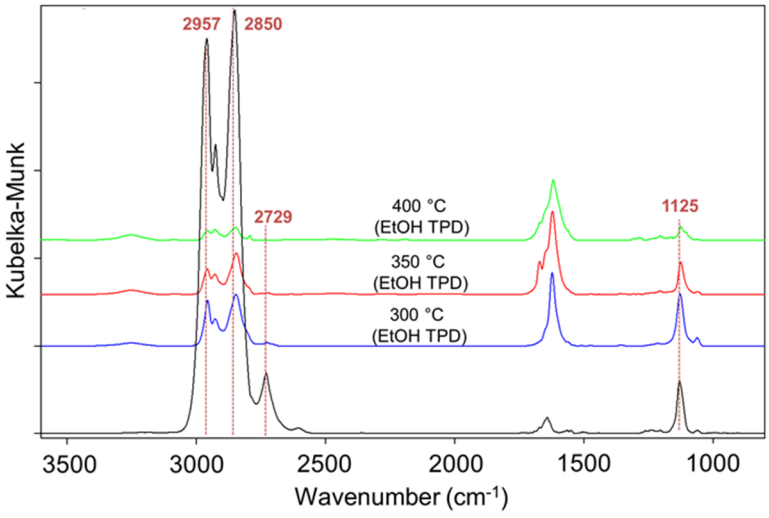

Figure 32. Ethanol continuous adsorption on MgO at 400°C (black) and comparison with spectra obtained by desorbing ethanol at 300, 350 and 350°C.

3.1.4 Computational Studies

This part of the research attempted to, at least, clarify the very early stages of ethanol adsorption on basic oxides. The idea was to focus on the likely transient species and their formation mechanism. Several reaction pathways that may lead to the experimentally detected products were also considered. The technical details of this theoretical investigation were given in the methodology chapter.

Alcohol dehydrogenation

The dehydrogenation reaction generating the aldehyde was the first step considered. Table 8 reports the results of reaction (ΔE) and transition state (TS) energetics for ethanol dehydrogenation with respect to two alternative energy zeros. The calculations were performed using a previously validated approach [109]. Figure 33 shows the optimized structures for the reactants, TS, and products of this reaction.

Table 8.Alcohol adsorption, reaction and TS energies for the process leading to the dehydrogenation of ethanol and methanol onto $Mg_{10}O_{10}$, and for the formation of a carbanion via the methyl deprotonation in ethanol.

Alcohol/site	*Adsorption energy (kcal/mol)*	*Reaction energy (kcal/mol)*	*ΔE*	*Barrier (kcal/mol)*
Dehydrogenation				
EtOH/Mg3C	39.5	38.1 (-1.4)		44.7 (5.2)
EtOH/O3C	23.9	29.4 (5.5)		40.4 (16.5)
MeOH/O3C	25.1	37.0 (11.9)		44.5 (19.4)
MeOH/Mg3C	40.4	45.9 (5.5)		51.4 (11.0)
Carbanion formation				
EtOH/Mg3C		31.3 (-8.2)		33.4 (-6.1)
EtOH/O3C		36.4 (12.5)		36.7 (12.8)

The zero of the energy for the processes is assumed to be the adsorbed alcohol with the OH dissociated. Also shown in brackets, there are energetic quantities referring to the gas phase alcohols plus $Mg_{10}O_{10}$ as reactants.

From Table 8, it is evident the lower barrier (by 4.4 kcal/mol) and ΔE obtained when the dehydrogenation of the adsorbed ethanol takes place in the proximity of the O3C site. However, the energetic ordering in Table 8 changes if gas phase ethanol/MgO cluster is used as the reference energy zero, due to the adsorption energies. Nevertheless, both catalytic sites should be considered as being active due to the high temperature (400°C) employed during the reaction.

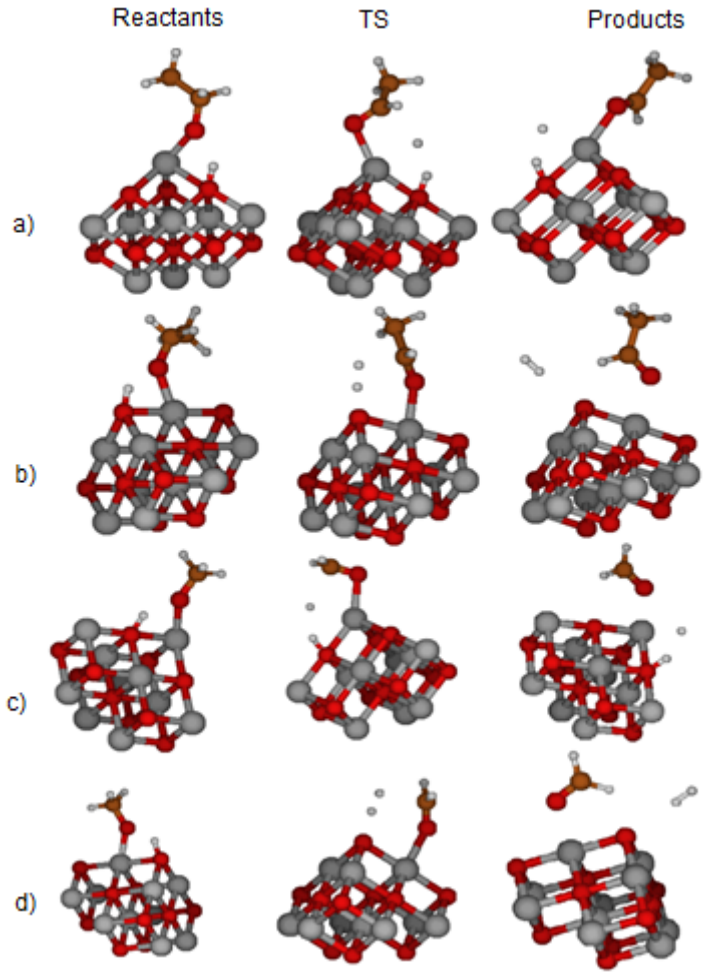

Figure 33. Reactant, TS and product (from left to right) of the alcohol (a and b, ethanol; c and d, methanol) dehydrogenation process on MgO near the Mg3C (a and c) and O3C (b and d) sites.

Enol formation

DFT calculations indicate that enol formation from acetaldehyde adsorbed onto Mg3C should release energy (2 kcal/mol) and require surmounting a low barrier (6.6 kcal/mol, see Figure 34 for the optimized structures). It is thus likely that a fast equilibrium between the two molecules is indeed present.

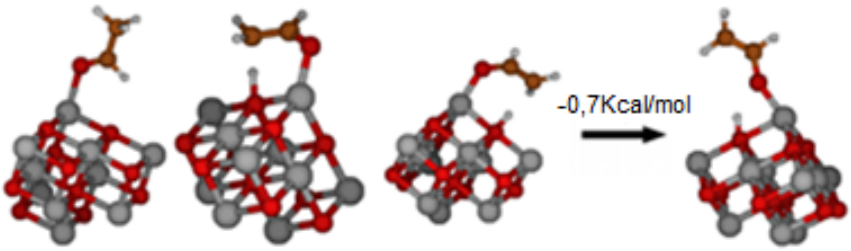

Figure 34. Reactant, TS and product for the enol formation from acetaldehyde near the Mg3C site. Notice the presence of two near-degenerate isomers for the enol coordinated onto the Mg3C site.

Carbanion formation

The presence of basic MgO surface sites may induce the deprotonation of the methyl group in ethanol and our calculations (see Table 8 and Figure 35) indicate that such process generates a carbanion 31.3 and 36.4 kcal/mol above the adsorbed ethanol in the vicinity, respectively, of the Mg3C and O3C sites. Deprotonation close to the Mg3C site generates a product that is 6.8 kcal/mol lower in energy than acetaldehyde plus adsorbed H_2 compared to MgO/gaseous ethanol; the TS barriers for such processes have also the same energy ordering. The carbanion produced close to the O3C site, instead, sits higher by 7.0 kcal/mol than acetaldehyde/adsorbed H_2, despite the TS barriers having the same ordering as happens close to Mg3C. Notice that the barrier for carbanion formation near O3C is just 0.3 kcal/mol above the energetic requirement for the reaction.

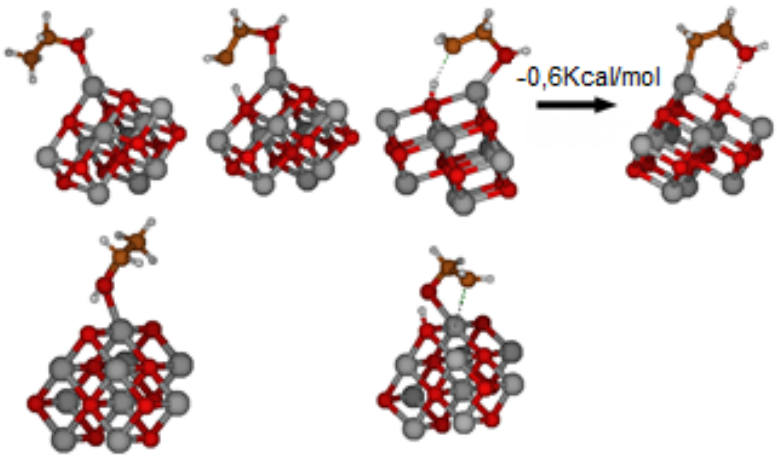

Figure 35. Reactant, TS and product for the carbanion formation from ethanol near the Mg3C (top) and O3C (bottom) sites. Notice the presence of two near-degenerate isomers for the carbanion coordinated onto the Mg3C site.

The data reported in Table 8 suggest that both Mg3C and O3C sites may produce both intermediates, albeit with a different activity and relative preference due to a disparity in acid-basic behaviour. Thus, the global energy profiles suggest that carbanion formation onto the Mg3C site ought to be the most likely process, followed by ethanol dehydrogenation on the same site and carbanion formation onto O3C.

The idea of a carbanion formation via deprotonation of the methyl group was previously considered by Iglesia and Gines,[121] although from an adsorbed aldehyde. In their study, the catalyst was a basic oxide (MgCeOx) modified with Cu and K and they used $^{12}C_2H_5OH$–$^{13}C_2H_4O$ reactant mixtures to establish that condensation reactions can proceed via direct reaction of ethanol without the intermediate formation of gas phase acetaldehyde. This means that acetaldehyde condensation may occur, but also that ethanol direct condensation contributes to the formation of the products. Besides, they discussed the fact that the condensation reactions become easier than the dehydrogenation in presence of a metal (e.g. Cu) since the latter helps removing the hydrogen as H_2.

Suggesting the carbanion formation onto the MgO surface rationalizes several experimental observations, the simplest one being the production of ethylene. In fact, we have located two TS leading from the Mg3C-adsorbed carbanion to ethylene and dissociated water (see Figure 36 for the reactant/TS structures) with fairly low (3.7 and 6.5 kcal/mol) barrier heights. Such finding places the barrier to be surmounted during the carbanion-formation plus dehydration sequence 4.8 kcal/mol below the barrier leading to acetaldehyde plus H_2. Thus, dehydration of ethanol is a competitive process compared to its dehydrogenation even onto the purely basic MgO. Besides, the carbanion normal mode at 1165 cm^{-1} also helps in assigning the IR feature at 1143 cm^{-1}, whose evolution is in line with the reactivity expected from such species (*vide supra*, DRIFTS Section, and Figure 37, showing the simulated IR spectrum of the carbanion). Similarly, the position of the two peaks around 1220 cm^{-1} in Figure 37 correlates well with the location of a shoulder appearing and then disappearing in the DRIFT spectra upon increasing the temperature. Notice, however, that the relative intensities in the 1143-1220 cm^{-1} region are not well reproduced by the calculations. We consider this finding as most likely due to the fact that the shoulder modes involve the displacement of the proton on MgO directly interacting with the anionic carbon; the effect of such motion on the molecular dipole may be improperly estimated by DFT due to shortcomings in describing electronic correlations. Instead, it remains for the moment unclear the lack of any feature in the DRIFT spectra around 1380 cm^{-1}, a mode connected to the wagging of OH-bearing CH_2 in the carbanion.

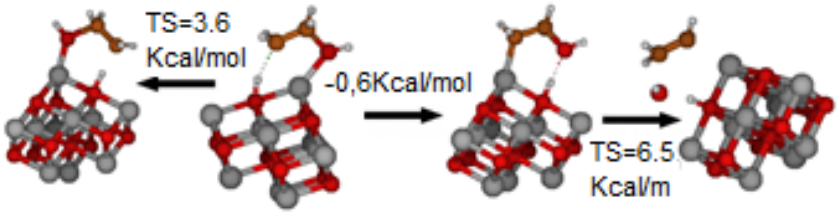

Figure 36.Reactants and TS for the dehydration of ethanol starting from the Mg3C-adsorbed carbanion.

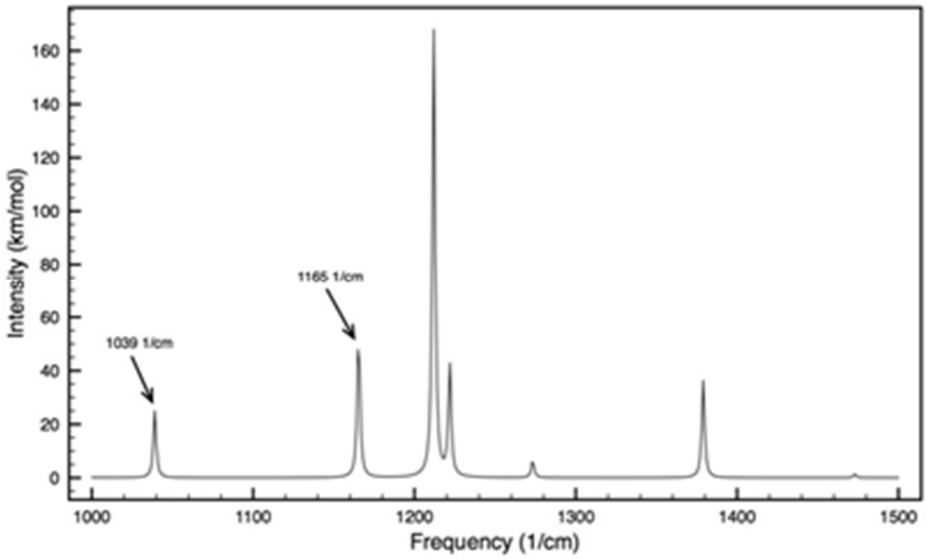

Figure 37.IR spectrum of the carbanion species adsorbed on MgO.

With the quantitative results just discussed, it is possible to draw a partial conclusion with respect to the importance of the aldolic path toward C_4 formation on MgO. As for this, the higher energetic cost to be paid to produce two molecules of acetaldehyde compared to a single carbanionic species or a carbanion and an acetaldehyde ought to make the surface concentration of the pair acetaldehyde/enol substantially less than for the carbanion/acetaldehyde couple (or the carbanion/ethanol pair, vide infra). In turn, this suggests the aldolic pathway as less likely than one involving the carbanion. Additional arguments against the aldolic scheme come from the fact that the adsorbed aldol lies substantially higher in energy than the adsorbed 1,3-BDO, and that our DFT calculations predict the aldolic condensation to be nearly energy neutral in the gas phase. Notice that the latter finding is valid whatever the catalyst employed and suggests that the presence of reduced metals (e.g. see work by Iglesia and Gines [121] and the butadiene catalyst by

Ivanova et al. [89]) may only favor the formation of acetaldehyde to be consumed along paths alternative to the aldolic one.

Carbanion reactivity

As suggested, the in-situ generation of a carbanion from ethanol may open alternative channels, among which two involving the attack to the acetaldehyde carbonyl group and the hydroxyl-bearing carbon in another ethanol molecule. The first reaction would lead to the alkoxide precursor of 1,3-BDO, while 1-butanol would be obtained by the SN2-like attack to the Mg-coordinated and activated ethanol. Table 9 provides the energetics for the two processes just mentioned; also shown, there is the energetics of the stationary points for the aldolic pathway. Figure 38, instead, shows the optimized structures of the species involved. While both processes are exergonic with respect to the reactants due to the formation of a stable single C-C bond, the carbonyl attack appears to be substantially more facile than the SN2-type reaction involving ethanol due to the electronic structure of the aldehydic group. Also, the charge-bearing carbon in the carbanion has to increase its distance from the stabilizing lattice Mg in order to approach the OH-bearing carbon in ethanol (see Figure 38).

Table 9. TS barrier heights and energetics of the carbanion attack to the acetaldehyde carbonyl and hydroxyl-bearing carbon in ethanol gauged from the co-adsorbed reactive species in the vicinity of the corner site.

Reactants	*TS barrier (kcal/mol)*[a]	*Reaction ΔE (kcal/mol)* [a]
Acetaldehyde/Carbanion	11.4 (19.1)	-28.9 (-21.2)
Ethanol/Carbanion	41.0 (28.9)	-42.0 (-54.1)
Acetaldehyde/Enol	7.2 (6.3)	-10.6 (-11.5)

[a]The energies referring to two ethanol molecules in the gas phase plus the MgO cluster are shown in brackets.

With the zero being conveniently set as two vapour ethanol molecules plus the MgO clusters, the energy profiles place the products of the ethanol/carbanion and acetaldehyde/carbanion reactions at -54.1 and -21.2 kcal/mol, respectively. This indicates that the adsorbed 1-butanol plus dissociated water is more stable than the dissociated 1,3-BDO, a result due to the cost of the dehydrogenation (see Table 8). With the same energy scale, the TS barrier for the two processes becomes, respectively, 28.9 and 19.1 kcal/mol; hence, either the two pathways have a similar activity, at least basing on the energy requirement alone, or the process for 1,3-BDO is somewhat faster than for 1-butanol.

Notice that the latter suggestion agrees nicely with the results in Figure 18, where a slightly lower yield is obtained for 1-butanol than for 3-buten-1-ol plus crotyl alcohol. Importantly, the latter compounds are likely to be produced by dehydration of the deprotonated 1,3-BDO via carbanion formation (Figure 38).

An additional consequence of the fact that adsorbed 1,3-BDO lies only 21.2 kcal/mol below the common energy zero is the possible retro-dissociation into ethanol and acetaldehyde, a process requiring only -0.3 kcal/mol onto MgO and being apparent in both Figure 20 and Figure 21. Importantly, this conclusion does not contradict the proposed mechanism of 3-buten-1-ol and crotyl alcohol formation, as the latter are formed in the vicinity of corner sites. Feeding directly 1,3-BDO onto MgO is instead likely to lead toward terrace adsorption, at least initially; this is a situation in which the diol may easily gather the energy to decompose.

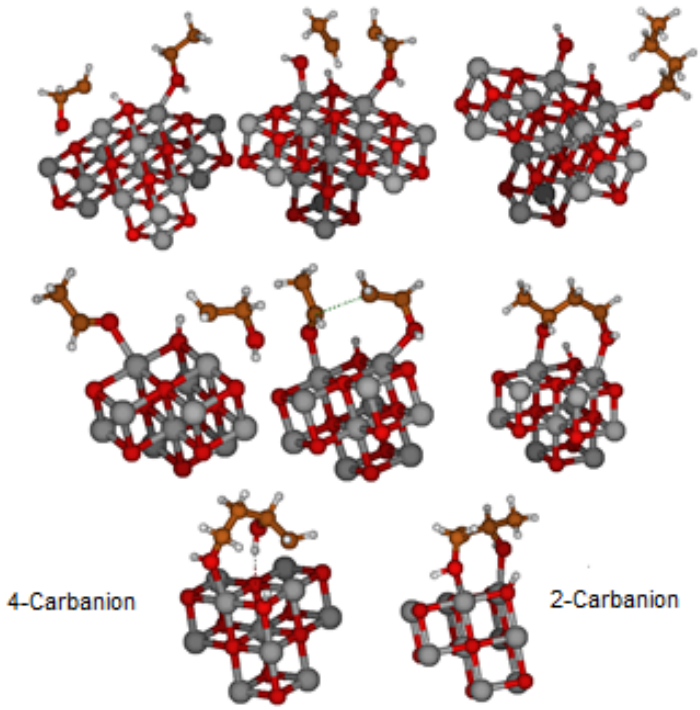

Figure 38.Reactants, TS and products of the reaction between the carbanion and an adsorbed ethanol molecule (top) or acetaldehyde (middle). Also shown, are the two carbanion obtained from 1,3-BDO (bottom).

Aldol formation thermodynamics

As the commonly suggested pathway for C_4 production via the Guerbet/Lebedev reaction is represented by the aldol condensation of two acetaldehyde molecules, one may wish to rationalize the finding that products derived from the subsequent transformation of the aldol are scarcely present compared to the ones deriving from reactions involving directly ethanol and its carbanion. In this respect, one ought to begin noticing that the higher energetic cost to be paid in order to produce two molecules of acetaldehyde compared to a single carbanionic species or a carbanion and an acetaldehyde ought to make the surface concentration of the pair acetaldehyde/enol substantially less than for the carbanion/acetaldehyde or carbanion/ethanol. Thus, statistically, there should be a lower likelihood for the related reactive encounter.

An additional argument against the aldolic pathway is the fact that the adsorbed aldol lies substantially higher in energy than the adsorbed 1,3-BDO. In fact, we have found that condensing the enol and acetaldehyde decreases the system energy by only 11.5 kcal/mol with respect to the common energy zero defined in Table 9 (See also Figure 39). The results presented, clearly, indicate the aldol as thermodynamically less stable than any of the other products investigated by us; thus, the equilibrium between acetaldehyde and the aldol should be tilted more toward the separated reactants due to the entropic factor (two molecules instead than only one) than in the 1,3-BDO and 1-butanol cases due to the higher product energy in the common energy scale. In turn, this suggests the aldolic condensation pathway as the one contributing the least to the production of C_4 compounds. Despite the lower TS barrier present along the aldolic path than for the reaction between acetaldehyde and carbanion. This finding is likely due to the energetic cost to be paid for distancing the carbon bearing the negative charge from the lattice Mg. Additional support to the idea that the aldol pathway has a limited importance for C_4 synthesis comes from its gas phase energetics, which our DFT calculations show to be:

$$2CH_3CHO \rightarrow CH_3CH(OH)CH_2CHO\ \Delta E = -8.5\ kcal/mol$$
$$CH_3CH(OH)CH_2CHO \rightarrow CH_3CH = CHCHO + H_2O\ \Delta E = +11.0\ kcal/mol$$
$$2CH_3CHO \rightarrow CH_3CH = CHCHO + H_2O\ \Delta E = +2.5\ kcal/mol$$
$$2CH_3CH_2OH \rightarrow CH_3CH = CHCHO + H_2O + 2H_2 \Delta E = +44.8\ kcal/mol$$

Due to energetically demanding nature of the dehydration step, the energetics of the coupled aldolic/dehydration steps suggests crotonaldehyde to be in facile equilibrium with acetaldehyde. The latter is continuously subtracted from this equilibrium by the non-reversible processes leading to 1-butanol and crotyl alcohol.

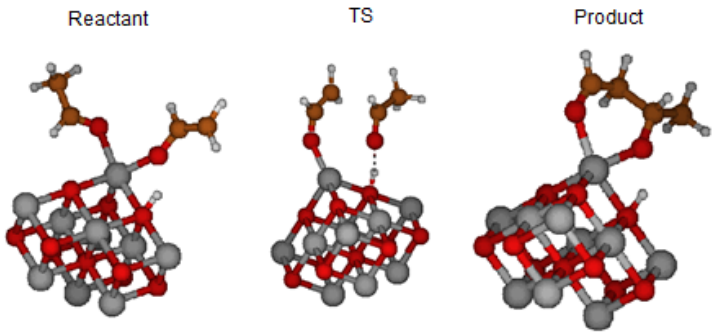

Figure 39.Reactants and product of the aldolic condensation

Production of 3-buten-1-ol and crotyl alcohol.

To investigate what mechanism may allow the production of 3-buten-1-ol and crotyl alcohol from 1,3-BDO, we have explored the possible formation of carbanions from the latter species, as well as the possibility that its alkoxy form (see middle panel, Figure 38) may easily convert into the undissociated 1,3-BDO. From the DFT results, it emerges that the alkoxy version of 1,3-BDO is only 1.5 kcal/mol more stable than the undissociated species. It is also found that deprotonating it to form a carbanion in positions 2 requires only 27.8 kcal/mol, while 32.6 kcal/mol are needed to deprotonate position 4; these energy requirements are indeed similar to the obtained in the ethanol case. The structures of the carbanions are shown in the lower panel of Figure 38. With the reasonable assumption that barriers similar to the one found for ethanol in the vicinity of O3C (Table 8) are associated with the TS leading toward the latter species, this finding suggests that 3-buten-1-ol and crotyl alcohol can be produced via the same mechanism generating ethylene, i.e. via dehydration following carbanion formation.

3.1.5 Guerbet vs Lebedev reactions on MgO: common features and differences in mechanisms

From the data collected so far by reactivity tests, DRIFT-TPD/MS and theoretical modelling, it is possible to suggest a new mechanism capable of explaining not only the evidence reported in this work but also the data published in many decades of literature on both the Lebedev and the Guerbet reactions.

First, ethanol is adsorbed on the basic oxide surface and dissociates into acetaldehyde and hydrogen; this is a rate-determining step and it requires a relatively high temperature (>200°C) in order to take place. Adsorbed acetaldehyde is in equilibrium with the related enolic form. At the same time, ethanol can be adsorbed on the catalyst surface as an ethoxide onto low coordination sites, although the latter anion always remains in equilibrium with its undissociated alcoholic form. This happens especially near O3C (the alcoholic oxygen is coordinate onto a Mg4C site), where the molecular ethanol may undergo a proton abstraction from the α-carbon, thus generating a carbanion whose negative charge is stabilized by the cations present in the oxide lattice as the near-sp^3 type orbital that contains the lone pair electrons points toward one of them. Carbanion may undergo 3 different reactions, each path being facilitated or hindered depending on temperature, catalyst acid-basic features, and likelihood of molecular encounter (*vide infra*):

The first option is that the hydroxyl group present in carbanion reacts with the previously dissociated H^+ (adsorbed on the catalyst surface) to produce water and ethylene, which desorb in the gas phase (route 1 in Figure 40);

Secondly, it could happen that the carbanion reacts with another ethanol molecule via a SN2-like attack, thus losing a water molecule to directly produce 1-butanol (route 2 in Figure 40);

Finally carbanion could also react with an acetaldehyde molecule to directly produce an adsorbed species which desorbs while producing either crotyl alcohol (route 3 in Figure 40) or 3-buten-1-ol and a water molecule. Alkenols may then dehydrate to 1,3-butadiene or rearrange into 3-buten-2-ol.

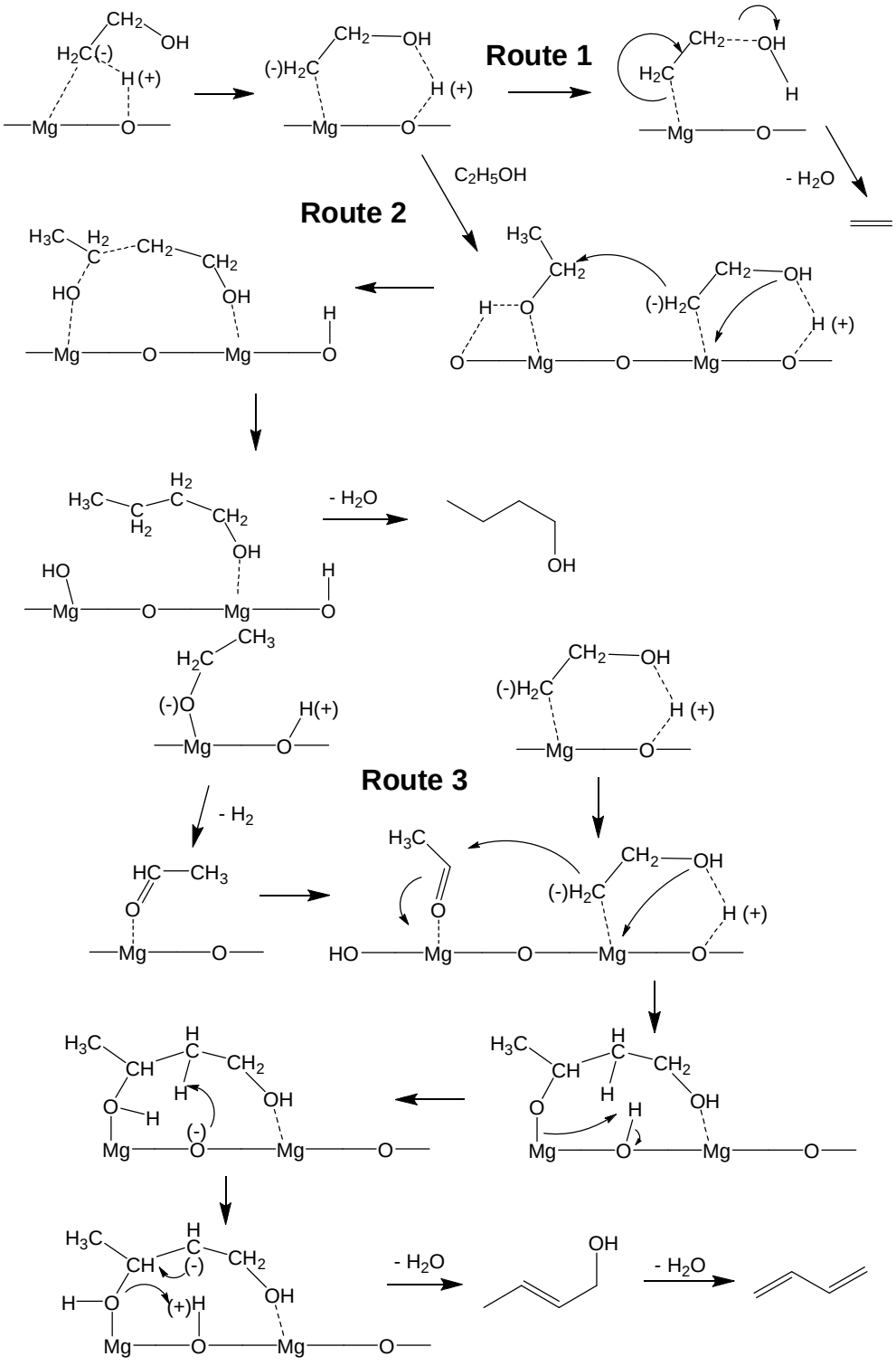

Figure 40. Hypothesized reaction pathways leading to ethylene (route 1), 1-butanol (Guerbet reaction, route 2) and crotyl alcohol, precursor of butadiene (Lebedev reaction, route 3).

As far as the first path is concerned, the harder the cation is, the more stable the carbanion is; this is why calcium oxide produces much more ethylene than magnesium oxide [83]. It is also important to note that the aldol condensation (which is endoergonic by 33.8 kcal/mol, accordingly to our theory level)[68] can be definitely ruled out as the main path in the Lebedev process since the encounter of two molecules of acetaldehyde is hindered due to their scarce concentration on the surface (for the same reason the Tishchenko dimerization to ethylacetate is also slow) and the large prevailing concentration of adsorbed ethanol. The latter is activated either as ethoxide or carbanion species. A reaction between the former and acetaldehyde is indeed possible, even though it would yield the hemiacetal (possible precursor of ethylacetate, which we observed only in traces). Its formation, however, is thermodynamically hindered at high temperature.

The second reaction is the main path followed by ethanol to produce Guerbet alcohols, i.e. mainly 1-butanol. The latter reaction is therefore aided by catalysts capable of stabilizing the carbanion (but not too much, in order to avoid ethylene formation) and by the lack of acetaldehyde on a vicinal site. These conditions may be reached by decreasing the temperature, so as to limit ethanol dehydrogenation to acetaldehyde (see different selectivity to 1-butanol in Figure 18 and Figure 19) and/or by tuning catalyst features. For example, hydroxyapatite [83] shows the highest yield to 1-butanol because, as pointed out by the authors, Lewis acid sites (Ca^{2+}) and basic sites (O^{2-}) have a higher atomic distance compared to MgO, and this might play an important role in the likelihood of molecular encounter. Moreover, for hydroxyapatite with high Ca/P ratio, the acid sites needed to perform alcohol dehydration are almost nil, thus avoiding consecutive reactions that might possibly take place from 1-butanol or crotyl alcohol, the latter being a competitive path.

Route 3 is the one leading to 1,3-butadiene from ethanol, i.e. the Lebedev reaction; the latter process has clearly been demonstrated to require complex catalysts capable, firstly, of dehydrogenating to acetaldehyde, secondly, of condensing C_2 intermediates, and lastly, dehydrating the formed C_4 [114],[68]. Moreover, it is well known that acetaldehyde has a beneficial effect on 1,3-butadiene yield and this is why this aldehyde is recycled to the reactor in the industrial process [71]. All these evidences are confirmed by our model. Acetaldehyde must react with ethanol carbanion to form crotyl alcohol as the key intermediate, and the precursor for butadiene formation via further dehydration. The final and kinetically consecutive dehydration of the alkenol to butadiene is likely to involve a

mechanism quite similar to that observed for both ethanol and 1,3-butanediol dehydration.

The reaction between acetaldehyde and ethanol is in competition with the direct production of 1-butanol: this is why an external source of aldehyde is needed to decrease the probability of carbanion reacting with ethanol and increase the selectivity to butadiene. The condensating features of catalysts must be carefully tuned since the atomic distance of two active sites (one bounding the aldehyde and the other the carbanion) must be right in order to facilitate the process. Lastly, dehydrating properties are essential for dehydrating the intermediate alkenol by shifting the equilibrium to 1,3-butadiene and butenes. In fact, in the case of the purely basic system investigated here, yield and selectivity to butadiene are much lower than those observed with mixed acidic-basic systems (e.g. Mg/Si/O). However, it is important to note that the presence of acid sites is required only to perform the consecutive steps concerning alcohols dehydrations (e.g. to lead to 1,3-butadiene), whereas they are not involved in the generation of primary products and intermediates shared by both the Lebedev and the Guerbet reactions.

It is also important to note that the dehydration of alcohols on acid systems involves energy barriers which are similar to those calculated with MgO;[122] this means that with bifunctional catalysts, an additional and acid-catalysed pathway leads to higher butadiene (and butene) selectivity and less by-product formation than with a purely basic catalyst, with which several other side reactions contribute to the formation of a wide spectrum of products.

Finally, it should be noticed that the mechanism proposed by Meunier et al [2] for the Guerbet reaction, based mainly on thermodynamic calculations, has analogies with the mechanism proposed here. In particular, it was reported that at least two reaction pathways take place simultaneously, the main pathway involving the condensation of two ethanol molecules with no intermediate gaseous compounds (so-called ‘‘direct’’ route), whereas a minor ‘indirect’’ route involves the condensation of ethanol with acetaldehyde (formed from ethanol dehydrogenation) to form butenol, which is subsequently converted to butanol by hydrogen transfer from a sacrificial ethanol molecule.

3.1.6 Conclusions of the chapter

The mechanism suggested here discards the key role of both acetaldol and crotonaldehyde as the reaction intermediates of the ethanol transformation on basic oxides. This species are usually accepted as being shared between the two pathways leading either to the alcohol or the diolefin; conversely, we have found that the two reactions involve different intermediates. In fact, our proposal is that crotyl alcohol is the key intermediate of the Lebedev process and precursors for butadiene formation. On the other hand, the reaction between ethanol and its activated form (carbanion) might explain the formation of the Guerbet alcohol as a kinetically primary product.

The mechanism suggested here also explains the formation of dehydration compounds even on purely basic materials. Furthermore, we also note that the mechanism proposed does not include H-transfer (MPV) reactions from ethanol to any reaction intermediate.

3.2 Mg-Si catalysts (varying the Mg to Si ratio)

Part of this chapter was included in the publication "An analysis of the chemical, physical and reactivity features of MgO–SiO_2 catalysts for butadiene synthesis with the Lebedev process". Velasquez Ochoa, J., Bandinelli, C., Vozniuk, O., Chieregato, A., Malmusi, A., Recchi, C., and Cavani, F. *Green Chemistry*, (advanced article) 2016. Doi: 10.1039/C5GC02194D. [123]

3.2.1 The synthesis of MgO–SiO_2 by the sol–gel method

The MgO-SiO_2 catalyst for ethanol transformation into butadiene can be prepared by several different methods such as mechanical mixing, co-precipitation, hydrothermal, wet kneading, sol-gel and so on. Among the methods considered, the sol-gel synthesis has been found suitable for obtaining an intimate mixing of components [124]–[128]. The above-mentioned methods are conventionally used to prepare materials with a Mg/Si atomic ratio ranging from 1 to 5. For instance, in recent studies, it has been stated that the wet kneading method is best suited for obtaining active catalysts for the Lebedev reaction (with a max. 16% yield to butadiene), but this concerned the case of an equimolar Mg/Si ratio [88], [129]. Conversely, in this research a wider ratio between the two cations is explored with the aim of investigating the role of Si^{4+} when used as a dopant for MgO and how it affects the performance in ethanol transformation into olefins.

3.2.2 Characterization of MgO–SiO_2 catalysts

The results of powder X-ray diffraction (XRD) for the synthesized samples are presented in Figure 41. There it is possible to observe that the materials with higher Si content were mainly amorphous with just weak reflections corresponding to MgO. Instead, when the Mg/Si ratio was increased, the intensity of lines attributable to the MgO phase increased concomitantly. In the intermediate range (Mg/Si=2-9), some small reflections were detected corresponding to another crystalline phase. These peaks (whose relative maximum intensity was for Mg/Si=3) were identified as a forsterite-like phase

(Mg_2SiO_4). On the other hand, when the Mg/Si ratio was higher than 9 the Si atoms (or silica domains) were well dispersed in the crystalline matrix of MgO. This interstitial dispersion was verified by the fact that the lines corresponding to MgO in the mixed samples were shifted toward lower 2θ values compared to pure MgO (Figure 42) and this suggests an expansion of the cubic cell volume for MgO, which cannot be explained by a replacement of the Mg^{2+} cation (size 86 pm) for Si^{4+} (size 54 pm).

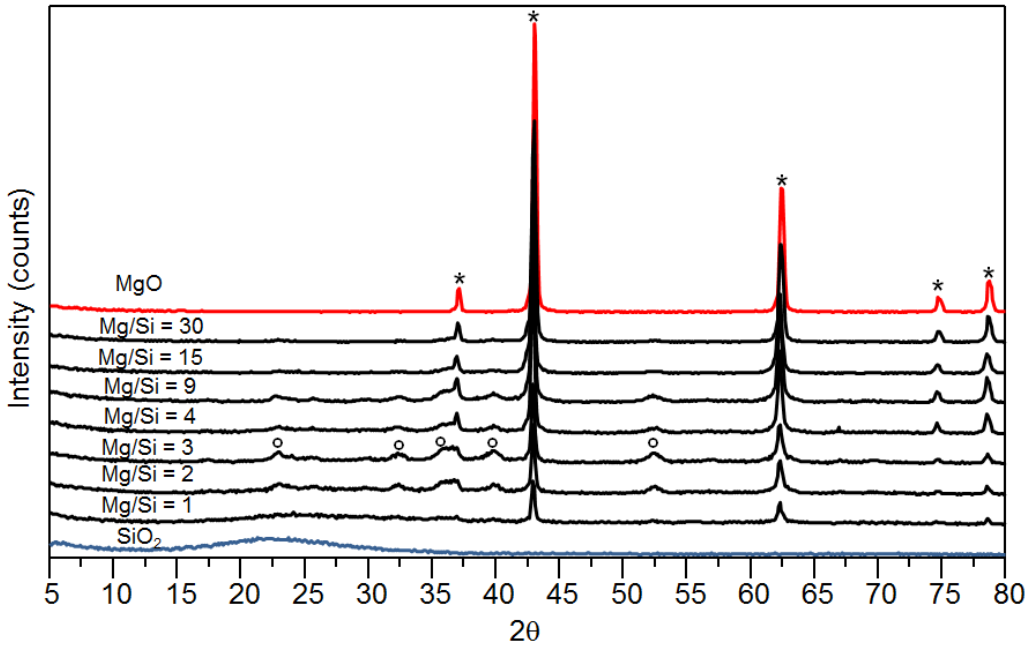

Figure 41. XRD patterns for the synthesized materials (*) MgO diffraction peaks (JCPDS 01-077-2364) (°) Mg2SiO4 (Forsterite) diffraction lines (JCPDS 01-085-1364).

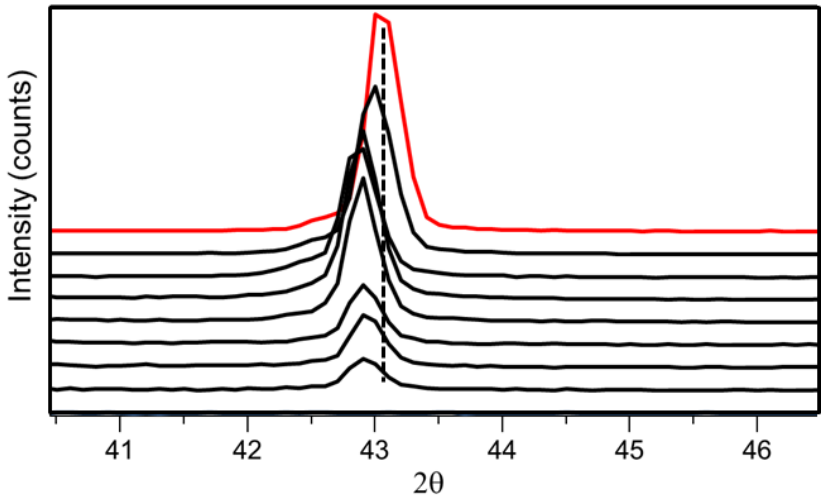

Figure 42. Zoom of the main peak for Figure 41

The analysis by Attenuated Total Reflectance (ATR, Figure 43) showed that Si^{4+} was not segregated as amorphous SiO_2 but instead it formed silicates (except, perhaps, for materials with Mg/Si ratio equal to 1 and 2). For samples with Mg/Si ratios from 3 to 9, the spectra correspond well to a forsterite-like compound, which was in agreement with XRD results. On the other hand, materials with Mg/Si ratios of 15 and 30 showed more defined vibration bands. These bands in the region from 800 to 1100 cm^{-1} are related to the internal Si–O vibration modes of SiO_4 tetrahedra. The shift of bands could be due to the combination of Mg–O stretching force constants with that of the Si–O bond, which results in a higher silicate stretching frequency. Especially the highest-frequency band appears predominantly shifted, due to the particular environment of these Si–O tetrahedral when surrounded mainly by Mg–O species. These shifts and the fact that in the XRD pattern only MgO is visible confirm that – in this case – Si atoms were well dispersed in MgO.

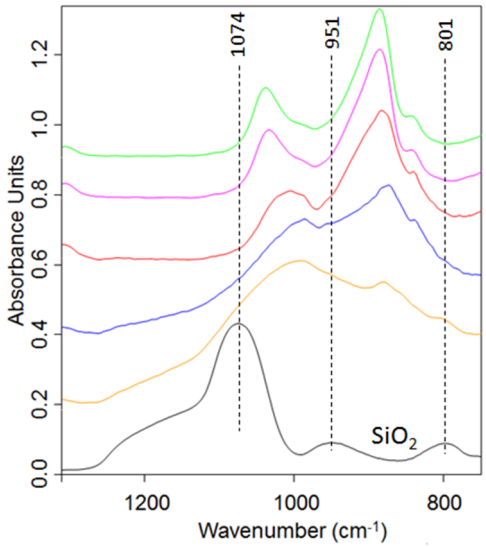

Figure 43. ATR spectra of the samples having different Mg/Si ratio

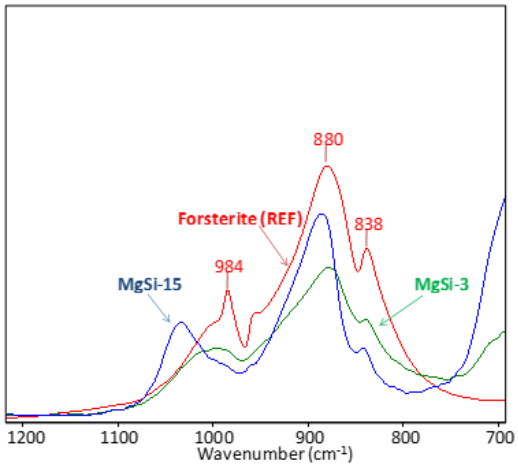

Figure 44. ATR comparison with forsterite

The samples were also analyzed by means of NH_3 temperature programed desorption (NH_3-TPD). Results presented in Table 10 show that the acidity was greatly affected by the Mg/Si ratio. In fact, the number of acid sites per unit surface area increased from SiO_2 up to sample MgSi-9, where the concentration of acid sites was almost 6 times that of silica. However, a further increase in the Mg/Si ratio led to a slight decrease in acid site density up to MgO, which showed no ammonia adsorption at all. It is worth noting that this was not due to its low surface area, since an analogous result was observed with a MgO sample prepared by the conventional precipitation method from a $Mg(NO_3)_2$ solution, showing a surface area of around 80 $m^2\ g^{-1}$ after the calcination treatment.

Table 10. Surface area and acidity results for the synthesized samples

Catalyst	A_BET (m^2/g)	Acid sites number*(10^{-6} mol/g) (Tmax)	Acid sites density*(10^{-6} mol/m^2)
MgO	2	--	--
Mg/Si = 30	12	23,5 (204°C)	2
Mg/Si = 15	21	44,5 (255°C)	2,1
Mg/Si = 9	25	57,5 (232°C)	2,3
Mg/Si = 4	38	56,0 (252°C)	1,5
Mg/Si = 3	47	69,3 (281°C)	1,5
Mg/Si = 2	63	51,6 (249°C)	0,8
Mg/Si = 1	102	72,0 (256°C)	0,7
SiO_2	24	10,8 (190°C)	0,4

Observing the ammonia desorption profiles of samples (Figure 45) it is possible to state that MgSi-1 has a greater acidity than silica, not only in terms of acid site density but also of strength, with a broad desorption band that covered almost the whole temperature range. Instead, the increase in Mg/Si ratio caused the desorption profile to narrow, while the temperature at which it reached its peak shifted to lower temperatures, indicating a weaker acidity. The sample with Mg/Si=30 showed the weakest acid strength. These results are similar to Niiyamas' findings, in the sense that the most acid material (holding the strongest sites) is the equimolar one (Mg/Si = 1) [79].

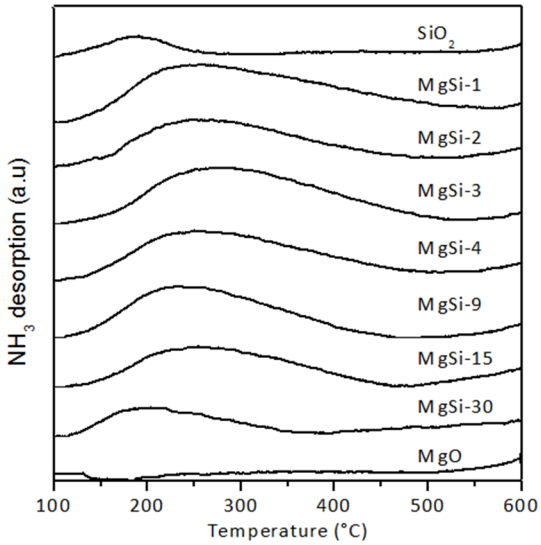

Figure 45. NH3-TPD profiles for the different Mg/Si sol-gel materials

Some samples were selected to perform studies of pyridine adsorption. Figure 46 A shows the results during adsorption on MgSi-4 at 50°C. From these spectra it is clear that the dominant acid sites in this material are of Lewis type (strong): 1436 cm^{-1} and 1599 cm^{-1} for the 19b and 8a modes [130] and the bands arising at 1580 and 1484 cm^{-1} are due to the adsorption of pyridine on weaker Lewis sites. However, the spectrum acquired after the flushing with He for at 400°C, showed that only the bands for the strong Lewis sites remained (Figure 46 B). The adsorption of pyridine was repeated by first inducing a water pre-adsorption (Figure 46 C) and it is shown that water generated Brønsted acid sites (bands at 1542 and 1648 cm^{-1}) by interaction with Lewis sites and this is important because during the reaction there is water formation and the generation of this type of site can induce dehydration or other acid-catalyzed reactions.

For the synthesized materials it can be said that the Mg^{2+} ion, which is a very weak Lewis acid site, acts as a medium-strength Lewis acid site in the mixed catalyst. In fact, the acidity-enhancement effect on Mg^{2+} increased when the Si content in catalysts increased being the MgSi-30 the sample that showed the weakest acid strength. This may be due to the fact that the charge withdrawal on Mg^{2+} sites – due to the presence of neighboring Si^{4+} atoms – was more efficient when the number of Si atoms close to each Mg^{2+} site was increased compared to MgSi-30. It is important to notice however, that even though the number of acid sites clearly increased with the concentration of Si in catalysts, their number was not simply directly proportional to the latter value (Table 10), as may be expected if the relative amount of the two cations in the structure (and on the surface) is taken into account.

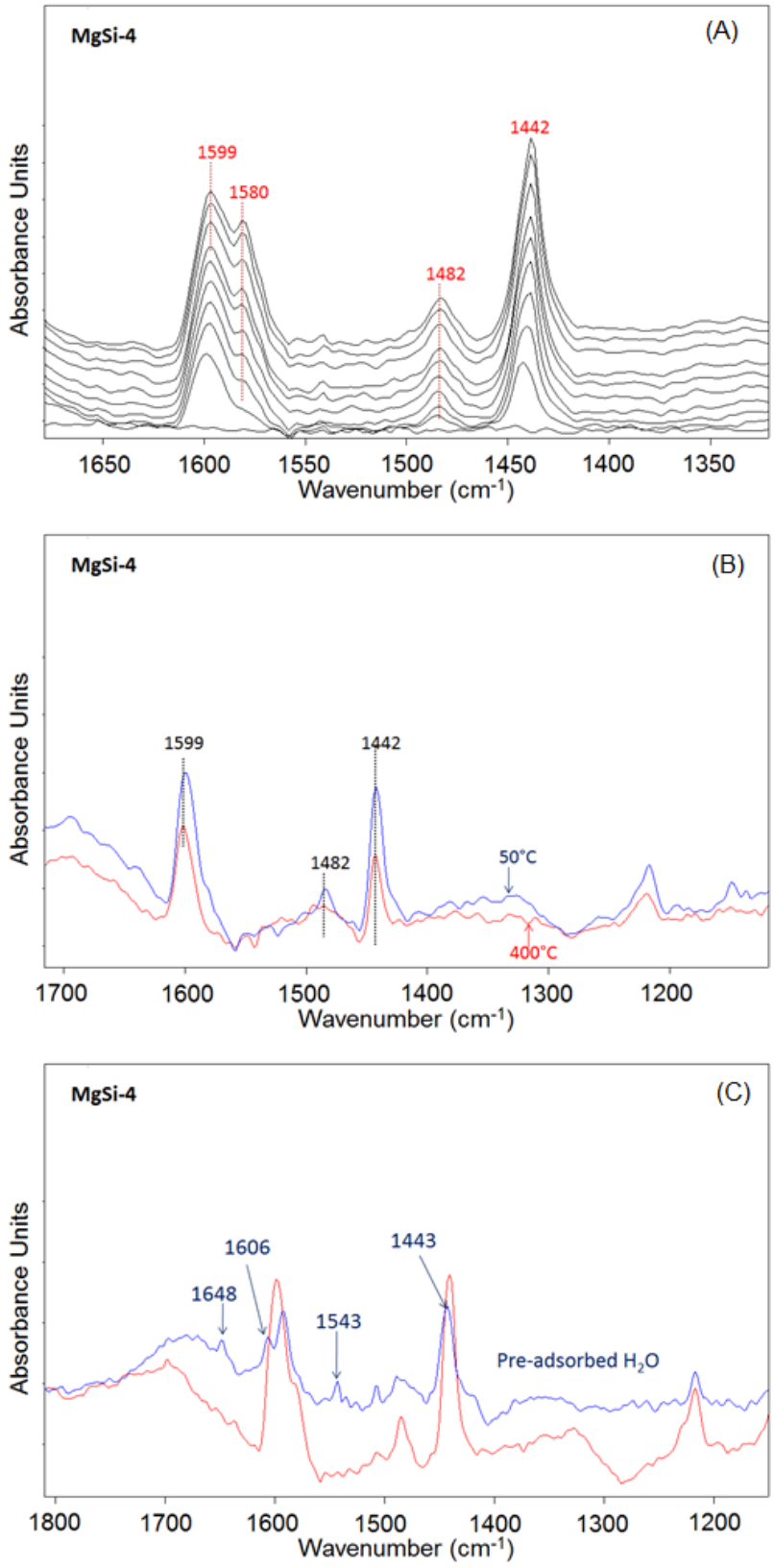

Figure 46. Continuous adsorption of pyridine on MgSi-4 at 50°C (A). Pyridine remaining on the surface after evacuation with He at 50°C and 400°C (B) and comparison with pyridine adsorption but pre-adsorbing water (C),

When pyridine adsorption was carried out with the sample MgSi-1 a blue-shift of the band attributed to the interaction of pyridine with the Lewis site indicated a stronger acidity of that site (see Figure 47).

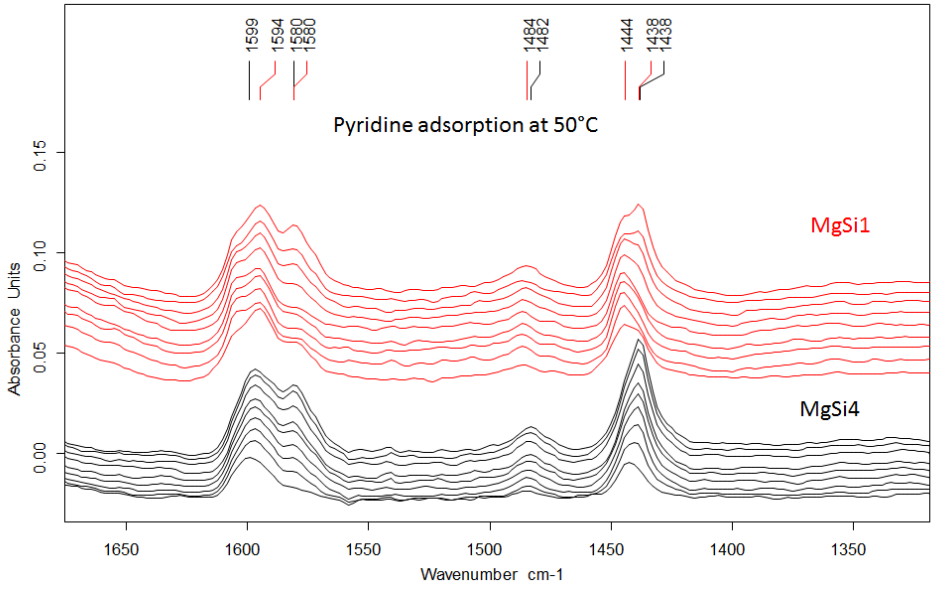

Figure 47. Continuous adsorption of pyridine at 50°C on MgSi-1 (UP, red) and MgSi-4 (BOTTOM, black)

The acid–base properties of MgO–SiO_2 catalysts prepared by kneading magnesium hydroxide with colloidal silica, in terms of Mg/Si ratio, have been investigated previously by other authors. For example, Niiyama et al., [79] concluded that acidity reaches its peak for the equimolar Mg/Si ratio while, on the other hand, basicity increases continuously with the increase of MgO. However, they also observed a "limit" in the rate of butadiene formation, which reached its peak for a content of MgO of 85% mol (Mg/Si = 5.7; higher ratios were not explored). Weckhuysen and co-workers [129] studied the acidity of the equimolar MgO–SiO_2 catalysts prepared by different methods, and concluded that the wet kneaded ones were performing better due to the appropriate balance among a small amount of strong basic sites, combined with an intermediate amount of acidic sites and weak basic ones. Makshina et al., [85] studied systems prepared by different methods in the Mg/Si range of 0–3. They observed that even large variations in dispersion and crystallinity of the basic component (MgO) had little impact on the butadiene yield, whereas a change in the acidic component (silica) could drastically modify the selectivity; in their case, when Grace silica gel 254 was used as the support, the optimal ratio was Mg/Si = 2. On the other hand, our acidity measurement experiments highlight that in

samples prepared by means of sol–gel, the dispersion of Si^{4+} in the MgO lattice occurring when the Mg/Si value is high generates Lewis acid sites which are associated with Mg^{2+} cations in the proximity of Si^{4+}. Not only the number, but also the strength of these sites is affected by the Mg/Si atomic ratio used. In addition, in the presence of steam, these sites are transformed into Brønsted sites. In samples with the lowest Mg/Si ratio (lower than 9 but higher than 2), the formation of Mg silicate domains (forsterite) leads to an even higher acid strength, with levelling in the number of acid sites and reduced density. Finally, samples showing the strongest acidity were those having the lower Mg/Si ratio (MgSi-1 and MgSi-2); for these samples no evidence for the formation of Mg silicate was seen, and domains of SiO_2 and MgO were likely formed.

Analyses via SEM–EDX were also performed in order to check the homogeneity of samples. In general, with samples having the lower Mg/Si ratio (Figure 48) the presence of particles of different sizes was observed; larger particles, of more regular shapes, showed a Mg/Si atomic ratio close to the expected one, whereas other smaller particles were made of MgO alone, more rarely of SiO_2, or showed a Mg/Si ratio higher than the nominal one. This is shown, for example, in Figure 48 for the sample MgSi-4. Conversely, samples with higher Mg/Si ratios were more homogeneous, with all spots analyzed containing both Mg and Si (Figure 49).

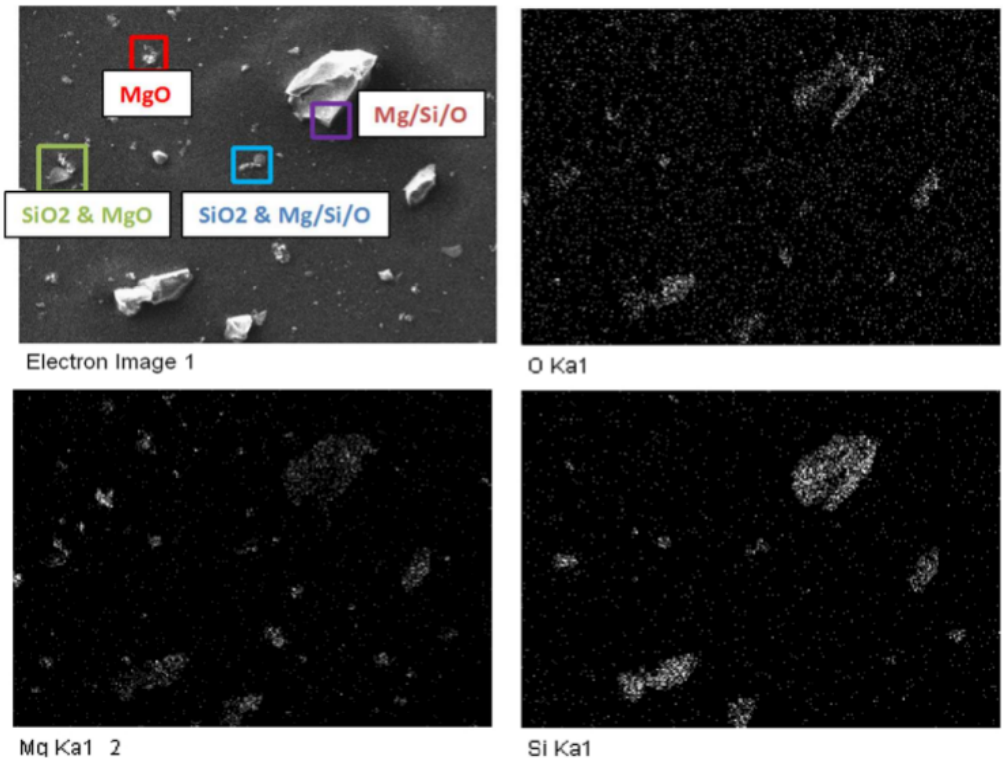

Figure 48. SEM-EDX analysis for the MgSi-4 sample

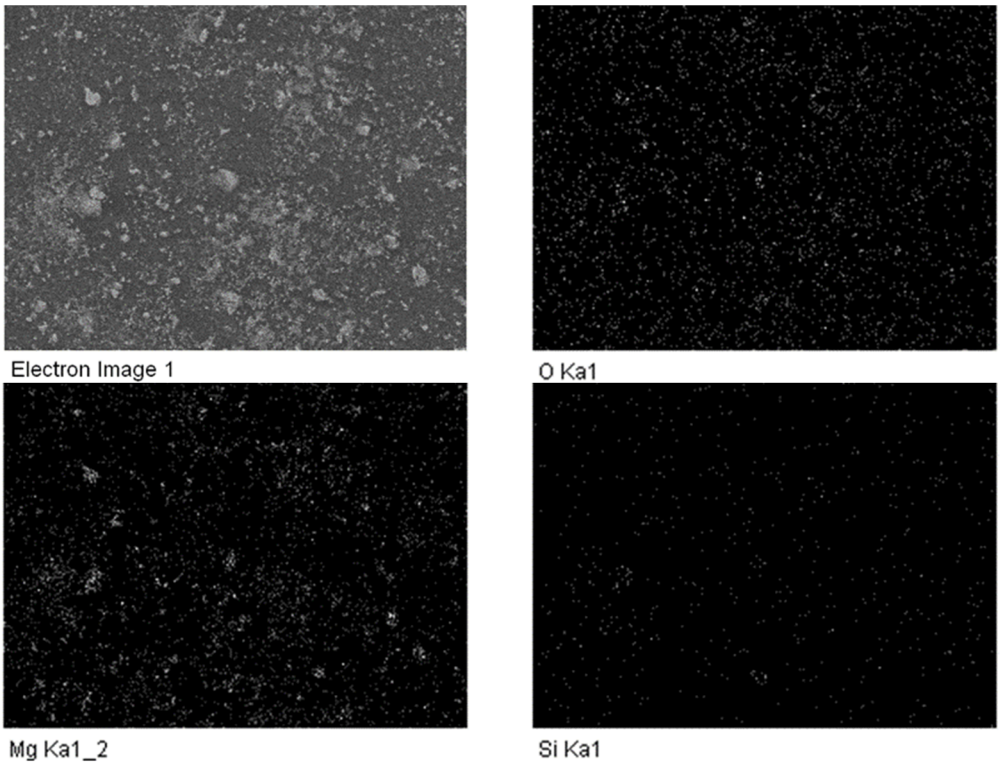

Figure 49. SEM-EDX analysis for the MgSi-15 sample

3.2.3 Reactivity of MgO–SiO_2 catalysts in the Lebedev reaction

Mixed Mg–Si oxides are the main components of industrial catalysts for the Lebedev process (butadiene from ethanol). However, their catalytic performance is highly dependent on the synthesis method, the Mg to Si ratio, and experimental conditions. A recent review by Sels and co-workers [73] shows that the yields obtained (for undoped Mg–Si materials) cover a broad range between 9–37% with a 20–62% selectivity (not taking into account the values reported by Ohnishi et al., since their results were not reproducible and were obtained at the very beginning of the catalyst lifetime). These studies, however, are limited to materials with a Mg/Si molar ratio between 0.8 and 6, and higher values were not explored in the literature, even when the best results were obtained with a Mg/Si > 3. In the present study, in fact, the best results were obtained for the materials with a Mg/Si ratio ranging between 4 and 15, higher than that reported in the literature for this type of catalyst. This can be seen in Figure 50, which shows the conversion of ethanol (top) and the selectivity to (i) butadiene, (ii) ethylene, (iii) acetaldehyde + alkenols + butadiene, and (iv) 1-butanol + butenes (bottom), as a function

of the Mg/Si ratio, under fixed reaction conditions. Details of the yields of all products are shown in Table 11.

As reported in the precedent chapter, with MgO the formation of ethylene and the main C4 products (1-butanol and butadiene) occurs by means of kinetically parallel routes, where the alcohol is formed by the direct condensation of two ethanol molecules (Guerbet reaction), whereas the diolefin is formed by reaction between ethanol and acetaldehyde, leading to alkenols (mainly crotyl alcohol) via water elimination; the latter dehydrates in the end to butadiene (Figure 51). Therefore, if this is what happens for MgO–SiO_2 samples as well, the selectivity to (i) ethylene, (ii) 1-butanol + butenes, and (iii) acetaldehyde + alkenols + butadiene should be almost independent from ethanol conversion. In fact, tests carried out with MgSi-4 by varying the contact time under isothermal conditions (Figure 52) demonstrated that within a certain range of ethanol conversion (between 40 and 60%), the distribution of products was only marginally affected.

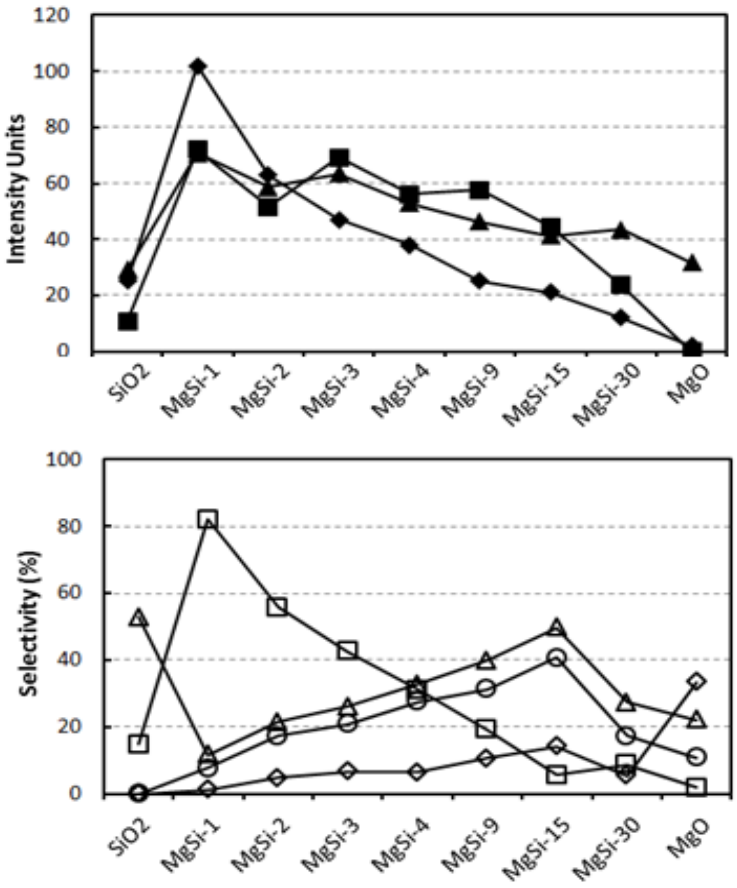

Figure 50. Top: % conversion of ethanol (▲) (reaction conditions: feed ethanol 2% in N2, T=400°C contact time 0.41 s), surface area (m2/g) (◆), and overall number of acid sites (10-6mol NH3/g, see Table 1) (■) for the various MgSi samples. Bottom: selectivity to ethylene (□), acetaldehyde + alkenols + butadiene (△), 1-butanol + butenes (◇) and butadiene (○) at 400°C for various MgSi samples.

Table 11. Results of catalytic experiments with catalysts at 400°C and 0.4 s contact time.

Yield (%)/ Catalyst	*SiO2*	*MgSi-1*	*MgSi-2*	*MgSi-3*	*MgSi-4*	*MgSi-9*	*MgSi-15*	*MgSi-30*	*MgO*
Ethanol conversion.	29.2	70.8	58.6	63.5	52.8	46.2	41.2	43.5	31.6
Butadiene	0	5.4	10.1	13.2	14.5	14.5	16.8	7.5	3.4
Ethylene	4.3	53.2	32.7	27	16.4	8.9	2.3	3.8	0.6
Butenes	0	0.7	2.8	4.0	2.8	1.4	0.5	0.1	0
propylene	0	0.2	1.4	2.4	1.5	0.8	0.3	0	0.1
Acetaldehyde	15.4	2.8	2.4	3.0	2.3	2.2	2.4	2.0	3.6
Acetone	0.5	1.1	1.9	3.0	1.9	3.7	3.1	1.9	3.6
Diethylether	5.3	7	4.6	4.1	2.9	1.6	1.1	0.7	0.4
Butanal	0	0	0	0	0.1	0	1.3	0.2	0
Ethylacetate	0.3	0	0	0	0.1	0.9	1.5	0.4	0.5
Alkenols	0	0	0.1	0.4	0.5	1.7	1.3	2.4	0
1-butanol	0	0	0.1	0.2	0.4	3.6	5.3	2.2	10.5
balance	88	99	96	90	82	85	87	49	72

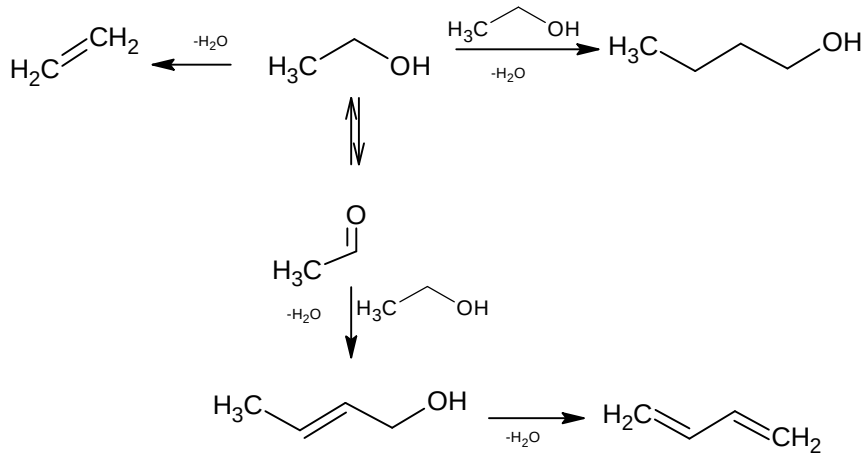

Figure 51. The three main parallel reaction pathways by which ethanol is transformed over MgO-based catalysts

Ethanol conversion (Figure 50, Top) with MgSi-1 was higher than that shown by SiO_2, and a further decrease of Si content led to a decreased conversion, until the lowest value shown by MgO. Conversion was not obviously correlated with the overall amount of acid sites, and did not correspond to the acidity strength. This fact, agrees with our recent findings that on MgO, key steps in ethanol activation are the formation of ethoxide species (which evolves to the formation of acetaldehyde), and the generation of a

stabilized carbanion species of ethanol, which further evolves either by dehydration to ethylene or by reaction with adsorbed ethanol and acetaldehyde (See precedent chapter); and both events are obviously related to catalyst basicity.

On the other hand, it may be expected that acid sites are also involved in ethanol conversion with MgO–SiO_2, because of the primary reaction of ethanol dehydration, which provides an additional contribution to ethylene formation. In this case, a correlation between ethanol conversion and surface area was seen (Figure 50, Top), even though the relationship between the two was not that of a direct proportionality; in other words, the increase in conversion seen for samples at increasing Si content (until MgSi-1) was lower than the increase in the surface area. This may be attributed to the basic strength of MgSi samples with a higher Mg/Si ratio which was greater than that of samples with a lower ratio (see below). It may thus be concluded that a low Mg/Si ratio leads to a decrease in surface basicity (and an increase in acidity), with a concomitant increase in the surface area and activity (conversion).

As regards the distribution of products (Figure 50, Bottom), an increase in the content of Mg from MgSi-3 to MgSi-15 improved the selectivity to butadiene and, even though the conversion decreased, the butadiene yield was slightly higher (13.2 vs. 16.8% for MgSi-3 and MgSi-15, respectively), the maximum selectivity to butadiene was seen at Mg/Si = 15. The selectivity to 1-butanol (added to the one of butenes, a consecutive product of alcohol dehydration) showed a similar trend, with the exception of MgO, whose selectivity was higher than that shown by MgSi-30. The latter sample was the one providing the lowest overall yield of useful C4 products and the greatest yield of heavy compounds (see Table 11). Conversely, when the Si content was too high (at low Mg/Si ratio), the materials showed high yield and selectivity toward ethylene. The intermediate Mg/Si ratio values (samples MgSi-9 and MgSi-15) were those showing both the greatest selectivity to C4 compounds and the lowest selectivity to ethylene. Silica gave a high selectivity to acetaldehyde, but with low ethanol conversion. It is also noteworthy that while MgO showed some butadiene production, SiO_2 alone produced mainly acetaldehyde, diethylether, and some ethylacetate, but not butadiene (Table 11).

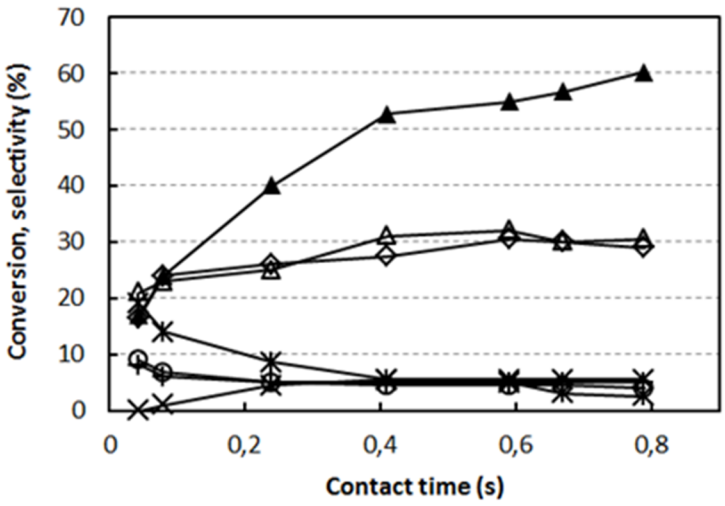

Figure 52.Effect of contact time on catalytic performance of MgSi-4 catalyst. Temperature 400°C, feed 2% ethanol in N2. Symbols: ethanol conversion (▲), selectivity to butadiene (◇), ethylene (△), acetaldehyde (✳), acetone (+), butenes (×), diethylether (○).

Interestingly, when comparing kinetic results for MgSi-4 (Figure 52) with those obtained with MgO (Figure 19) the same products were obtained with the two catalysts, with similar trends as well. The relative amount of each compound was different in the two cases but this is clearly related to the introduction of acid properties on the samples. For the former case (MgSi-4) the most abundant products detected for the whole range of residence times investigated were ethylene and butadiene, followed by acetaldehyde and butenes, at lower and higher contact times, respectively, and by acetone and diethylether. Other minor by-products (not shown in the figure) were 1-butanol, propylene, butyraldehyde, and the three alkenol isomers: 3-buten-1-ol, 2-buten-1-ol (crotyl alcohol) and 1-buten-3-ol. Taking into account all products, the C balance was in the 80–90% range, and was not much affected by the conversion degree; indeed, heavy compounds formed under all conditions, and were not identified, although eluted in the GC column. As expected, acetaldehyde appeared to be a kinetically primary product undergoing consecutive transformations, whereas both butadiene and butenes were consecutive products: indeed, the extrapolation of butadiene selectivity toward zero contact time was approximately nil, and butenes were not detected even at the lowest contact time value.

Regarding ethylene, its behavior seemed to be the result of two contributions: when selectivity was extrapolated to nil residence time it was clearly higher than zero, indicating its kinetically primary nature; however, the selectivity trend increased with residence time, which is the typical behavior for a consecutive product. Several studies on the reaction mechanism of ethanol dehydration to ethylene over acid catalysts have been reported in the literature, but this mechanism is still controversial [9]. The major

controversy lies in whether ethylene is directly generated from ethanol or also consecutively from diethylether (DEE), which is the main by-product of the process with several acid catalysts. In order to verify DEE involvement as an intermediate molecule in ethanol conversion into ethylene on our catalytic systems, the ether was fed over MgSi-4 at the reaction temperature of 400 °C and 0.4 s residence time. A low DEE conversion of 7% was observed, with ethylene actually being the main reaction product. Therefore, in this case, direct ethanol dehydration appears to give the greatest contribution to ethylene formation. However, a minor contribution deriving from DEE cracking should also be taken into account.

As suggested in the previous chapter, the formation of butadiene occurs by reaction between acetaldehyde and ethanol which form an adsorbed species (chemically related to 1,3-butanediol) that then dehydrates and desorbs into the gas phase, yielding the precursors of butadiene (alkenol). With regard to the latter step, the dehydration of 1,3-butanediol can give rise to three different isomers: 3-buten-1-ol, 2-buten-1-ol (crotyl alcohol), and 3-buten-2-ol. It is expected, however, that these three compounds are not formed in equal amounts, with the formation depending on the two types of mechanism by which dehydration occurs (either acid- or basic-catalyzed). Therefore, in order to infer more details of the reaction mechanism with $MgO–SiO_2$ catalysts, the three C4 alkenols were fed over MgSi-4, at 400 °C and 0.4 s residence time (results reported in Table 12).

Table 12. Direct dehydration of alkenols

Reagent	*Conversion (%)*	*Yield (%)*		
		1,3-BDE	propene	2-butenal
2-buten-1-ol	99,9	86	0,3	traces
3-buten-1-ol	95	13	15	9
3-buten-2-ol	99,9	68	0,3	-

It is evident that crotyl alcohol (2-buten-1-ol) was more efficiently dehydrated into butadiene, showing yields up to 86% on total conversion. 3-Buten-2-ol was also converted into butadiene quite efficiently (68% yield on total conversion) but a greater amount of heavy compounds was observed. Conversely, 3-buten-1-ol behaved in a very different manner, showing a much lower yield of butadiene (only 13% at 95% conversion) together with extensive formation of heavy compounds. Moreover, significant yields of propylene and crotonaldehyde were obtained. This might suggest that

the final dehydration step (from alkenols to butadiene) preferably occurs in the presence of acid sites; otherwise, if an anionic-type mechanism via H+ abstraction by a basic site would take place, the dehydration of 3-buten-1-ol should lead to the formation of butadiene. Conversely, an acid-catalyzed dehydration would occur preferably on crotyl alcohol, because of the delocalization of the positive charge generated on the primary C atom after water elimination, and on 3-buten-2-ol as well, because of the formation of a cation on the secondary C atom.

Kinetic experiments were also performed by co-feeding water with ethanol on MgSi-4. Since water is generated during the transformation of ethanol into butadiene and other by-products, the aim of this experiment was to determine whether the presence of water may affect the reactivity of the catalyst. Therefore, we co-fed an amount of water which corresponds to approximately 70% of the amount which is generated in situ during the reaction. The results of these experiments are presented in Table 13, and compared with tests without co-fed water carried out under the same conditions.

Table 13. Ethanol conversion at 400°C over MgSi_4 at 0,4s residence time: effect of water in the inlet feed.

Feed	*Ethanol 2% in N_2*	*Ethanol 2% + 0,5% H_2O In N_2*
X EtOH (%)	53	24
1,3 BDE (%)	29	18
Ethylene	27	49
Butenes	6	tr
Propylene	3	tr
Acetaldehyde	4	10
Acetone	4	9
Ethylether	4	8
1-Butanol	1,5	1
Heavies	16	-

When water was co-fed, a poisoning effect was seen; indeed, the presence of water led to a considerable decrease in ethanol conversion and also greatly affected product selectivity. A selectivity increase was recorded for ethylene, and also, to a minor extent, for the other kinetically primary products such as DEE and acetaldehyde, and for acetone as well. On the other hand, a drop in the selectivity of secondary products such as butadiene, butenes, and propylene was also observed. This effect may in part be related to the strong decrease in ethanol conversion, but also to the change in the nature of active sites, as in the case of ethylene, whose formation mainly comes from Brønsted-type acid sites. These results, together with FTIR spectra recorded during water + pyridine adsorption, reveal that water generated during the reaction is responsible for the in situ generation of Brønsted sites; unfortunately, this leads primarily to a strong increase in ethylene selectivity.

3.2.4 In situ DRIFTS studies

First a DRIFT spectrum of each catalyst after thermal treatment at 400°C in a flux of He was acquired. Figure 53 shows the results obtained for the samples with different Mg/Si ratio. It is usually agreed that OH stretching is highest for terminal OH groups, whereas intermediate and low frequencies indicate bridging OH groups [131], [132]. Here, the parent MgO shows a band at 3745 cm^{-1} assigned to a Mg–OH hydroxyl group in which the oxygen is mono-coordinated with Mg. When the amount of Si in the material was low, the OH stretching shifted to 3678 cm^{-1} which indicates an increase in the coordination number of the oxygen, but in this case the OH group is multi-coordinated to Mg and Si atoms (or the Mg–OH is affected by the neighboring Si^{4+}). However, when the Si content increased, the intensity of this band decreased and the band at 3738 cm^{-1} started to raise, a phenomenon which might be due to the presence of isolated Si–OH groups on the surface. The presence of this acid group correlates with the tendency of materials to produce ethylene (which means that the presence of free terminal Si–OH induces dehydration). The band at 3481 cm^{-1} may be assigned to OH groups which interact with O^{2-} species [132], and this band is only present when Mg/Si > 4.

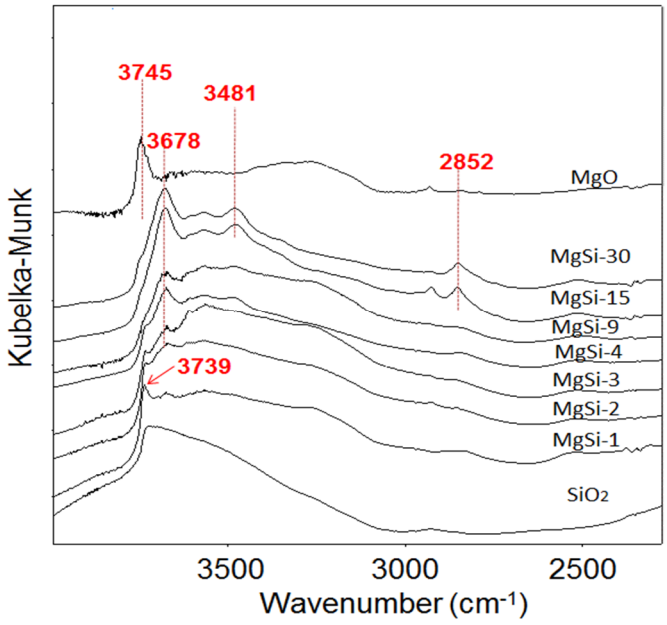

Figure 53. DRIFT spectra of the Mg-Si catalysts at 400°C.

In order to understand the interaction of the alcohol with the surface of this catalysts, some experiments were performed by adsorbing ethanol at 85 °C (see Figure 54 A) and then desorbing it at 400 °C (Figure 54 B). The spectrum of the catalyst was subtracted, so the bands observed correspond to the surface species created by ethanol adsorption and transformation.

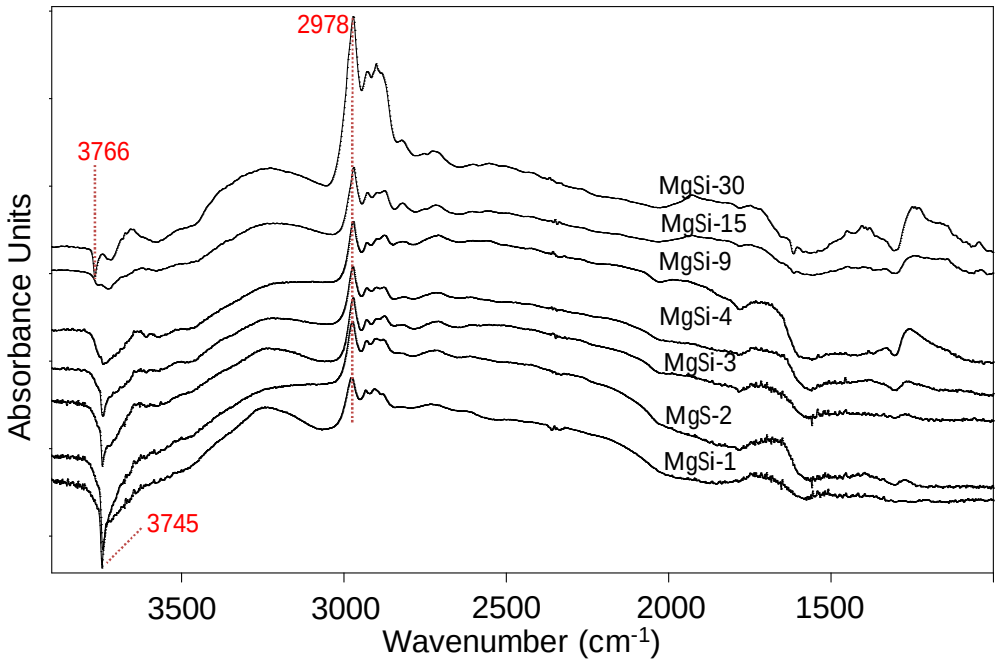

(A)

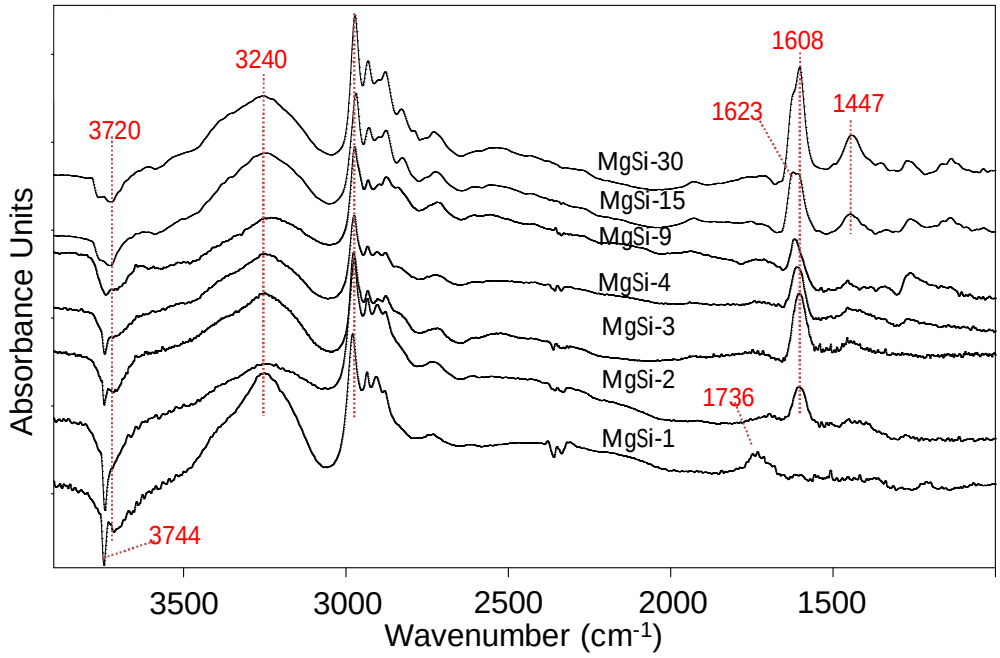

(B)

Figure 54.Ethanol adsorbed at 85°C on the different Mg-Si materials (A) and after thermal treatment at 400°C (B).

In the case of adsorption of ethanol at 85 °C, a sharp negative band in the OH stretching region appeared for MgSi-1 (3745 cm^{-1}). This negative band indicates that the alcohol interacts with the terminal OH groups but when the Mg/Si ratio was increased, the intensity of this band decreased and it became broader, suggesting that the adsorption of ethanol was less strong and that it took place at different sites, including the multi-coordinated OH groups observed before (Figure 53). The fact that some OH groups were disappearing (since the subtracted OH band is negative), might indicate that a direct dehydration reaction plays an important role especially when the Si content is high. After the thermal treatment at 400 °C and quenching, the negative band still was present, suggesting that the loss of the hydroxyl groups is an irreversible process. In this case, also some bands in the low frequency region appeared (Figure 54 B). For MgSi-1, the band at 1743 cm^{-1} can be attributed to the C=O stretching of acetaldehyde (thus in this case it does not desorb easily) but then, starting from MgSi-2, a band appeared at 1604 cm^{-1} whose intensity increased for MgSi-3 but then decreased when the Mg/Si ratio was ≥4, and a band at around 1623 cm^{-1} started to appear and grow (See a zoom in Figure 55). This band has been previously assigned in the MgO chapter to an adsorbed form of crotyl alcohol, which is the butadiene precursor. Starting from MgSi-9 and above, a band at 1605 cm^{-1} increased again but in this case it might be attributed to the formation of

carbonates in the most basic materials or even acetates (as shown by the presence of other bands at 1447 and 1338 cm^{-1}, the OCO ν(s) and CH3 δ(s) typical of this moiety). Therefore, catalyst basicity should be strong enough to favor the dehydrogenative pathway until crotyl alcohol, but when it is too strong (as for the MgSi-30), it favors the formation of acetates and carbonates and lowers butadiene selectivity as well.

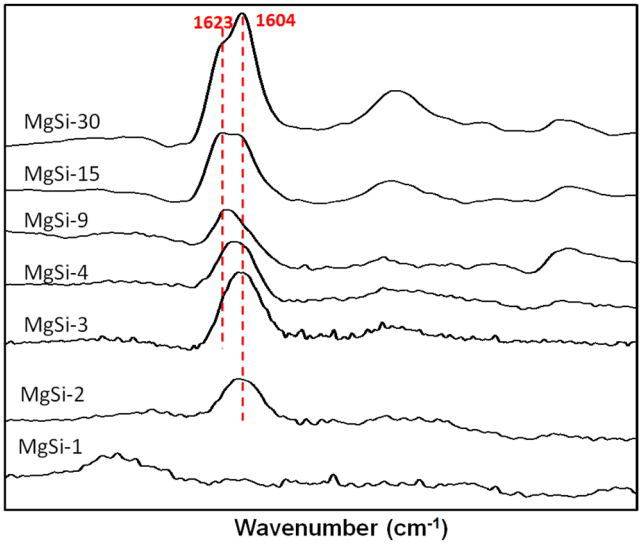

Figure 55. zoom centered at 1500 cm-1 for Figure 54

In order to verify that the band at about 1620 cm^{-1} is associated with intermediates for butadiene formation, more realistic conditions were reproduced by continuously feeding ethanol during the temperature program (Figure 56). In this case it was observed that the formation of intermediates such as ethoxy (the band at 1065 cm^{-1}), ethanol anion (1143 cm^{-1}) and adsorbed crotyl alcohol (1620 cm^{-1}) took place much more easily in the case of MgSi-15 compared to materials with a low Mg/Si ratio (MgSi-4), indicating that the former has a more appropriate balance of acid/base properties to promote the dehydrogenative pathway instead of the dehydration (ethylene) or condensation (butanol) routes.

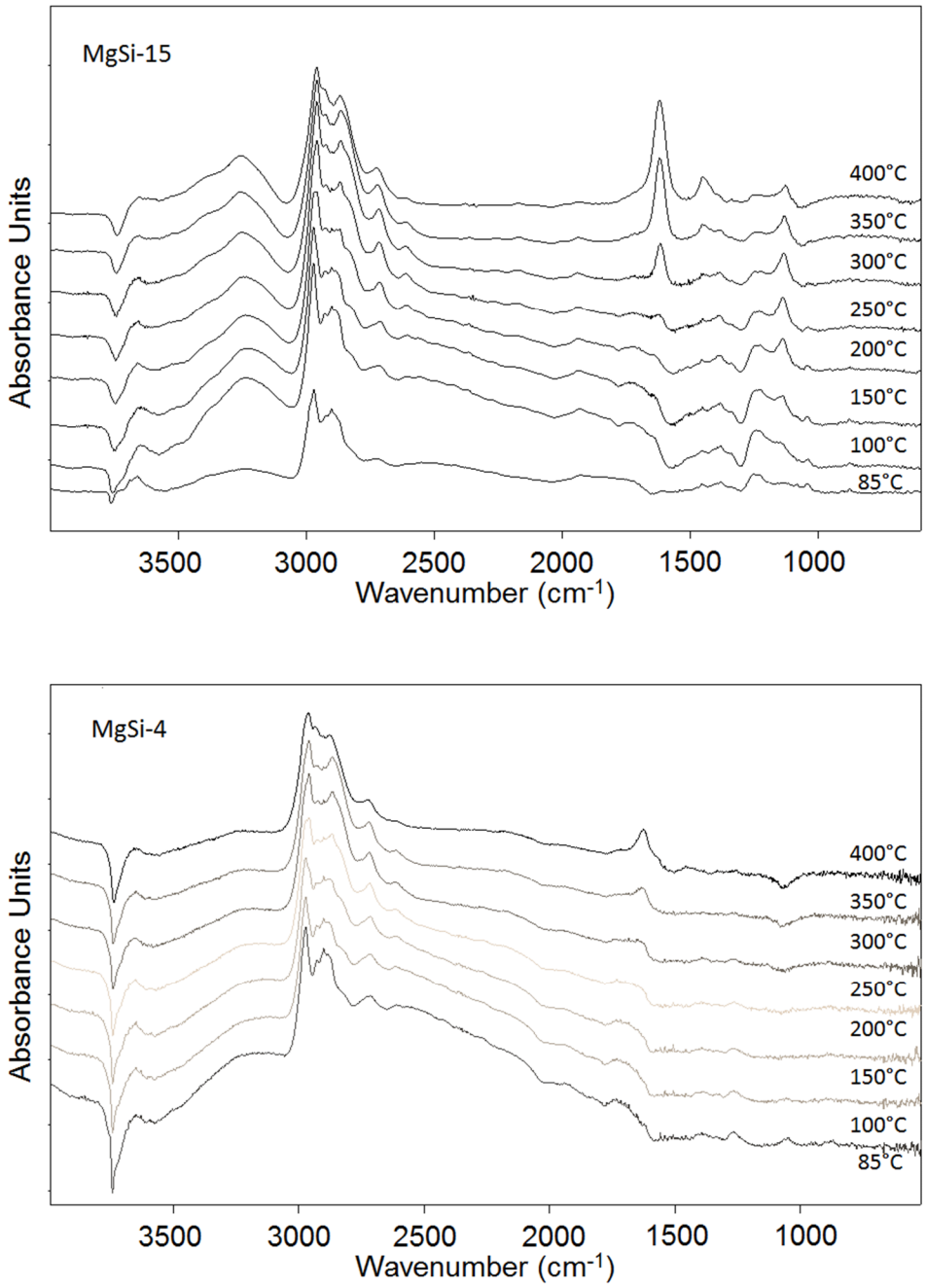

Figure 56. In-situ DRIFTS spectra of the MgSi-15 (Top) and MgSi-4 (Bottom)

Further tests were made by adsorbing CO_2 over MgSi-1 and MgSi-15 (Figure 57). The amount of CO_2 adsorbed at 400 °C on the latter catalyst was significantly higher than that shown for MgSi-1, which demonstrates the higher basicity of the MgSi-15 sample and also makes it possible to exclude the formation of carbonates in previous experiments, while facilitating the assignment of the bands observed.

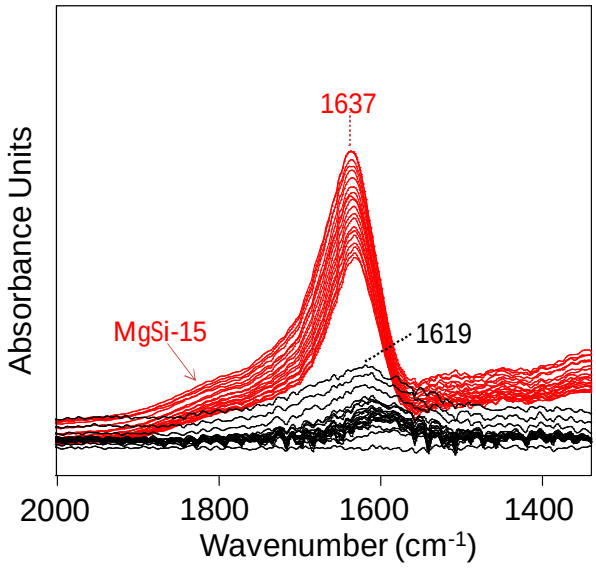

Figure 57. Adsorption of CO2 at 400°C over MgSi-15 (Red) and MgSi-1 (Black).

3.2.5 A model for the nature of active sites in MgO–SiO_2

In the literature, some studies have tried to explain the nature of active sites in MgO-SiO_2 systems. In this regard, Kvisle et al. [81] studied the mechanical and chemical mixtures of Mg and Si oxides and concluded that it is unlikely that their synergic effect is solely due to the presence of MgO in the SiO_2 or vice versa. Conversely, they mentioned the possibility that this result is related either to defects created on the MgO structure during synthesis or to new Mg–O–Si interactions. The review by Sels and co-workers states that the synthesis procedure should promote the formation of Mg–O–Si species, at the same time keeping the remaining MgO highly dispersed [73]. Natta and Rigamonti also mentioned a relationship between the activity and high dispersion of magnesia on silica and the presence of a limited amount of amorphous magnesia hydrosilicate phase resulting from the interaction of dissolved Mg^{2+} with the silanols of the silica surface [74], [114]. In the case of the present research, with the information discussed and the results obtained so far, it is possible to propose a model for these complex heterogeneous catalysts. In samples showing a high Mg/Si ratio, new sites characterized by a Lewis-type acidity are generated, associated with Mg^{2+}–O–Si^{4+} pairs; the acid strength of this site is related to the number of neighbouring Si^{4+} sites. These sites interact with the water generated in the reaction environment and are transformed into Brønsted acid sites; the latter possess the acid strength needed for the dehydration of intermediately formed alkenols into butadiene. Conversely, when the content of Si is too high, it segregates in a

forsterite phase and also as SiO_2 domains, creating a stronger acidity, which is detrimental for selectivity, because it favors ethanol dehydration to ethylene. Therefore the optimal acid strength is neither too weak (not sufficient for an efficient dehydration and leading mainly to the formation of heavy compounds, in an amount even greater than that observed with MgO only, as for MgSi-30) nor too high, because, in this case, the formation of ethylene becomes the prevailing reaction. Thus the optimal acidity is observed for Mg/Si values between 15 and 9, i.e. when the catalyst is made of Si^{4+} dispersed in MgO, and the formation of forsterite is minimal.

3.2.6 Relationship between acidic–basic properties and catalytic behavior

In the previous chapter, it was stated that ethanol activation and transformation into ethylene, 1-butanol, or butadiene (the latter via alkenols as intermediate compounds) may occur on MgO catalyst with the involvement of basic sites only. Combining the information reported in there and the one of this chapter, the following statements can be done:

a) The activation of ethanol occurs with the contribution of both basic sites (especially in samples showing greater basic strength, i.e., those with the higher Mg/Si ratio), and acid sites, especially in samples showing the greater acid strength (i.e., those with the lower Mg/Si ratio). Basic sites extract the proton either from the OH group, so generating an ethoxide species which is the precursor for acetaldehyde, or from the methyl group with the formation of a carbanion species. The latter reaction is as energetically demanding as the ethoxide dehydrogenation to acetaldehyde. The carbanion may then react with either another molecule of ethanol, generating 1-butanol, or with acetaldehyde, with the formation of crotyl alcohol, in both cases after elimination of one water molecule. Instead, acid sites contribute to ethanol dehydration to ethylene. The most active catalyst was MgSi-1, which showed a greater surface area. Silica was less active than MgSi-1 because of both its relatively low surface area and the absence of basic sites, whereas catalysts with higher Mg/Si atomic ratio were less active than MgSi-1, despite the stronger basicity, because of both the lower surface area and the lower number of acid sites.

b) The products distribution is affected by the number and strength of both acidic and basic sites, in a non-obvious manner. In the reaction pathway leading to butadiene, acidity plays a role in causing the dehydration of the intermediately formed alkenols. The presence of a small amount of Si^{4+} (as in MgSi-30) led to an increased surface area compared to MgO, and to the generation of acid sites, albeit of weak strength. In this case, only a limited increase in selectivity to butadiene was shown when compared to MgO, but the selectivity to 1-butanol (whose formation may occur with the involvement of basic sites only) was lower than that with MgO, while, at the same time, the formation of heavier compounds was considerably enhanced. A further increase in Si content, as in samples with Mg/Si ratios of 15, 9 and 4, led to an increased acidity in terms of the number, density, and strength of sites, which fostered the dehydration of intermediately formed alkenols to butadiene, thus finally leading to a strongly enhanced formation of butadiene, still with a low yield of ethylene. An even higher acidity, in samples with low Mg/Si ratio (<4), led to a considerably increased contribution of the acid-catalyzed dehydration of ethanol to ethylene: a reaction which greatly prevailed over the formation of C4 compounds. The same was true for 1-butanol dehydration to butenes; in samples with the highest Mg/Si ratio, 1-butanol selectivity largely prevailed over butenes, while the opposite was true for Mg/Si ratios lower than 9. Therefore, the greater selectivity to butadiene was shown by those samples which combined a strong basicity –necessary for dehydrogenating the ethoxide to acetaldehyde and for generating the carbanion species – with a medium strength acidity and a moderate density of acid sites, needed to efficiently dehydrate alkenols, while limiting ethylene formation. DRIFTS experiments confirmed the stronger interaction of ethanol with catalysts having greater Si content, which induced the preferred dehydration to ethylene.

c) Both key species, previously identified with MgO, crotyl alcohol and the carbanion formed by deprotonation of the methyl group, were also identified with MgO–SiO_2 catalysts, an event which confirms that the same mechanism formerly proposed for ethanol to C4 compounds with MgO is also valid with these bifunctional catalysts. Spectroscopic measurements also validated that the pathway leading to butadiene was the preferred one with catalysts having a higher Mg/Si atomic ratio, i.e., with MgSi-9 and MgSi-15, which agrees with the greater selectivity shown by these samples. Previously Niiyama et al [79] reported that a catalyst with 79 wt% of MgO (Mg/Si atomic ratio 5.7) showed a good acid–base balance, reaching a high butadiene formation rate, since at lower values ethylene formation was too high and after this value, butadiene formation

decreased. Unfortunately, 5.7 was the highest Mg/Si molar ratio investigated and the yield of products was not reported in this case. A thorough analysis of the role of basic and acid sites in $MgO–SiO_2$ catalysts was also reported by Angelici et al [129]. These authors found that the best performing catalysts are those containing a small amount of strong basic sites, combined with an intermediate amount of acidic sites. This statement is in line with our findings, with the difference that our results led us to conclude that the best Mg/Si ratio, showing the optimal combination of the different sites needed, is obtained for higher Mg/Si ratios than those reported in the literature, at least with our sol–gel catalysts.

3.2.7 Conclusions of the chapter

The reactivity of $MgO–SiO_2$ materials prepared by means of the sol–gel method, used as catalysts for the one-pot ethanol transformation into butadiene, was affected by the nature and amount of both basic and acid sites. The best catalysts, showing greater selectivity to butadiene, were those which combined a limited number of medium-strength acid sites with stronger basic properties. Samples showing these features were those with a Mg/Si atomic ratio between 9 and 15. In fact, a greater content of Si led to the formation of either forsterite or silica domains, with a considerable fraction of strong acid sites which finally gave rise to the preferred formation of ethylene. Conversely, in samples having a Mg/Si ratio higher than 15, the generation of a limited number of weak acid sites did not provide the acidity feature needed to efficiently dehydrate intermediately formed alkenols. An important role is played by Lewis acid sites of medium strength generated by Mg–O–Si pairs; these site might transform into Brønsted sites by interaction with the water generated during the reaction.

3.3 Mg-Si catalysts (varying the synthesis method)

In this chapter, a catalytic screening was performed with samples prepared by different synthesis methods and with the Mg-to-Si ratio in the range from 1 to 30. The following table summarizes the set of samples considered.

Table 14. List of samples to compare Mg/Si ratio and synthesis method

Label	*Mg/Si*	*Sources*	*Synthesis method*
MS1-O	1	$Mg(OH)_2$ and SiO_2 (from TEOS)	Wet kneading
MS2-O	2	$Mg(OH)_2$ and SiO_2 (from TEOS)	Wet kneading
MS9-O	9	$Mg(OH)_2$ and SiO_2 (from TEOS)	Wet kneading
MS15-O	15	$Mg(OH)_2$ and SiO_2 (from TEOS)	Wet kneading
MS30-O	30	$Mg(OH)_2$ and SiO_2 (from TEOS)	Wet kneading
MS1-L	1	MgO and SiO_2 (grace)	Wet kneading
MS2-L	2	MgO and SiO_2 (grace)	Wet kneading
MS9-L	9	MgO and SiO_2 (grace)	Wet kneading
MS15-L	15	MgO and SiO_2 (grace)	Wet kneading
MS30-L	30	MgO and SiO_2 (grace)	Wet kneading
MS1-SG	1	$Mg(NO_3)_2$ and TEOS	Sol-gel
MS2-SG	2	$Mg(NO_3)_2$ and TEOS	Sol-gel
MS9-SG	9	$Mg(NO_3)_2$ and TEOS	Sol-gel
MS15-SG	15	$Mg(NO_3)_2$ and TEOS	Sol-gel
MS30-SG	30	$Mg(NO_3)_2$ and TEOS	Sol-gel

3.3.1 Catalytic tests

The catalysts synthesized were tested under the "Lebedev conditions": 400°C, 2% Ethanol in N_2, 0,65 s of contact time and during 4 h of time on stream. The results are presented in the following graphs and discussed afterwards.

A) Figure 58. **Catalytic Results (SERIE MS*X*-O)** Wet kneading $Mg(OH)_2$ and SiO_2 (from TEOS) with X= Mg/Si atomic ratio= 1, 2, 9, 15 or 30.
B) Figure 59. **Catalytic Results (SERIE MS*X*-L)** Wet kneading MgO and SiO_2 (Grace) with X= Mg/Si atomic ratio= 1, 2, 9, 15 or 30.
C) Figure 60. **Catalytic Results (SERIE MS*X*-SG)** Silica-Gel method, using $Mg(NO_3)_2$ and TEOS with X= Mg/Si atomic ratio= 1, 2, 9, 15 or 30

MS1-O

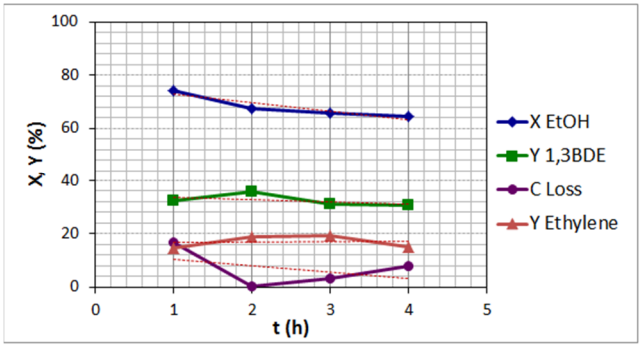

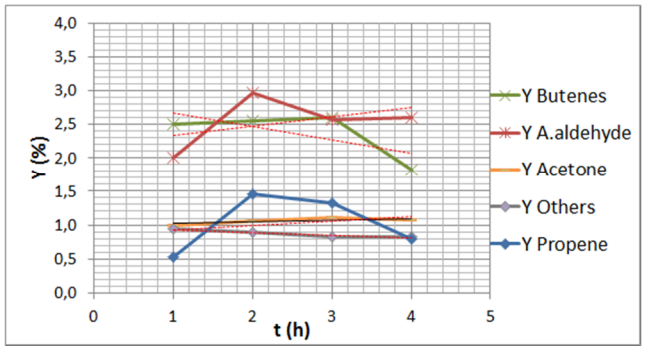

MS2-O

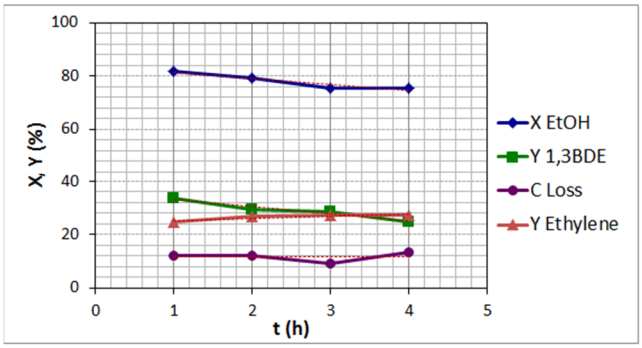

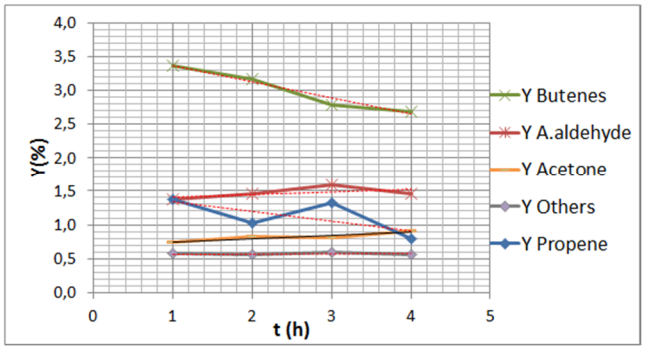

MS9-O

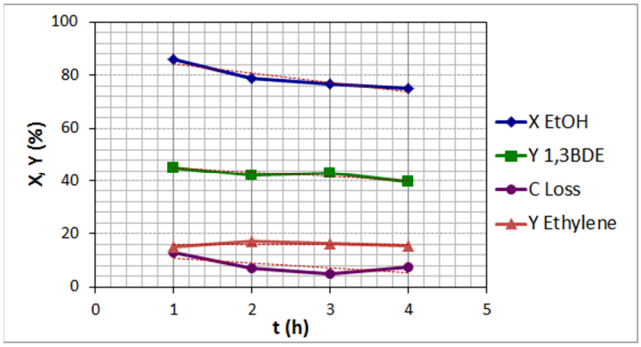

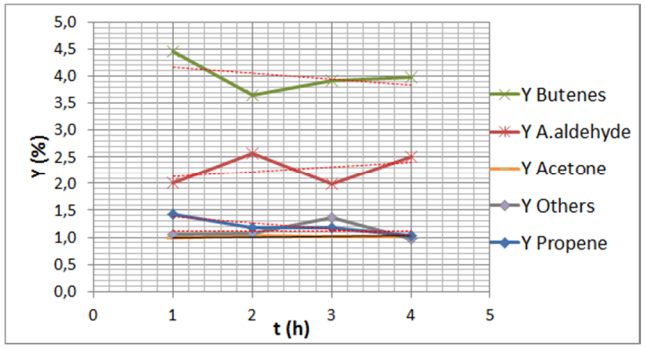

MS15-O

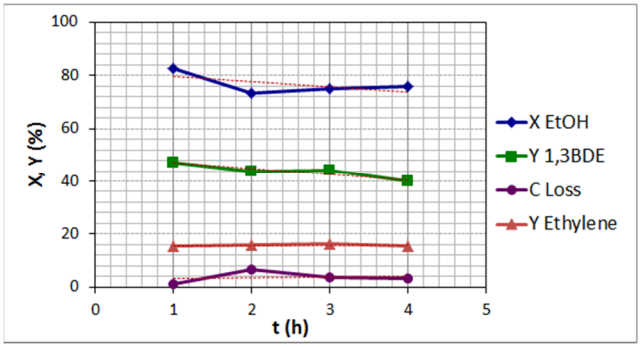

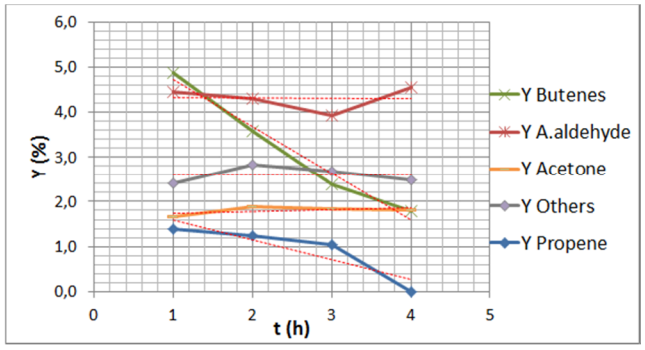

MS30-O

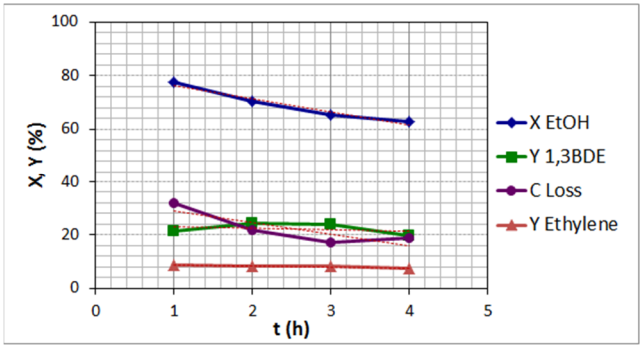

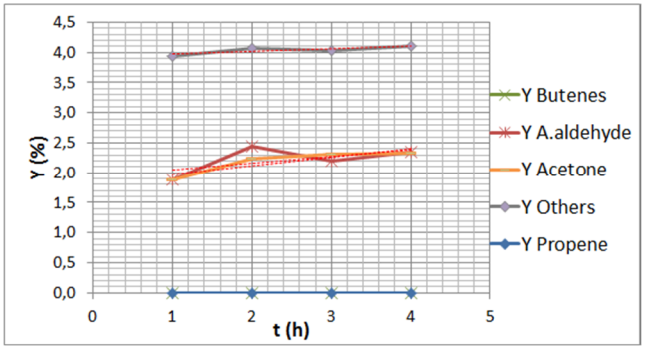

MS1-L

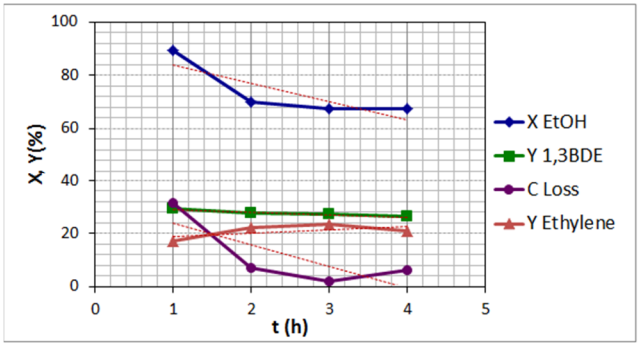

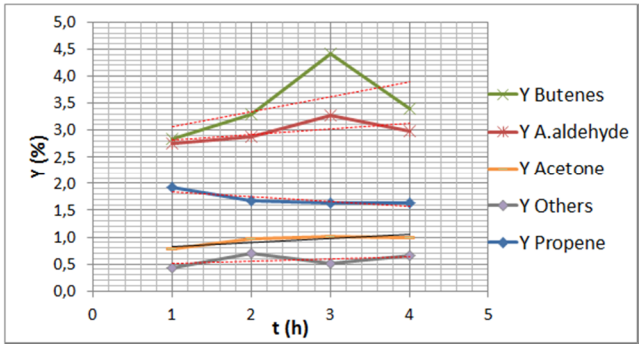

MS2-L

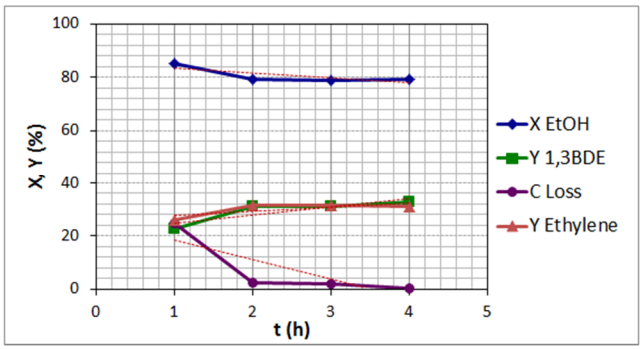

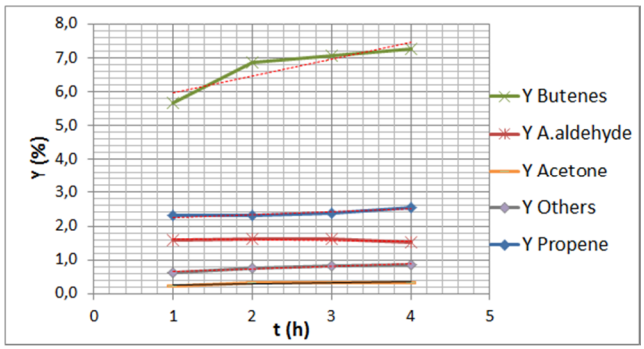

MS9-L

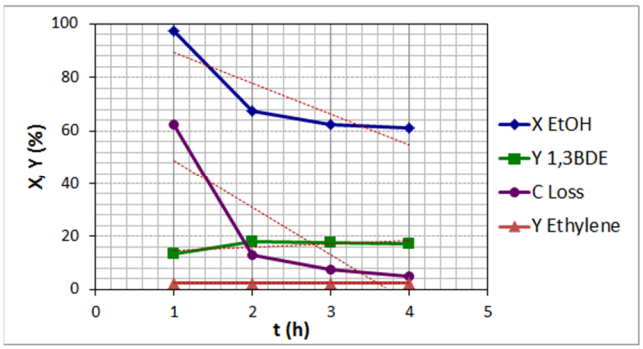

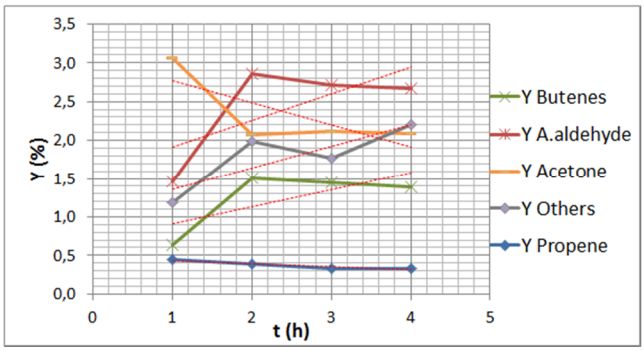

MS15-L

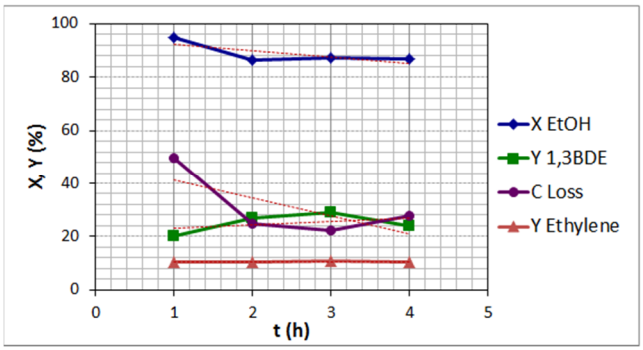

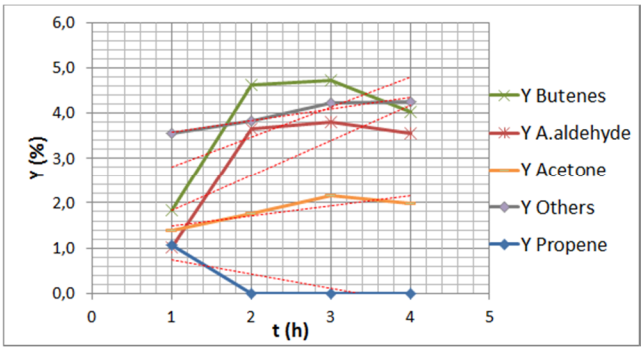

MS30-L

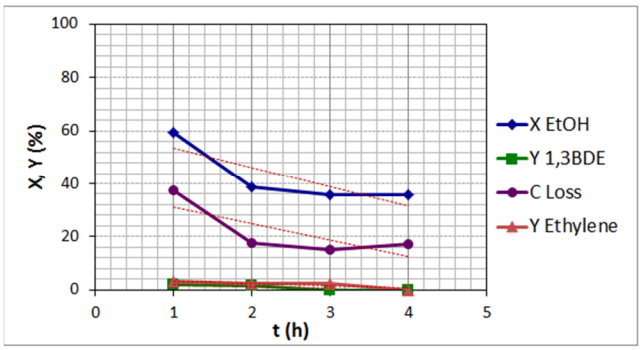

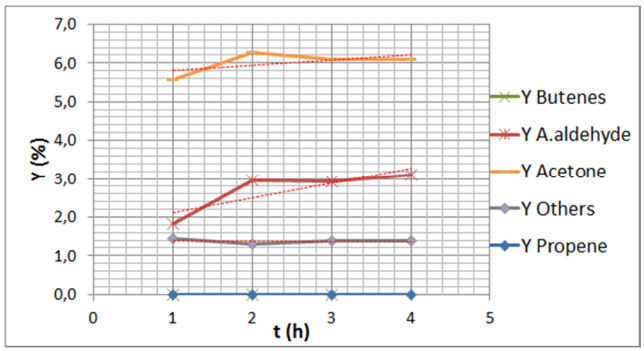

MS1-SG

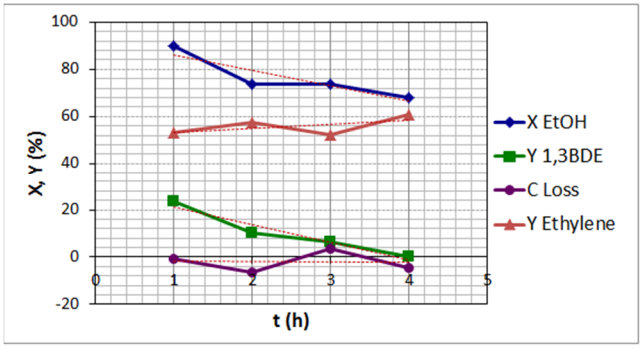

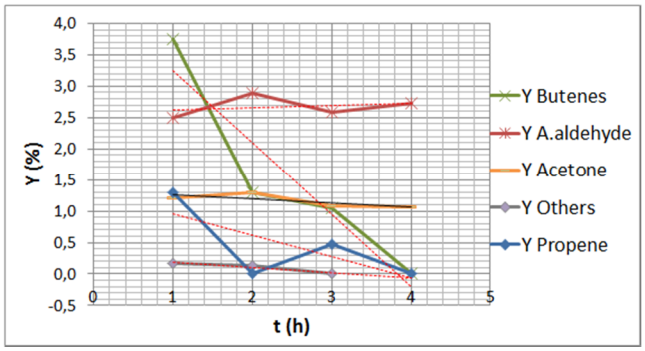

MS2-SG

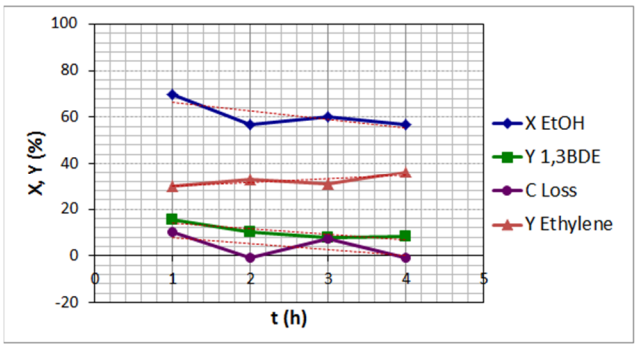

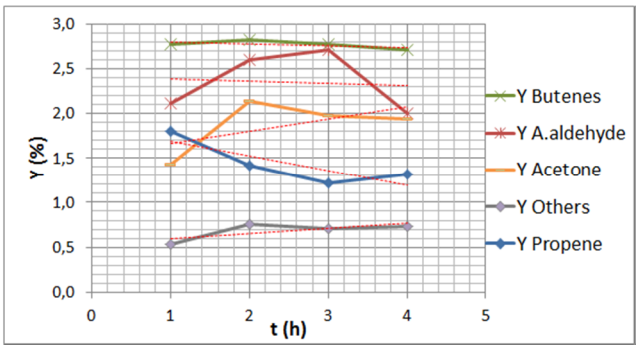

MS9-SG

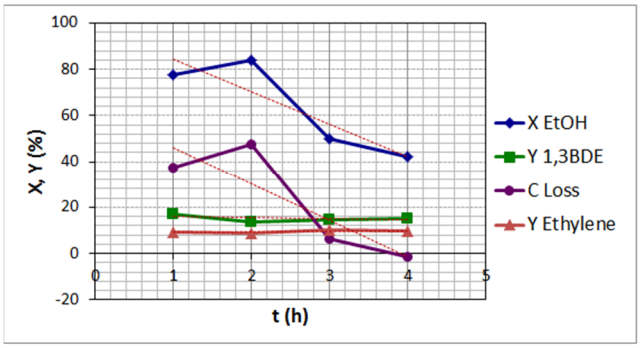

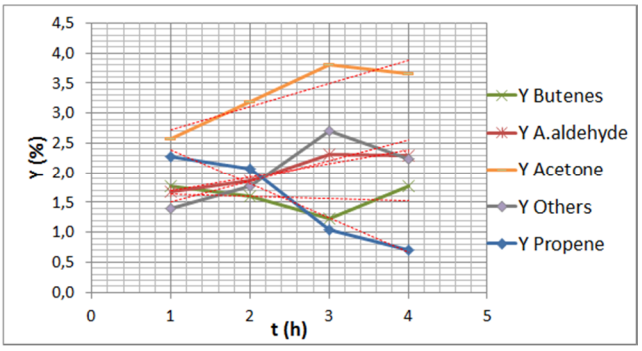

MS15-SG

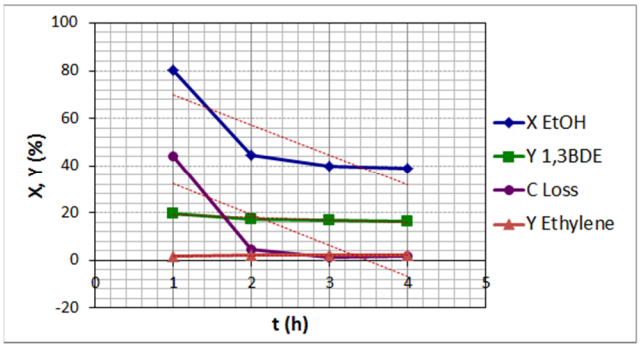

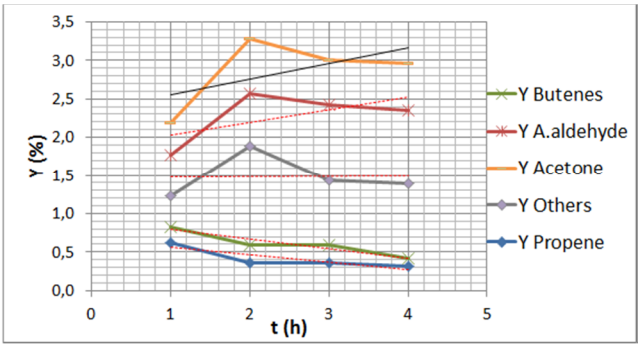

MS30-SG

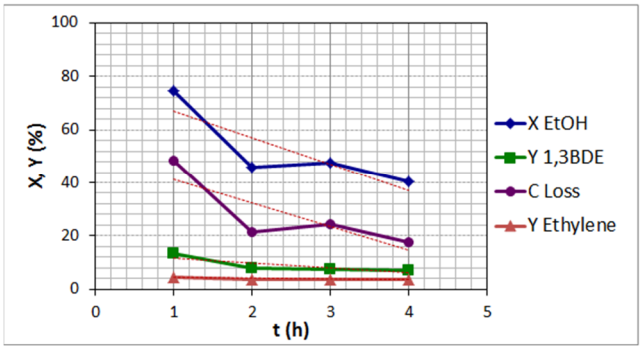

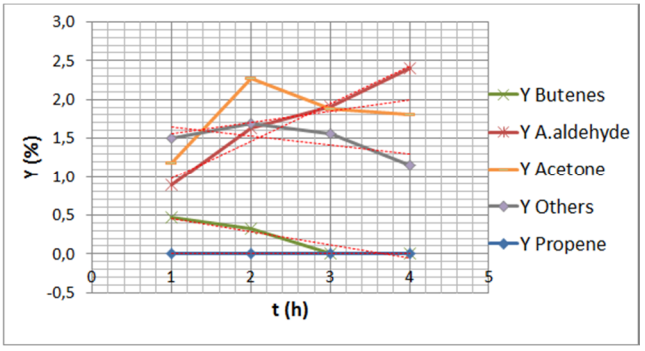

The following table summarizes the results of the catalytic tests performed with the different catalyst under the same conditions.

Table 15.Catalytic performance of different Mg-Si catalysts at 400°C, 0,65 g/mL.s and TOS of 4h.EtOH 2% in N_2

	Mg/Si	*X EtOH*	*Y 1,3 BDE*	*S 1,3 BDE*	*S ethylene*	*AREA BET*
MS1-O	1	65,9	32,5	49,3	26,7	82
MS2-O	2	76,7	27,7	36,1	35,4	54
MS9-O	9	76,9	41,5	54,0	21,2	58
MS15-O	15	74,7	42,7	57,1	21,2	71
MS30-O	30	66,2	22,7	34,3	12,2	47
MS1-L	1	68,2	27,0	39,6	22,7	341
MS2-L	2	79,1	31,9	40,4	39,7	231
MS9-L	9	63,6	17,6	27,7	3,9	145
MS15-L	15	86,8	26,6	30,6	12,2	67
MS30-L	30	36,8	0,5	1,2	4,3	36
MS1-SG	1	70,8	5,4	7,6	82,2	102
MS2-SG	2	58,6	10,1	17,2	55,8	63
MS9-SG	9	46,2	14,5	31,3	19,2	25
MS15-SG	15	41,2	16,8	40,8	5,5	21
MS30-SG	30	43,5	7,5	17,1	8,7	12

3.3.2 Discussion of the results

Evidently the synthesis method has an influence on the performance of the different materials as well as the Mg-to-Si ratio. However the optimal value of this last parameter showed to vary in different way depending on the preparation method adopted. In order to try to understand why the materials showed such a different behavior we started to analyze the low Mg/Si range (1-2) which is the one usually investigated in the literature [88]. Figure 61 shows a comparison of the results for these two values and from there it is evident that the wet kneaded samples perform better with respect to the sol-gel. Among them, the most selective catalyst is MS1-O which is in agreement with what has been reported previously in the open literature [73].

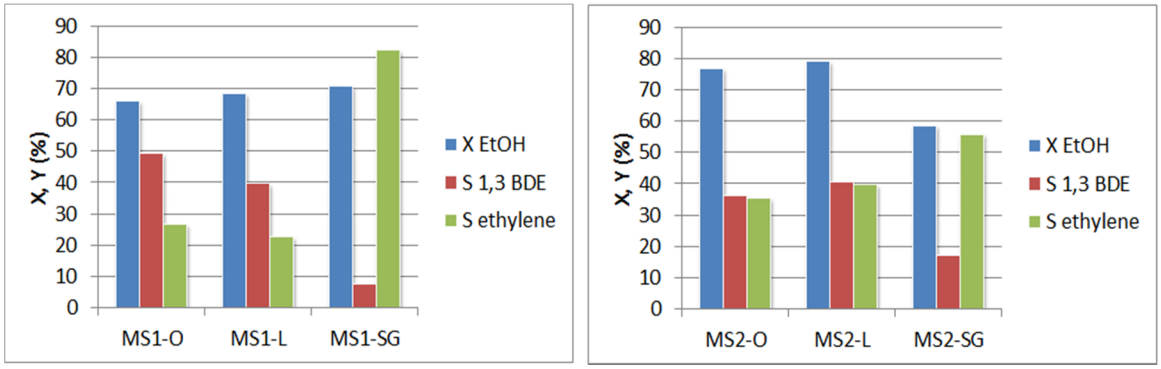

Figure 61. Comparison of the catalytic results for the samples with Mg/Si = 1 (Left) and Mg/Si = 2 (Right)

On the other hand, in the higher range of Mg/Si ratio (15-30) that is usually not considered in the literature we observe a different behavior (Figure 62). For the Ohnishi-like preparation method (Serie MS*X*-O) and the sol-gel (Serie MS*X*-SG) the selectivity to butadiene reached the maximum value at Mg/Si =15 (On the left) to then decrease again, whereas for the Lewandowsky-like preparation the selectivity did not improve with respect to samples with Mg/Si = 1 or 2.

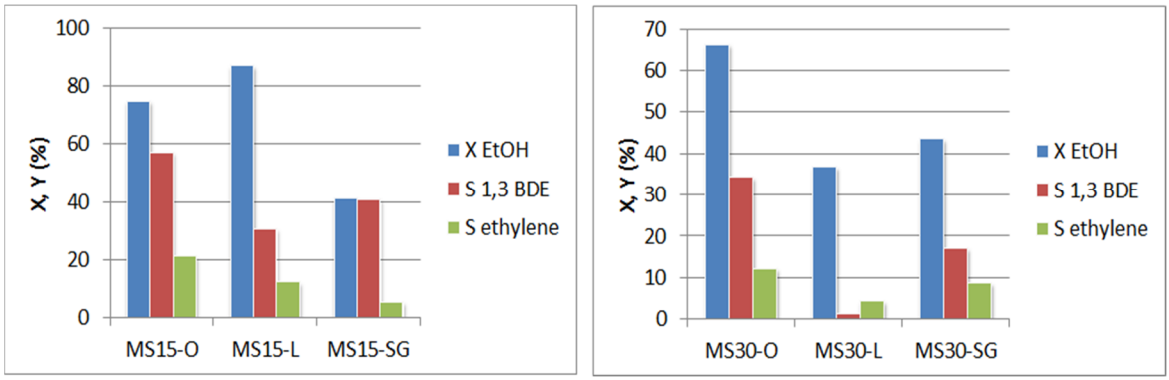

Figure 62. Comparison of the catalytic results for the samples with Mg/Si = 15 (Left) and Mg/Si = 30 (Right)

3.3.3 Characterization

In an attempt to understand these differences, analyses by X-ray diffraction (XRD) and attenuated total reflection (ATR) were performed. Figure 63 presents the diffraction patterns corresponding to the MS*X*-O series (Left) and the MS*X*-L series (Right); it is possible to observe that the only crystalline phase formed in all cases corresponds to MgO. It is clear as well that for the two series the crystallinity increased when the Mg/Si

ratio was increased. However, it is not possible to say much about the Si-containing phase which is mainly amorphous.

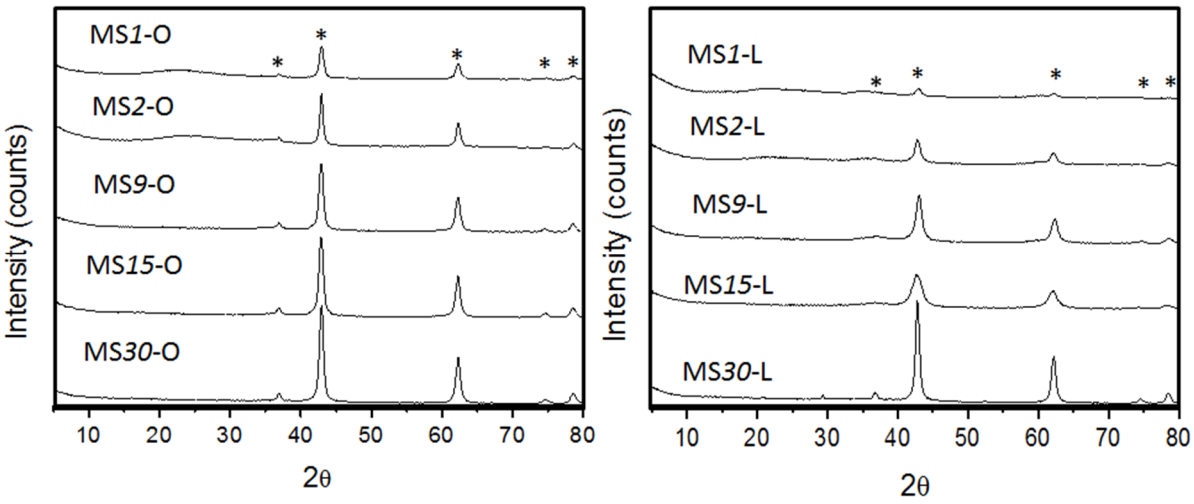

Figure 63. X-ray diffraction patterns for the MSX-O series (Left) and the MSX-L series (Right). (*) MgO diffraction peaks (JCPDS 01-077-2364)

Infrared absorption spectroscopy is widely used to characterize materials containing amorphous SiO_2. Especially the variation in the frequency of the vibrational mode (transverse optic, TO) associated with the asymmetric stretch motion of the bridging oxygen atoms moving in the plane of adjacent Si atoms, has been used to characterize the environment of the Si in the network [133].

Figure 64 shows the spectra obtained for the Ohnishi-like materials (Serie MS*X*-O) compared with the spectrum of silica (bottom). For silica, a typical spectrum was obtained with the very strong and broad IR band at 1074 cm^{-1} and a shoulder at 1176 cm^{-1} that is usually assigned to the transverse and longitudinal optical modes (TO and LO) of the Si-O-Si asymmetric stretching vibrations. The IR band at 951 cm^{-1} can be assigned to silanol groups (Si-OH stretching vibration) and the band at 801 cm^{-1} is ascribed to Si-O-Si symmetric stretching vibrations. In chapter 3.3.2 the analysis was made for the silica-gel samples and there it was found that the samples with a spectrum similar to a Mg-silicate (forsterite) were performing worse. Instead those with a Si stretching shifted towards higher wavenumbers (due to the presence of surrounding Mg-O) were more selective. In the case of the Ohnishi-like materials we found a particular situation. The sample with Mg/Si =1 has a spectrum very similar to that one of the amorphous SiO_2 but when the Mg/Si ratio was increased the band assigned to the TO of asymmetric Si-O-Si stretching (1073 cm^{-1}) became broader and shifted towards lower wavenumbers (1007 cm^{-1}). Interestingly, the samples where this band was stronger were the most selective

ones, whereas the sample with Mg/Si =2 had the shoulder at 1200cm^{-1} and thus it still had an amorphous silica-like character; for the sample with Mg/Si = 30 this band almost disappeared.

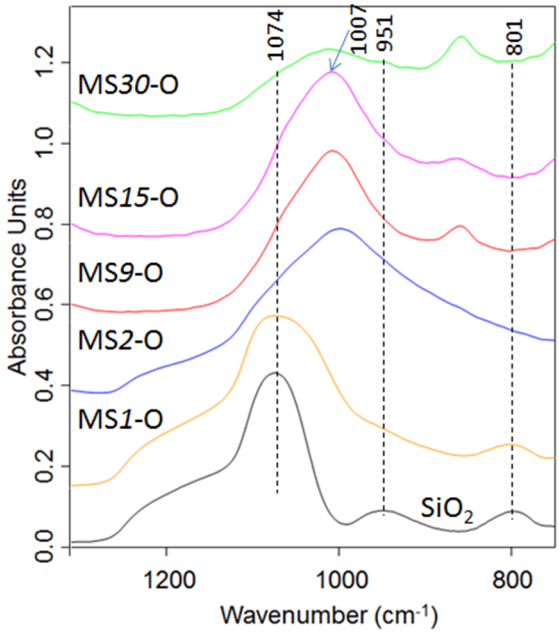

Figure 64. ATR spectra for the Ohnishi-like samples (MSX-O)

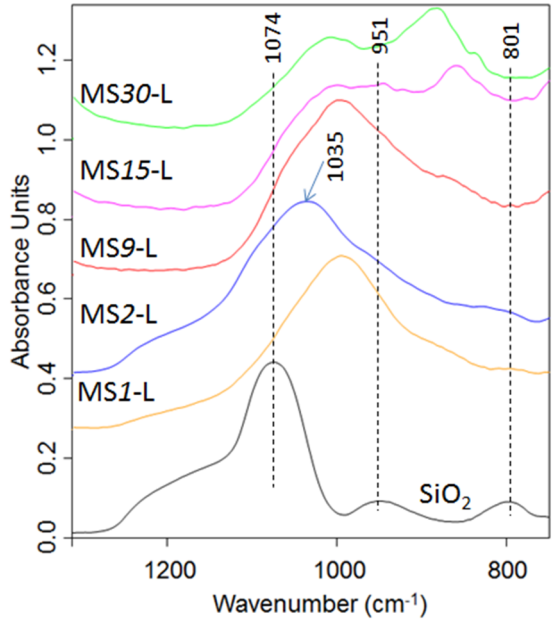

Figure 65. ATR spectra for the Lewandowsky-like samples (MSX-L)

The results of ATR for the MSX-L series are presented in Figure 65. In this case as well there is a red shift of the Si-O-Si stretching band that is quite particular. For the sample MS2-L the band appears at 1035 cm^{-1} whereas for the other samples the shift is bigger

and in the extreme case of MS30-L the spectrum is coincident with that one of a Mg-silicate (as in the case of sol-gel samples) [134]. The appearance of a particular shift for the MS2-L band, the most selective catalyst of this series, seems to indicate that there is a certain environment for the Si-O site that makes the catalyst more selective towards butadiene. In fact, comparing the three series of synthesized materials, the more selective ones have a band in the range 1007-1035 cm^{-1} (Figure 66) which might be related to an active and selective site for butadiene production. In the case of the sol-gel sample, this band is not the main one and this could be related to its poor performance when compared to the wet-kneaded samples.

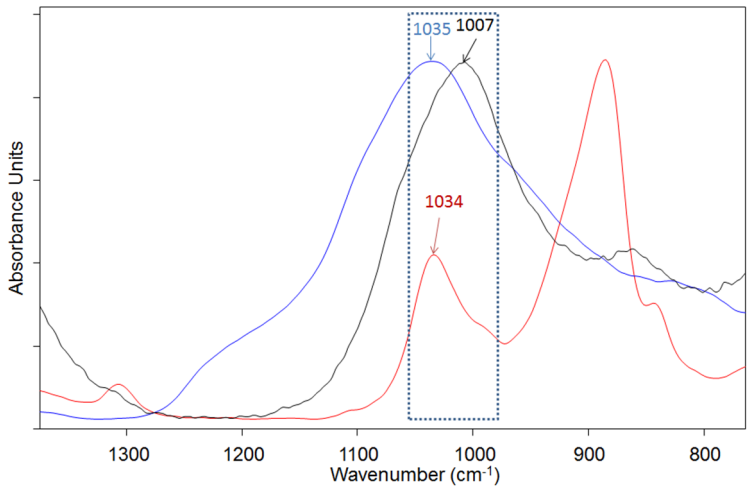

Figure 66. Comparison of the ATR spectra for the most selective sample with the different preparation methods

3.3.4 Conclusions of the chapter

The variation of the optimal Mg-to-Si ratio is related to the preparation method, that is, taking a single Mg/Si value and evaluating different types of synthesis might give an incomplete perspective of the best performance of a material, since each method might have the optimal Mg/Si value falling in a different range. Especially for materials prepared by wet kneading of $Mg(OH)_2$ and SiO_2 (Ohnishi-like method) it has been found that they have a better selectivity and butadiene yield at higher Mg/Si ratios that despite this being one of the most active catalysts for this reaction, were not explored before. Moreover, it has been found a particular spectral range in the infrared (ATR spectroscopy) where the more active catalysts usually present the Si-O-Si stretching band.

3.4 Modified catalysts: Ga/Mg-Si oxides

Another topic of research was the effect of Ga incorporation into MgO-SiO_2 catalysts. Gallium was chosen because it was proven to enhance the performance of metal catalysts in a variety of catalytic reactions such as a hydrocarbon dehydrogenation and cyclization, methane activation, methanol to hydrocarbon conversion, Friedel–Crafts benzylation and acylation reactions, reforming of methanol and its reverse, methanol synthesis [135]. Moreover, the presence of formate species as key intermediates in some of these reactions has been reported [136].

3.4.1 Catalysts preparation and characterization

The MS1-O catalyst was impregnated with different loading of Ga. The method used was the wet impregnation with aqueous solutions of $Ga(NO_3)_3$ in different weight percentage (of Ga), from 0.5 to 10%. Figure 67 shows the X-ray diffraction patterns of the original (MS1-O) and the impregnated samples after calcination at 500°C for 3h. Before impregnation, the catalyst presents reflections attributable to MgO and SiO_2. The impregnated samples were mainly amorphous with some broad reflections that seem attributable, with some uncertainty, to $MgSiO_3$, SiO_2 and $MgGa_2O_4$. However due to their broadness and low intensity, an unambiguous assignment could not be done. Anyway, it is clear that the impregnation method caused changes in the original structure and that probably during the stirring of the catalyst with the $Ga(NO_3)_3$ solution, hydration and re-dissolution of the Mg and Si phases took place, and an interaction of the Ga^{3+} ion with MgO and silica that led to the generation of new phases. Table 16 presents the result of N_2 physisorption for the synthesized samples. The trend indicates that the low Ga content originated compounds with a higher surface area; conversely, at higher load of the metal, the area sensibly decreased probably due to the formation of aggregates and clusters.

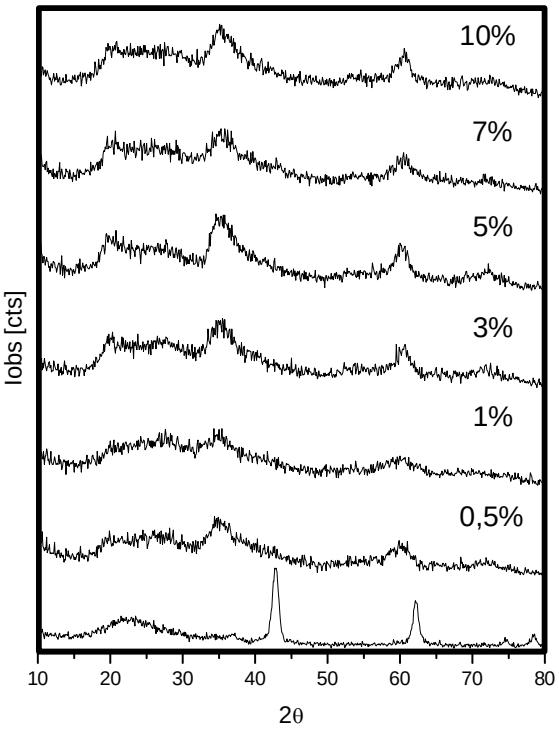

Figure 67. X-ray diffraction pattern of the original sample and the samples impregnated with different Ga content (wt % Ga) after calcination at 500°C

Table 16. Results of N_2 physisorption for the samples impregnated at different Ga percentage

Sample	*Surface area BET* m^2/g
MS1-O	82
MS1-O+0,5% Ga	262
MS1-O+1,0% Ga	149
MS1-O+3,0% Ga	168
MS1-O+5,0%Ga	48
MS1-O+7,0%Ga	51
MS1-O+10%Ga	63

3.4.2 Catalytic tests

The samples were tested in the direct conversion of ethanol to butadiene (Lebedev process). Results for ethanol conversion and yield to products are shown in Figure 68 for the reaction carried out at 400°C and 0,65 s contact time; time-on-stream was equal to 4h, and the molar concentration of ethanol was 2% in N_2. On the left-hand side, yields to the main products are shown, on the right side those produced with lower yields.

An increase of the conversion was shown in the presence of Ga. Already at 0,5 wt % Ga, total conversion was reached. 1,3-Butadiene yield also increased in all the cases with respect to the sample without Ga. However, the production of by-products also increased mainly ethylene and butenes.

Table 17 summarizes the conversion and selectivity results for the different samples. These results show the increase in the selectivity to butadiene that has a maximum of 48-52% for the samples with 3 and 5%w of Ga, respectively. However, the sample with the 5% of Ga presents a lower co-production of ethylene.

A) MS1-O (0%Ga)

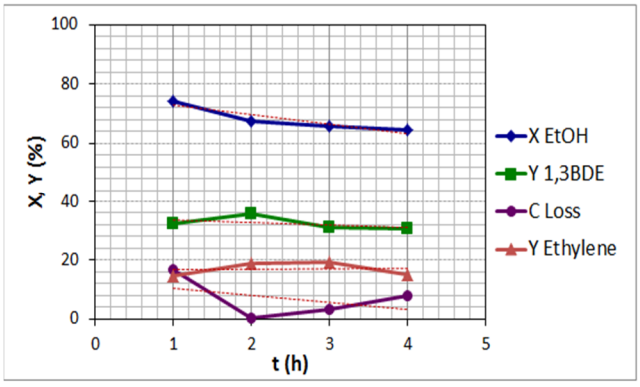

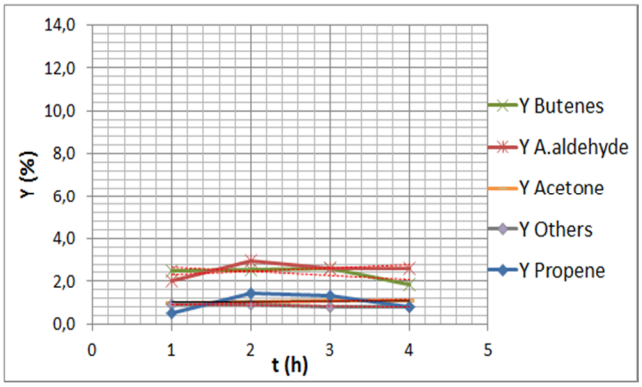

B) 0,5% Ga

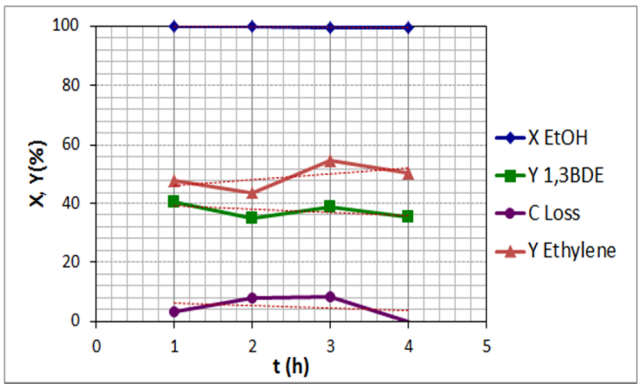

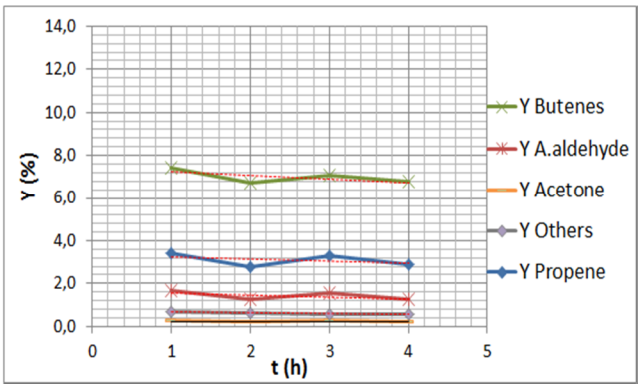

C) 1,0% Ga

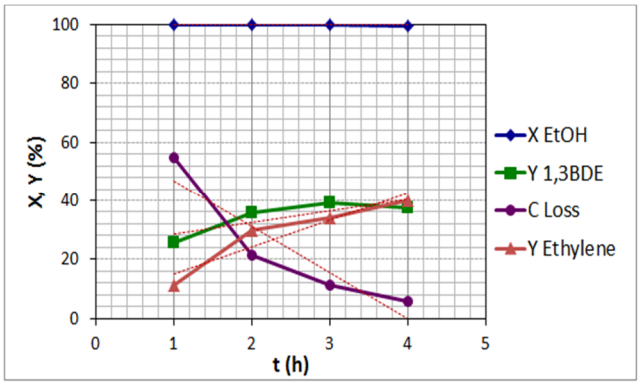

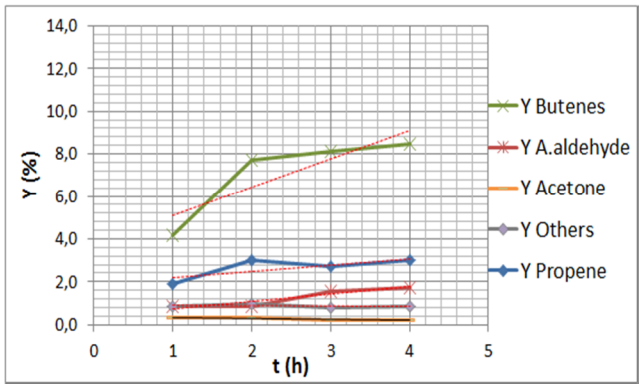

D) 3% Ga

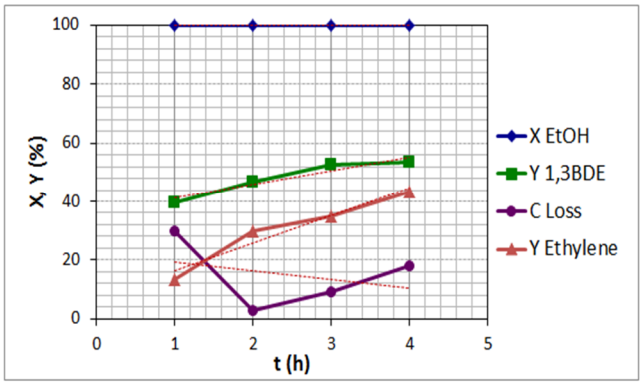

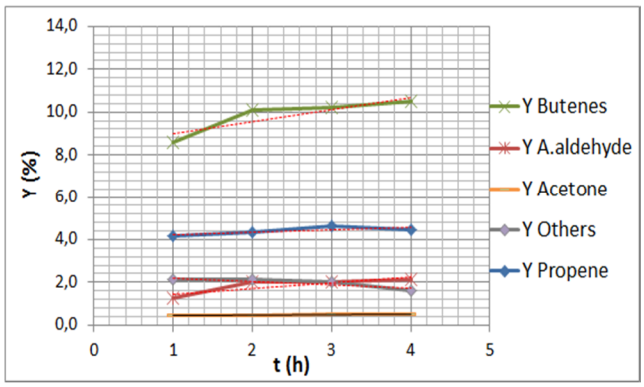

E) 5% Ga

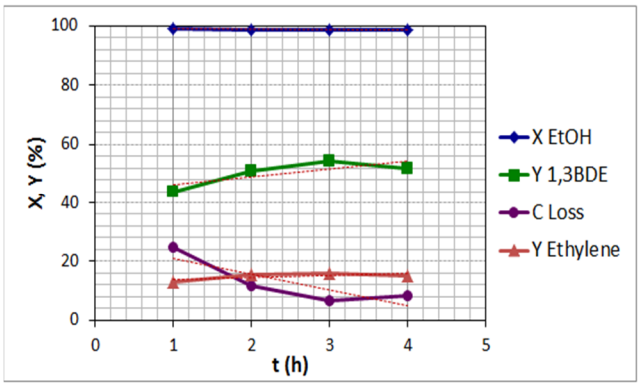

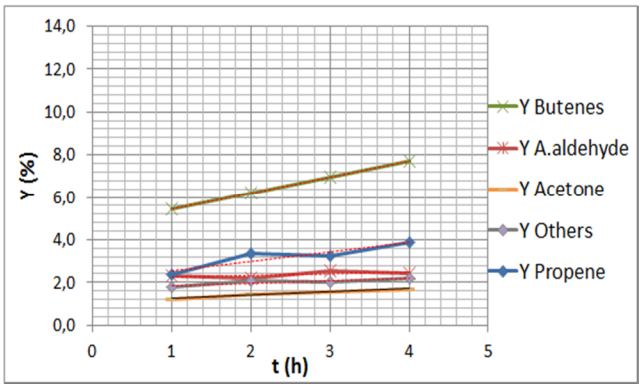

F) 7% Ga

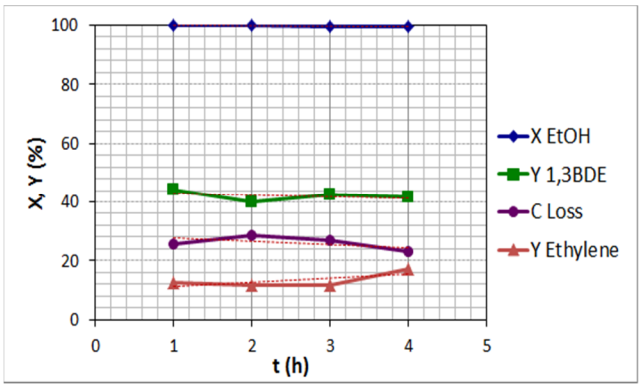

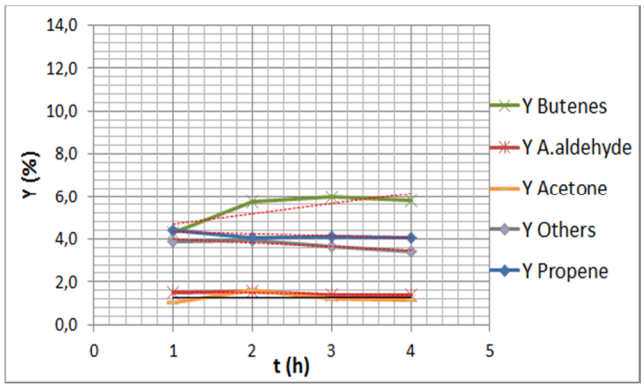

G) 10 % Ga

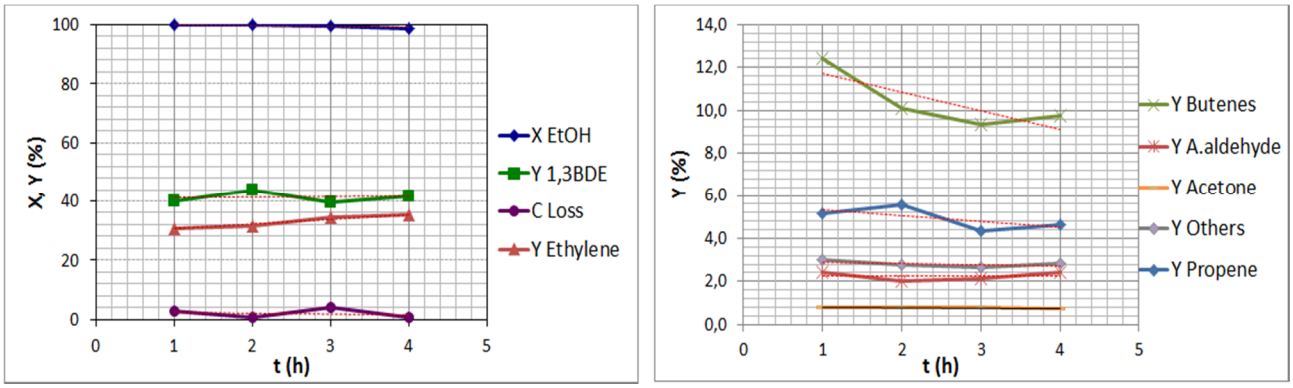

Figure 68. Catalytic results for the sample MS1-O containing different amounts of Ga (0 - 10%)

Table 17. Catalytic performance of MS1-O impregnated with different amounts of Ga. Conditions: 2% Ethanol, contact time 0,65s, 4h of TOS

Sample	*Ethanol conversion*	*Butadiene Yield*	*Butadiene Selectivity*	*Ethylene Selectivity*
MS1-O	65,9	32,5	49,3	26,7
MS1-O+0,5% Ga	99,7	37,5	37,6	49,4
MS1-O+1,0% Ga	99,9	34,6	34,6	28,8
MS1-O+3,0% Ga	99,9	48,2	48,2	30,4
MS1-O+5,0%Ga	98,8	52,4	53,1	15,7
MS1-O+7,0%Ga	99,7	42,1	42,2	13,3
MS1-O+10%Ga	99,5	41,4	41,6	33,3

The effect of the temperature for the best performing catalyst (MS1-O+5%Ga) was studied. Results presented in Table 18 confirm that 400°C is the more suitable temperature to maximize the yield to 1,3-BDE; below this temperature the conversion is lower whereas at higher temperatures the production of heavy compounds is greater (as seen from the C loss).

Table 18. Temperature effect for ethanol transformation on MS1-O + 5%Ga.

Temperature	*Ethanol conversion*	*Butadiene Yield*	*Butadiene Selectivity*	*Ethylene Selectivity*	*C loss*
255 °C	6,7	4,5	73,8	0,0	6,4
300 °C	13,1	8,0	65,0	5,3	6,2
350 °C	37,8	18,4	48,4	9,1	4,8
400 °C	98,8	52,4	53,1	15,7	9,0
450 °C	99,1	39,9	40,2	11,3	19,9

3.4.3 The effect of the impregnation method

The introduction of 5%w Ga was performed using deposition methods other than wet impregnation; specifically, the Ga source was directly added to the gel during the synthesis of the catalyts (in-situ method), or deposited by means of incipient wetness impregnation. Figure 69 compares the XRD patterns for samples prepared with the three different methods used. It is observed that only the wet impregnation method produced changes in the structure of the sample; in fact, the other two samples presented the same diffraction pattern as the original MS1-O, albeit with different intensity (all patterns are on the same intensity scale).

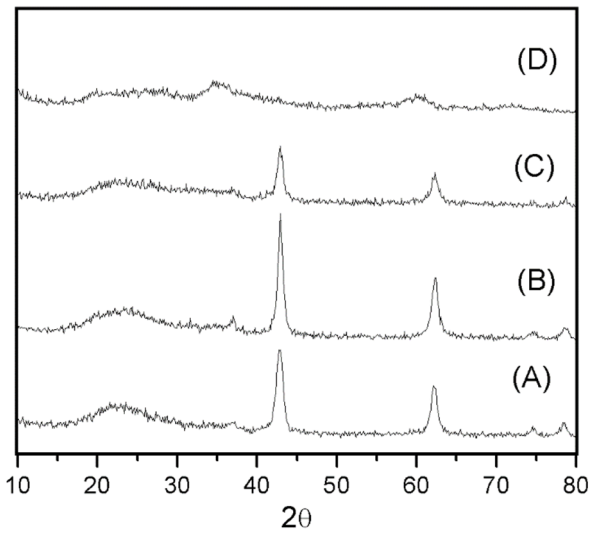

Figure 69. XRD pattern for Sample MS1-O without Ga (A) and with 5% of Ga introduced in-situ (B), by incipient wetness impregnation (C) and the wet impregnation (D).

The following figure shows the catalytic results for the samples. It is observed that the sample prepared with the in-situ method had a slightly lower conversion (96,5% average) and it also formed more by-products (ethylene and others). The butadiene yield was slightly higher for the in-situ sample (33% vs 28%). Nevertheless, both samples presented a lower yield to butadiene and the carbon balance was worse than in the case of the sample prepared by wet impregnation.

A) Incipient wetness impregnation

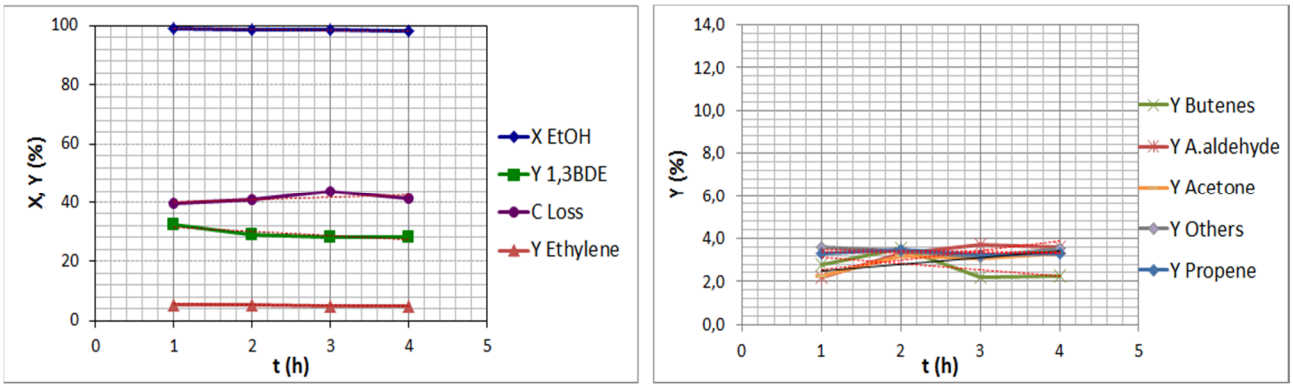

B) In-situ preparation

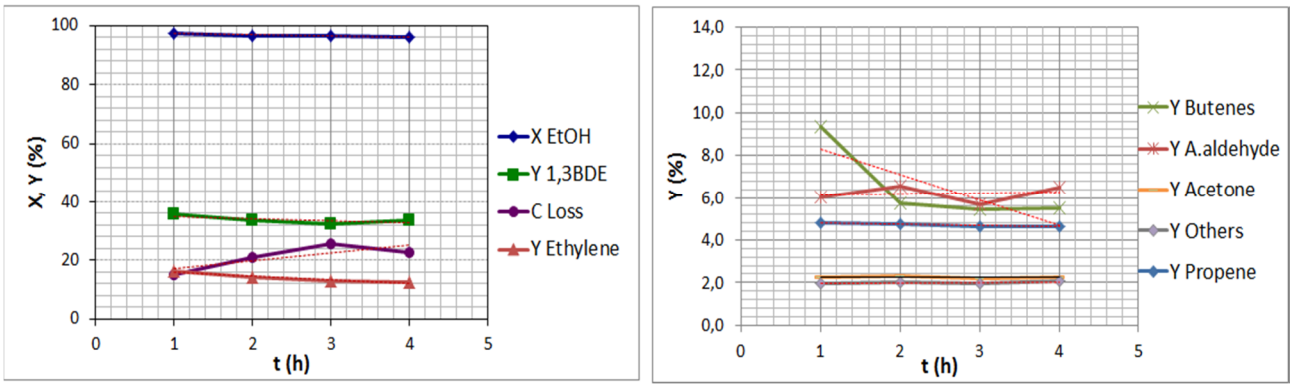

Figure 70. Catalytic results for ethanol conversion over MS1-O modified with 5% Ga by incipient wetness impregnation (A) and in-situ synthesis (B)

3.4.4 Varying the impregnated sample

Two more Mg-Si-O samples were chosen for the impregnation with 5% of Ga, the one synthesized by sol-gel and calcined at high temperature (forsterite, FS), and the one synthesized by wet-kneading of the oxides (MS2-L). Catalytic results for FS without Ga showed an average of 19% yield to butadiene; results presented in Figure 71B show that Ga addition increased the conversion of this sample. However, there was a considerable amount of heavy compounds formed (measured as C-loss), that was even greater than

butadiene yield; therefore this catalyst might not be a good choice. For catalyst MS2-L the measured butadiene yield was ca 34%. In presence of 5% Ga (Figure 71D) the yield was very high at the beginning (54%), but then it decreased down to ca. 40%, which is still better than without Ga, but not better than for MS1-O with 5% Ga.

A) FS (Forsterite)

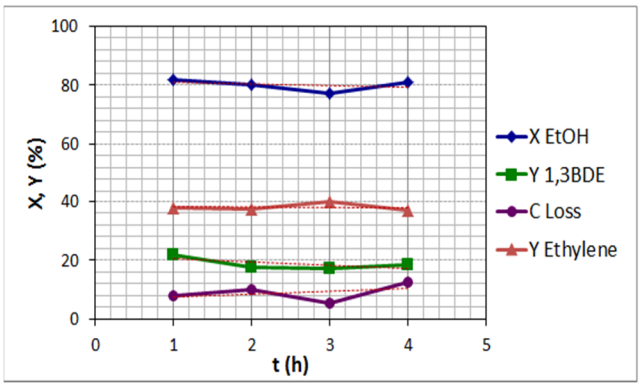

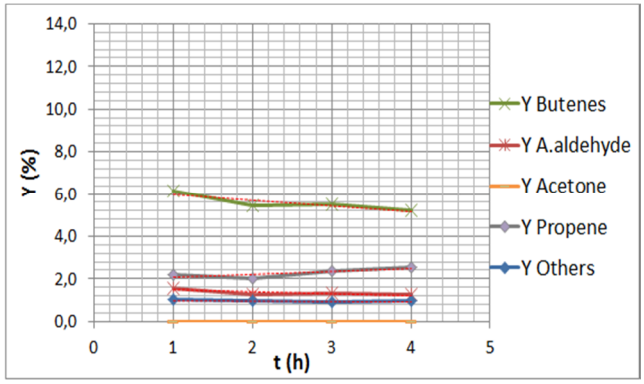

B) FS + 5%Ga

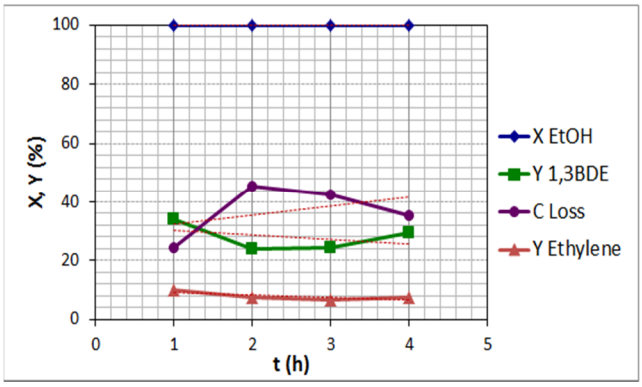

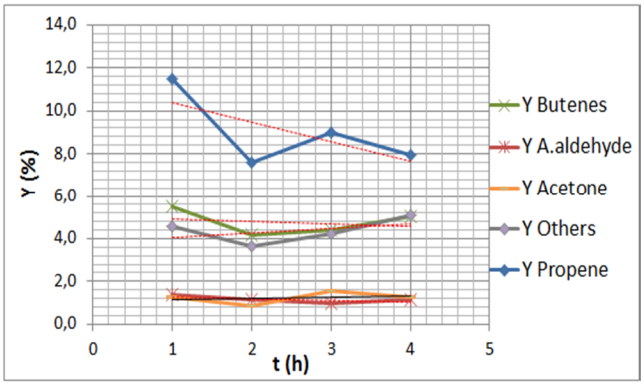

C) MS2-L

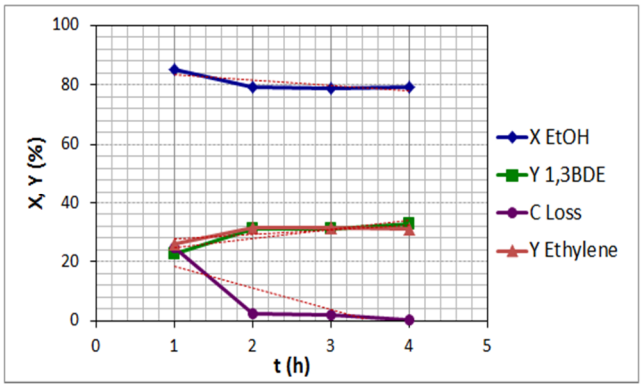

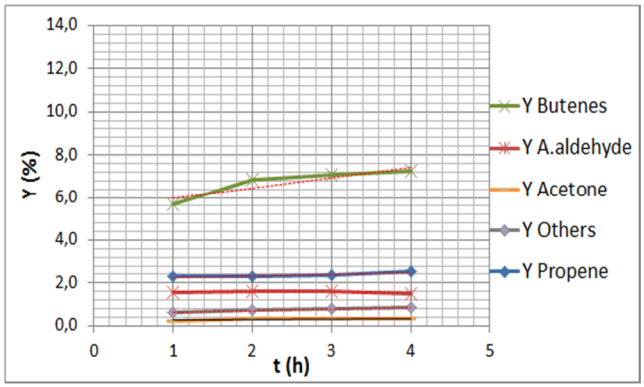

D) MS2-L + 5%Ga

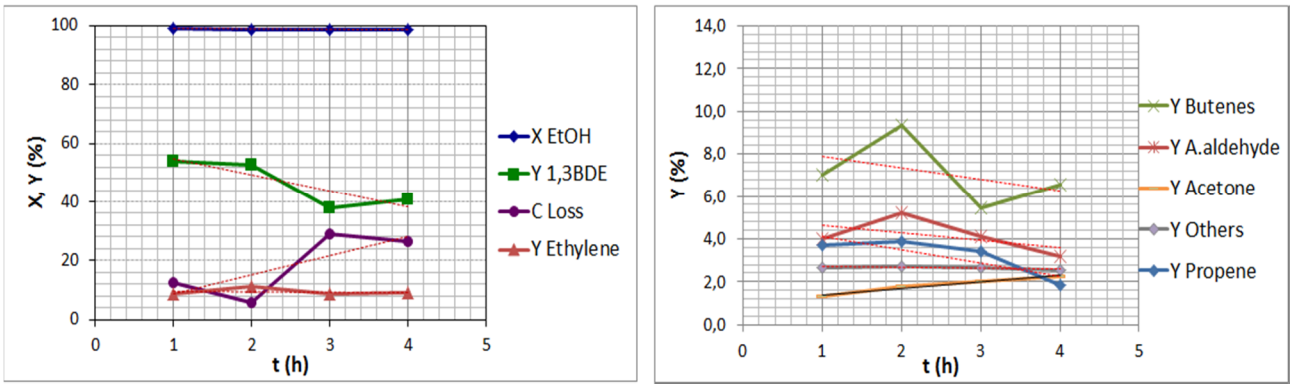

Figure 71. Catalytic conversion of ethanol with the catalysts FS2+5%Ga (A) and MS2L+5%Ga (B)

3.4.5 Spectroscopic study of the best performing catalyst

Figure 72 shows the DRIFT spectra of the unmodified catalyst MS1-O and of the same sample impregnated with 5% Ga, at both 85°C and 400°C. A sharp band at 3672 cm^{-1} is shown, especially at high temperature, for the sample containing Ga. This band has been ascribed to the vibration of surface OH multi-coordinated to Ga^{3+} in an octahedral environment. The band at 3730 cm^{-1} may be assigned to mono-coordinated OH groups [137].

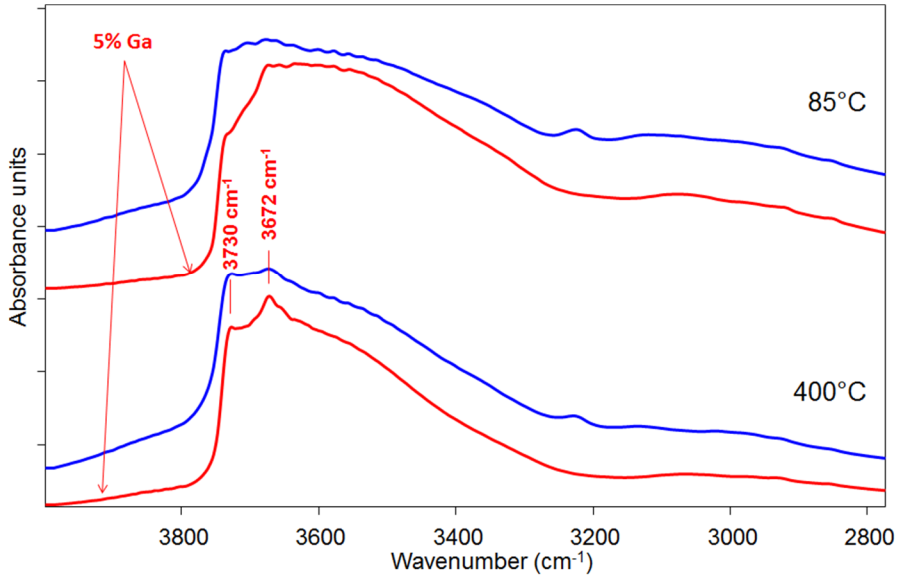

Figure 72. DRIFT spectra of the sample MS1-O (Blue) and MS1-O+5%Ga (Red) at 85 and 400°C under He flow.

For the same samples, attenuated total reflection spectra (ATR) were taken in order to observe the spectral range at lower wavenumbers that it is difficult to analyse by means of DRIFT for these samples. Spectra are shown in Figure 73; it is possible to observe that the presence of Ga caused the broadening of the Si-O-Si stretching band (at 1078 cm^{-1}), which is attributable to a newly developed interaction, i.e., to a Ga-O-Si bond. The fitting of the spectra in the region of this band (Figure 74) confirms that the component at around 1004 cm^{-1} is not present in the sample without Ga.

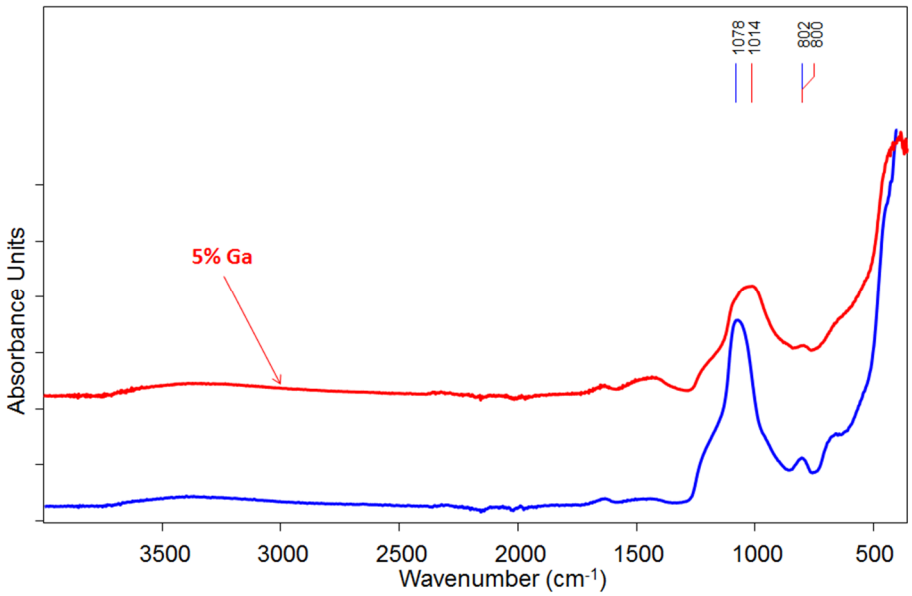

Figure 73. ATR spectra of MS1-O (Blue, bottom) and MS1-O+5%Ga (Red, Top)

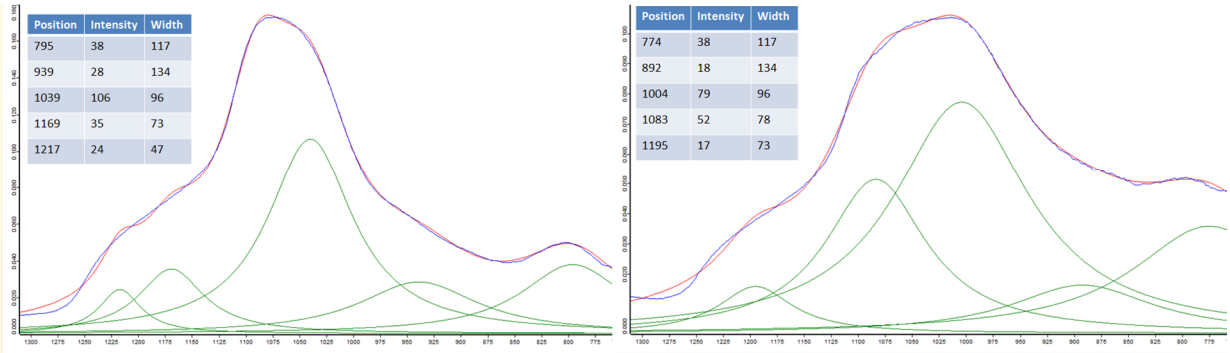

Figure 74. Fitting in the region 750-1200 cm-1 for the ATR spectra of Figure 73

In situ- DRIFTS of Ethanol Adsorption

Due to its better performance, the MS1-O sample containing 5% wt Ga was chosen to carry out studies of ethanol adsorption and to make a comparison with the non-impregnated sample. Figure 9 shows the spectra during ethanol adsorption at room

temperature for both samples (after subtraction of the catalyst spectrum). The intermediates correspond to adsorbed ethanol and to the ethoxy group ($C_2H_5O^-$). Table 19 shows the assignment of the bands highlighting the most characteristic bands for each species, whereas the others are in common to both species adsorbed, ethanol and ethoxy [116], [138], [139].

Table 19. Assignment of the bands after ethanol adsorption on the samples MS1-O with and without Ga

	MS1-O	*MS1-O + 5%Ga*
Metal-O	878	878
$\nu_{as}(C\text{-}O)_{bident}/\nu_{as}(C\text{-}C)$ ethoxy	1039	1043
$\nu_{as}(C\text{-}O)_{monodentent}$ ethoxy	1076	1078
δ(OH) in ethanol	1272	1276
$\delta_s(CH_3)$ in ethanol	1394	1392
$\delta_{as}(CH_3)$	1451	1450
$\delta_{as}(CH_2)$	--	1479
$\delta_s(H_2O)$ (negative)	1630	1630
ν_{as}(α-C-H) ethoxy	2732	2732
$\nu_s(CH_2)$	2885	2885
$\nu_s(CH_3)$	2900	2900
$\nu_{as}(CH_2)$	2933	2933
$\nu_{as}(CH_3)$ in ethoxy	2975	2975
ν(OH) in ethanol	3261	3245
ν(free OH) (negative)	3727	3720

From the spectra it seems that the sample with Ga (bottom spectrum) adsorbs more ethanol (more or less twice as much the total intensity). This might be true if we take into account that the quantity of sample used in the experiment was the same in the two cases, but the surface area was smaller for the sample with Ga (48 vs 82 m^2g^{-1} for the Ga-impregnated and the unmodified MS1-O samples, respectively). On the other hand, when

an integration of the different peaks to measure their relative intensity with respect to the negative peak (free OH groups) was carried out, a higher intensity was shown in all cases for the unmodified MS1-O (see

Table 20). This could be due to the fact that in the case of impregnation with Ga, the adsorbed intermediates were transformed or desorbed more easily. This was verified afterwards in the experiments increasing the temperature (vide infra). Another observation is that the C-O in the ethoxy group vibrates at higher wavenumbers for the sample with Ga compared to the unmodified one, which probably indicates a coordination of some of these groups with Ga^{3+}.

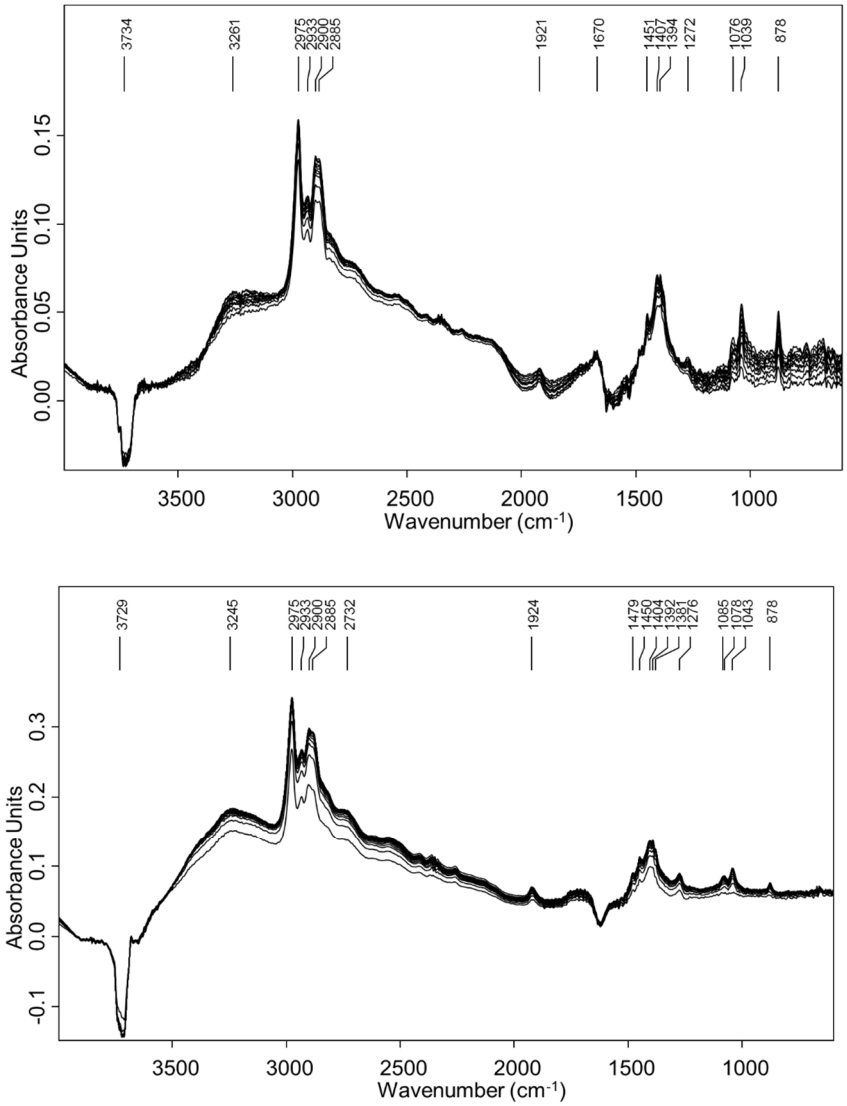

Figure 75. DRIFTS of ethanol adsorption at room temperature for the MS1-O (Top) and the MS1-O+5%Ga (bottom) at increasing time until saturation.

Table 20. Integration results for the DRIFTS spectra in Figure 75

pp	Peak	MS1-O	MS1-O + 5%Ga
Peak 1	837 -965	0,00	0,00
Peak 2	915-1105	0,56	0,15
Peak 3	1200-1585	2,99	1,46
Peak 5	1999-3600	26,73	22,60
Peak 5	3640-3835	1,00	1,00

After the saturation with ethanol was reached at room temperature, the cell temperature was increased until 400°C at 10°C min^{-1} (with continuous flow of ethanol in He). Figure 76 shows the result of ethanol reaction at different temperatures for the unmodified and the Ga-impregnated catalysts.

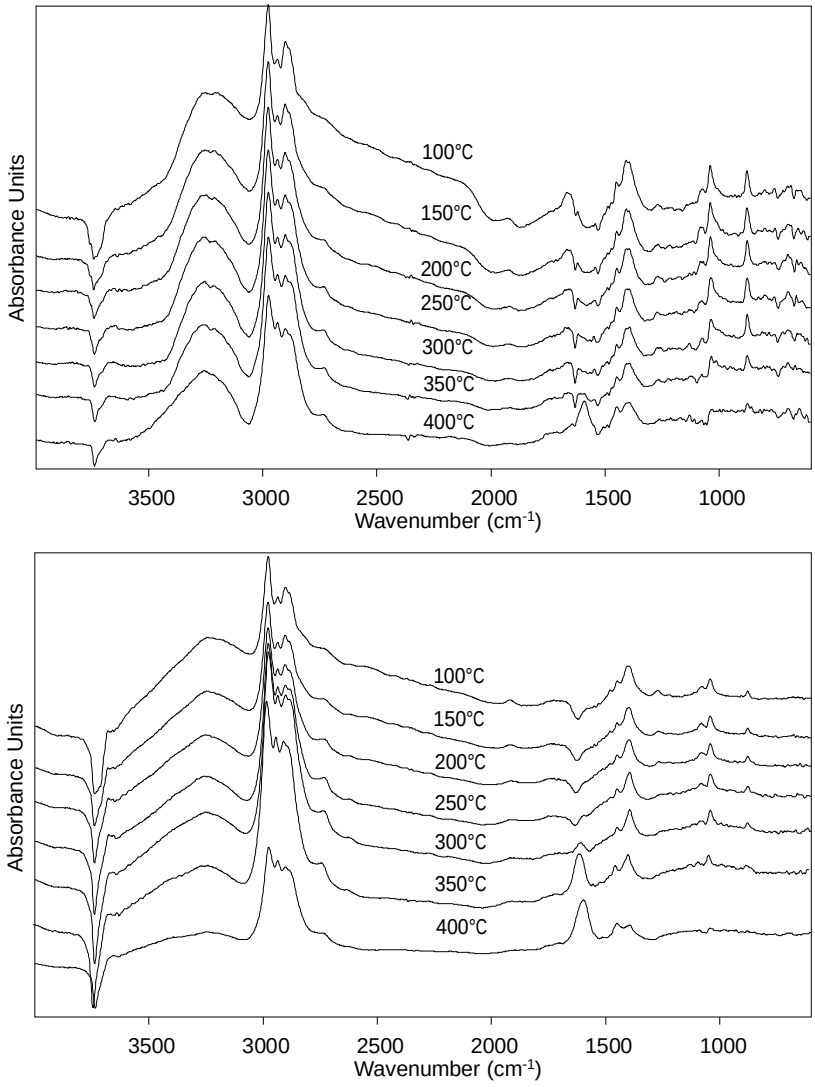

Figure 76. DRIFT spectra of MS1-O (Top) and MS1-O+5%Ga (Bottom) during Ethanol adsorption at increasing temperatures.

The spectra are those obtained after subtraction of the background (bare catalyst) registered at each temperature. At high wavenumbers there is a negative band that corresponds, in both catalysts, to an interaction of the alcohol with the free OH groups, so making them no longer available; therefore, with the subtraction of the corresponding reference spectrum they seem to disappear. This interaction is stronger in the case of the catalyst with Ga, due to the presence of additional Ga-OH groups that can interact with ethanol, and even at high temperature this negative band continued to be strong, whereas in the case of the unmodified MS1-O catalyst (Top spectrum), it seems to be less intense with the increasing temperature. One important difference is that the sample with Ga showed a band at around 1600 cm^{-1} that has been attributed to the ν_{as} of the intermediate crotyl-like species, precursor of butadiene formation. This band can be seen at lower temperature (starting at 300°C) in comparison with the sample without Ga, that presents this band only at 400°C (Top spectrum). Moreover, the increase of this band is concomitant with the disappearance of the ethoxy bands (< 1100 cm^{-1}) and this indicates that the sample with Ga is more active, since it transforms the ethoxy intermediate into crotyl-like species, the key-intermediate in the formation of butadiene, at milder conditions compared to MS1-O. Figure 77 shows a comparison for the two samples at 350°C.

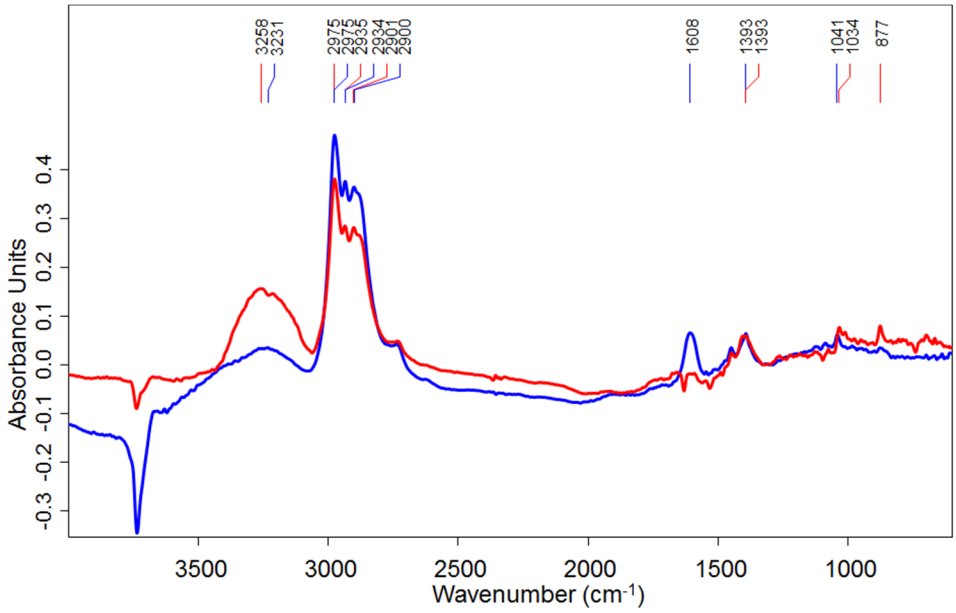

Figure 77. Comparison of the spectra at 350°C for the samples MS1-O (Blue) and MS1-O+5%Ga (Red)

In-situ DRIFTS-MS of Ethanol temperature programmed desorption (Ethanol-TPD)

Another set of experiments was performed on the samples with and without Ga. In this case, ethanol was sent at low temperature as a pulse (0,6ul min^{-1} for 5 min). Afterwards, the samples were left under He flow until weakly adsorbed ethanol was removed (ca 30 min) and then a temperature program was performed (until 400°C at 10°C min^{-1}). Figure 78 shows the result of the ethanol temperature programmed desorption (Ethanol-TPD) experiments for MS1-O and MS1-O+5%Ga. In this case, samples were not diluted in KBr in order to evaluate the adsorption of the alcohol in the absence of phenomena which might affect spectra. For both samples, at low temperature the bands corresponding to adsorbed ethanol and ethoxy species are present, even if some of the characteristic bands below 1000 cm^{-1} are not seen probably due to the high absorbance of the undiluted samples in this region.

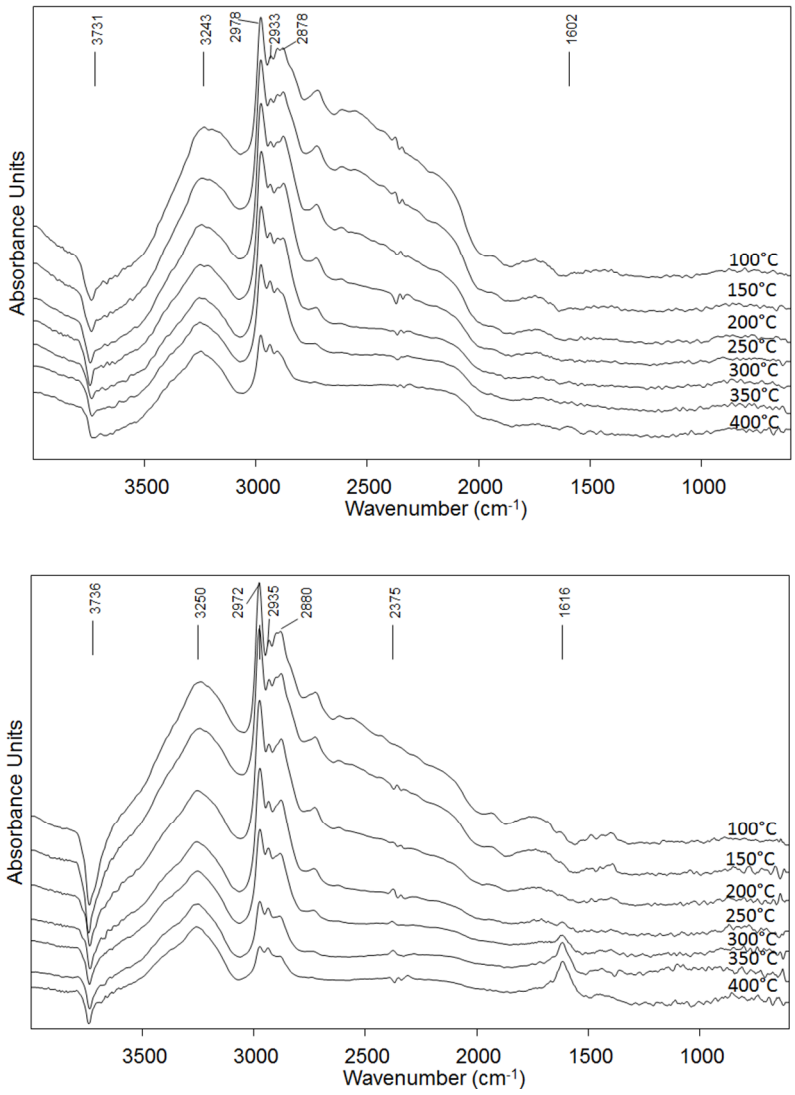

Figure 78. DRIFTS spectra during Ethanol TPD of the MS1-O sample (UP) and MS1-O+5%Ga(BOTTOM)

There are two main differences between the samples; the first is the way the OH groups interact (negative band at around 3730cm^{-1}): a sharper band was observed for the sample with Ga, which might indicate that ethanol interacts preferentially with only one type of OH group, the one monocoordinated with Ga (observed in the spectra for the catalysts before ethanol adsorption (Figure 78). Instead, in the sample without Ga this band was broader and less strong, indicating an interaction with different types of OH in the catalyst (Mg-OH or Si-OH). The second difference was that the sample with Ga gave rise to a band at around 1617 cm^{-1} that has been ascribed to the formation of a crotyl-like intermediate, precursor for butadiene formation; this band is observed already at 300°C.

During the TPD experiments, the desorbed products were followed by an on-line quadrupole (mass spectrometer). The main products detected for the two samples are shown in Figure 79. It can be inferred that for both samples, at low temperature; there was desorption of unreacted ethanol and acetaldehyde formation and desorption. Ethylene formed as well with both samples; the profile of the MS signal in this case was particular, since ethylene formed at least in two stages, the first one probably due to ethanol dehydration, whereas the second one can be explained by a particular mechanism of ethanol adsorption as a carbanion and its decomposition to ethylene, as proposed before in the chapter for MgO (Figure 80). On the other hand, it can be observed that ethylene and butadiene (the two main products of the reaction) showed similar trends for the two samples, but both compounds were released earlier for the sample with Ga (see Figure 81 for a comparison), which agrees with the spectroscopic observations and the fact that the sample with Ga holds a bigger total number of acid sites (as seen from the intensity of the NH_3 desorption signal in Figure 82) and besides, the Lewis acid sites are slightly stronger, as seen from pyridine adsorption experiments (Figure 83, the band around 1600 is shifted for the sample with Ga).

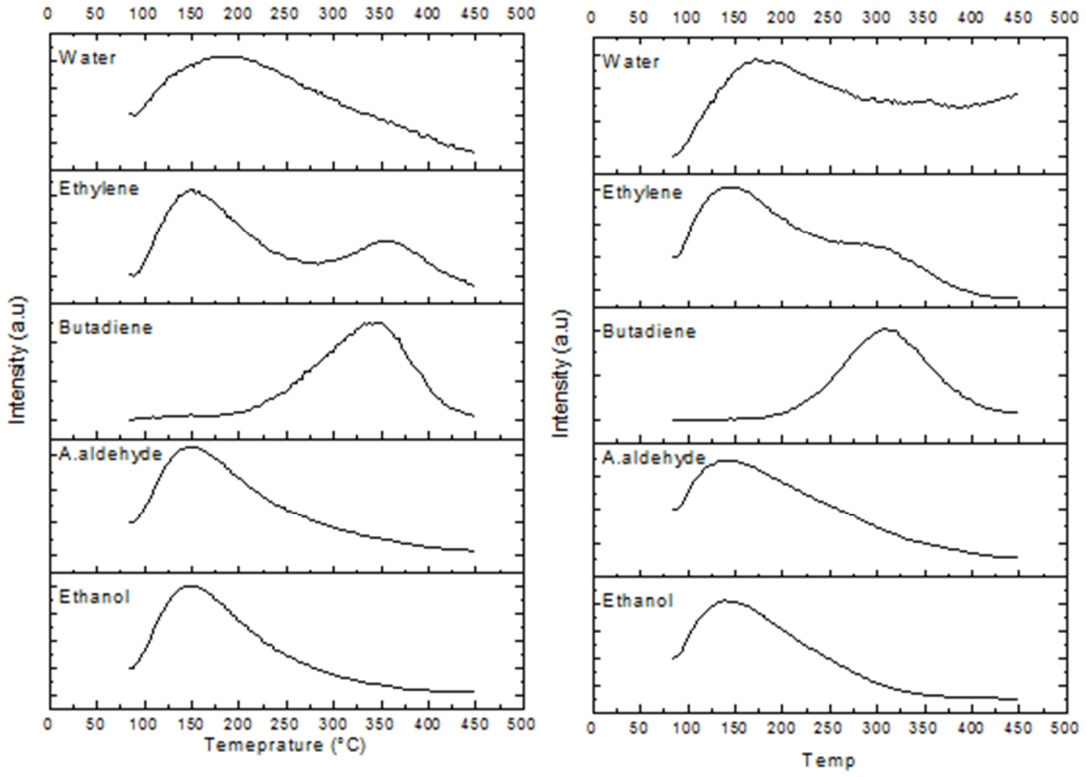

Figure 79. Main products during the Ethanol desorption for the samples MS1-O (Left) and MS1-O+5%Ga (Right)

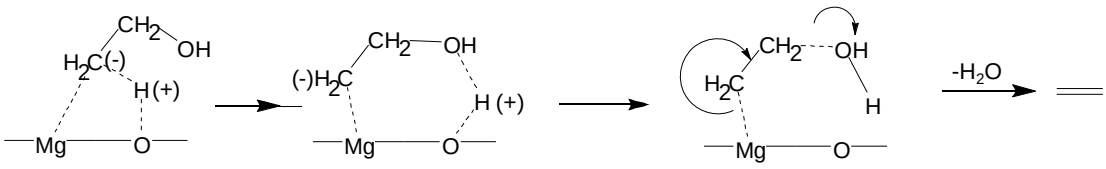

Figure 80. Formation of ethylene from ethanol via carbanion.

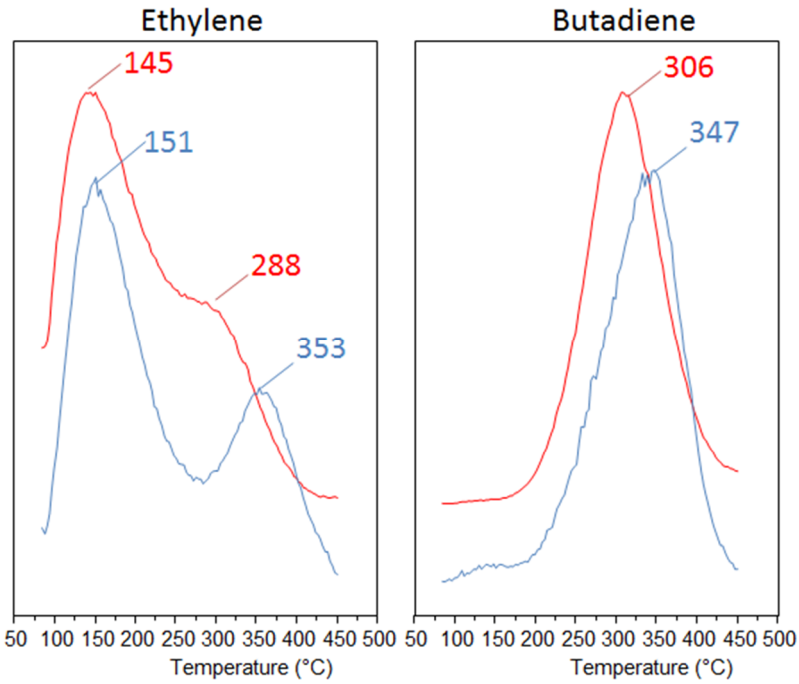

Figure 81. Main products during Ethanol-TPD of the samples MS1-O (blue) and MS1-0+5%Ga (red) with a vertical offset.

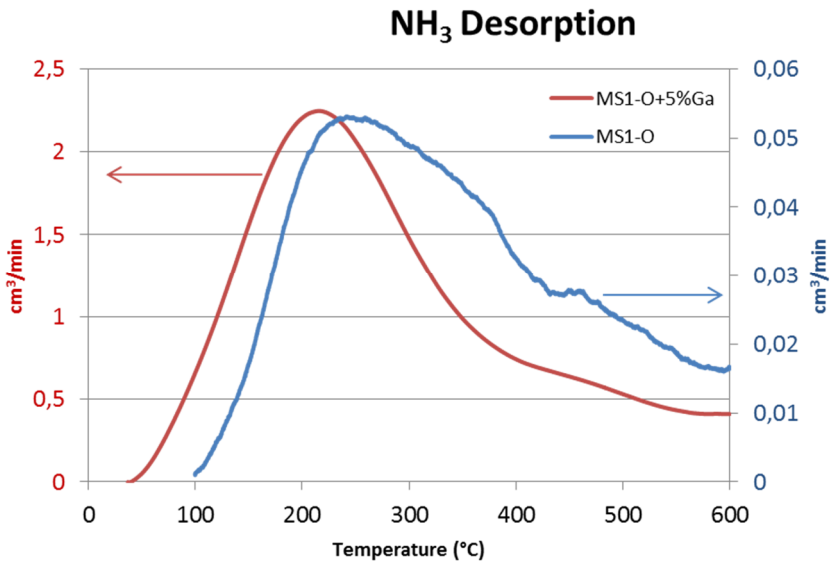

Figure 82. Ammonia desorption for the MS1-O sample (Left, red) and the sample MS1-O+5%Ga (right, blue)

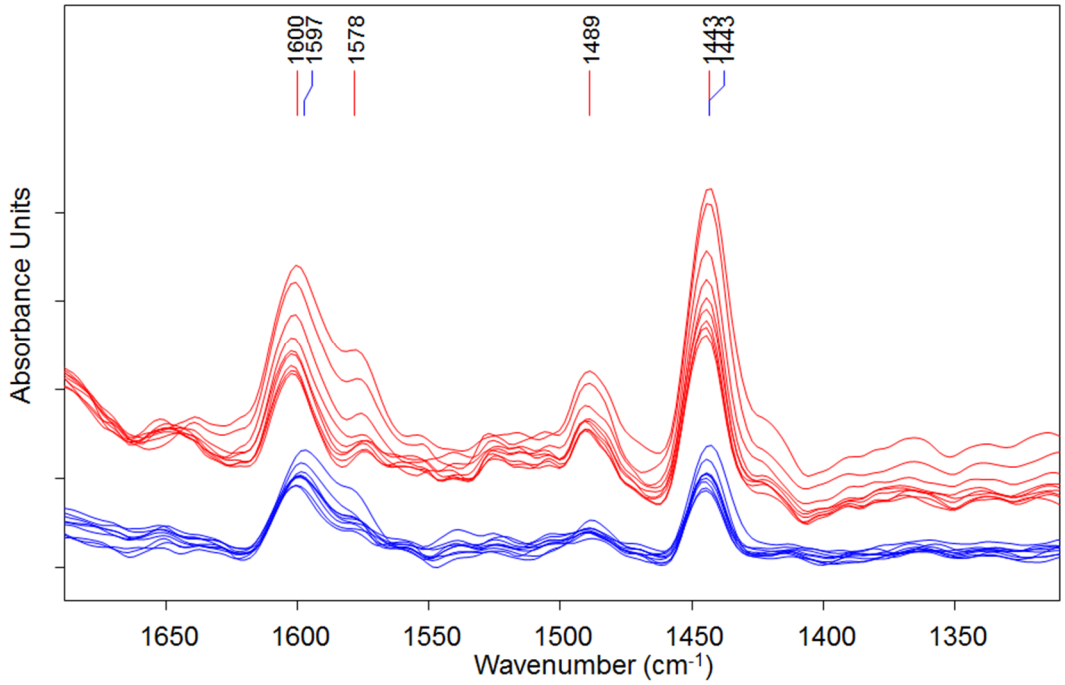

Figure 83. DRIFTS Spectra of pyridine adsorption at 50°C with time for the MS1-O sample (Bottom, blue) and the sample MS1-O+5%Ga (Top, red)

3.4.6 Conclusions of the chapter

The deposition of Ga^{3+} onto Mg-Si-O samples affects positively the performance for butadiene production. In general, it enhances butadiene yield by increasing the conversion of ethanol and decreasing the selectivity to byproducts as ethylene. When Ga is impregnated by means of the wet impregnation method, it affects the structure and creates new surface OH groups (and Ga-O-Si-OH), that interact with ethanol. This interaction seems to be more effective on the OH groups coordinated to only one cation, and these groups form the intermediate crotyl-like species, which is the precursor for butadiene formation, and whose formation is observed at lower temperature with the sample containing Ga. It is important to make clear however, that the conditions used are aimed at understanding catalysts behavior from the mechanistic point of view. Instead, different conditions such as higher ethanol concentration and time on stream should be considered in order to make this reaction an attractive industrial process.

3.5 Alternative systems (Hydrotalcites)

In this chapter the research was devoted to the synthesis of catalysts with hydrotalcite-like structure (HT) having Zn, Mg and Al as active metals and Si (as a silicate) in the interlayer as the charge-compensating anion. These materials were chosen due to their particular properties that could result useful in the transformation of ethanol into olefins. These properties include an intrinsic basicity (with some weak acid sites), flexible composition, better dispersion of the metals and a high surface area. Besides, the acid/base properties of these materials can be tuned by varying the composition [140]. An example of the particular layered structure of these materials is displayed in Figure 84.

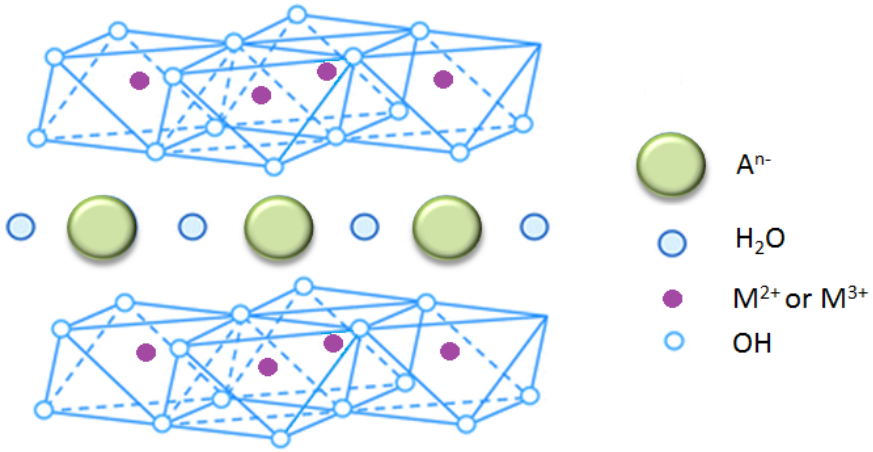

Figure 84. Hydrotalcite (HT) structure

3.5.1 Synthesis

-Synthesis of hydrotalcites containing carbonate as compensating anion

A precursor was prepared with the composition ZnMgAl-CO_3 in order to have a reference material without the presence of Si in the interlayer.

-Synthesis of hydrotalcites containing silicate as a compensating anion

The synthesized precursors were treated with different sources of Si (either TEOS or SiO_2) with the aim of introducing dispersed Si-O moieties that could act as active sites in catalysis of ethanol transformation. The following table summarizes the synthesized materials:

Table 21. Set of synthesized hydrotalcites

Composition (Metals-Anion)	*Synthesis method*
ZnMgAl-CO_3	Base to metals (final pH10)
ZnMgAl-SiO_4 (TEOS)	Base to metals (final pH10) (TEOS dissolved in the metallic sln.)
ZnMgAl-SiO_4 (Silica)	Base to metals (final pH10) (basic sln. containing SiO_2)

3.5.2 Characterization

X-ray diffraction (XRD)

Synthesized samples were analyzed by x-ray diffraction in order to verify their crystalline structure. XRD patterns of the carbonate and silicate-containing compounds are shown in Figure 85. The diffractogram for the ZnMgAl-CO_3 sample shows the characteristic pattern of hydrotalcite-like compounds with sharp and intense diffraction lines due to basal reflection planes and broad and less intense peaks related to non-basal planes; the basal spacing is 7.7 Å. The incorporation of silicates, rather than carbonates, in the interlayer leads to a solid with a lower crystalline degree and with a somewhat similar basal spacing (only a slight shift towards lower 2θ values was observed). Decreased crystallinity was shown not only in the basal direction but also within layers, as can be seen by the considerable reduction in the intensity of the first reflection line (especially for the TEOS case) and the poor resolution of the doublet (recorded in the 60–65 2θ range) related to the 1 1 0 and 1 1 3 diffraction planes. The basal spacing obtained in the Si-containing materials synthesized here was lower than the 12 Å reported by other authors [141], but it was similar to the value obtained by Depege et al and Albertazzi et al [142], [143]. This low basal spacing was explained as due to the formation of a polysilicate where the SiO_4 units condense with the same orientation. However, in the solids prepared, the presence of some silicate species adsorbed on the particle surface cannot be ruled out.

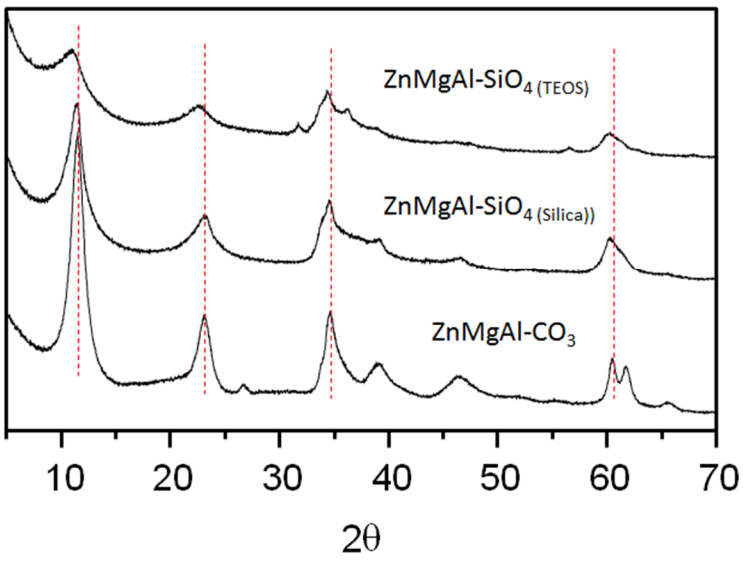

Figure 85. XRD patterns of the hydrotalcite-like materials

Infrared spectroscopy (FTIR)

The synthesized materials were analyzed by means of infrared spectroscopy. This analysis gave useful information about the structure of the compounds and interlayer anions. The FT-IR spectra of the HT precursors are shown in Figure 86. The broad band at 3466 cm^{-1} common for the three materials was ascribed to the stretching vibrations of hydroxyl groups and surface or interlayer water molecules, which are found at a lower frequency in the hydrotalcites compared to the O–H stretching in free water at 3600 cm^{-1} due to the formation of hydrogen bonds between the interlayer water and the different guest anions as well as with the hydroxide groups of the layers [144]. A weaker band at 1640 cm^{-1}, common for the three materials as well, is assigned to the bending mode of water molecules. The unmodified ZnMgAl-CO_3 material presented a band at 1369 cm^{-1} typical for the ν_3 mode (asymmetric stretching) of CO_3^{2-} anion [145]. On the other hand, there was a sharp band at 1384 cm^{-1} for the Si-containing materials, which corresponds to the ν_3 vibration of NO_3 ions that were incorporated to the interlayer structure due to the higher affinity of this ion (present in the metallic sources) with respect to the silicate ions in this kind of structure.

In addition, the infrared spectra of the HT silicate samples showed a strong Si–O stretching band at around 1000 cm^{-1} characteristic of silicate moieties, due to the antisymmetric stretching vibrations of Si–O–Si bridging sequences. No band was recorded at 800 cm^{-1} (symmetric stretching vibrations of Si–O–Si) or 1200 cm^{-1} (bending

vibrations of Si–O–Si). The absence of the latter band suggests the condensation of SiO_4 polyhedron with the same orientation in the interlayer. This feature agrees with data obtained by XRD, since the basal spacing obtained was lower than that expected in an inverted connecting frame between two straight-linked SiO_4 tetrahedral groups.

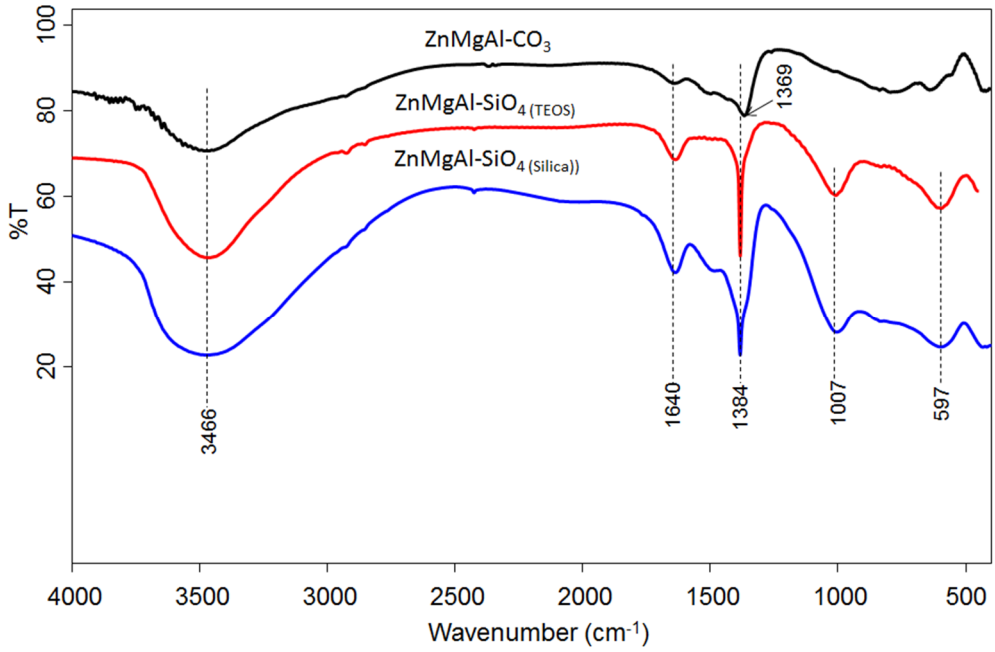

Figure 86. Infrared spectra of the synthesized samples

Thermogravimetric analysis

The evolution of volatile compounds was followed by thermogravimetric analysis observing that the weight loss varied from 34% for the ZnMgAl-CO_3 to 25 and 23% for Si-containing samples (From TEOS and silica respectively) since non-volatile silicate anions remain in the structure of the catalysts even after thermal treatment. Weight losses occur at temperatures similar to those of carbonate-containing compounds; thus the thermal stability is mainly determined by the nature of the hydroxide layers rather than interlayer anions [142]. In the bottom part the differential thermal analysis (DTA) results are shown. The reference sample ZnMgAl-CO_3 presents the typical events for the hydrotalcites materials: Loss of humidity (until 100°C), then loss of structural water (at ca 200°C) and then dehydroxilation and decarboxilation (T>250°C). All these events are endothermic. On the other hand the samples containing Si showed a more intense peak relative to physysorbed water (probably due to a lower crystallinity as observed by Albertazzi et al [142]) whereas they show a relatively less intense peak due to interlayer water (also at lower temperature) and less intense hydroxilation and nitrates decomposition peak which confirms the absence of interlayer carbonate ions.

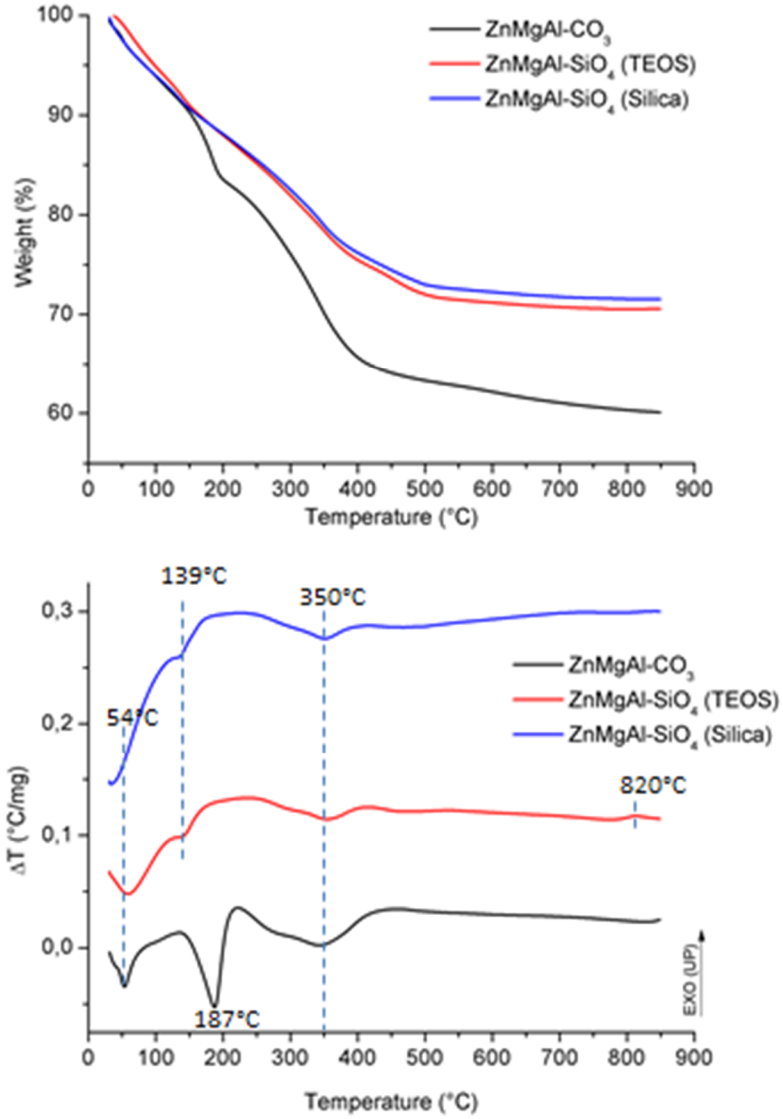

Figure 87. TGA and DTA analysis for the synthesized samples

Calcined samples

The samples were calcined at 450°C for 3h and analyzed by nitrogen physisorption; results presented in Table 22 showed that these are very high surface materials. It is observed that the incorporation of silicates into the structure led to a significant increase of the specific surface area as reported before for this type of anionic exchange [146].

Table 22. Results of surface area analysis for the calcined HT samples

Composition (Metals-Anion)	*Area (m^2/g)*	*BET*
ZnMgAl-CO_3	103	
ZnMgAl-SiO_4 (TEOS)	188	
ZnMgAl-SiO_4 (Silica)	161	

After the thermal treatment, samples were analyzed by means of X-ray diffraction in order to verify their transformation into mixed oxides. Patterns presented in Figure 88 show that the samples became a complex system of different superposed phases that include the original hydrotalcite phase (formed probably by reconstruction) and segregated ZnO and SiO_2 together with some unidentified phases.

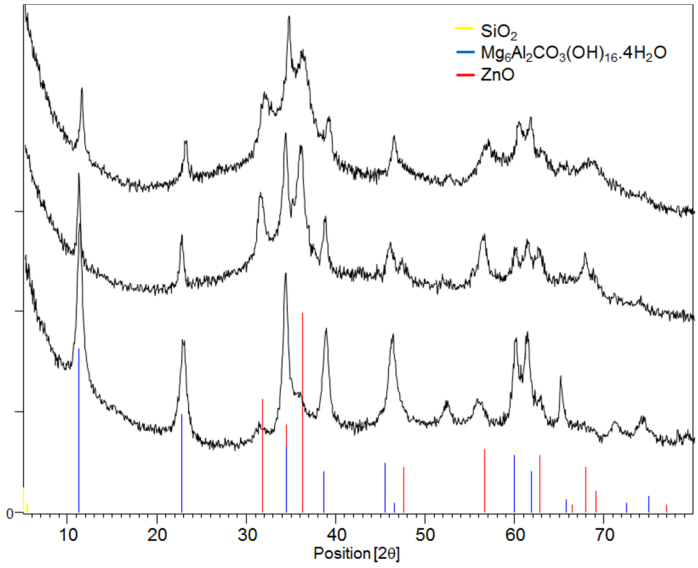

Figure 88. XRD patterns for the HT samples calcined at 450°C and comparison with some probable phases formed

Catalytic tests

The synthesized materials were tested on ethanol transformation with the aim of understanding better their differences. As regards conversion, it was found that samples containing Si were slightly more active: 97% of conversion for the ZnMgAl-CO_3 and 99% for the other two samples. However, the C-loss was very high in all cases (40-50%) which indicates that samples were likely too active and rapidly formed heavy products

that were deposited on the catalysts and are not eluted. Yields to the different products are presented in Figure 89. From there it is clear that these samples were not suitable for butadiene production, in fact because the yield to this product was negligible; instead they produced other compounds which were not the target. However it is interesting to notice that the Si-containing sample prepared with silica, produced more acetaldehyde but then was not able to transform it to butadiene whereas the catalyst prepared with TEOS produced the olefin with a higher yield together with a high amount of acetone. The formation of the latter compound can be explained by a retroaldolisation reaction of a 4-hydroxy-2-butenone, thus in the case of the Si-containing samples the catalysts took this route preferentially instead of producing crotyl alcohol, which needs at the same time more acidic sites in order to be dehydrated efficiently to butadiene. Another interesting fact is that the Si-containing samples produced less ethylene and since this fact is related in part to the acid properties it seems that the Si does not increase the acidity in this case.

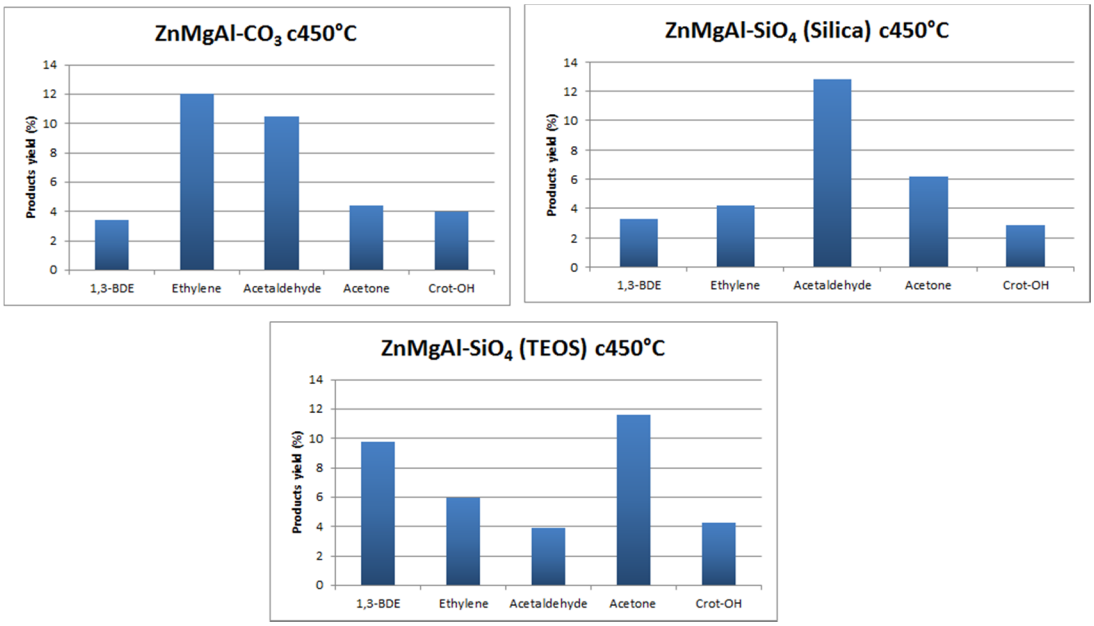

Figure 89. Results of ethanol transformation for the calcined HT samples

3.5.3 Conclusions of the Chapter

The synthesis of materials with hydrotalcite structure containing silicate in the interlayer is an interesting approach in the aim of obtaining mixed oxides with particular properties (such as high surface area). However, under the reaction conditions studied these materials were not selective for butadiene production.

4 DRIFTS STUDIES OF THE INTERACTION OF ALCOHOLS WITH DIFFERENT MATERIALS

4.1 Ethanol Ammoxidation on supported vanadia catalysts

4.1.1 Catalytic behaviour of V/Zr/O and V/Ti/O materials in ethanol ammoxidation

The catalytic behavior of V_2O_5/ZrO_2 and V_2O_5/TiO_2 in ethanol ammoxidation was previously investigated in this research group by Federico Folco [147] and the most important findings are summarized here:

a) The superior performance of V/Zr/O in ethanol ammoxidation compared to V/Ti/O, is due in part to its greater efficiency in the conversion of acetaldehyde into acetonitrile, together with lower formation of both CO_2 and N_2 from acetaldehyde and ammonia combustion respectively. This reaction occurs mainly on oxidized V sites since in the absence of oxygen, but in the presence of ammonia, the catalysts converted ethanol into acetaldehyde but the latter, however, did not react with ammonia. Thus, there is a difference in the redox properties between the two catalysts that in presence of O_2 makes the V/Zr/O able to keep the V sites more oxidized, so making the latter more able to activates ammonia for its reaction with the intermediately formed acetaldehyde.

b) Another difference between the two systems is the different efficiency in the conversion of ethanol into acetaldehyde. Experiments of ethanol oxidation showed that in fact the two catalysts differ greatly in regard to their redox behaviour. The fresh V/Ti/O is unselective, but this behavior changes notably during reaction in the presence of ethanol and oxygen, and it becomes progressively more selective to acetaldehyde. The considerable change in the observed catalytic behavior may be related to a modification of the nature of the active V sites; the fully oxidized (and unselective) V sites become progressively more reduced and thus more selective in the formation of acetaldehyde and CO and less in the formation of CO_2. However, even under the best conditions, this catalyst was less selective than V/Zr/O. Conversely, with V/Zr/O, catalyst changes had less effect on products distribution, which indicates that the active V sites do not undergo

important modifications on exposure to the reactant stream. These differences may be explained by taking into account a different type of rate-determining step in the redox process. In V/Ti/O, V^{5+} reduction (by ethanol) is faster than re-oxidation of the reduced V species, giving rise to a working V species which, under steady-state conditions, is strongly reduced. The opposite is true for V/Zr/O, where the rate-determining step is the reduction of the V species, and the working V species is fully or almost fully oxidized under steady-state conditions.

c) In the case of ethanol anaerobic oxidation the experiments demonstrated that ethanol is able to reduce V^{5+} both in V/Ti/O and V/Zr/O. In this case (in absence of oxygen) the oxidized V species selectively form CO_2, but upon reduction CO_2 formation was prevented and the disproportionation of ethanol (to give acetaldehyde, ethane and water) became the main reaction. However, the extent of V^{5+} reduction in the two catalysts was quite different: it is totally reduced to almost metallic V with V/Ti/O, whereas with V/Zr/O only a partial reduction occured.

4.1.2 Spectroscopic Study of V/Zr/O and V/Ti/O catalysts

With the aim of gaining new insights on the redox behaviour of the previously described catalysts, studies of temperature-programmed ethanol desorption using in-situ DRIFT spectroscopy were performed. Figure 90 shows the results for ethanol adsorption and desorption at different temperatures using air as carrier gas. In this case for the low temperature range (85-150°C), the band for chemically bound ethanol (1380 cm^{-1} $\delta_s CH_3$) was dominant in the spectrum of V/Ti/O (bottom), while the spectrum of V/Zr/O showed bands corresponding to ethoxy species (dissociated ethanol, 1057, 1097 and 1143 cm^{-1} $\nu_{(as)}$ *C-O bident.,* $\nu_{(as)}$ *C-C and* $\nu_{(as)}$ *C-O monodent.*) [139] and a negative band at 1630 cm^{-1} (δ *H-O-H*), indicating that water is desorbed from the catalyst (Figure 90, bottom). Water desorption suggests an oxidative dehydrogenation over V/Zr/O which instead is not observed on the V/Ti/O.

With increasing temperature, several broad bands appeared in the spectra of both catalysts. The bands at 1356, 1442 and 1536 cm^{-1} correspond to the stretching of acetate-like moieties (δ_s *CH3,* $\nu_{(as)}$ *O-C-O* $\nu_{(s)}$ *O-C-O)* [148] and they seem to be the predominant surface species in the case of the V/Ti/O from 200°C and then they decreased in intensity

at higher temperatures. However, in the case of V/Zr/O there were additional bands especially in the C=O region indicating more oxidized products. Even if an unambiguous assignment is not possible, the evolution of bands at 1402, 1670 and 1689 cm^{-1} in the case of the V/Zr/O suggests the formation of acetic acid or ethylacetate, and the band at 1562 cm^{-1} is typical for a surface carbonate [138], [149]. Figure 91 shows the deconvoluted spectrum for both catalysts at 350°C. From there is more evident the presence of additional bands in the case of V/Zr/O that correspond to more oxidized products.

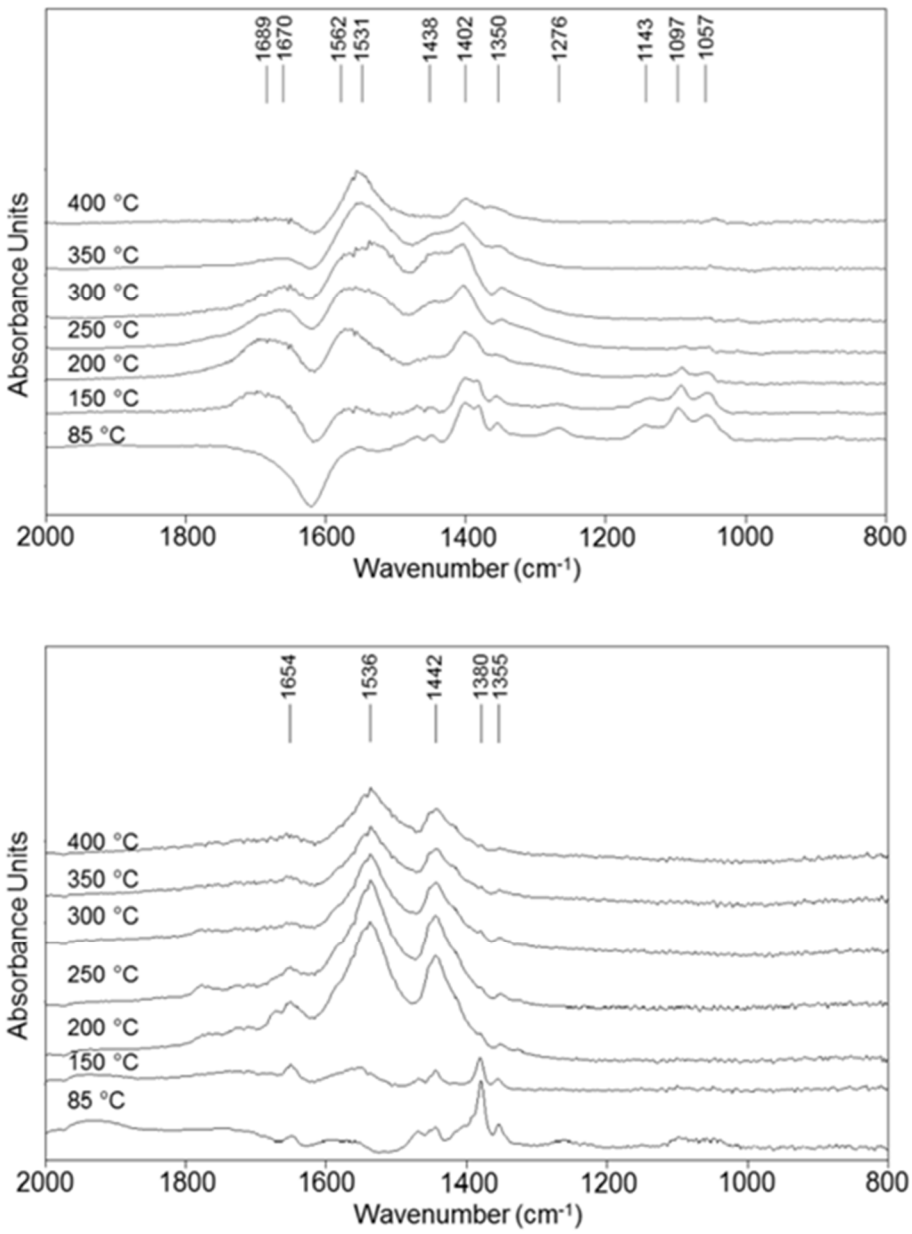

Figure 90. DRIFT spectra recorded during ethanol temperature-programmed-desorption using air as carrier (10 mL min^{-1}).Top: V/Zr/O, Bottom: V/Ti/O.

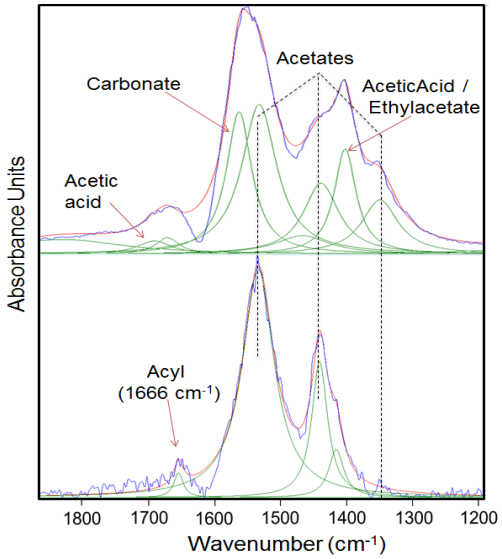

Figure 91. Detail of the DRIFT spectra recorded at 350°C for V/Zr/O (Top) and V/Ti/O (bottom) catalysts after adsorption of ethanol.

Thus, from this analysis it can be inferred that in the case of V/Zr/O, the formation of acetaldehyde results mainly from the oxidative dehydrogenation of activated ethanol (ethoxy species). The resulting reduced V species is promptly reoxidized by O_2 and is able to continue the oxidation process towards the formation of acetic acid, ethylacetate, carbonates and so on. Conversely, in the case of V/Ti/O, acetaldehyde might form mainly by disproportionation of ethanol (with co-formation of ethane), and then it evolves to acetates. However, after V^{5+} has been reduced, the reoxidation process is more difficult, leading the pathway towards the decomposition of the acetates. Figure 92 depicts the proposed routes for ethanol oxidation over the two catalysts.

Experiments were also conducted with V/Zr/O in the absence of O_2, i.e., with a feed of ethanol and He as the carrier gas. Ethanol was first adsorbed at room temperature and then the temperature was increased while recording DRIFT spectra (Figure 93). It can be seen that at low temperatures ethanol dissociated forming the ethoxy species. At 150°C, however, a band at 1632 cm^{-1} appeared. The presence of this band, attributable to the C=O stretching of acetaldehyde, and the lack of a negative band for water desorption confirm that under anaerobic conditions the aldehyde is formed mainly by disproportionation. Interestingly, the spectrum of V/Zr/O under inert atmosphere was similar to that one shown for V/Ti/O in air, confirming that the latter catalyst reduced quickly but it was not easily reoxidised.

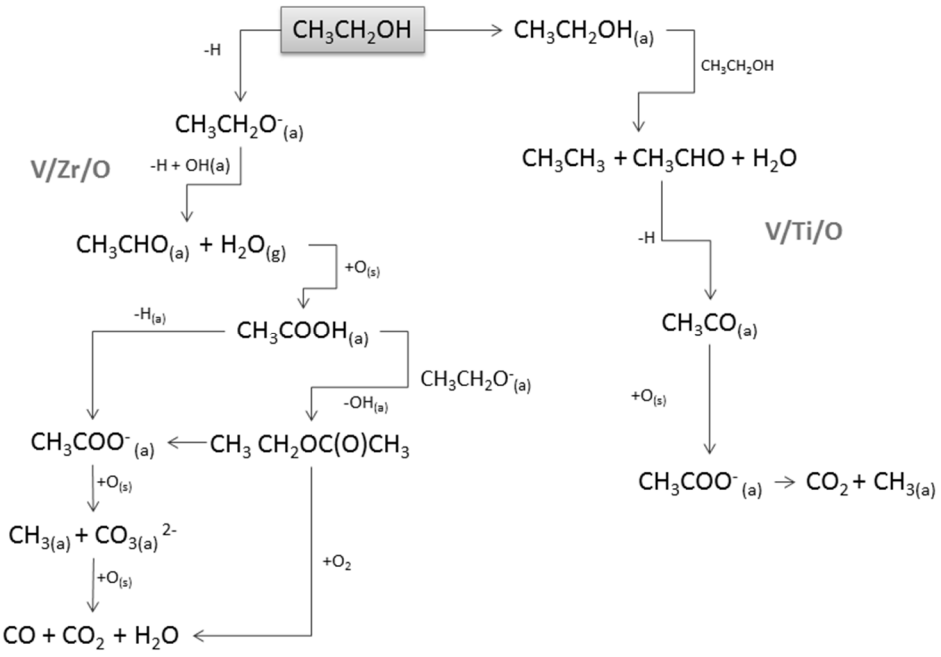

Figure 92. Main pathways for ethanol oxidation on the surface of V/Zr/O (Left) and V/Ti/O2 (Right) catalysts.

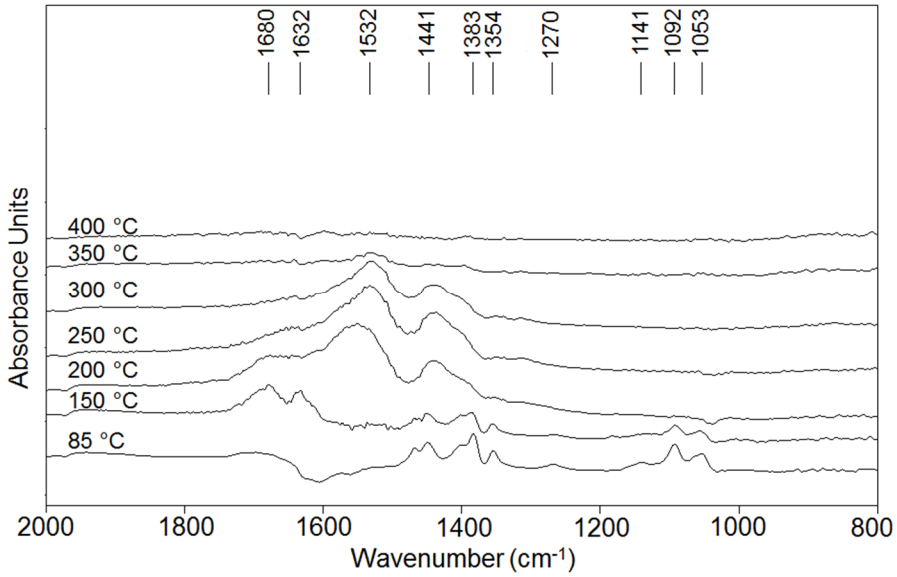

Figure 93. DRIFT spectra of the V/Zr/O recorded during temperature-programmed- ethanol desorption using He as a carrier gas.

Figure 94 compares the main mass spectrometry signals recorded during ethanol TPD measurements conducted with and without oxygen for V/Zr/O. Under anaerobic conditions, even at low temperature, desorption of ethanol, CO_2, acetaldehyde and water was observed. At high temperature desorption of CO_2 was not due to total oxidation (because there was no water formation), but to a decomposition of the intermediates. Conversely, in the presence of air the concomitant desorption of CO_2 and water in several

steps was the evidence for the occurrence of combustion reactions. This confirms once again the previously discussed hypothesis that V/Zr/O is partially reduced by ethanol, but in the presence of oxygen it is able to recover its oxidation state and transform the intermediate acetaldehyde into CO_2 and H_2O.

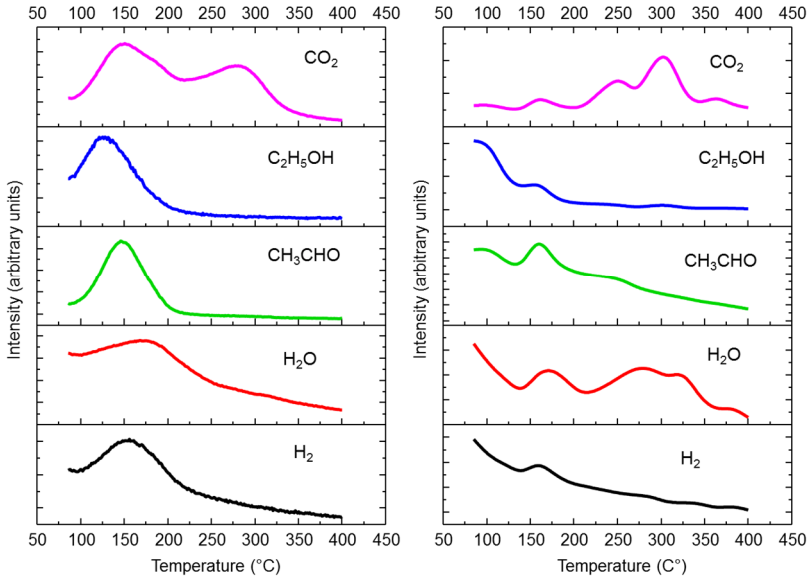

Figure 94. Signals of selected ions as function of temperature recorded after ethanol adsorption in He (left) and in air (right) for the V/Zr/O catalyst.

4.1.3 Conclusions

The investigation by in-situ DRIFT spectroscopy under different conditions of two vanadium oxide catalysts, supported on titania or zirconia were in line with findings from reactivity tests. In fact, these studies reinforce the statements that explain the different catalytic behaviours for the V/Zr/O sample, which is more active and more selective to acetonitrile than V/Ti/O.

The different behaviours were attributed to the fact that V/Zr/O is more selective than V/Ti/O in the oxidative dehydrogenation of ethanol to acetaldehyde, which is a key reaction intermediate in ammoxidation to acetonitrile. This is because the rate-determining is different in the two cases: in V/Ti/O, is the reoxidation of V by O_2, whereas with V/Zr/O it is the reduction by ethanol. It is also important to note that the fully oxidized V^{5+} is intrinsically unselective under anaerobic conditions, giving rise to the formation of CO_2 and H_2O only. The more efficient activation of ammonia with V/Zr/O has been attributed to the greater availability of oxidized V sites in this catalyst.

4.2 Ethanol on Metal-Organic Frameworks (MOFs)

In this case, DRIFTS experiments were performed to shed light on the adsorbent-adsorbate interactions of two MOFS using ethanol as a model probe. The two samples analysed were called Ni(BPEB) and Ni(BTP) and they consist in a metallic centre of Ni surrounded by pyrazolate ligands, either H_2BPEB = 1,4-bis(1*H*-pyrazol-4-ylethynyl)benzene; or H_3BTP = 1,3,5-tris(1*H*-pyrazol-4-yl)benzene) which are depicted in Figure 95. This work was performed in collaboration with the University of Insubria (Universita degli Studi dell'Insubria, Dipartimento di Scienza e Alta Tecnologia, Varese, Italy) where the catalysts were synthesized.

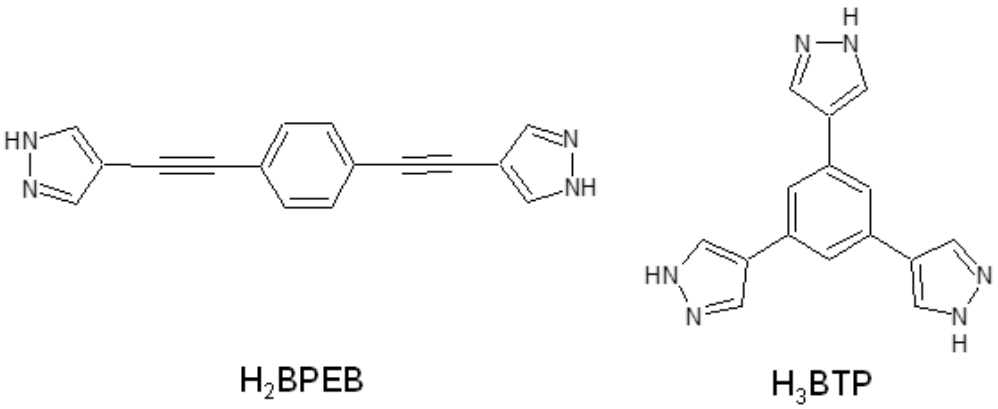

Figure 95. poly(pyrazolato)-based ligands

The resulting MOFs display of course different structural motifs, closely depending on the coordination capacity of the ligand. However, when thermally activated, both MOFs possess potentially accessible open metal sites, which might be involved in adsorbent-adsorbate interactions beneficial, e.g., for gas adsorption or separation, and catalysis [150]. This favourable aspect is further valorised by the high thermal stability imparted, to the whole material, by the poly(pyrazolato)-based spacers: decomposition temperatures, in air, as high as 422 and 430 °C were indeed found for Ni(BPEB) and Ni(BTP), respectively. However, the catalytic performance of these two samples in the (base-free) transformation of 5-hydroxymethyl-2-furfural (HMF) to diformylfuran (DFF) was quite different: Ni(BTP) showed almost 30% yield and 100% selectivity, whereas Ni(BPEB) showed no conversion at all under the same experimental conditions (results obtained in this research group).

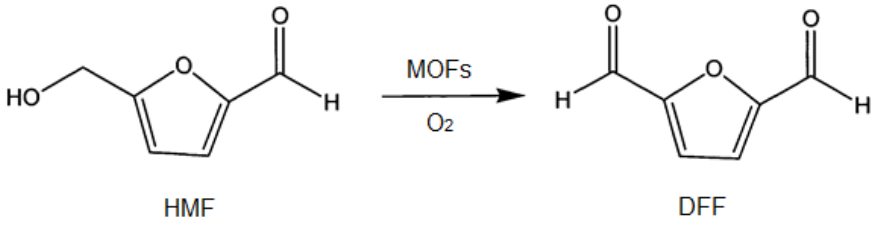

Figure 96. Selective oxidation of HMF to DFF

A first approach aimed to understanding this behaviour was the in-situ observation of their performance during the adsorption of an alcohol. Figure 97 shows the DRIFT spectra acquired at 85 °C during ethanol adsorption on the clean surface of thermally activated Ni(BPEB) and Ni(BTP), while Table 23 lists the most relevant bands detected during the experiment, together with their assignment. On the whole, three events appeared to take place during adsorption on these catalysts. First of all, the progressive growth of the bands centred at 3582 and 3465 cm^{-1} demonstrates that the adsorbate interacts with the MOF through hydrogen bonds. Moreover, as suggested by the bands in the 1090-1040 cm^{-1} region, which can be confidently ascribed to the C-O and C-C stretching of ethoxy species, the alcohol partially dissociates. Finally, and definitely more interesting in the frame of catalysis, the band peaked at 879 cm^{-1} can be interpreted as the Ni-O(H) bending, indicating that the probe interacts with the MOF not only by means of hydrogen bond interactions, but also binding the metal centres *via* its oxygen atoms.

The insurgence of Ni-O(H) interactions between Ni(BTP) and the Lewis basic probe adopted in the present work can be tentatively explained on the basis of previously reported theoretical calculations and experimental observations: by means of FT-IR spectroscopy, Shearer and colleagues [151] could not observe a Ni(II)-probe interaction when using the weak Lewis base CO. This evidence was ascribed to the absence of a positive electrostatic potential at the Ni_4 nodes when Ni(II) is in low-spin state (as typical for Ni(II) in square planar coordination). A positive region could be conversely calculated under the assumption that the metal centres were in high-spin state. It can be suggested that more basic probes like ethanol, can establish Ni(II)-probe interactions energetic enough to overcome the 75 kJ necessary to a mol of Ni(II) ions to switch from low- to high-spin state, in spite of its higher kinetic diameter (4.5 Å for ethanol vs. 3.3 Å for CO).

In the case of thermally activated Ni(BPEB), the bands peaked at 1086 and 1045 cm^{-1} indicate partial dissociation of the alcohol also in this case. The intensity of the bands centred at 3593, 3492 (witnessing the formation of hydrogen bond interactions) and 881

cm^{-1} (indicating the formation of Ni-O(H) bonds) was lower than in the case of Ni(BTP), suggesting less pronounced interactions between the adsorbent and the adsorbate (See also Figure 98 for the ethanol remaining after He flushing).

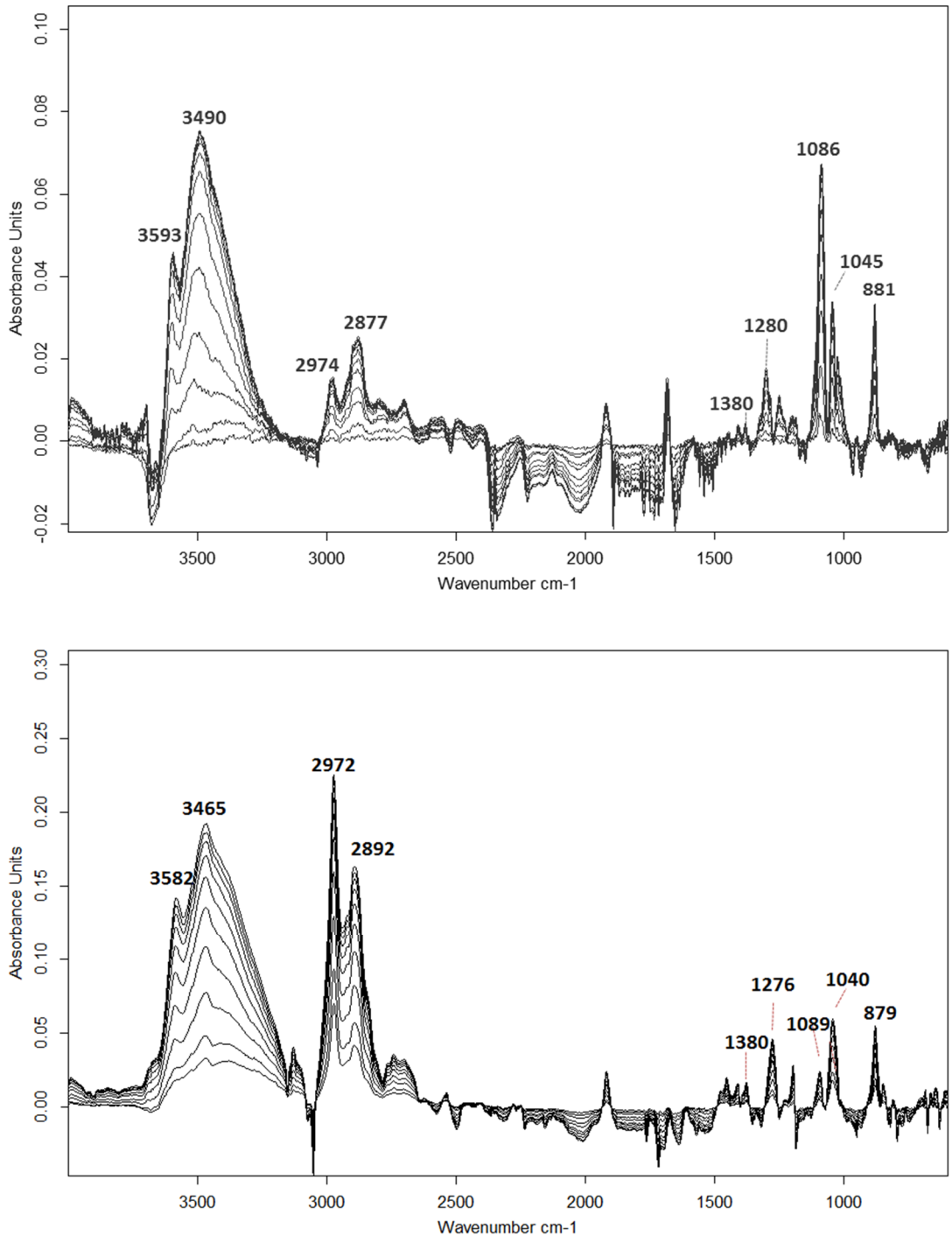

Figure 97. Evolution of the FT-IR spectra acquired at 85 °C on the clean surface of Ni(BPEB) (Top) and Ni(BTP) (Bottom) during ethanol adsorption.

The insurgence of Ni-O(H) bonds between Ni(BPEB) and the Lewis basic probes ethanol/ethoxy can be *qualitatively* explained on the basis of previous theoretical calculations and experimental observations on the isostructural MOF Ni(BDP): Albanese and colleagues [152] explained the lack of insurgence of metal-probe interactions between Ni(BDP) and the apolar probe H_2 or the weak Lewis acid CO_2 in terms of the presence of a positive electrostatic potential around the low-spin state metal centres, the negative cavities near the Ni(II) ions being partially shielded by the ligands. In spite of the positive electrostatic potential around the metal centres, also the weak base CO underwent only physisorption: this occurrence was ascribed to the amount of energy (65 kJ *per* mol of Ni(II) ions) required by Ni(II) to switch from low- to high-spin state. Given the fact that Ni(BPEB) and Ni(BDP) are isostructural and their metal centres possess very similar stereochemistry and second shell environment, the features just described for Ni(BDP) can be qualitatively extended to Ni(BPEB). On the basis of this assumption, it can be proposed that stronger bases like ethanol or ethoxy may establish Ni(II)-probe interactions energetic enough to pass the low-to-high-spin barrier. On the other hand, the higher difficulty faced by ethanol to be adsorbed on Ni(BPEB) rather than on Ni(BTP) could be explained in terms of the different pore aperture and thus possibility of alcohol-Ni interaction in the two cases.

Table 23. Assignment of the DRIFTS bands for ethanol adsorbed on Ni(BPEB) and Ni(BTP)

Vibrational frequency (cm^{-1})	***Vibrational mode***	***Adsorbed species***
3582	ν OH	Intramolecular H-bonds
3465	ν OH	Intermolecular H bonds
2972	$\nu_{(as)}$ CH_3	Ethoxy
2892	$\nu_{(s)}$ CH_3	Ethanol/Ethoxy
1379	δ CH_3	Ethanol
1275	δ OH	Ethanol
1094	$\nu_{(as)}$ CO/ $\nu_{(as)}$ CC	Ethoxy (monodent.)
1043	$\nu_{(s)}$ CO	Ethoxy (bident.)
879	δ Ni-O(H)	Ethanol/Ethoxy-Ni

After the pulse of ethanol, He was let to flow in order to remove physically adsorbed alcohol and again a spectrum was taken. Moreover, in order to further confirm the insurgence of Ni(II)-ethanol interactions on Ni(BTP) and Ni(BPEB), ethanol was adsorbed, under the same experimental conditions, also over $NiCl_2$ and results for the three samples are shown in Figure 98. As expected, FT-IR monitoring of the adsorption on $NiCl_2$ (Figure 98 C) revealed the appearance and progressive growth of a band centred at 877 cm^{-1}. It is interesting to notice as well that besides the general lowered intensity of the absorption bands, in the case of the Ni(BPEB) the band of monodentate ethoxy species was more intense with respect to the bidentate one (band around 1090 vs 1045 cm^{-1}) whereas the contrary was true for the Ni(BTP). This indicates that there is a difference in the accessibility to the active site but also in the way the alcohol can attach to it.

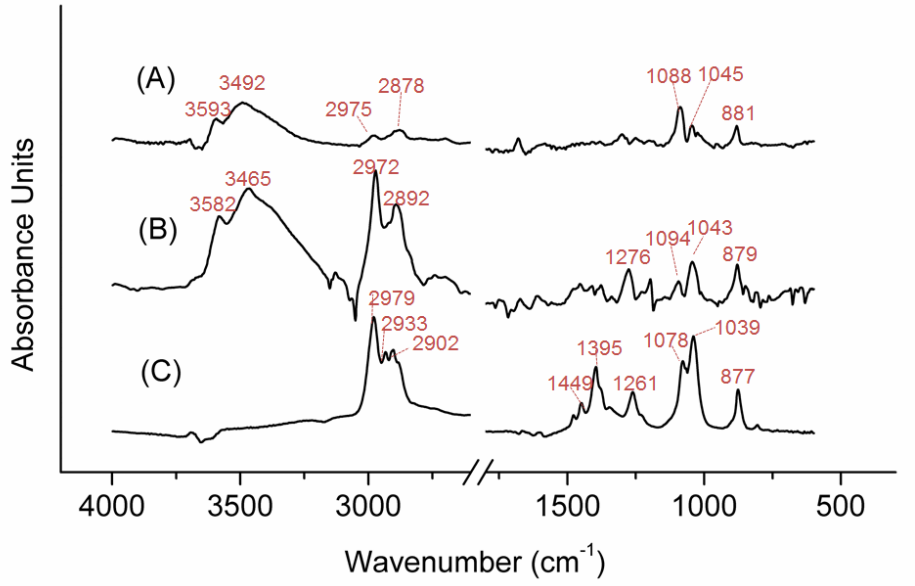

Figure 98. Ethanol chemically adsorbed (after He flushing) at 85 °C on Ni(BPP) (A), Ni(BTP) (B) and NiCl2 (C).

For the sake of completeness, DRIFTS monitoring of ethanol adsorption was performed, in the same experimental conditions, also on non-activated Ni(BTP), still containing Dimethyl-formamide (DMF) within the pores. The comparison of the spectra acquired on activated and non-activated Ni(BTP) after the ethanol pulse and further He flushing (Figure 99), highlights that, on the whole, the same events described above occur, namely insurgence of hydrogen bond interactions, partial deprotonation of the probe and formation of Ni-O(H) bonds. Nonetheless, while the bands ascribed to ethoxy species are more intense for the non-activated adsorbent, the one witnessing the presence of Ni-O(H)

bonds is less intense: this evidence concurs to confirm that not only the metal sites on the surface, but also those inside the pores contribute to the catalytic activity of the MOF, solvated Ni(BTP) being consequently less active than the evacuated counterpart.

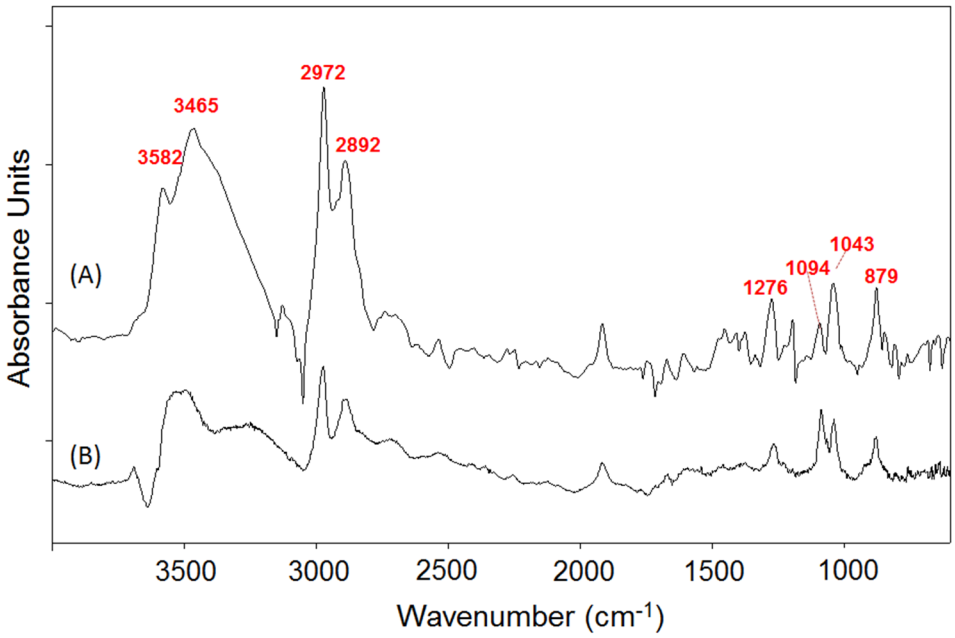

Figure 99.Comparison of ethanol adsorption over Ni(BTP) without DMF (A) and with DMF (B)

Concluding, the differences in the catalytic behavior of the two MOFs samples considered can be related to the way the alcohol group interacts with the active center, because it seems that is more accessible and the interaction is stronger in the case of the Ni(BTP) and because it interacts in a different way with it (bidentate vs. monodentate).

4.3 Ethanol on TiO_2@CeO_x Core-Shells

Ethanol was used to study the particular properties of a ceria layer deposited on bulk titania. This work was made in collaboration with the group "Chimica delle superfici e catalisi" of Professor Gaetano Granozzi at the University of Padova, where the catalysts were synthesized. It was previously investigated by that team the formation of core-shell materials using a core of titania Degussa-P25 (anatase and rutile mixed phase) and a ceria shell [153], finding that the modulation of the layer thickness was important for regulating the $C^{4+/}Ce^{3+}$ ratio. In this case the idea was to use a single phase of titania (rutile) as a core, and characterize the resulting materials.

Two samples were synthesized and labelled TCR1, and TCR3 referring to the titania rutile after one or three impregnations with a solution 0.45M of Ce(III)-ethylhexanoate in hexane (to avoid Ce oxidation). The samples were characterized by N_2 adsorption and XPS. Results are presented in Table 24. The surface area of the mixed samples is higher than that for the titania rutile alone and the Ce/Ti ratio for the TCR3 sample is in fact three times that of the TCR1.

Table 24. Surface area and XPS results for the ceria, titania and mixed TCR samples

Catalysts	*Surface area m^2 g^{-1}*	*Ce/Ti [a]*	*Ce/Ti [b]*
Rutile	17	--	
Ceria	43	--	
TCR1	25	0.06	
TCR3	23	0.18	

Ethanol temperature programmed desorption

Ethanol was sent as a pulse and adsorbed at room temperature over the 4 samples. Afterwards, the carrier gas was let to flow in order to remove the alcohol physically adsorbed. Later the temperature was raised at a constant rate of 10°C min^{-1} and spectra at different temperatures were registered. Results are presented in the following figures. At 30°C it can be observed that the ceria sample presented a particularly complex profile whereas the TCR samples resembled more to the behavior of the titania. For all samples

there was a negative peak at ca 3679 cm^{-1} that is attributed to the loss of surface free OH groups when they become bounded to the alcohol or when they combine with the H of ethanol to desorb as water (See equations below). In fact, another negative band observed at 1631 cm^{-1} is related to the bending of water. The bands of ethoxy species ($C_2H_5O^-$) were also visible, especially for the ceria. They included the C-C and C-O stretching around 1063, 1105 and 1123 cm^{-1}. Also those bands at 2972, 2930 and 2872 cm^{-1} were the characteristic CH bands associated to ethoxides (ν_aCH_3, ν_aCH_2 and ν_sCH_3) [116]. Another particularity for the ceria is the fact that even at this low temperature it presents bands for the acetate species (1312, 1445, and 1561 cm^{-1} corresponding to δCH_3, ν_sOCO and $\nu_{as}OCO$, respectively). Moreover, the bands at 885 and 903 cm^{-1} can be ascribed to new Ce^{4+}-O (O from ethanol) interactions and these were not observed in the other samples. On the contrary, in TCR samples and in titania the prevailing bands were those attributable to ethanol molecularly adsorbed at 1273, 1356, 1380 cm^{-1} ascribed to $\delta(OH)$, $\omega(CH_2)$, and $\delta_s(CH_3)$ respectively and the broad band at 3200 cm^{-1} for the OH stretching.

$$C_2H_5OH(g) \longrightarrow C_2H_5OH(ad)$$

$$C_2H_5OH(ad) \xrightarrow{OH(s)} C_2H_5O^-(ad) + H_2O(g)$$

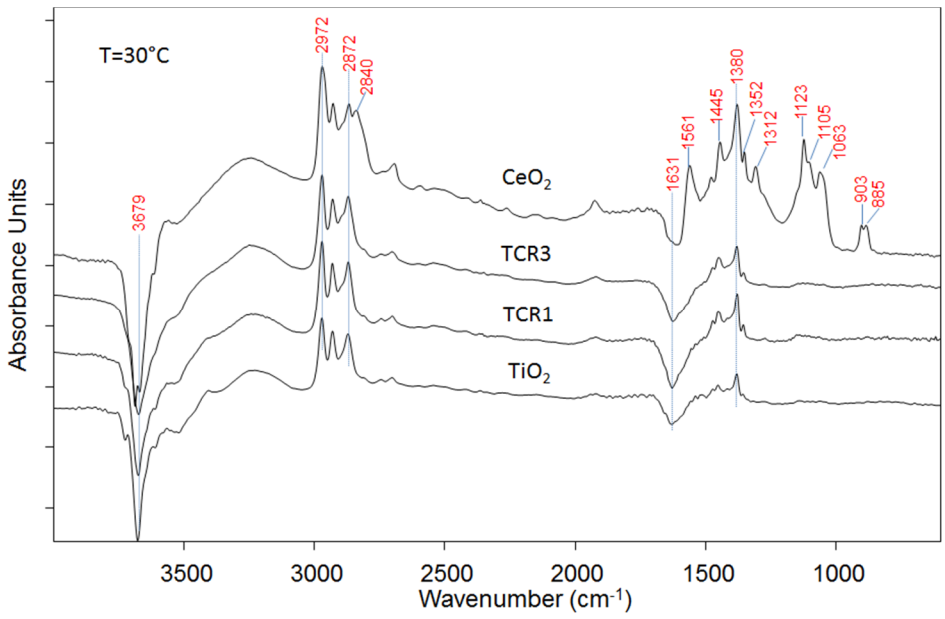

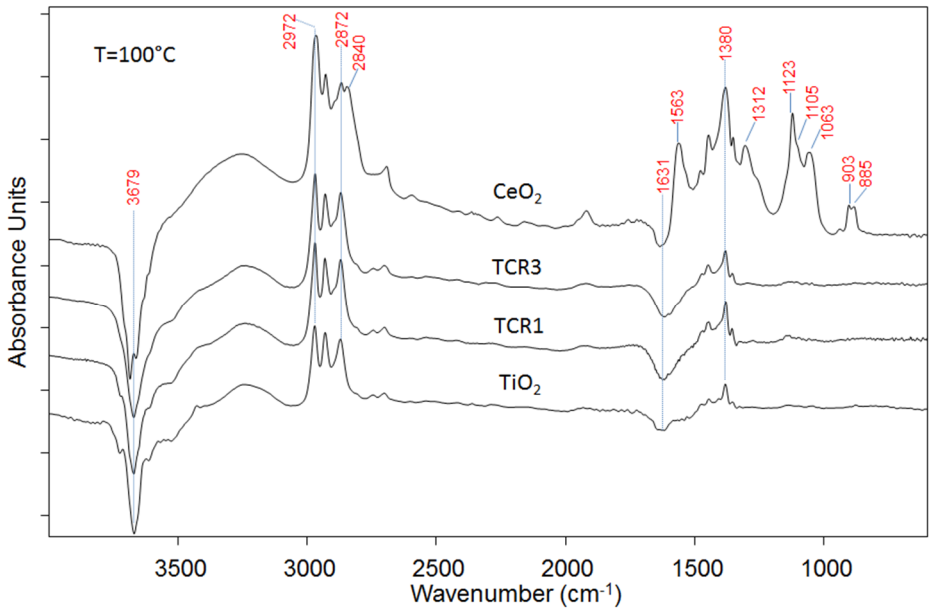
T=100°C
2972
2872
2840
1380
1563
1312
1123
1105
1063
3679
1631
903
885
CeO2
TCR3
TCR1
TiO2
Absorbance Units
3500
3000
2500
2000
1500
1000
Wavenumber (cm-1)

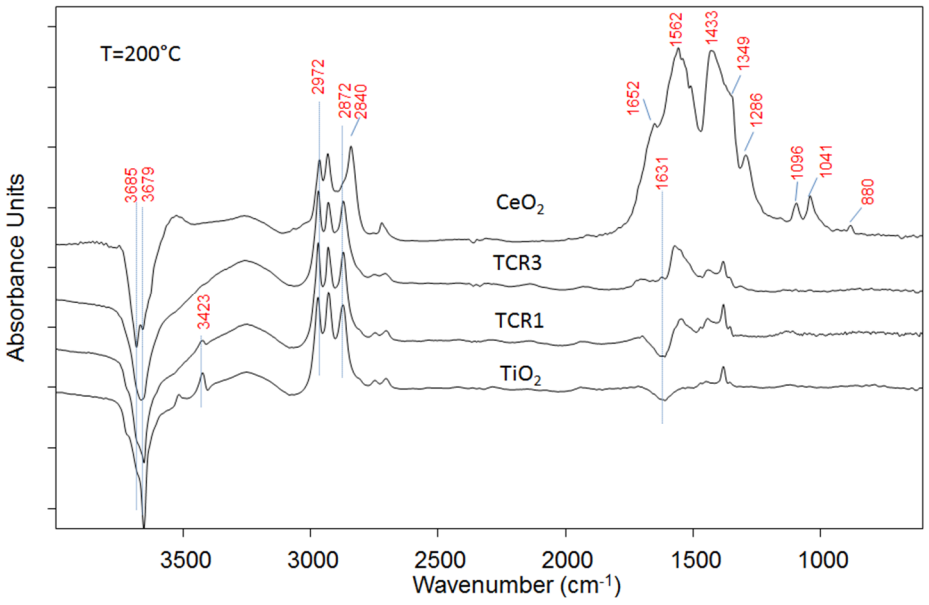
T=200°C
1562
1433
1349
2972
2872
2840
1652
1286
1096
1041
3685
3679
1631
880
CeO2
TCR3
3423
TCR1
TiO2
Absorbance Units
3500
3000
2500
2000
1500
1000
Wavenumber (cm-1)

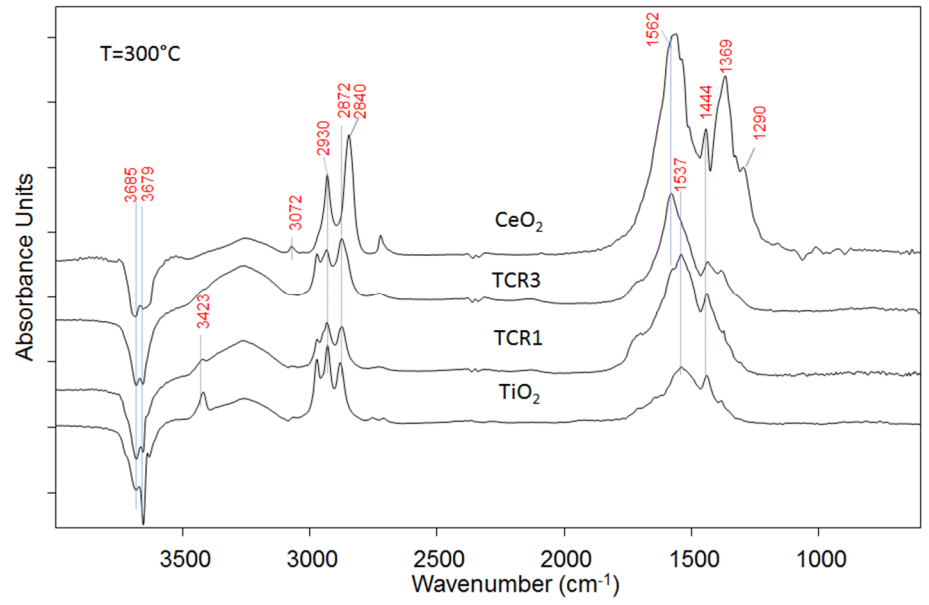
T=300°C
1562
1369
1444
2930
2872
2840
1290
3685
3679
1537
3072
CeO2
TCR3
3423
TCR1
TiO2
Absorbance Units
3500
3000
2500
2000
1500
1000
Wavenumber (cm-1)

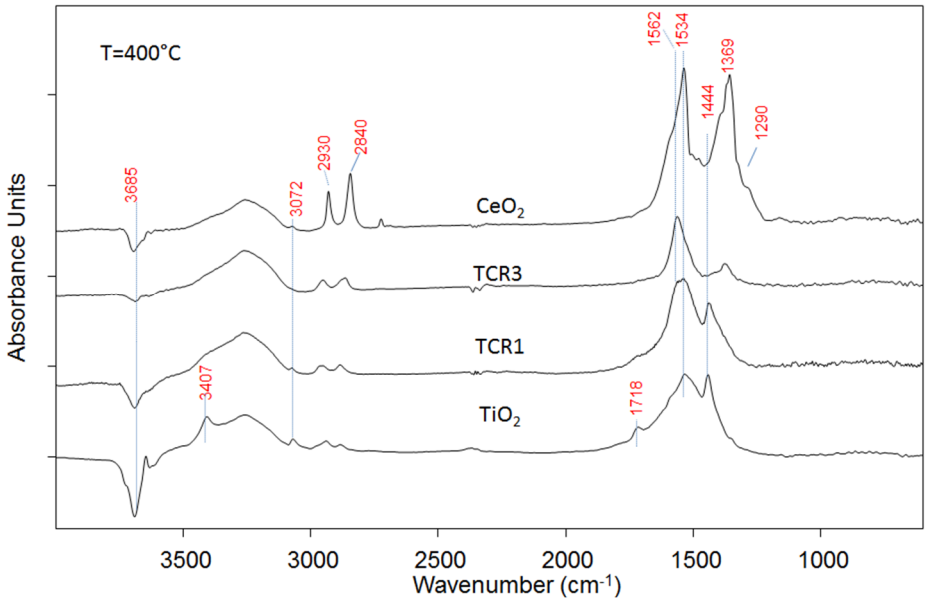

Figure 100. DRIFT spectra during Ethanol TPD for the ceria, titania and mixed TCR samples (T=30 to 400°C)

At increasing temperature (100°C) the spectra did not change much with respect to the one recorded at 30°C. Instead, when the temperature arrived up to 200°C the intensity of acetate bands in ceria increased considerably, and the band at 1562 cm^{-1} appeared as well in TCR3. A new band at 1652 cm^{-1} appeared for the ceria indicating the presence of adsorbed acetaldehyde (C=O stretching). At this temperature, for TCR1 and titania the prevailing bands were still those of ethanol. At 300°C, the acetaldehyde band for ceria disappeared and bands attributable to acetates were the prevailing ones in all samples; however they were shifted toward higher wavenumbers for TCR3 and to lower wavenumbers for both TC1R and titania, indicating a different strength in the two cases. At 400°C, for CeO_2 evidence for the transformation of acetate species to carbonate was shown, since the intensity of band at 1562 cm^{-1} decreased while a new band was formed at 1534 cm^{-1}. This band, together with that one at 1369 cm^{-1} was similar to other bands attributed in literature to bidentate carbonates [154]. These bands fell at the same wavelenght for TCR3, whereas in the case of TC1R and titania they might still correspond to acetates.

In general these spectra showed that the Ce present in TCR samples is stabilized as Ce^{3+} since (especially at lower temperatures) the TCR samples did not present the typical acetate and carbonate bands associated with the oxidized Ce. It is important to notice that in this case when rutile was used as a core, the formation of the shells was incomplete (as

seen from the TEM analysis, not shown) and DRIFT spectra confirmed that especially in the case of TCR1 ethanol had access to the exposed titania surface.

Nevertheless, a synergic effect was observed while monitoring on-line the desorbed products (Figure 101). From there it was clear that the TC1R had increased dehydrogenating properties since it was able to produce acetaldehyde at lower temperature and with relative higher intensity. This phenomenon cannot be related to Ce oxidation state, since in both TCR samples it was mainly present in the reduced form; therefore the explanation can be given by taking into account that TCR1 presents a lower quantity of Ce, that being better dispersed that in the case of TCR3 (as observed by TEM analysis, not shown), a greater fraction of Ce/Ti interface is available (together with more titania borders exposed) and it might become active for ethanol dehydrogenation. In fact, the Ce-Ti interface was observed to have a particular enhanced activity in the production of formaldehyde from methanol [155].

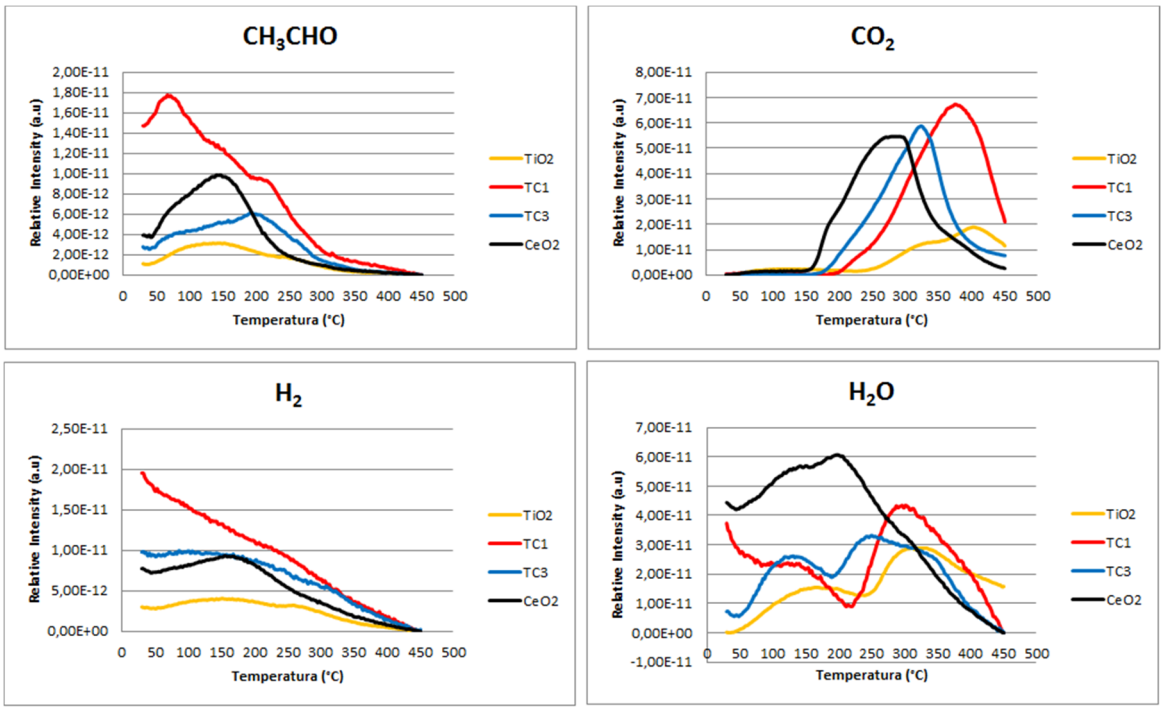

Figure 101. Main products monitored during ethanol TPD on ceria, titania and TCR mixed samples

4.4 1-Butanol Oxidehydration to Maleic Anhydride

The catalytic behavior of vanadyl pyrophosphate (VPP) in the transformation of 1-butanol to maleic anhydride (MA) was previously investigated by Giulia Pavarelli et al [156]. It was found that the VPP catalyst is very selective in ethanol dehydration to butenes (it does not form the dehydrogenation product, butyraldehyde). However, the kinetically consecutive step of butene oxidation into MA shows a limited selectivity, because of the several side reactions. Moreover, it was observed that there is an optimal range of oxygen partial pressure to carry out the reaction. In fact, both low (less than 0.10 molar fraction) and high (more than 0.20) oxygen partial pressure led to poor selectivity either because of the prevailing selectivity to olefins, or because of the dominant CO and CO_2 formation.

4.4.1 A DRIFTS study of butanol interaction with the VPP

In order to understand the interaction of the alcohol with the catalyst surface and investigate on the reaction mechanism, a DRIFT spectroscopic investigation was performed first by adsorption of 1-butanol over VPP at 140°C using inert (He) or oxidizing carrier gas (air). Figure 102 shows the spectra obtained and in both cases it can be stated that 1-butanol interacted strongly with the OH groups present on the catalyst surface as seen by the negative peaks at 3743 and 3663 cm^{-1}. The positive peaks at around 3250 and 2970-2880 cm^{-1} correspond to the OH and C-H stretching of adsorbed butanol, respectively. In the case of air as a carrier, the peaks at 1727, 1627, and 1468 cm^{-1} indicate the presence of oxidised species even at this low temperature; these bands may be attributed to either crotonic or maleic acid [157]. These experiments confirm the strong interaction of the alcohol with the VPP, and this probably caused the saturation of the surface.

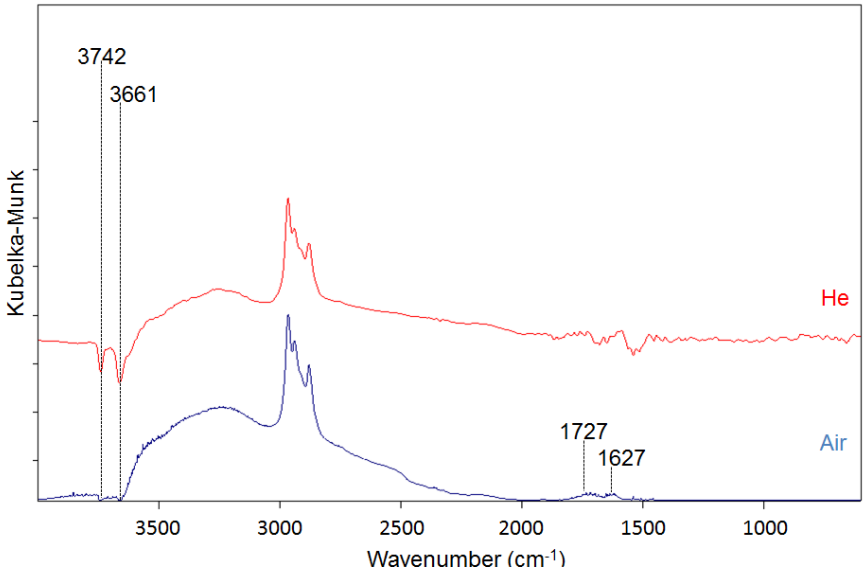

Figure 102. 1-Butanol adsorption on VPP catalyst at 140°C.

The alcohol adsorption was performed also at 300°C. In this case the differences among spectra recorded under different conditions were more evident (Figure 103). In the case of inert atmosphere, the most important features were the negative peaks at high frequency and some broad bands at around 1630 cm^{-1} and 973 cm^{-1}. The former may correspond to a C=C stretching of an olefin (butene) adsorbed on the surface, while the latter is usually attributed to a V=O stretching [158]. Therefore, in this case (when no air is present) the catalyst was able to dehydrate the butanol producing butenes, but this altered the catalyst surface. On the other hand, when air was present, olefins were also formed (butenes and butadiene in this case) but they were further oxidised as evidenced by both the sharp peak present at 1778 cm^{-1} and the shoulder at 1850 cm^{-1}, which have been attributed previously in literature to the O-C=O stretching of adsorbed MA [157], [159]. The bands at 1730 and 1616 cm^{-1} indicate either the presence of species with a C=O and/or C=C bond, such as butyraldehyde, 2-propanal, furan, and alkenals, or some adsorbed unreacted olefins. Since there were no changes in the low frequency range, this confirms that oxygen is necessary to keep the catalyst surface species unaltered. As regards the OH interaction, clearly in oxidant atmosphere the bands were less intense and this agrees with the fact (observed in reactivity tests) that air (O_2) is needed in order to have a less adsorbed and thus more reactive molecule, which is more quickly oxidised because of the greater availability of V^{5+} sites.

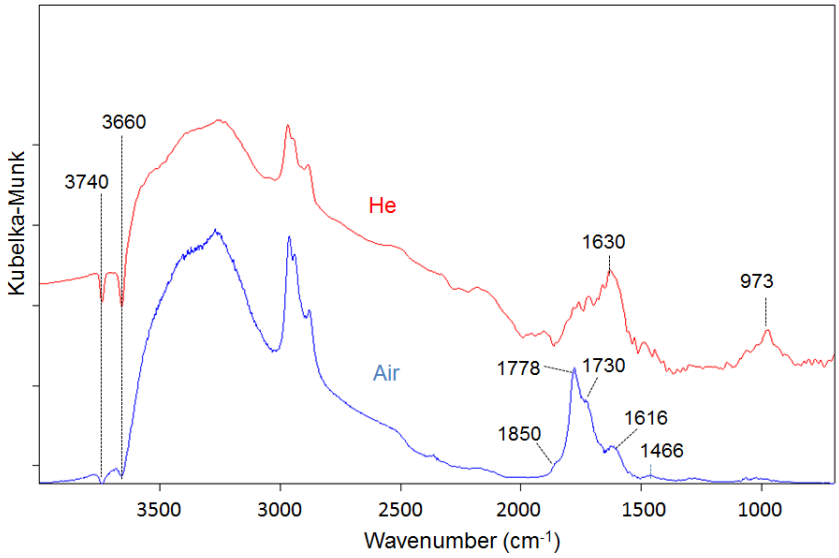

Figure 103. 1-Butanol adsorption on VPP catalyst at 300°C

Temperature programmed desorption (TPD) of butanol was also carried out. In this set of experiments, the adsorption was performed at 140°C and then stopped to monitor the reactive transformations of the adsorbed species with temperature. As observed from the spectra (Figure 104), in the case of inert atmosphere adsorbed butanol evolved mainly towards butadiene (broad band centred at 1602 cm^{-1}) but then other olefins and carbonylic species also formed (C=C and C=O bands around 1630-1724 cm^{-1}); this occurred concomitantly with the increase of the band at 978 cm^{-1}, thus confirming that vanadyl (V^{4+}) surface species developed during the transformation of 1-butanol under inert atmosphere. The OH interaction was so strong that it was maintained throughout the whole temperature program (negative bands); in fact, a slightly decreased intensity was seen only at T>320°C. On the other hand, when air was present, oxidised carbonyl species were more readily formed, corresponding to further oxidation compounds; particularly, the bands at around 1780 and 1850 cm^{-1} were assigned to adsorbed MA.

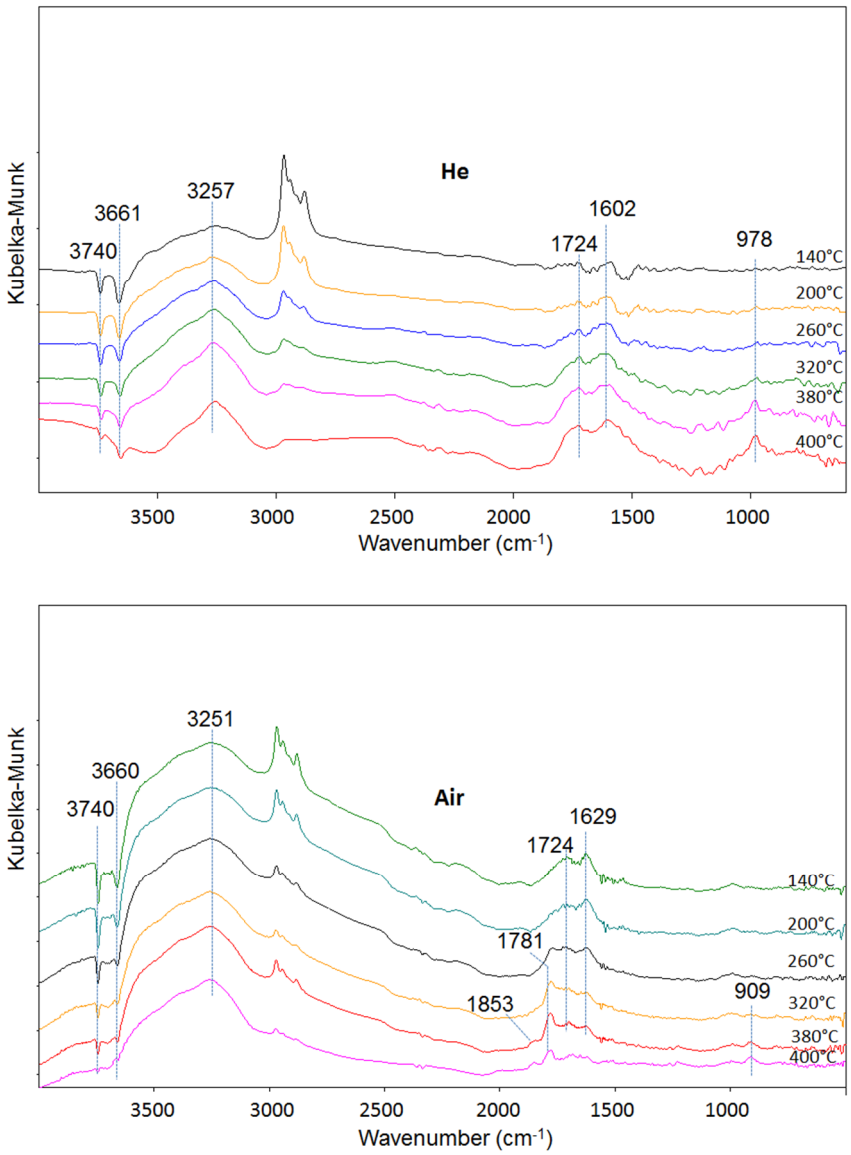

Figure 104. 1-Butanol adsorption on VPP catalyst at 140°C and its transformation with temperature in inert atmosphere (top) and oxidising environment (bottom).

From these experiments it may be concluded that the catalyst under anaerobic conditions is able to dehydrate 1-butanol and oxidise olefins (until crotonic or maleic acid); however, oxygen from the gas phase becomes necessary because it helps to keep the vanadium centres effectively oxidised, while also making it possible for the intermediate to dehydrate and desorb, in the end producing MA.

5 GENERAL CONCLUSIONS

- Ethanol is easily obtained from biomass fermentation and already available in big amounts and this makes it one of the pillar building blocks in the bio-refineries model. The possibility to obtain high added value molecules such as butadiene from ethanol and other bio-alcohols is a driving force to continue the research in this field, since it would reduce the dependence on fossil fuels availability to obtain this olefin and many other compounds such as ethylene, acetonitrile, n-butanol, maleic anhydride and so on.
- In spite of the long history of ethanol in the chemical industry, the details of its catalytic transformation (especially over basic materials), continues to be an active subject of debate. The present research was an attempt to clarify the key points of the mechanism currently accepted for ethanol conversion into butadiene or butanol and it gave as a result an alternative mechanistic proposal that allowed the explanation of several experimental observations and literature statements.
- The in-situ spectroscopic observation of the catalysts under working conditions was an important tool to identify intermediates and to propose reaction pathways for ethanol transformation; the DFT calculations were useful in demonstrating the feasibility of such proposed routes. Moreover, the different characterization techniques allowed identifying the physical properties having influence in directing the selectivity of the reaction to a desired product.
- Besides the study of the transformation of ethanol to butadiene, other important reactions of great interest such as ethanol ammoxidation to acetonitrile or 1-butanol oxidehydration to maleic anhydride were also considered and studied by means of in-situ DRIFT spectroscopy.
- Ethanol was used as well as a probe molecule to investigate the properties of materials with particular features such as Ni-Metallic organic frameworks or CeOx-TiO_2-nanocomposites

6 PUBLICATIONS

Book chapters:

"Gas-Phase Oxidation of Alcohols: Innovation in Industrial Technologies and Recent Developments". Velasquez Ochoa, J. and Cavani, F.; CHAPTER 8 in *Transition Metal Catalysis in Aerobic Alcohols Oxidation*. (2014), p. 203-230. Print ISBN: 978-1-84973-823-1. Doi: 10.1039/9781782621652-00203. Royal Society of Chemistry.

"Olefins from Biomass" Chieregato, A., Velasquez Ochoa, J. and Cavani, F.; CHAPTER 1 in *Chemicals and Fuels from Bio Based Building Blocks*. (2016), p. 1-32. Print ISBN: 978-3-527-33897-9. Doi: 10.1002/9783527698202.ch1. Wiley-VCH Verlag GmbH & Co. KGaA.

Journals:

"An analysis of the chemical, physical and reactivity features of $MgO–SiO_2$ catalysts for butadiene synthesis with the Lebedev process". Velasquez Ochoa, J., Bandinelli, C., Vozniuk, O., Chieregato, A., Malmusi, A., Recchi, C., and Cavani, F. *Green Chemistry*, (advanced article) 2016. Doi: 10.1039/C5GC02194D.

"On the Chemistry of Ethanol on Basic Oxides: Revising Mechanisms and Intermediates in the Lebedev and Guerbet reactions" Chieregato, A., Velasquez Ochoa,J., Bandinelli, C., Fornasari, G., Cavani, F., and Mella, M. *ChemSusChem*, 8 (2015) 377–388.

"A New Process for Maleic Anhydride Synthesis from a Renewable Building Block: The Gas-Phase Oxidehydration of Bio-1-butanol". Pavarelli G., Velasquez Ochoa J., Caldarelli A., Puzzo F., Cavani F., and Dubois JL. *ChemSusChem*. 8 (2015) 2250-2259.

"Gas-Phase Ammoxidation: An Alternative Process for Acetonitrile Synthesis" Folco, F., Velasquez Ochoa, J., Cavani, F., Ott, L., Janssen, M. *Submitted.*

7 ACKNOWLEDGEMENTS

The financial support of Università di Bologna (for the PhD grant) is gratefully acknowledged.

Versalis SpA is also thankfully acknowledged for sponsoring part of the research activity described in this thesis.

We can only be said to be alive in those moments when our hearts are conscious of our treasures. ~Thornton Wilder

I'm very grateful to all the treasures (persons) I've found on my way during the years of this doctorate (included those who could not remain); and even more grateful with the people who have been with me for several years now and keep holding my back. Figure 105 summarizes some of the persons who make part of my life and which I keep close to my heart.

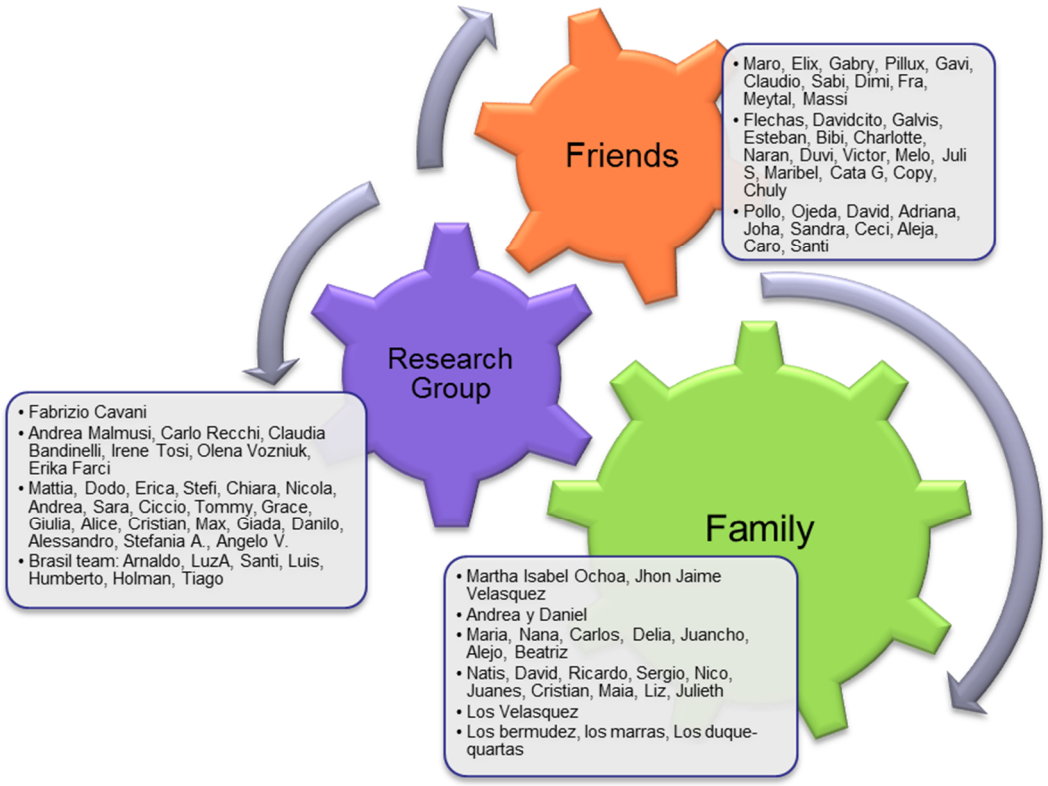

Figure 105. Best team ever

8 REFERENCES

[1] A. Chieregato, J. Velasquez Ochoa, C. Bandinelli, G. Fornasari, F. Cavani, and M. Mella, "On the Chemistry of Ethanol on Basic Oxides: Revising Mechanisms and Intermediates in the Lebedev and Guerbet reactions," *ChemSusChem*, vol. 8, pp. 377–388, 2015.

[2] J. Scalbert, F. Thibault-Starzyk, R. Jacquot, D. Morvan, and F. Meunier, "Ethanol condensation to butanol at high temperatures over a basic heterogeneous catalyst: How relevant is acetaldehyde self-aldolization?," *J. Catal.*, vol. 311, pp. 28–32, Mar. 2014.

[3] J. Rass-Hansen, H. Falsig, B. Jørgensen, and C. H. Christensen, "Bioethanol : fuel or feedstock ?," *J. Chem. Technol. Biotechnol.*, vol. 82, pp. 329–333, 2007.

[4] S. Kim and B. E. Dale, "Global potential bioethanol production from wasted crops and crop residues," *Biomass and Bioenergy*, vol. 26, no. 4, pp. 361–375, Apr. 2004.

[5] J. A. Posada, A. D. Patel, A. Roes, K. Blok, A. P. C. Faaij, and M. K. Patel, "Potential of bioethanol as a chemical building block for biorefineries: preliminary sustainability assessment of 12 bioethanol-based products.," *Bioresour. Technol.*, vol. 135, pp. 490–9, May 2013.

[6] P. Lanzafame, G. Centi, and S. Perathoner, "Evolving scenarios for biorefineries and the impact on catalysis," *Catal. Today*, vol. 234, pp. 2–12, Oct. 2014.

[7] J. Althoff, K. Biesheuvel, A. De Kok, H. Pelt, M. Ruitenbeek, G. Spork, J. Tange, and R. Wevers, "Economic Feasibility of the Sugar Beet-to-Ethylene Value Chain," *ChemSusChem*, vol. 6, no. 9, pp. 1625–1630, 2013.

[8] D. Fan, D.-J. Dai, and H.-S. Wu, "Ethylene Formation by Catalytic Dehydration of Ethanol with Industrial Considerations," *Materials (Basel).*, vol. 6, no. 1, pp. 101–115, Dec. 2012.

[9] M. Zhang and Y. Yu, "Dehydration of Ethanol to Ethylene," *Ind. Eng. Chem. Res.*, vol. 52, no. 28, pp. 9505–9514, Jun. 2013.

[10] D. Minoux, N. Nesterenko, W. Vermeiren, and D. Sander Van, "Dehydration of alcohols in the presence of an inert component," *WO2009098268A1*, vol. Total Petr, Aug. 2009.

[11] F. Maiko and A. Kimura, "Process for the manufacture of ethylene by dehydration of ethanol," EP2594546A1.2013.

[12] B. Patrick Gracey and S. R. Partington, "Process for preparing ethene," WO2009050433A1.2009.

[13] T. K. Phung and G. Busca, "Diethyl ether cracking and ethanol dehydration: Acid catalysis and reaction paths," *Chem. Eng. J.*, vol. 272, pp. 92–101, Jul. 2015.

[14] M. Kang, J. F. DeWilde, and A. Bhan, "Kinetics and Mechanism of Alcohol Dehydration on γ-Al2O3: Effects of Carbon Chain Length and Substitution," *ACS Catal.*, vol. 5, no. 2, pp. 602–612, Feb. 2015.

[15] T. Hou, S. Zhang, Y. Chen, D. Wang, and W. Cai, "Hydrogen production from ethanol reforming: Catalysts and reaction mechanism," *Renew. Sustain. Energy Rev.*, vol. 44, no. 0, pp. 132–148, Apr. 2015.

[16] M. A. Christiansen, G. Mpourmpakis, and D. G. Vlachos, "DFT-driven multi-site microkinetic modeling of ethanol conversion to ethylene and diethyl ether on γ-Al2O3(111)," *J. Catal.*, vol. 323, pp. 121–131, Mar. 2015.

[17] M. E. Potter, M. E. Cholerton, J. Kezina, R. Bounds, M. Carravetta, M. Manzoli, E. Gianotti, M. Lefenfeld, and R. Raja, "Role of Isolated Acid Sites and Influence of Pore Diameter in the Low-Temperature Dehydration of Ethanol," *ACS Catal.*, vol. 4, no. 11, pp. 4161–4169, Nov. 2014.

[18] J. F. DeWilde, C. J. Czopinski, and A. Bhan, "Ethanol Dehydration and Dehydrogenation on γ-Al2O3: Mechanism of Acetaldehyde Formation," *ACS Catal.*, vol. 4, no. 12, pp. 4425–4433, Dec. 2014.

[19] M. Mascal, "Chemicals from biobutanol: technologies and markets," *Biofuels, Bioprod. Biorefining*, vol. 6, no. 4, pp. 483–493, Jul. 2012.

[20] G. Pavarelli, J. Velasquez Ochoa, A. Caldarelli, F. Puzzo, F. Cavani, and J.-L. Dubois, "A New Process for Maleic Anhydride Synthesis from a Renewable Building Block: The Gas-Phase Oxidehydration of Bio-1-butanol.," *ChemSusChem*, vol. 8, no. 13, pp. 2250–9, Jul. 2015.

[21] P. Lanzafame, G. Centi, and S. Perathoner, "Catalysis for biomass and CO2 use through solar energy: opening new scenarios for a sustainable and low-carbon chemical production.," *Chem. Soc. Rev.*, vol. 43, no. 22, pp. 7562–80, Nov. 2014.

[22] T. Tsuchida, S. Sakuma, T. Takeguchi, and W. Ueda, "Direct Synthesis of n-Butanol from Ethanol over Nonstoichiometric Hydroxyapatite," *Ind. Eng. Chem. Res.*, vol. 45, no. 25, pp. 8634–8642, Dec. 2006.

[23] C. Yang and Z. Y. Meng, "Bimolecular Condensation of Ethanol to 1-Butanol Catalyzed by Alkali Cation Zeolites," *J. Catal.*, vol. 142, no. 1, pp. 37–44, 1993.

[24] J. T. Kozlowski and R. J. Davis, "Heterogeneous Catalysts for the Guerbet Coupling of Alcohols," *ACS Catal.*, vol. 3, no. 7, pp. 1588–1600, Jul. 2013.

[25] G. R. M. Dowson, M. F. Haddow, J. Lee, R. L. Wingad, and D. F. Wass, "Catalytic Conversion of Ethanol into an Advanced Biofuel: Unprecedented Selectivity for n-Butanol," *Angew. Chemie Int. Ed.*, vol. 52, no. 34, pp. 9005–9008, Aug. 2013.

[26] M. Eckert, G. Fleischmann, R. Jira, H. M. Bolt, and K. Golka, "Acetaldehyde," in *Ullmann's Encyclopedia of Industrial Chemistry.*, Weinheim: Wiley-VCH Verlag GmbH & Co. KGaA, 2006.

[27] J. Velasquez Ochoa and F. Cavani, "Gas-Phase Oxidation of Alcohols: Innovation in Industrial Technologies and Recent Developments," in *Transition Metal Catalysis in Aerobic Alcohol Oxidation*, F. Cardona and C. Parmeggiani, Eds. Cambridge: Royal Society of Chemistry, 2014, pp. 203–230.

[28] A. Corma and H. Garcia, "Supported gold nanoparticles as catalysts for organic reactions.," *Chem. Soc. Rev.*, vol. 37, no. 9, pp. 2096–126, Sep. 2008.

[29] M. Stratakis and H. Garcia, "Catalysis by supported gold nanoparticles: beyond aerobic oxidative processes.," *Chem. Rev.*, vol. 112, no. 8, pp. 4469–506, Aug. 2012.

[30] T. Ishida and M. Haruta, "Gold catalysts: towards sustainable chemistry.," *Angew. Chem. Int. Ed. Engl.*, vol. 46, no. 38, pp. 7154–6, Jan. 2007.

[31] N. Dimitratos, J. A. Lopez-Sanchez, and G. J. Hutchings, "Selective liquid phase oxidation with supported metal nanoparticles," *Chem. Sci.*, vol. 3, no. 1, pp. 20–44, 2012.

[32] A. S. K. Hashmi and G. J. Hutchings, "Gold Catalysis-the journey continues," *Catal. Sci. Technol.*, vol. 3, no. 11, p. 2861, 2013.

[33] G. J. Hutchings and J. K. Edwards, "Application of gold nanoparticles in catalysis," *Frontiers of Nanoscience*, vol. 3, no. 1. pp. 249–293, 2012.

[34] C. Della Pina, E. Falletta, and M. Rossi, "Update on selective oxidation using gold," *Chem. Soc. Rev.*, vol. 41, no. 1, pp. 350–369, 2012.

[35] C. Della Pina, E. Falletta, and M. Rossi, "Gold Nanoparticles-catalyzed Oxidations in Organic Chemistry," in *Nanoparticles and Catalysis*, D. Astruc, Ed. Wenheim: Wiley-VCH Verlag GmbH & Co. KGaA, 2008, pp. 427–455.

[36] C. Della Pina, E. Falletta, and M. Rossi, "Liquid Phase Oxidation of Organic Compounds by Supported Metal-Based Catalysts with a Focus on Gold," in *Liquid Phase Oxidation via Heterogeneous Catalysis: Organic Synthesis and Industrial Applications*, M. G. Clerici and O. Kholdeeva, Eds. Wiley-VCH Verlag GmbH & Co. KGaA, 2013, pp. 221–262.

[37] C. Della Pina, E. Falletta, and M. Rossi, "Oxidation of Alcohols and Carbohydrates," in *Modern Gold Catalyzed Synthesis*, S. K. Hashmi and F. D. Toste, Eds. Wenheim: Wiley-VCH Verlag GmbH & Co. KGaA, 2012, pp. 309–329.

[38] C. H. Christensen, B. Jørgensen, J. Rass-Hansen, K. Egeblad, R. Madsen, S. K. Klitgaard, S. M. Hansen, M. R. Hansen, H. C. Andersen, and A. Riisager, "Formation of acetic acid by aqueous-phase oxidation of ethanol with air in the presence of a heterogeneous gold catalyst.," *Angew. Chem. Int. Ed. Engl.*, vol. 45, no. 28, pp. 4648–51, Jul. 2006.

[39] B. Jorgensen, S. E. Christiansen, M. L. D. Thomsen, and C. H. Christensen, "Aerobic oxidation of aqueous ethanol using heterogeneous gold catalysts: Efficient routes to acetic acid and ethyl acetate," *J. Catal.*, vol. 251, no. 2, pp. 332–337, Oct. 2007.

[40] P. Liu and E. J. M. Hensen, "Highly efficient and robust Au/MgCuCr2O4 catalyst for gas-phase oxidation of ethanol to acetaldehyde.," *J. Am. Chem. Soc.*, vol. 135, no. 38, pp. 14032–5, Sep. 2013.

[41] M. Gubelmann-Bonneau, "Process for the production of acetic acid by controlled oxidation of ethanol," US5840971 (A)1998.

[42] B. Jørgensen, S. B. Kristensen, A. J. Kunov-Kruse, R. Fehrmann, C. H. Christensen, and A. Riisager, "Gas-Phase Oxidation of Aqueous Ethanol by Nanoparticle Vanadia/Anatase Catalysts," *Top. Catal.*, vol. 52, no. 3, pp. 253–257, Jan. 2009.

[43] X. Li and E. Iglesia, "Selective catalytic oxidation of ethanol to acetic acid on dispersed Mo-V-Nb mixed oxides.," *Chem. A Eur. J.*, vol. 13, no. 33, pp. 9324–30, Jan. 2007.

[44] V. I. Sobolev and K. Y. Koltunov, "MoVNbTe Mixed Oxides as Efficient Catalyst for Selective Oxidation of Ethanol to Acetic Acid," *ChemCatChem*, vol. 3, no. 7, pp. 1143–1145, Jul. 2011.

[45] G. Litt and C. Almquist, "An investigation of CuO/Fe2O3 catalysts for the gas-phase oxidation of ethanol," *Appl. Catal. B Environ.*, vol. 90, no. 1–2, pp. 10–17, Jul. 2009.

[46] C. P. Rodrigues, V. T. da Silva, and M. Schmal, "Partial oxidation of ethanol over cobalt oxide based cordierite monolith catalyst," *Appl. Catal. B Environ.*, vol. 96, no. 1–2, pp. 1–9, Apr. 2010.

[47] R. D. Weinstein, A. R. Ferens, R. J. Orange, and P. Lemaire, "Oxidative dehydrogenation of ethanol to acetaldehyde and ethyl acetate by graphite nanofibers," *Carbon N. Y.*, vol. 49, no. 2, pp. 701–707, Feb. 2011.

[48] I. F. McConvey, D. Woods, M. Lewis, Q. Gan, and P. Nancarrow, "The Importance of Acetonitrile in the Pharmaceutical Industry and Opportunities for its Recovery from Waste," *Org. Process Res. Dev.*, vol. 16, no. 4, pp. 612–624, Apr. 2012.

[49] T. Ishida, H. Watanabe, T. Takei, A. Hamasaki, M. Tokunaga, and M. Haruta, "Metal oxide-catalyzed ammoxidation of alcohols to nitriles and promotion effect of gold nanoparticles for one-pot amide synthesis," *Appl. Catal. A Gen.*, vol. 425–426, pp. 85–90, May 2012.

[50] S. J. Kulkarni, R. R. Rao, M. Subrahmanyam, A. V Rama Rao, A. Sarkany, and L. Guczi, "Oxidation and ammoxidation of toluene and benzyl alcohol over silico-aluminophosphate and metal-silico-aluminophosphate catalysts," *Appl. Catal. A Gen.*, vol. 139, pp. 59–74, 1996.

[51] T. Oishi, K. Yamaguchi, and N. Mizuno, “An Efficient One-Pot Synthesis of Nitriles from Alcohols or Aldehydes with NH3 Catalyzed by a Supported Ruthenium Hydroxide,” *Top. Catal.*, vol. 53, no. 7–10, pp. 479–486, Apr. 2010.

[52] T. Oishi, K. Yamaguchi, and N. Mizuno, “Catalytic oxidative synthesis of nitriles directly from primary alcohols and ammonia.,” *Angew. Chem. Int. Ed. Engl.*, vol. 48, no. 34, pp. 6286–8, Jan. 2009.

[53] K. Yamaguchi and N. Mizuno, “Green Functional Group Transformations by Supported Ruthenium Hydroxide Catalysts,” *Synlett*, vol. 2010, no. 16, pp. 2365–2382, Sep. 2010.

[54] M. O. Guerrero-Pérez and M. A. Bañares, “New reaction: conversion of glycerol into acrylonitrile.,” *ChemSusChem*, vol. 1, no. 6, pp. 511–3, Jan. 2008.

[55] S. J. Kulkarni, R. Ramachandra Rao, M. Subrahmanyam, and A. V Rama Rao, “Ammoxidation of ethanol to acetonitrile over molecular sieves,” *J. Chem. Soc. Chem. Commun.*, p. 273, 1994.

[56] R. R. Rao, N. Srinivas, S. J. Kulkarni, M. Subrahmanyarn, and K. V. Raghavan, “Selective prepartion of acetonitrile from etahnol over vnadium modified silicoaluminophosphate catalysts,” *Indian J. Chem.*, vol. 36A, pp. 708–711, 1997.

[57] “One Step Synthesis of Acetonitrile from ethanol via Ammoxidation over Sb-V-P-O/Al2O3 catalyst.” .

[58] W. Yin, C. Wang, and Y. Huang, “Highly practical synthesis of nitriles and heterocycles from alcohols under mild conditions by aerobic double dehydrogenative catalysis.,” *Org. Lett.*, vol. 15, no. 8, pp. 1850–3, Apr. 2013.

[59] S. P. Godbole, M. J. J. Seely, and D. Suresh, “Ammoxidation of a mixture of alcohols to a mixture of nitriles to acetonitrile and HCN,” 6,204,4072001.

[60] K. Yamaguchi, H. Kobayashi, T. Oishi, and N. Mizuno, “Heterogeneously catalyzed synthesis of primary amides directly from primary alcohols and aqueous ammonia.,” *Angew. Chem. Int. Ed. Engl.*, vol. 51, no. 2, pp. 544–7, Jan. 2012.

[61] K. Yamaguchi, K. Yajima, and N. Mizuno, “Facile synthesis of nitriles via manganese oxide promoted oxidative dehydrosulfurization of primary thioamides.,” *Chem. Commun. (Camb).*, vol. 48, no. 91, pp. 11247–9, Nov. 2012.

[62] J. He, K. Yamaguchi, and N. Mizuno, “Aerobic oxidative transformation of primary azides to nitriles by ruthenium hydroxide catalyst.,” *J. Org. Chem.*, vol. 76, no. 11, pp. 4606–10, Jun. 2011.

[63] R. H. Nielsen, “On-purpose Butadiene Production,” *Process Econ. Progr. Rep. 35E*, no. December 2012, 2012.

[64] J. Grub and E. Löser, “Butadiene,” *Ullmann’s Encyclopedia of Industrial Chemistry*. Wiley-VCH Verlag GmbH & Co. KGaA, pp. 1–17, Jul-2011.

[65] H. N. Sun and J. P. Wristers, “Butadiene,” *kirk othmer encyclopedia of chemical technology*, vol. 4, no. 8. John Wiley & Sons, Inc., pp. 365–392, 2000.

[66] K. Weissermel and H.-J. Arpe, “1,3-Diolefins,” in *Industrial Organic Chemistry*, Wiley-VCH Verlag GmbH, 2007, pp. 105–124.

[67] A. Chieregato, J. Velasquez Ochoa, and F. Cavani, “Olefins from Biomass,” in *Chemicals and Fuels from Bio-based Building Blocks*, Wiley-VCH Verlag GmbH & Co. KGaA, 2016, pp. 1–32.

[68] C. Angelici, B. M. Weckhuysen, and P. C. a Bruijnincx, “Chemocatalytic conversion of ethanol into butadiene and other bulk chemicals.,” *ChemSusChem*, vol. 6, no. 9, pp. 1595–614, Sep. 2013.

[69] J. L. Marsh, I. L. Murray, and J. S. P. Smith, “Process for making butadiene,” US2403741 A1946.

[70] W. J. Toussaint, J. T. Dunn, and D. R. Jackson, “Production of butadiene from alcohol,” *Ind. Eng. Chem.*, vol. 39, no. 2, pp. 120–125, 1947.

[71] W. J. Toussaint and J. T. Dunn, “Process for making diolefins,” US 24213611947.

[72] I. L. Murray, “Recovery method for cyclic vapor phase reaction products,” US2249847A22-Jul-1941.

[73] E. V Makshina, M. Dusselier, W. Janssens, J. Degrève, P. a Jacobs, and B. F. Sels, “Review of old chemistry and new catalytic advances in the on-purpose synthesis of butadiene.,” *Chem. Soc. Rev.*, pp. 7917–7953, 2014.

[74] G. Natta and G. Rigamonti, “Studio roentgenografico e chimico dei catalizzatori usati per la produzione del butadiene dall’acool etilico,” *La Chim. e l’Industria*, vol. 29, pp. 239 – 244, 1947.

[75] I. R. László, B. Falkay, and L. Hegyessy, *Hungarian J. Chem.*, vol. 60, pp. 54–74, 1954.

[76] B. Kovarik, “Einfluss der magnesiumsilikate auf die aktivitat des lebedew-katalysators,” *Collect. Czechoslov. Chem. Commun.*, vol. 26, pp. 1918–1924, 1960.

[77] S. K. Bhattacharyya and B. N. Avasthi, “One-Step Catalytic Conversion of Ethanol to Butadiene in a Fluidized Bed,” *Ind. Eng. Chem. Process Des. Dev.*, vol. 2, no. 1, pp. 45–51, Jan. 1963.

[78] J. M. Berak, R. Guczalski, and J. Wojcik, *Acta Chim. Acad. Sci. Hung.*, vol. 50, pp. 163–166, 1966.

[79] H. Niiyama, S. Morii, and E. Echigoya, “Butadiene formation from ethanol over silica-magnesia catalysts,” *Bull. Chem. Soc. Jpn.*, vol. 45, pp. 655–659, 1972.

[80] R. Ohnishi, T. Akimoto, and K. Tanabe, “Pronounced catalytic activity and selectivity of MgO–SiO2–Na2O for synthesis of buta-1, 3-diene from ethanol,” *J. Chem. Soc., Chem. Commun.*, pp. 1613–1614, 1985.

[81] S. Kvisle, A. Aguero, and R. P. A. P. A. Sneeden, “Transformation of ethanol into 1,3-butadiene over magnesium oxide/silica catalysts,” *Appl. Catal.*, vol. 43, no. 1, pp. 117–131, Jan. 1988.

[82] Y. Kitayama, M. Satoh, and T. Kodama, “Preparation of large surface area nickel magnesium silicate and its catalytic activity for conversion of ethanol into buta-1,3-diene,” *Catal. Letters*, vol. 36, no. 1–2, pp. 95–97, 1996.

[83] T. Tsuchida, J. Kubo, T. Yoshioka, S. Sakuma, T. Takeguchi, and W. Ueda, “Reaction of ethanol over hydroxyapatite affected by Ca/P ratio of catalyst,” *J. Catal.*, vol. 259, no. 2, pp. 183–189, Oct. 2008.

[84] M. D. Jones, C. G. Keir, C. Di Iulio, R. A. M. Robertson, C. V. Williams, and D. C. Apperley, “Investigations into the conversion of ethanol into 1,3-butadiene,” *Catal. Sci. Technol.*, vol. 1, no. 2, pp. 267–272, 2011.

[85] E. V. V Makshina, W. Janssens, B. F. F. Sels, and P. a. A. Jacobs, “Catalytic study of the conversion of ethanol into 1,3-butadiene,” *Catal. Today*, vol. 198, no. 1, pp. 338–344, Dec. 2012.

[86] M. Lewandowski, G. S. Babu, M. Vezzoli, M. D. Jones, R. E. Owen, D. Mattia, P. Plucinski, E. Mikolajska, A. Ochenduszko, and D. C. Apperley, “Investigations into the conversion of ethanol to 1,3-butadiene using MgO:SiO2 supported catalysts,” *Catal. Commun.*, vol. 49, pp. 25–28, Apr. 2014.

[87] G. O. Ezinkwo, V. F. Tretjakov, R. M. Talyshinky, A. M. Ilolov, and T. A. Mutombo, “Creation of a continuous process for bio-ethanol to butadiene conversion via the use of a process initiator,” *Catal. Commun.*, vol. 43, pp. 207–212, Jan. 2014.

[88] C. Angelici, M. E. Z. Velthoen, B. M. Weckhuysen, and P. C. a Bruijnincx, "Effect of preparation method and CuO promotion in the conversion of ethanol into 1,3-butadiene over SiO2-MgO catalysts," *ChemSusChem*, pp. 2505–2515, 2014.

[89] V. L. Sushkevich, I. I. Ivanova, V. V Ordomsky, and E. Taarning, "Design of a Metal-Promoted Oxide Catalyst for the Selective Synthesis of Butadiene from Ethanol," *ChemSusChem*, vol. 7, no. 9, pp. 2527–2536, 2014.

[90] W. Janssens, E. V. Makshina, P. Vanelderen, F. De Clippel, K. Houthoofd, S. Kerkhofs, J. a. Martens, P. a. Jacobs, and B. F. Sels, "Ternary Ag/MgO-SiO 2 Catalysts for the Conversion of Ethanol into Butadiene," *ChemSusChem*, vol. 8, no. 6, pp. 994–1088, 2015.

[91] O. Larina, P. Kyriienko, and S. Soloviev, "Ethanol Conversion to 1,3-Butadiene on ZnO/MgO–SiO2 Catalysts: Effect of ZnO Content and MgO:SiO2 Ratio," *Catal. Letters*, vol. 145, no. 5, pp. 1162–1168, 2015.

[92] V. Sushkevich, I. I. Ivanova, and E. Taarning, "Ethanol Conversion into Butadiene over Zr-containing Molecular Sieves doped with Silver," *Green Chem.*, pp. 2552–2559, 2015.

[93] E. A. Redina, A. A. Greish, I. V Mishin, G. I. Kapustin, O. P. Tkachenko, O. A. Kirichenko, and L. M. Kustov, "Selective oxidation of ethanol to acetaldehyde over Au–Cu catalysts prepared by a redox method," *Catal. Today*, vol. 241, pp. 246–254, Mar. 2015.

[94] D.-W. Kim, H. Kim, Y.-S. Jung, I. Kyu Song, and S.-H. Baeck, "Synthesis of tungsten–vanadium mixed oxides for ethanol partial oxidation," *J. Phys. Chem. Solids*, vol. 69, no. 5–6, pp. 1513–1517, May 2008.

[95] F.-W. Chang, H.-C. Yang, L. S. Roselin, and W.-Y. Kuo, "Ethanol dehydrogenation over copper catalysts on rice husk ash prepared by ion exchange," *Appl. Catal. A Gen.*, vol. 304, no. 0, pp. 30–39, May 2006.

[96] Y. Guan and E. J. M. Hensen, "Ethanol dehydrogenation by gold catalysts: The effect of the gold particle size and the presence of oxygen," *Appl. Catal. A Gen.*, vol. 361, no. 1–2, pp. 49–56, Jun. 2009.

[97] I. Ostromislensky, *Russ. J. Phys. Chem.*, vol. 47, pp. 1472–1506, 1915.

[98] A. . Balandin, *Russ. J. Phys. Chem.*, vol. 6, p. 357, 1935.

[99] S. Lebedev, *Russ. J. Gen. Chem.*, no. 3, pp. 698–717, 1933.

[100] V. Gruver, a. Sun, and J. J. Fripiat, "Catalytic properties of aluminated sepiolite in ethanol conversion," *Catal. Letters*, vol. 34, no. 3–4, pp. 359–364, 1995.

[101] H. Jones, E. Stahly, and B. Corson, "Butadiene from Ethanol. Reaction Mechanism," *J. Am. Chem. Soc.*, vol. 767, pp. 1822–1828, 1949.

[102] F. Zaera, "New advances in the use of infrared absorption spectroscopy for the characterization of heterogeneous catalytic reactions," *Chem. Soc. Rev.*, vol. 43, no. 22, pp. 7624–7663, 2014.

[103] G. Busca, "Infrared studies of the reactive adsorption of organic molecules over metal oxides and of the mechanisms of their heterogeneously-catalyzed oxidation," *Catal. Today*, vol. 27, no. 3–4, pp. 457–496, 1996.

[104] F. C. Meunier, "The design and testing of kinetically-appropriate operando spectroscopic cells for investigating heterogeneous catalytic reactions," *Chem. Soc. Rev.*, vol. 39, no. 12, pp. 4602–4614, 2010.

[105] M. J. Frisch, G. W. Trucks, H. B. Schlegel, G. E. Scuseria, M. A. Robb, J. R. Cheeseman, J. A. Montgomery, Jr., T. Vreven, K. N. Kudin, J. C. . Burant, J. M. . Millam, S. S. . Iyengar, J. . Tomasi, V. . Barone, B. . Mennucci, M. . Cossi, G. . Scalmani, N. . Rega, and G. A. . Petersson, "Gaussian, Inc," *Gaussian, Inc*, 2009.

[106] A. D. Becke, "Density-functional thermochemistry. III. The role of exact exchange," *J. Chem. Phys.*, vol. 98, no. 7, p. 5648, Apr. 1993.

[107] A. G. Pelmenschikov, G. Morosi, A. Gamba, S. Coluccia, G. Martra, and E. A. Paukshtis, "Single and Multiple Lewis Sites of MgO: A Combined IR and ab Initio Study with CD 3 CN as a Molecular Probe," *J. Phys. Chem.*, vol. 100, no. 12, pp. 5011–5016, Jan. 1996.

[108] M. Cavalleri, A. Pelmenschikov, G. Morosi, A. Gamba, S. Coluccia, and G. Martra, *Oxide-based Systems at the Crossroads of Chemistry, Second International Workshop*, vol. 140. Elsevier, 2001.

[109] T. Pasini, A. Lolli, S. Albonetti, F. Cavani, and M. Mella, "Methanol as a clean and efficient H-transfer reactant for carbonyl reduction: Scope, limitations, and reaction mechanism," *J. Catal.*, pp. 206–219, 2014.

[110] G. Szöllösi and M. Bartók, "Vapour-phase heterogeneous catalytic transfer hydrogenation of alkyl methyl ketones on MgO: Prevention of the deactivation of MgO in the presence of carbon tetrachloride," *Appl. Catal. A Gen.*, vol. 169, pp. 263–269, 1998.

[111] M. Balat and H. Balat, "Recent trends in global production and utilization of bio-ethanol fuel," *Appl. Energy*, vol. 86, no. 11, pp. 2273–2282, Nov. 2009.

[112] M. León, E. Díaz, and S. Ordóñez, "Ethanol catalytic condensation over Mg–Al mixed oxides derived from hydrotalcites," *Catal. Today*, vol. 164, pp. 436–442, 2011.

[113] M. León, E. Díaz, A. Vega, S. Ordóñez, and A. Auroux, "Consequences of the iron–aluminium exchange on the performance of hydrotalcite-derived mixed oxides for ethanol condensation," *Appl. Catal. B Environ.*, vol. 102, no. 3–4, pp. 590–599, Feb. 2011.

[114] G. Natta and R. Rigamonti, "Sintesi del butadiene da alcool etilico," *La Chim. e L'industria*, vol. 29, pp. 195–202, 1947.

[115] W. M. Quattlebaum, W. J. Toussaint, and J. T. Dunn, "Deoxygenation of Certain Aldehydes and Ketones: Preparation of Butadiene and Styrene," *J. Am. Chem. Soc.*, vol. 69, no. 3, pp. 593–599, 1947.

[116] M. Dömök, M. Tóth, J. Raskó, and A. Erdőhelyi, "Adsorption and reactions of ethanol and ethanol–water mixture on alumina-supported Pt catalysts," *Appl. Catal. B Environ.*, vol. 69, no. 3–4, pp. 262–272, Jan. 2007.

[117] T. W. Birky, J. T. Kozlowski, and R. J. Davis, "Isotopic transient analysis of the ethanol coupling reaction over magnesia," *J. Catal.*, vol. 298, pp. 130–137, Feb. 2013.

[118] C. Resini, S. Cavallaro, and F. Frusteri, "Initial steps in the production of H2 from ethanol: A FT-IR study of adsorbed species on Ni/MgO catalyst surface," *React. Kinet. Catal. Lett.*, vol. 90, no. 1, pp. 117–126, 2007.

[119] A. M. da Silva, K. R. de Souza, L. V. Mattos, G. Jacobs, B. H. Davis, and F. B. Noronha, "The effect of support reducibility on the stability of Co/CeO2 for the oxidative steam reforming of ethanol," *Catal. Today*, vol. 164, no. 1, pp. 234–239, Apr. 2011.

[120] M. G. Rosmaninho and F. C. C. Moura, "Investigation of iron oxide reduction by ethanol as a potential route to produce hydrogen," *Appl. Catal. B Environ.*, vol. 115–116, pp. 45–52, Apr. 2012.

[121] M. J. L. Gines and E. Iglesia, "Bifunctional Condensation Reactions of Alcohols on Basic Oxides Modified by Copper and Potassium," *J. Catal.*, vol. 176, no. 1, pp. 155–172, 1998.

[122] M. J. Janik, J. Macht, E. Iglesia, and M. Neurock, "Correlating Acid Properties and Catalytic Function: A First-Principles Analysis of Alcohol Dehydration Pathways on Polyoxometalates," *J. Phys. Chem. C*, vol. 113, no. 5, pp. 1872–1885, Feb. 2009.

[123] J. V. Ochoa, C. Bandinelli, O. Vozniuk, A. Chieregato, A. Malmusi, C. Recchi, and F. Cavani, "An analysis of the chemical, physical and reactivity features of MgO–SiO2 catalysts for butadiene synthesis with the Lebedev process," *Green Chem.*, DOI: 10.1039/C5GC02194D, Nov. 2016.

[124] R. Brambilla, C. Radtke, J. H. Z. dos Santos, and M. S. L. Miranda, "Silica-magnesia mixed oxides prepared by a modified Stöber route: Structural and textural aspects," *Powder Technol.*, vol. 198, no. 3, pp. 337–346, Mar. 2010.

[125] F. Ciesielczyk, M. Przybysz, J. Zdarta, A. Piasecki, D. Paukszta, and T. Jesionowski, "The sol-gel approach as a method of synthesis of xMgO·ySiO 2 powder with defined physicochemical properties including crystalline structure," *J. Sol-Gel Sci. Technol.*, vol. 71, no. 3, pp. 501–513, 2014.

[126] T. Lopez, R. Gomez, and M. E. Llanos, "On the surface basic properties of sulfated magnesia – silica sol – gel mixed oxides," *Mater. Lett.*, vol. 39, no. April, pp. 51–57, 1999.

[127] T. López, R. Gomez, M. E. Llanos, and E. López-Salinas, "Acidic – base properties of silica – magnesia sol – gel mixed oxides : use of 2 butanol as test reaction," *Mater. Lett.*, vol. 38, no. February, pp. 283–288, 1999.

[128] S. Mitra and S. Sampath, "Sol – gel derived , magnesium based ionically conducting composites," *Ratio*, no. May, pp. 2531–2537, 2002.

[129] C. Angelici, M. E. Z. Velthoen, B. M. Weckhuysen, and P. C. a. Bruijnincx, "Influence of acid–base properties on the Lebedev ethanol-to-butadiene process catalyzed by SiO 2 – MgO materials," *Catal. Sci. Technol.*, vol. 5, pp. 2869–2879, 2015.

[130] G. Busca, "The surface acidity of solid oxides and its characterization by IR spectroscopic methods. An attempt at systematization," *Phys. Chem. Chem. Phys.*, vol. 1, no. 5, pp. 723–736, 1999.

[131] G. Busca, "Spectroscopic characterization of the acid properties of metal oxide catalysts," *Catal. Today*, vol. 41, no. 1–3, pp. 191–206, 1998.

[132] O. Diwald, M. Sterrer, and E. Knözinger, "Site selective hydroxylation of the MgO surface," *Phys. Chem. Chem. Phys.*, vol. 4, pp. 2811–2817, 2002.

[133] C. Martinet and R. A. B. Devine, "Analysis of the vibrational mode spectra of amorphous SiO2 films," *J. Appl. Phys.*, vol. 77, no. 9, p. 4343, 1995.

[134] S. W. Kieffer, "Thermodynamics and Lattice Vibrations of Minerals" *Rev. Geophys. Sp. Phys.*, vol. 17, no. 1, pp. 20–34, 1979.

[135] a Vimont, J. C. Lavalley, a Sahibed-Dine, C. Otero Arean, M. Rodríguez Delgado, and M. Daturi, "Infrared spectroscopic study on the surface properties of gamma-gallium oxide as compared to those of gamma-alumina.," *j. phys.chem. B*, vol. 109, no. 19. pp. 9656–9664, 2005.

[136] M. Calatayud, S. E. Collins, M. A. Baltanás, and a L. Bonivardi, "Stability of formate species on beta-Ga2O3.," *Phys. Chem. Chem. Phys.*, vol. 11, no. 9, pp. 1397–405, 2009.

[137] S. E. Collins, M. A. Baltanás, and A. L. Bonivardi, "Infrared spectroscopic study of the carbon dioxide adsorption on the surface of Ga2O3 polymorphs.," *J. Phys. Chem. B*, vol. 110, no. 11, pp. 5498–5507, 2006.

[138] J. Velasquez Ochoa, C. Trevisanut, J.-M. M. Millet, G. Busca, and F. Cavani, "In Situ DRIFTS-MS Study of the Anaerobic Oxidation of Ethanol over Spinel Mixed Oxides," *J. Phys. Chem. C*, vol. 117, no. 45, pp. 23908–23918, 2013.

[139] A. M. Nadeem, G. I. N. Waterhouse, and H. Idriss, "The reactions of ethanol on TiO2 and Au/TiO2 anatase catalysts," *Catal. Today*, vol. 182, no. 1, pp. 16–24, Mar. 2012.

[140] F. Cavani, F. Trifirò, and A. Vaccari, “Hydrotalcite-type anionic clays: Preparation, properties and applications.,” *Catal. Today*, vol. 11, no. 2, pp. 173–301, Dec. 1991.

[141] A. Schutz and P. Biloen, “Interlamellar chemistry of hydrotalcites,” *J. Solid State Chem.*, vol. 68, no. 2, pp. 360–368, 1987.

[142] S. Albertazzi, F. Basile, P. Benito, P. Del Gallo, G. Fornasari, D. Gary, V. Rosetti, and A. Vaccari, “Effect of silicates on the structure of Ni-containing catalysts obtained from hydrotalcite-type precursors,” *Catal. Today*, vol. 128, no. 3–4, pp. 258–263, 2007.

[143] C. Depège, F.-Z. El Metoui, C. Forano, A. de Roy, J. Dupuis, and J.-P. Besse, “Polymerization of Silicates in Layered Double Hydroxides,” *Chem. Mater.*, vol. 8, no. 4, pp. 952–960, 1996.

[144] R. L. Frost, H. J. Spratt, and S. J. Palmer, “Infrared and near-infrared spectroscopic study of synthetic hydrotalcites with variable divalent/trivalent cationic ratios,” *Spectrochim. Acta - Part A Mol. Biomol. Spectrosc.*, vol. 72, no. 5, pp. 984–988, 2009.

[145] M. J. Hernandez-Moreno, M. A. Ulibarri, J. L. Rendon, and C. J. Serna, “IR characteristics of hydrotalcite-like compounds,” *Phys. Chem. Miner.*, vol. 12, no. 1, pp. 34–38, 1985.

[146] M. H. Kim, S. H. Jang, I. M. Kang, Y. Song, J. J. Lee, J. S. Hong, and M. Lee, *Synthesis of novel mesoporous material through intercalation of anionic silicates into cationic charged layered material hydrotalcite*. Elsevier B.V., 2007.

[147] F. Folco, “Catalytic processes for the transformation of ethanol into acetonitrile,” Università di Bologna, 2013.

[148] M. Schmal, D. V Cesar, M. M. V. M. Souza, and C. E. Guarido, “Drifts and TPD analyses of ethanol on Pt catalysts over Al2O3 and ZrO2—partial oxidation of ethanol,” *Can. J. Chem. Eng.*, vol. 89, no. 5, pp. 1166–1175, 2011.

[149] H. Idriss and E. G. Seebauer, “Reactions of ethanol over metal oxides,” *J. Mol. Catal. A Chem.*, vol. 152, no. 1–2, pp. 201–212, Mar. 2000.

[150] A. H. Chughtai, N. Ahmad, H. A. Younus, A. Laypkov, and F. Verpoort, “Metal-organic frameworks: versatile heterogeneous catalysts for efficient catalytic organic transformations.,” *Chem. Soc. Rev.*, vol. 44, no. 19, pp. 6804–49, Oct. 2015.

[151] G. C. Shearer, V. Colombo, S. Chavan, E. Albanese, B. Civalleri, A. Maspero, and S. Bordiga, “Stability vs. reactivity: understanding the adsorption properties of Ni3(BTP)2 by experimental and computational methods.,” *Dalton Trans.*, vol. 42, no. 18, pp. 6450–8, May 2013.

[152] E. Albanese, B. Civalleri, M. Ferrabone, F. Bonino, S. Galli, A. Maspero, and C. Pettinari, “Theoretical and experimental characterization of pyrazolato-based Ni(ii) metal–organic frameworks,” *J. Mater. Chem.*, vol. 22, no. 42, p. 22592, Oct. 2012.

[153] L. Artiglia, S. Agnoli, M. Cristina Paganini, M. Cattelan, and G. Granozzi, “TiO2@CeOx core-shell nanoparticles as artificial enzymes with peroxidase-like activity,” *ACS Appl. Mater. Interfaces*, vol. 6, no. 22, pp. 20130–20136, 2014.

[154] A. Yee, S. J. Morrison, and H. Idriss, “A Study of the Reactions of Ethanol on CeO2 and Pd/CeO2 by Steady State Reactions , Temperature Programmed Desorption , and In Situ FT-IR,” *J. Catal.*, vol. 186, no. 2, pp. 279–295, 1999.

[155] S. Agnoli, A. E. Reeder, S. D. Senanayake, J. Hrbek, and J. A. Rodriguez, “Structure and special chemical reactivity of interface-stabilized cerium oxide nanolayers on TiO2(110).,” *Nanoscale*, vol. 6, no. 2, pp. 800–10, Jan. 2014.

[156] G. Pavarelli, “The Synthesis of Maleic Anhydride: Study of a New Process and Improvement of the Industrial Catalyst,” Università di Bologna, 2015.

[157] R. Wenig and G. Schrader, “In situ Fourier transform infrared study of crotyl alcohol, maleic acid, crotonic acid, and maleic anhydride oxidation on a vanadium-phosphorus-oxide industrial catalyst,” *J. Phys. Chem.*, vol. 91, no. 12, pp. 5674–5680, 1987.

[158] B. Sakakini, “A Study of the Kinetics and Mechanism of the Adsorption and Anaerobic Partial Oxidation of n-Butane over a Vanadyl Pyrophosphate Catalyst,” *J. Catal.*, vol. 189, no. 2, pp. 253–262, Jan. 2000.

[159] R. W. Wenig and G. L. Schrader, “I n Situ FTIR Spectroscopy of 1-Butene and 1,3-Butadiene Selective Oxidation to Maleic Anhydride on V-P-0 Catalysts,” *J. Phys. Chem.*, vol. 91, pp. 1911–1918, 1987.